Antonio Renê Benevides de Melo

The role of extracellular polymeric substances during biodegradation of contaminants
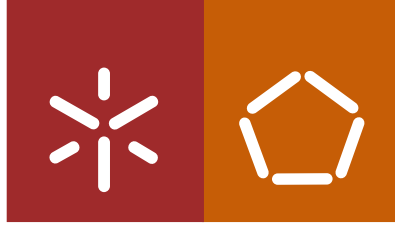
The role of extracellular polymeric substances during biodegradation of contaminants

Antonio Renê Benevides de Melo

UMinho | 2023

abril de 2023

Universidade do Minho
Escola de Engenharia

Antonio Renê Benevides de Melo

The role of extracellular polymeric substances during biodegradation of contaminants

Tese de Doutoramento
Doutoramento em Engenharia Química e Biológica

Trabalho efetuado sob a orientação da
Doutora Daniela Patrícia Bernardino Mesquita
e do
Professor Doutor Eugénio Campos Ferreira

abril de 2023

COPYRIGHT AND WORKING CONDITIONS BY THIRD PARTIES

This is an academic work that may be used by third parties, provided that the international rules and good practices accepted in respect of copyright and related rights are respected.

Thus, the present work can be developed in terms of public availability.

If the user needs to be authorized to use this work in conditions not subject to prior agreement, contact the author through the University of Minho's RepositóriUM.

ACKNOWLEDGEMENTS

First, I would like to give special thanks to my supervisors.

I want to express my sincere gratitude and respect to my advisor, Dr. Daniela Mesquita. I would like to thank her for allowing me to complete my PhD under her guidance. Her insight and advice helped me achieve and realize my academic goals. I learned a lot under her supervision, and that experience will continue to help me throughout my career. To Professor Dr. Eugénio Ferreira for the great opportunity granted me to carry out my PhD in the Biosystems group. I also thank you for all your contributions to the construction of this thesis.

I would also like to thank especially Dr. Cristina Quintelas for her advice, discussion and enthusiasm on my research. I am also grateful for her guidance on my laboratory work. Actually, I cannot find the right words to express how thankful I am for all your contributions on this long journey. Thanks a lot, Dr. Quintelas!

I want to thank my friend Joana Costa for supporting the microscopy sampling campaign and for all your collaboration and friendship.

I would also like to thank all my colleagues at the Laboratory of Sustainable Bioprocesses and Bioproducts (LBBS), Laboratory of Environmental Biotechnology (LBA), and Laboratory of Environmental Microbiology (LMAmb). Thank you, Jorge Padrão, Salomé Duarte and Vânia Ferreira, for sharing the laboratories and experimental devices.

I also want to thank my dear friends from the Doctoral Program: Dr Cristiano Leal for his friendship, companionship during the PhD journey and advice on various subjects, Dr Enrique Pino, Dr Andreia Vaz, Silvia Fernandes, Joana Costa and José Roberto for their friendship, kindness and moral support during all the time we spent there. Finally, I could not forget my dear friend João Carlos; thank you for welcoming me at the beginning of this challenge.

Last but not least, I would like to thank my family for all their support and always believing in me. Special thanks to my wife, Soraia, for her patience and encouragement and for always being by my side during this long journey. To my beloved little António and my wife, I dedicate this thesis!

STATEMENT OF INTEGRITY

I hereby declare having conducted this academic work with integrity. I confirm that I have not used plagiarism or any form of undue use of information or falsification of results along the process leading to its elaboration.

I further declare that I have fully acknowledged the Code of Ethical Conduct of the University of Minho.

The role of extracellular polymeric substances during biodegradation of contaminants

ABSTRACT

In this thesis, a sequencing batch reactor (SBR) inoculated with activated sludge (AS) was operated initially in the absence of micropollutants, and later with ibuprofen (IBU), desloratadine (DESL), and atrazine (ATZ). The system performance, the production and composition of extracellular polymeric substances (EPS), as well as the morphology of the biomass using quantitative image analysis (QIA) techniques were evaluated. The three-dimensional fluorescence spectroscopy (3D-EEM) technique was used enlightening the changes in functional groups of EPS affected by the addition of DESL and ATZ. Different chemometric techniques were also applied, mainly principal component analysis (PCA) and partial least squares (PLS), to the system operational parameters, EPS results and morphological parameters of the biomass. The activity of both heterotrophic and autotrophic microrganisms was impacted by the micropollutants decreasing the chemical oxygen demand removal and interfering with the nitrification process. After adding the selected compounds, a significant change in biomass properties was observed, demonstrating that EPS, more specifically TB-EPS forms, played a crucial role in the aggregates morphology. Also, the LB-EPS influenced the biomass properties, especially during experiments with DESL and ATZ, lowering the biomass's capacity to settle despite the lower contents of filamentous bacteria. Morphological parameters were extremely helpful, demonstrating that the dysfunctions in the biomass settling ability were caused by filamentous content or by viscous bulking related to the overproduction of LB-EPS. The PCA carried out allowed identifying the clusters corresponding to the experimental periods with the addition of DESL and ATZ and evaluating the interrelationships of the studied parameters. Finally, this study also provided an alternative approach to estimate the different forms of EPS, saving time in the operation and monitoring of AS systems.

Keywords: Activated sludge, chemometric tools, extracellular polymeric substances, micropollutants, quantitative image analysis.

O papel das substâncias poliméricas extracelulares durante a biodegradação de contaminantes

RESUMO

Nesta tese foi operado um reator descontínuo sequencial (SBR) inoculado com lamas ativadas (AS), inicialmente sem a adição de micropoluentes e posteriormente adicionando ibuprofeno (IBU), desloratadina (DESL) e atrazina (ATZ). Avaliou-se o desempenho do sistema, a produção e composição das substâncias poliméricas extracelulares (EPS), bem como a morfologia da biomassa por técnicas de análise quantitativa de imagens (QIA). Foi utilizada a técnica de espectroscopia de fluorescência tridimensional (3D-EEM) para esclarecer as alterações nos grupos funcionais de EPS causadas pela adição dos micropoluentes. Foram ainda utilizadas diferentes técnicas quimiométricas, incluindo análise de componentes principais (PCA) e mínimos quadrados parciais (PLS), aos parâmetros operacionais do sistema, resultados globais de EPS e parâmetros morfológicos da biomassa. A atividade dos microrganismos heterotróficos e autotróficos foi impactada pelos micropoluentes diminuindo a remoção da carência química de oxigénio e interferindo no processo de nitrificação. Após a adição dos compostos selecionados, observou-se uma mudança significativa nas propriedades da biomassa, demonstrando que os EPS, mais especificamente a forma *tighly bound* (TB-EPS), tiveram um papel crucial na morfologia dos agregados. Além disso, a forma *loosely bound* (LB-EPS) influenciou as propriedades da biomassa, principalmente durante os experimentos com DESL e ATZ, diminuindo a sua capacidade de sedimentação apesar da menor incidência de bactérias filamentosas. Os resultados morfológicos obtidos foram extremamente úteis e demonstraram que as disfunções na capacidade de sedimentação da biomassa foram causadas pela proliferação de bactérias filamentosas ou pelo *bulking* viscoso relacionado com a superprodução de LB-EPS. O PCA realizado permitiu identificar os *clusters* correspondentes aos períodos experimentais com adição de DESL e ATZ e avaliar as inter-relações dos parâmetros estudados. Este estudo forneceu ainda uma abordagem alternativa para estimar as diferentes formas de EPS, economizando tempo na operação e monitorização de sistemas AS.

Palavras chave: Análise quantitativa de imagem, lamas ativadas, micropoluentes, substâncias poliméricas extracelulares, técnicas quimiométricas.

TABLE OF CONTENTS

LIST OF FIGURES

LIST OF TABLES

SCIENTIFIC OUTPUTS

Papers in international journals with peer review:

- Melo, A., Costa, J., Quintelas, C., Ferreira, E.C., Mesquita, D.P., 2022. Effects of desloratadine on activated sludge: Behaviour of EPS and sludge properties. Journal of Environmental Chemical Engineering. 10, 108415. https://doi.org/10.1016/j.jece.2022.108415
- Melo, A., Quintelas, C., Ferreira, E.C., Mesquita, D.P., 2022. The Role of Extracellular Polymeric Substances in Micropollutant Removal. Frontiers. Chemical Engineering. 4, 1–13. https://doi.org/10.3389/fceng.2022.778469
- Melo, A., Costa, J., Quintelas, C., Ferreira, E.C., Mesquita, D.P., 2021. Effect of ibuprofen on extracellular polymeric substances (EPS) production and composition, and assessment of microbial structure by quantitative image analysis. Journal of Environmental Management. 293, 112852. https://doi.org/10.1016/j.jenvman.2021.112852
- Assessing extracellular polymeric substances in activated sludge under atrazine exposure (in preparation).

Abstract and poster in international congress:

- Antonio Melo, Jorge Padrão, Ana Nicolau, Cristina Quintelas, Eugénio Campos Ferreira, Daniela Mesquita. Toxicity assessment of ibuprofen on activated sludge by respirometric technique. Microbiotec19 – Congress of Microbiology and Biotechnology 2019. Coimbra, Portugal during December from 05 to 07, 2019.

CHAPTER 1 – INTRODUCTION

1.1 Research Motivation

The micropollutants found in wastewater are numerous and diverse, among which include pesticides (atrazine) (Campo *et al.*, 2013; Sharma *et al.*, 2019) and pharmaceutical compounds (ibuprofen and desloratadine) (Fick *et al.*, 2009; Ternes, 1998; Verenitch *et al.*, 2006). The presence of these micropollutants in the environment has become a growing concern worldwide. Albeit these compounds are present at low concentrations (<1 mg L^{-1}) in aquatic environments, they are capable of triggering extremely harmful effects in the systems in which they can be found (Joss *et al.*, 2006; Rani *et al.*, 2021; Sacher *et al.*, 2001; Santos *et al.*, 2010). The occurrence in the environment has become increasingly worrying because their toxicity effects on the environment and health are unknown. In conventional wastewater treatment plants (WWTP), the micropollutants are not entirely removed from the wastewater with primary and secondary treatment (Fick *et al.*, 2009; Santos *et al.*, 2013; Ternes, 1998). Thus, these micropollutants have received wide attention in the scientific community since their presence in the different environmental compartments (soil, water, etc.), even at low concentrations (ranging from ng L^{-1} to mg L^{-1}), can have detrimental impacts on the environment and human health (Kalyabina *et al.*, 2021; Kosonen and Kronberg, 2009; Rodriguez-Narvaez *et al.*, 2017).

In biological wastewater treatment (WWT), microorganisms live and grow held together by a slime matrix comprised of extracellular polymeric substances (EPS), forming a three-dimensional microbial structure of aggregates (flocs or granules) and by chemical binding forces. Furthermore, microscopic observations showed that microbial cells within the flocs were cross-linked with EPS, forming a network of polymers with pores and channels. The EPS are typically composed of organic substances such as polysaccharides (PS), proteins (PN), humic acid substances (HAS), nucleic acids, lipids, and deoxyribonucleic acid (DNA).

It has been established that EPS plays an essential role in the aggregates flocculation, settling, and dewatering (Bala Subramanian *et al.*, 2010; Sheng *et al.*, 2010). Moreover, in the presence of toxic substances, such as pharmaceutical compounds and pesticides, EPS forms a protective layer for the aggregated biomass against environmental disturbances that might play an important role in the adsorption process, transport and transformation of micropollutants (Szewczyk *et al.*, 2020; Tian *et al.*, 2019; Wang *et al.*, 2018; Zhang *et al.*, 2019).

The conventional characterisation of EPS by chemical methods cannot reveal in detail the particular functional groups of involved in the interaction with micropollutants because the characterisation is based chiefly on fractionated EPS components such as PN, PS and HAS, through

colorimetric methods, without considering their high compositional and structural heterogeneity. However, to solve the lack regarding their fundamental composition, new instruments and techniques for the characterization of EPS, such as three-dimensional fluorescence spectroscopy (3D-EEM), have been used in the last few years, generating a large amount of information about the structural and functional properties of EPS (Yu, 2020).

Some researchers indicated that there is an increase in EPS concentration under toxic conditions, which can induce a change in the formation of the microbial aggregates due to the complex influence of EPS in aggregates flocculation and biomass arrangement. Thus, several effects of EPS on aggregates may affect the AS flocs structure leading to the poor performance regarding biomass-water separation, or even improve the biomass aggregation. In biological WWT, microscopy investigations have been widely used to monitor the AS flocs structure and morphology (Amaral and Ferreira, 2005). As a result, many studies have addressed using quantitative image analysis (QIA) to extract quantitative data and remove the subjectivity of human analysis. Indeed, QIA methodology has already been applied for the identification of AS flocs structure and morphology (Campbell *et al.*, 2019), identification of different types of bulking (Mesquita *et al.*, 2011), and to monitor the dysfunction in granular AS during shock loadings of pharmaceutical compounds (Leal *et al.*, 2021).

Due to the large amount of data generated during operational routine in AS systems, including basic performance parameters, EPS data and QIA results, multivariate statistical methods are crucial to handle all data and extract crucial information. Principal component analysis (PCA) is one of the most multivariate statistical techniques used in monitoring biological WWT systems (Tomita *et al.*, 2002). Furthermore, the PCA has been applied in a different context, either in monitoring AS operational parameters (Tomita *et al.*, 2002), AS flocs structure and morphology (Amaral and Ferreira, 2005; Campbell *et al.*, 2019), or disfunction in the performance of AS systems (Mesquita *et al.*, 2011).

Thus, to properly monitor and optimize biological WWT systems, it is crucial to understand the role of EPS commonly involved in flocculation, settling, and ultimately in the protection of microorganisms against toxic compounds (Sheng *et al.*, 2010; Tian *et al.*, 2019).

1.2 Main Objectives

The main objective of this work was to evaluate the role of EPS on AS properties in a sequencing batch reactor (SBR) treating wastewater containing micropollutants. For that purpose, different experiments were conducted containing ibuprofen (IBU), desloratadine (DESL) and atrazine (ATZ) to assess their impact on EPS production and composition measured through chemical methods.

Fluorescence characteristics of EPS components were also evaluated using 3D-EEM. Furthermore, biomass activity, mainly heterotrophic and autotrophic biomass, and AS flocs structure and morphology were also assessed.

For AS flocs structure and morphology, microscope monitoring accomplished with QIA techniques were used, resulting in large datasets of parameters. Moreover, chemometric techniques were employed, including PCA, to enlighten the interrelationships between EPS and morphological parameters, and PLS to evaluate the feasibility of predicting the forms and content of EPS in a faster, more economical and environmentally friendly method.

1.3 Thesis Outline

This dissertation is divided into seven chapters, as described in Table 1.1. The current one provides the context, research aim and outline of this work (Chapter 1). Chapter 2 provides a general review regarding the role of EPS on biological WWT systems, including the influence of EPS on AS flocculation, settling, morphological changes and the effect of micropollutants on EPS production and composition. In Chapter 3 the material and methods are presented. The following three chapters discuss the experimental work and results (Chapter 4, 5, and 6). Finally, the last chapter states the most relevant conclusions of this work and future perspectives (Chapter 7).

Table 1.1 – Thesis structure.

Chapter	Description
Chapter 1	Consists of a context, main objectives and outline.
Chapter 2	Literature review.
Chapter 3	Material and methods.
Chapter 4	Provides information about the effect of IBU on EPS production and composition, and assessment of microbial structure by QIA.
Chapter 5	Provides information about the characteristics of EPS from AS under DESL exposure.
Chapter 6	Provides information about the assessment of EPS in activated sludge under ATZ exposure.
Chapter 7	Presents the main conclusions and gives some suggestions for further research in this field.

CHAPTER 2 - LITERATURE REVIEW

2.1 Activated sludge systems

2.1.1 General description

Activated sludge (AS) system is widely used for wastewater treatment, being one of the processes most used worldwide. In the AS process, mixed cultures of microorganisms convert contaminants present in municipal, industrial, and hazardous wastewaters to new cell mass, carbon dioxide, water, and other end products, which depend upon the nature of the contaminants and the organism distribution present (Irvine *et al.*, 1989). Microorganisms in reactors are organized as microbial consortia, being composed by a wide variety of bacteria, fungi, protozoa, and some metazoa (Jenkins *et al.*, 2003), that depending on their physical structure, can be classified mainly as suspended growth (flocs and granules - bioaggregates) and fixed-filme systems (biofilms), in which the organisms grow attached to surfaces. The syntrophic association between microorganisms and its organization in bioaggregates facilitates the solid-liquid separation, improves the retention of the sludge, and optimizes the accessibility to the nutrients (Ding *et al.*, 2015). The organic material (dissolved and particulate biodegradable constituents) will be removed from wastewater while more biomass is produced in the form of suspended flocs in the liquid. The equation 2.1, describes the aerobic biological oxidation of organic matter (e.g. dissolved and particulate carbonaceous organic matter) into simple end products and additional biomass,

$$\nu_1 \cdot (\text{organic matter}) + \nu_2 \cdot O_2 + \nu_3 \cdot NH_3 + \nu_4 \cdot PO_4^3 \xrightarrow{\text{Microorganisms}} \nu_5 \cdot (\text{new cells}) + \nu_6 \cdot CO_2 + \nu_7 \cdot H_2O \quad (2.1)$$
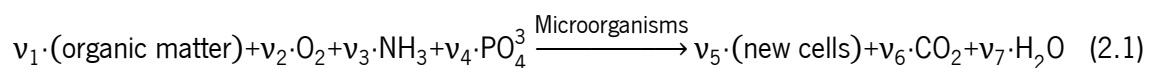
where ν_i is equal to stoichiometric coefficient.

This process consists of a treatment in which aerobic heterotrophic bacteria oxidize the organic matter forming CO_2 and H_2O. Depending on its configuration, an AS WWT can achieve biological nitrogen and phosphorus removal due to development of specific microorganisms, besides removal of organic carbon substances (Weber, 2002).

In Equation (2.1), oxygen (O_2), ammonia (NH_3), and phosphate (PO_4^3) are used to represent the nutrients needed for the convertion of the organic matter to simple end products (i.e., CO_2 and H_2O).

Because the biomass has a specific gravity slightly greater than that of water, the biomass can be removed from the treated liquid by gravity settling. The amount of suspended material in the process is normally controlled by means of adding a sedimentation tank at the end of the process, where the biomass is either recirculated back to the biological process or removed from the system as excess

sludge, whereas the purified wastewater is withdrawn from the top of the sedimentation tank. The conventional configuration of the AS system can be seen in Figure 2.1.

To maintain aerobic conditions and to keep the active biomass suspended, a constant and well-timed supply of oxygen is required. Different configurations of the AS process can be employed to ensure that the wastewater is mixed and aerated in an aeration tank.

Clarifier

Activated Sludge Tanks

Treated Effluent

Return Activated Sludge
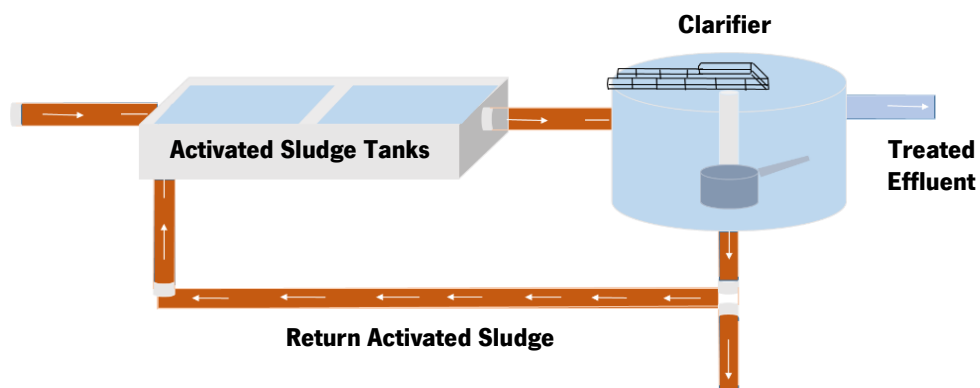
Figure 2.1 – Conventional activated sludge process.

The AS process was developed around 1913 at the Lawrence Experiment Station in Massachusetts by Clark and Gage, and by Ardern and Lockett (1914) at the Manchester Sewage Works in Machester, England. AS process used today may incorporate nitrification, biological nitrogen removal, and/or biological phosphorus removal. These designs employ reactors in series, operated under aerobic, anoxic, and anaerobic conditions.

In the aeration tank, the contact time is the time in which occur the mixture of the influent wastewater and suspended biomass, generally referred to as mixed liquor suspended solids (MLSS) or mixed liquor volatile suspended solids (MLVSS) mixture.

To maintain high levels of treatment performance with AS process under a wide range of operating conditions, special attention must be given to process control. The principal approaches to process control are: (i) maintaining dissolved O_2 levels in aeration tanks, (ii) regulating the amount of return AS, and (iii) controlling the waste AS. The sludge retention time (SRT) is the parameter commonly used for controlling the AS process. Return and waste flow of AS is important in maintaining the MLSS concentration and controlling the sludge blanket level in the secondary clarifier. Oxygen uptake rates (OURs) are also measured as a means of monitoring and controlling the AS process. Routine microscopic observations are important in monitoring the microbial characteristics and for early detection of changes that might negatively impact sludge settling and process performance. Routine

microscope observations provide valuable information about the condition of the microbial population in the AS process. Specific information includes changes in floc size and density, the status of filamentous organisms growth in the floc, foam/scum formation caused by nocardioforms and *Microthrix parvicella*, and the type and abundance of higher life-forms such as protozoa and rotifers. Changes in these characteristics can provide an indication of variations in wastewater characteristics or an operational problem. Early detection of filament growth allows time for corrective measures, minimizing potential problems associated with excessive growth of these organisms.

The most operational problems encountered in the AS process are bulking sludge, rising sludge, and *Nocardia* foam (Jenkins *et al.*, 2003). In filamentous bulking, biomass presents poor settling characteristics due to inadequate AS floc structure (Mesquita *et al.*, 2011) like excess of protrunding filaments bacteria or growth of free filamentous bacteria, creating a bridge between the flocs or developing diffuse flocs, that in the clarifier interfere with compaction, settling and thickening, causing higher effluent suspended solids, and decreasing the treatment performance. Filamentous-growing bacteria form filaments of single-cell organisms that attach end-to-end, and filaments typically extend outside the AS floc. This structure has a higher surface area to mass ratio than the preferred dense floc with strong settling properties, which leads to poor settling. Figure 2.2, present flocs containing good settling properties and non filamentous bacteria (Figure 2.2a) as well as a floc containing protruding filaments growth (Figure 2.2b). Other common type of AS bulking problem is caused by the production or release of EPS by bacteria, given a sludge with slimy, a jellylike consistency known as viscous bulking (Jenkins *et al.*, 2003). Viscous bulking is usually related with nutrient-limited systems or in a very high organic loading condition. Also, this type of bulking could be related to the presence of toxic compounds in the wastewater inflow (Zhang *et al.*, 2019).

Different methods have been developed for the diagnosis and resolution of AS solids separation problems. Microscopic evaluation of AS floc characteristics, filaments content, and floc and filamentous organisms types provide useful information regarding AS structure (Jenkins *et al.*, 2003). The classification system of AS is based on morphology (floc size and shape) and filaments length and identification. Earlier methods used to counting filamentous length (i.e. total extended filament length and filament count) have the disadvantage of being dependent on the technician's skill. Currently, describing the AS floc structure using microscopic inspection in conjunction with QIA techniques has proven to be quite helpful (Amaral and Ferreira, 2005; Campbell *et al.*, 2019).
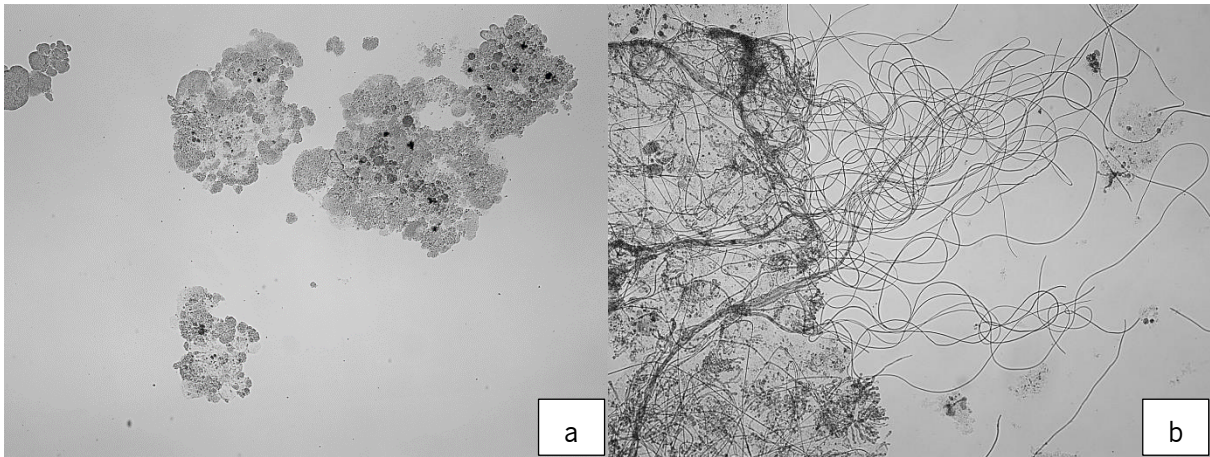
Figure 2.2 – Microscopy images of aggregates (a) with good settling properties, and (b) with overgrowth of filamentous bacteria and low settling ability (images obtained during this work).

2.1.2 Sequencing Batch Reactor (SBR)

The SBR, is a time-oriented system, with flow, energy input, and tank volume varying according to some predetermined periodic operating strategy. The SBR process utilizes a fill-and-draw strategy with complete mixing during the batch reaction step, and after desired reaction time, the mixed liquor is allowed to settle and the clarified supernatant is drawn from the tank (Irvine *et al.*, 1989).

The essential difference between the SBR and a conventional AS system is that each SBR tank carries out functions such as equalization, aeration, and sedimentation in a time rather than in a space sequence. One advantage of the time orientation used in the SBR is flexibility of operation. The SBR can be operated either as a labor-intensive, low-energy, high-sludge yield system or a minimal-labor, high-energy, low-sludge yield system for essentially the same physical plant (Irvine *et al.*, 1989). The actual operating policy can be adjusted in accordance with prevailing economic conditions by simply modifying the settings of the control mechanism.

All SBR systems have five steps in common, which are carried out in sequence as follows: (1) fill, (2) react (aeration phase), (3) settle (biomass sedimentation), (4) draw (decant), and (5) idle. All these steps are presented with more detail in Table 2.1 and Figure 2.3. Technology development allowed to improve the control of SBR systems and modifications during some phases of SBR operation have been made to remove nitrogen and phosphorus (Gerardi, 2010).

Table 2.1 – Description of the five phases of an SBR (Adapted from Al-Rekabi *et al.* (2006) and Metcalf and Eddy (2003)).

Operational steps	Description
Fill	The influent to the tank may be either raw wastewater (screened and degritted) or primary effluent and may be either pumped in or allowed to flow in by gravity. During the fill step, the influent wastewater is added to the biomass (i.e., mixed-liquor suspended solids) which remained in the tank from the previous cycle. The liquid volume increases from the initial level to the maximum of 100%. The initial volume is determined based on a number of factors including desired loading and hydraulic retention time and expected settling characteristics of the organisms. The aeration system must be able to provide a range of mixing intensities, from zero to complete agitation, and the flexibility of mixing without aeration to achieve low dissolved oxygen (DO) concentration. In this way, the aeration system will provide various aeration/mixing strategies, including static, mixed and aerated fill.
React	During the reaction period, the biomass consumes the substrate under controlled environmental conditions. Reactions which were initiated during the filling phase are completed during this step, regardles of mixing intensities. Also during this phase, sludge wasting can take place as a simple means for controlling the sludge age.
Settle	Solids separation takes place quiescently (i.e., without inflow or outflow). The time in settling phase typically ranges between 0.5 and 1.5 h. This insures that the sludge blanket remains below the withdrawal mechanism during draw phase and does not rise (because of gas formation) before draw is completed.
Draw	The withdrawal mechanism may take one of several forms, with the most popular being floating or adjustable weirs. It may be as simple as a pipe fixed at some predetermined level with the flow regulated by an automatic valve or a pump, depending on the hydraulic grade line of the system. In any case, the withdrawal mechanism should be designed and operated in a manner that prevents floating matter from being discharged. The time dedicated to draw can range from 5 to more than 30% of the total cycle time. The time in draw, however, should not be overly extended because of possible problems with rising sludge.
Idle	The period between draw and fill is termed idle. An idle period is used in a multitank system to provide time for one reactor to complete its fill phase before switching to another unit. Because idle is not a necessary phase as it is sometimes omitted.
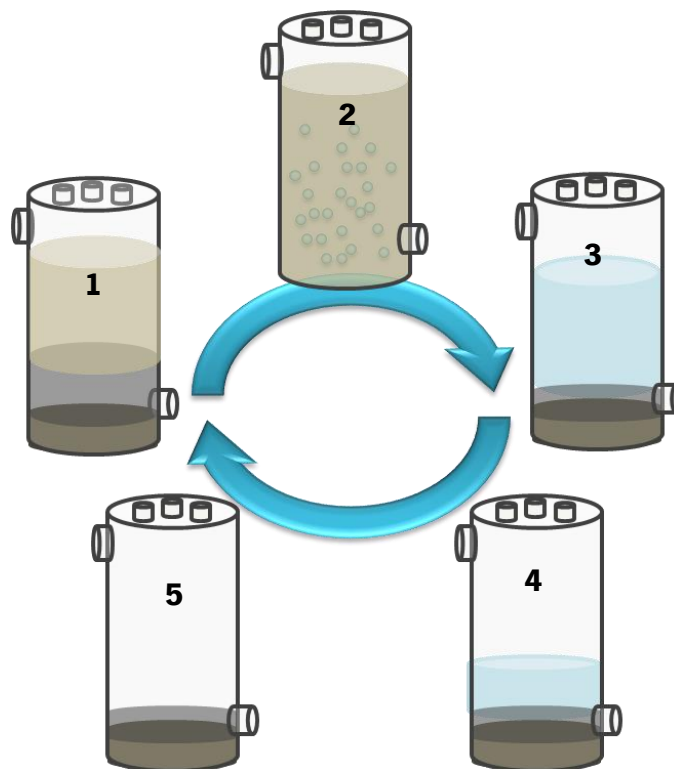
Figure 2.3 – The phases of SBR cycle consist of (1) fill, (2) react, (3) settle, (4) decant , and (5) idle.

2.2   Ocurrence of micropollutants in the environment

Micropollutants comprise a vast and expanding list of emerging contaminants, including pharmaceuticals, pesticides, personal care products, steroid hormones, industrial chemicals, and others. Although anthropogenic activity has led to an increase in the concentration of micropollutants, these compounds have been detected in various aquatic environments at trace concentrations, ranging from a few ng L^{-1} to high µg L^{-1} (Chaturvedi *et al.*, 2021; Kim *et al.*, 2007; Ryu *et al.*, 2014). The low concentration and diversity of micropollutants make the associated detection and analysis procedures difficult and create challenges for WWT processes (Luo *et al.*, 2014).

Regarding pharmaceuticals, the presence of these compounds in the environment has become a growing concern worldwide. For example, the presence of pharmaceutical compounds in the environment was highlighted in the United States (US) and England (UK) in the 1970s. Nevertheless, advances in analytical techniques in the mid-90s made meaningful progress in the knowledge of environmental contamination by those compounds, thus involving the scientific community to assess possible risks to humans and ecology (Santos *et al.*, 2010).

Albeit these compounds are present at low concentrations (mainly ng L^{-1} and µg L^{-1}) in aquatic environments, these substances are capable of triggering extremely harmful effects in the systems in

which they can be found (Joss *et al.*, 2006; Sacher *et al.*, 2001; Santos *et al.*, 2010). Furthermore, the metabolites and biotic and abiotic transformation products of parent pharmaceuticals can remain pharmacologically active in the aquatic environments (López-Serna *et al.*, 2013).

The use of pharmaceuticals by modern society is huge and steadily increasing. The intensive use of pharmaceutical compounds has been accelerated to treat common diseases, cancer treatment, open-heart surgery, and organ transplants (Hutchings *et al.*, 2019). Consequently, pharmaceuticals are continuously delivered to the environment, usually been detected in lake (ibuprofen, 0.58 ng L^{-1}) (Tran *et al.*, 2014), rivers (iopromide, 134 ng L^{-1}) (Kim *et al.*, 2007), groundwater (ibuprofen, 0.99 µg L^{-1}) (López-Serna *et al.*, 2013), hospital and pharmaceuticals effluents facilities (ciprofloxacin, 14 mg L^{-1}) (Fick *et al.*, 2009).

Figure 2.4 shows the main routes to the destination of pharmaceuticals in the environment. An important emission source of pharmaceuticals in the water cycle is via human metabolism; in fact, once administered, these compounds are only partially metabolized by the human body and therefore enter the water cycle either as parent (unchanged) compounds, which are mainly excreted through urine (generally 55–80% of the total, with few exceptions) and partially in the faeces, or as a mixture of metabolites and/or conjugated compounds (Al Aukidy *et al.*, 2012; Lienert *et al.*, 2007). Pharmaceuticals used in veterinary medicine are also excreted in urine and faeces by animals before being spread on land through manure application as green fertilizers. However, sources of contribution may be household disposal of unused and out-of-date pharmaceuticals discarded down the sink/flush toilet, waste collection or improper waste disposal (Patel *et al.*, 2019). Moreover, in some circumstances, the removal of micropollutants in WWTP is not complete. Accordingly, the entry of contaminants throughout poorly purified effluents into water bodies is a considerable concern (Campo *et al.*, 2013). Also, WWTP installed at pharmaceutical facilities contribute to the release of these substances into water bodies. In fact, concentrations higher than usually found in the environment (31 mg L^{-1} of antibiotic ciprofloxacin) were observed in a WWTP that receives wastewater from drug manufacturing companies (Larsson *et al.*, 2007). Furthermore, in developing countries with poor sewage treatment infrastructure, raw sewage is discharged directly into watercourses as a release route for these compounds (Patel *et al.*, 2019).
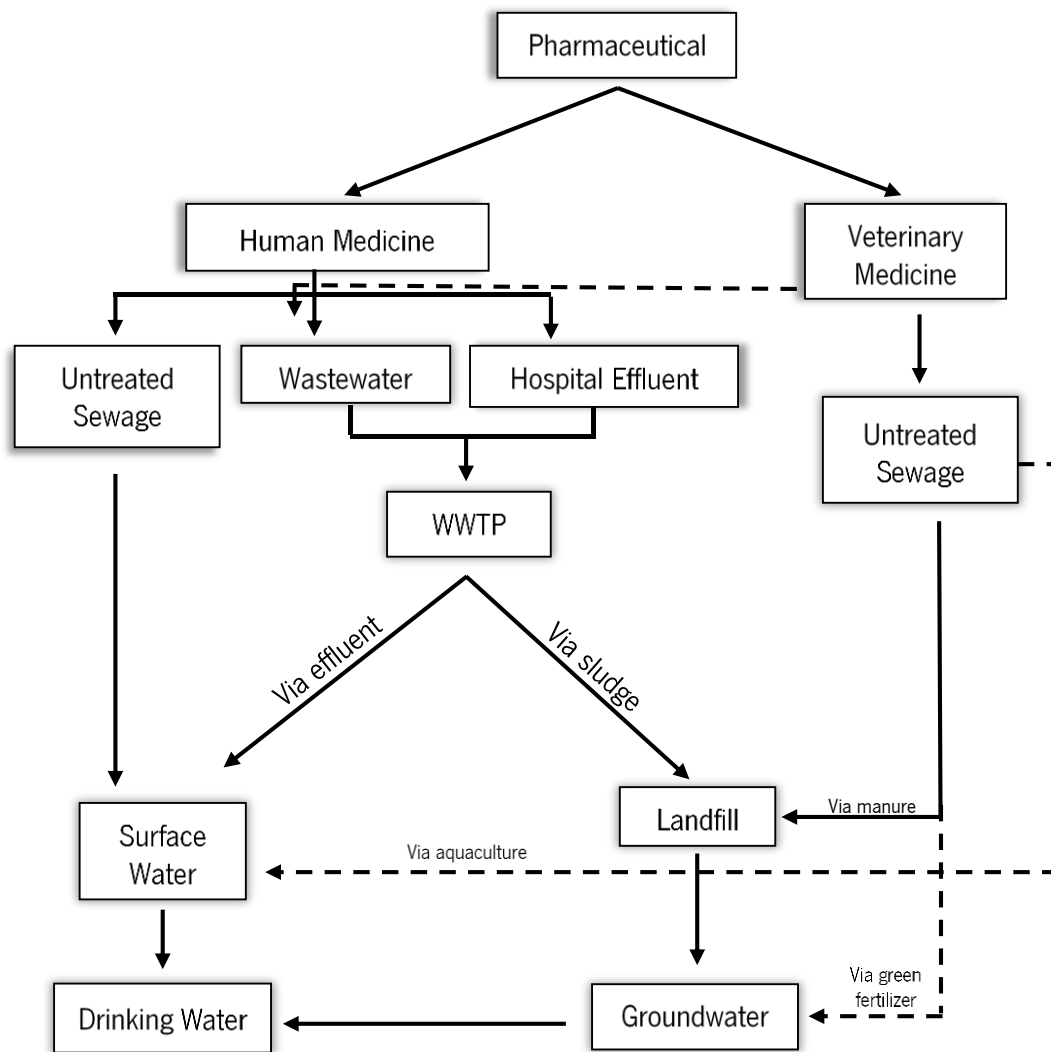
Figure 2.4 – Representative sources and fate of pharmaceuticals in the environment (adapted from Santos *et al.* (2010)).

In addition to the risk of direct soil contamination due to the reuse of effluent or sludge used as green fertiliser on agricultural land, there is also the risk of runoff with heavy rainfall, which may contaminate both the nearby surface and groundwater. Aquaculture is another example of anthropogenic activity, with the usage of pharmaceutical products, and discharge of metabolites and degradation products into surface waters (Santos *et al.*, 2010).

Pesticides are another important class of micropollutants that can potentially reach water bodies. They include various chemicals, which are increasingly being used worldwide. The European Union (EU) Pesticides Database lists more than 1378 active ingredients, 466 of which have been approved, and 858 have not been approved for use in the EU (Kalyabina *et al.*, 2021). Pesticides are consumed mainly in developed countries; the US, North-Western Europe and Japan use most pesticides employed worldwide (Alavanja, 2009). Every year about 2.36 million tons of chemical pesticides are being used

all over the world, of which 24% are used in the US and 45% in Europe (Rani *et al.*, 2021). Continuously pesticides including alachlor, acetochlor, simazine, metolachlor and atrazine were identified in waterways of cornbelt in the US, and in California, rivers were contaminated with prometon, diuron, chlorpyrifos, diazinon and 2,4-dichlorophenoxyacetic acid (Rani *et al.*, 2021). Pesticides include a wide range of herbicides, insecticides, fungicides, rodenticides, nematicides, etc., that are applied to control or kill the harsh pests like creatures, organisms causing plant diseases and weeds (Sharma *et al.*, 2019). Due to their propensity for toxicity, these compounds can bioaccumulate and have an impact on non-target organisms, especially in aquatic environments including diatom populations, aquatic invertebrate communities, among others (Chará-Serna *et al.*, 2019; Guasch *et al.*, 1997; Ricart *et al.*, 2010). These compounds are listed as priority substances by the Water Framework Directive in the EU due to their hazardous characteristics ("Directive 2000/60/EC of the European Parliament and of the Council of 23 October 2000 establishing a framework for Community action in the field of water policy (OJ L 327, 22.12.2000, p. 1), 2000.," 2000). In addition, pesticides can be broadly categorized based on applications, target organism and chemical nature. Regarding chemical nature, pesticides can be categorized as organochlorines, organophosphates, carbamates, pyrethroids, phenyl amides (carbanilates, acylanalides, toluidines and acetamides), phenoxyalkonates, trazines, benzoic acid derivatives, benzonitriles, phtalimide derivatives, dipyrids and miscellaneous category (Jayaraj *et al.*, 2016; Rani *et al.*, 2021). Among pesticides, herbicides are chemical agents used to suppress or eradicate weeds. There are approximately 150 herbicide-active ingredients; most are organic compounds containing carbon, hydrogen, oxygen, and other chemical elements, which are formulated into hundreds of commercial products (Holt, 2013). Herbicides must last long enough to kill the weeds they were designed to control in order to be successful. Persistence beyond that time, may result in injury to non-target plants and other organisms, residues in crops, and environmental contamination (Holt, 2013). As a result, persistent herbicides could pollute soil, water, grass as well as other flora. Furthermore, herbicides could be poisonous to other creatures such as frogs (Hayes *et al.*, 2010), fish (Santos and Martinez, 2012; Wang *et al.*, 2013), and insects (Oluah *et al.*, 2010).

2.2.1 Ibuprofen

Ibuprofen (IBU) is a non-steroidal anti-inflammatory drug used to reduce fever and treat pain or inflammation caused by many conditions, such as headache, toothache, back pain, arthritis, menstrual cramps or minor injury. IBU and/or its metabolites have been detected in aquatic ecosystems (Ashton

et al., 2004; Loos *et al.*, 2007; Ternes, 1998), sewage (Lee *et al.*, 2005; Quintana *et al.*, 2005; Verenitch *et al.*, 2006), and drinking water (Loraine and Pettigrove, 2006).

WWTP can act as entrance routes for IBU into the aquatic environment resulting from different sources, including pharmaceutical industries, hospital activities, and human excretion (up to 70%) (Buser *et al.*, 1999). IBU has been measured in raw wastewater from different sources in concentrations ranging from 200 ng L^{-1} to >370 μg L^{-1} (Santos *et al.*, 2007, 2013). In conventional WWTP, IBU is not entirely removed with primary and secondary treatment (Ternes, 1998). Thus, IBU and other micropollutants have received wide attention in the scientific community since the presence of these compounds in the different environmental compartments (soil, water, etc.), even at low concentrations (from ng L^{-1} to mg L^{-1}), can cause harmful effects to the environment and human health (Kosonen and Kronberg, 2009; Rodriguez-Narvaez *et al.*, 2017; Verenitch *et al.*, 2006). Moreover, several reports indicate the toxicity of IBU in the aquatic environment. Studies have been carried out on acute effects in organisms belonging to different trophic levels (e.g., algae, zooplankton, other invertebrates and fish) (Ortiz de García *et al.*, 2014; Santos *et al.*, 2010). Studies have also examined the toxic effects of IBU on the microbial communities in wastewater treatment systems in terms of microbial activity (Amariei *et al.*, 2017) and treatment performance, primarily by observing the decline in the ability to remove organic matter (Falås *et al.*, 2016; Jia *et al.*, 2020) and nitrogen compounds (Pasquini *et al.*, 2013).

2.2.2 Desloratadine

Allergic disorders are increasingly prevalent in modern industrialized countries, affecting up to 30% of the population and causing major public health concerns worldwide (Zhang *et al.*, 2021). Antihistamines have become the largest class of pharmaceuticals employed to treat allergic diseases, with more than 45 antihistamines currently on the market, due to their widespread use and diverse applications (Simons and Simons, 2011). In most cases, antihistamines have seasonal uses indicating that their influent load varies throughout the year. In the UK, monthly prescription information showed that antihistamines used to treat allergies peaked from May to August, when pollen production is highest (Petrie *et al.*, 2015). In the Norwegian WWTP, quantities of antihistamine cetirizine grew considerably during the summer months, with very similar results to those registered in the Norwegian prescription database (Harman *et al.*, 2011). Antihistamines have been commonly detected in influent wastewater (Kasprzyk-Hordern *et al.*, 2009), effluent discharges from WWTP (Fick *et al.*, 2009), and

surface waters (Du *et al.*, 2016). About 15 antihistamines, including desloratadine (DESL), have been detected in watercourses in concentrations ranging from ng L^{-1} to µg L^{-1} (Kristofco and Brooks, 2017; Moreno-González *et al.*, 2015), being also detected in higher ranges (mg L^{-1}) (cetirizine and ranitidine) (Fick *et al.*, 2009; Larsson *et al.*, 2007). DESL is a second-generation anti-histaminic drug causing less sedation and drowsiness than the first-generation antihistamines used to treat allergic reactions (Iesce *et al.*, 2019). DESL is a pharmacologically active compound metabolized from loratadine through the hepatic system. It was reported that 40% and 42% of the ingested loratadine dose is excreted unchanged in the urine and the faeces, respectively (Ramanathan *et al.*, 2007). Nearly 20% of DESL was excreted in monkey urine, being the majority of the dose (>55%) excreted by faeces (Ramanathan *et al.*, 2005). In general, antihistamines are gaining increasing attention due to their fate in the aquatic environment and partial removal in WWTP (Chaturvedi *et al.*, 2021; Golovko *et al.*, 2014; Loraine and Pettigrove, 2006). Besides that, the toxic effects of loratadine and DESL were reported to affect the organisms selected from two trophic levels (Iesce *et al.*, 2019). The parent compound loratadine, its metabolite DESL, the transformation products and the degradation mixture of DESL caused mortality in both crustaceans and rotifers with the lethal concentration (LC50) values, obtained after 24 h exposure, reported as 0.60 mg L^{-1} of loratadine in the cladoceran crustacean *Ceriodaphnia dubia*, and 1.21 mg L^{-1} and 6.22 mg L^{-1} of DESL in the rotifer *Brachionus calyciflorus* and in the anostracan crustacean *Thamnocephalus platyurus*, respectively. Furthermore, loratadine was the most chronically active compound in the rotifer with the median inhibition concentration (EC50) of 51.32 mg L^{-1}, while its metabolite DESL was the most active in *Ceriodaphnia* dubia, with an EC50 of 9.39 µg L^{-1}, and in the green alga *Pseudokirchneriella subcapitata* (EC50 = 220.20 µg L^{-1}) (Iesce *et al.*, 2019). Despite the previously reported presence of DESL in wastewater, the effect of DESL on biological WWT systems, namely AS, has not yet been studied. Therefore, in addition to the knowledge gap concerning the impact of DESL on biological treatment systems, it is crucial to understand the performance of AS under DESL exposure.

2.2.3 Atrazine

Atrazine (2-chloro-4-ethylamino-6-isopropylamino-s-triazine) is a kind of pesticide that was initially registered as a herbicide in 1958 (Guo *et al.*, 2016). ATZ, a member of s-triazine, is one of the most commonly used herbicides in agricultural activity worldwide (Sharma *et al.*, 2019). From 1992 to 2011,

reported annual usages on crops were 32,000–36,000 tons in the US. According to the US Environmental Protection Agency (EPA), ATZ is considered an endocrine disruptor, and EU has banned their use because of ubiquitous and unpreventable water contamination (2004/248/EC), and was then included in the list of priority substances by the Water Framework Directive in EU (2000/60/EC). Owing to its massive use, environmental persistence and various toxic properties (Araújo *et al.*, 2021; Camenzuli *et al.*, 2016; Torquetti *et al.*, 2021), it has a very high environmental significance (Ricart *et al.*, 2010). ATZ may cause an adverse effect on human beings, interfering in the endocrine system and producing disorders in fertility due to the ability to influence hormone signalling, including estrogens, thyroid, and androgens which are an essential part of usual embryonic growth (Rani *et al.*, 2021). Furthermore, ATZ is related to cause gastroschisis in young mothers who live in a region where the level of this compound was present in surface water (Rani *et al.*, 2021; Waller *et al.*, 2010). As a consequence of excessive usage and mobility, ATZ can be found in WWT systems and natural aquatic environments (Luo *et al.*, 2014). Also, unsuitable discharges to the environment from factories where these compounds present concentration in mg L^{-1} is an important source of micropollutants to reach water bodies (Rott *et al.*, 2017). ATZ was the most herbicide found in: (i) St. Lawrence river and tributaries (Canada) in concentrations from 4 to 666 ng L^{-1} (Montiel-León *et al.*, 2019); (ii) Susquehanna river (US) in concentrations between 26 to 241 ng L^{-1} (Foster *et al.*, 2000); and (iii) the Haihe river near Beijing (China) in concentrations from 5 to 590 ng L^{-1} (Heeb *et al.*, 2012). In EU, even after 2003 when the use of ATZ was banned, concentrations from 1 to 46 ng L^{-1} in riverine surface waters (Loos *et al.*, 2009), from 0.4 to 19 ng L^{-1} in Alqueva reservoir (Portugal) (Palma *et al.*, 2014), from 4.26 to 8.22 ng L^{-1} in Volturno river (Italy) (Triassi *et al.*, 2022), were found.

Different methods to degrade ATZ have been investigated (Luo *et al.*, 2014) such as advanced oxidative process (AOP) (Klamerth *et al.*, 2010), membrane bioprocess (Sahar *et al.*, 2011; Tadkaew *et al.*, 2011), moving bed biofilm reactor (MBBR) (Derakhshan *et al.*, 2018b) and AS system (Mahlalela *et al.*, 2021). Furthermore, some researchers reported that combining different technologies, like biological + AOP, reached satisfactory results compared with just one technique to degrade ATZ (Mahlalela *et al.*, 2021). Extensive studies on ATZ biotransformation during the biological treatment stage revealed that ATZ was partially removed, since biological treatment was not originally designed to remove ATZ (Fischer and Majewsky, 2014; Rodriguez-Narvaez *et al.*, 2017). ATZ was persistent to biotransformation in AS nitrifying systems, with low removal efficiency (< 20%) obtained compared to

other micropollutants. Thus, more insights are needed regarding the effect of micropollutants, such as ATZ during biological WWT.

2.3 Extracellular polymeric substances (EPS)

2.3.1 EPS definition and composition

EPS are defined as "organic polymers (biopolymers) of microbial origin which in microbial aggregate systems are frequently responsible for binding cells and other particulate materials together (cohesion) and to the substratum (adhesion)" (Wingender *et al.*, 1999).

EPS comprises soluble EPS (i.e., slime) and bound EPS (Yu *et al.*, 2009, 2008). The soluble EPS can move freely between sludge flocs and the surrounding liquor (Tu *et al.*, 2012), and the bound EPS exhibit a dynamic double-layer-like structure, with a distinct margin outside the cell wall. Bound EPS can be, in turn, classified as loosely bound EPS (LB-EPS) and tightly bound EPS (TB-EPS) (Li and Yang, 2007). However, research focusing on individual EPS components properties and functions in WWT has just started (Lin *et al.*, 2018; Sheng *et al.*, 2013; Wang *et al.*, 2015). Bound EPS are intimately adhered to the cells due to the functional groups (carboxyl, phosphoric, sulfhydryl, phenolic and hydroxyl) and nonpolar groups (i.e., aromatic, aliphatic in proteins, and hydrophobic regions in carbohydrates and proteins). On the other hand, soluble EPS are poorly adhered to the cells or dissolved within the solution, which can be explained by the hydrophilic fractions mainly consisting of carbohydrates (Nouha *et al.*, 2016).

A significant variety of functions has been attributed to EPS, most of them related to the performance of biomass-water separation. EPS matrix presents a sorption function that influences the exchange of nutrients and other molecules between the environment and bioaggregates. Substances captured from the water phase are maintained trapped into the matrix for possible consumption by cells in the bioaggregates. The sorption by the EPS matrix is not specific, indicating that toxic substances may accumulate surrounding bioaggregates. For this reason, the functions of the EPS matrix include the formation of a protective layer of cells against the harmful external environment, when the biomass is exposed to substances such as pesticides, pharmaceutical compounds, and sudden changes of pH, taking up exogenous nutrients and organic molecules, and aggregating bacterial cells in flocs. Consequently, it has been established that EPS plays an essential role in the flocculation, settling and dewatering of bioaggregates (Sheng *et al.*, 2010). Researchers have found differences in the EPS composition. The concentrations of the compounds are presented in different ways, depending on the extraction method, the analysing method for each component, the kind of sludge under study, the type

of effluent, among other factors. EPS production and function has been studied for decades; however, earlier studies of EPS in wastewater demonstrate that the major constituents are PS and PN, both representing 60% of the total content and in smaller quantities are the HAS, uronic acid, lipids, and DNA (Frølund *et al.*, 1995; Frølund *et al.*, 1996; Wang *et al.*, 2013). EPS generally contains small amounts of DNA, which are released after cell lysis. Large amounts of DNA in the EPS may indicate that the cells suffered cell lysis during the rigorous extraction process (Liu and Fang, 2002). Moreover, amphiphilic compounds (phospholipids), glycosylated proteins (glycoproteins), and HAS also appear in significant amounts or even predominate in EPS preparations from AS, trickling filter biofilms and granular sludge (Boleij *et al.*, 2018; Liu *et al.*, 2021; Melo *et al.*, 2021; Oliveira *et al.*, 2020). Additionally, HAS are constituted of complex heterogeneous mixtures of organic compounds, such as poly-aliphatic and poly-aromatic compounds, containing carboxylic, phenolic and hydroxyl groups, which give a highly negative charge. Thus, unlike many other natural organic products, they cannot be considered in terms of unique chemical structures (Filella *et al.*, 2005).

2.3.2 *Factors that influence EPS production*

Substrate

Some researchers have found different amounts of EPS produced when different types of substrates are used. On the one hand, LB-EPS contents increased slightly when the system was fed with starch and glucose. On the other hand, LB-EPS contents increased considerably when the system was fed with sodium acetate. Nevertheless, the substrate change caused an initial decrease in TB-EPS content from 54 to 45 mg TOC g^{-1} SS, increasing gradually and remaining relatively stable thereafter (Ye *et al.*, 2011). It has been observed that the production of EPS is related to the type and amount of the carbon source. Many types of carbohydrates are used as carbon sources, such as glucose, sodium acetate, peptone, and starch, but research shows that glucose, when used by bacteria, favours the production of EPS (Czaczyk and Myszka, 2007; Lee *et al.*, 1999; Miqueleto *et al.*, 2010). However, some contradictory results can be found in the literature. Wang *et al.* (2014) compared EPS production using starch and glucose as carbon sources and obtained higher productivity with starch. Geyik *et al.* (2016) assessed three different substrates (solely glucose; acetate + glucose + peptone; and solely peptone) in three parallel reactors. Albeit the carbon source affected EPS production, PN were the main component of EPS even when PN were absent in the medium. Furthermore, the variety and size of PN were clearly different when fed with PN. Moreover, in the absence of PN in the medium, as in the

experiment with glucose, it was assumed that the biomass used the PN found in different fractions of bound EPS. It was observed that, in the absence of an organic substrate, the microorganisms used their EPS as substrate for cell maintenance. In addition, this condition or ability can facilitate the adaptation of microorganisms in environments with nutritional limitations. It was also observed that the PS were consumed before the PN, indicating that under food shortage, the microorganisms degrade the sugars first (Zhang and Bishop, 2003).

Cell growth, pH, and temperature

The correlation between cell growth and EPS secretion has been reported in many studies. Differences in EPS composition were found at the molecular level observed between exponential and stationary growth phases (Badireddy *et al.*, 2010). The time of biomass cultivation may influence the amounts of EPS produced depending on the operational and environmental conditions. Under anaerobic conditions, longer bacteria culture time caused lower EPS production, and consequently, EPS production is commonly related to the stationary growth phase of bacteria (Sheng *et al.*, 2006). Under aerobic conditions, in AS and biofilms, the cell retention time caused a significant increase in EPS production (Miao *et al.*, 2017; Nielsen *et al.*, 1996; Sesay *et al.*, 2006). However, in other studies, the cell retention time did not correlate with EPS production (Liao *et al.*, 2001; Wang *et al.*, 2013).

Many studies, especially on lab-scale, have evaluated the effect of pH on EPS production. In general, the ideal pH value for EPS production is between 5.0 and 7.0 (Shu and Lung, 2004). In addition, extreme pH values (e.g. 2–3 and greater than 10) in the growth medium may inhibit EPS biosynthesis, affecting bacterial growth, causing morphological changes in aggregates, and influencing the molecular mass of EPS compounds (Chen *et al.*, 2001; Shu and Lung, 2004; Czaczyk and Myszka, 2007). However, most EPS-producing microorganisms require a constant pH value in the growth medium to achieve maximum EPS production (More *et al.*, 2014).

Temperature is one of the most important parameters that influence EPS production, affecting the microbial population and the enzymatic activity in the biological process (Li *et al.*, 2015; Wingender *et al.*, 1999). Most of the EPS-producing microorganisms show maximum performance when the temperature is in the range of 25 to 31 °C. It was previously found that the EPS biosynthesis process was inhibited when the temperature was reduced by 10 °C from the ideal temperature (Czaczyk and Myszka, 2007; More *et al.*, 2014; Sutherland, 2001).

2.3.3 The role of EPS on bioflocculation and settling ability

Bioflocculation

Several interactions and mechanisms are involved in the bioflocculation process, including electrostatic forces, hydrophobic interactions, and bridges of multivalent cations such as Ca^{2+}, Mg^{2+}, and Fe^{2+} (Liu and Fang, 2003; Sobeck and Higgins, 2002). In turn, the divalent cation bridge theory states that Ca and Mg are important for the bioflocculation process. In theory, divalent cations negatively carry functional groups within EPS, and this bridge helps to aggregate and stabilize the matrix of biopolymers and microorganisms, promoting bioflocculation. The biomass flocculation process allows an effective separation of the solid-liquid in sedimentation tanks (continuous flow) or sedimentation phase (SBR process), which is decisive for the performance of an AS process and is a crucial factor for low turbidity and high effluent quality (Sheng *et al.*, 2010). According to Bala Subramanian *et al.* (2010), EPS produced by microorganisms plays an essential role in bioflocculation, being the main constituent of microbial flocs (Frølund *et al.*, 1996) acting as a kind of glue that holds the cells together (Li and Yang, 2007). Furthermore, microscopic observations showed that microbial cells within the flocs were cross-linked with EPS, forming a polymer network with pores and channels (Liu and Fang, 2003). However, high EPS concentrations can adversely affect compaction, bioflocculation, and sedimentation due to strong electrostatic repulsion between the negatively charged components of the flocs as described in the DLVO theory (Derjaguin and Landau, Verwey and Overbeek) (Wilén *et al.*, 2008). Thus, many studies have stated that increasing EPS concentration appears to have a negative effect on bioflocculation properties (Wilén *et al.*, 2008). Nevertheless, recent studies suggest a significant role of specific EPS molecules rather than the quantity of EPS in determining the difference in sludge bioflocculation behavior (Liao *et al.*, 2011). In terms of EPS components, PS are recognised as key elements involved in the sludge floccular and granular matrix structure, providing structural support for microbial aggregates (Lin *et al.*, 2013). Adav and Lee (2008) revealed that hydrolysis of β-PS caused granules disintegration, whereas the use of specific enzymes to remove PN, lipids, and α-PS had minimal impacts on the structural stability of the granules. For these authors, the granule structure is viewed as a network with β-PS as the backbone for PN, lipids, α-PS, and cells that support the structural integrity of granules. Furthermore, the decrease in the PS content hindered the attachment of the bacteria to the filamentous skeleton and suppressed the formation of stable sludge flocs during filamentous bulking (Shen *et al.*, 2020). PN in the EPS contains many hydrophobic amino acids, such as alanine, and is therefore considered the hydrophobic component in the EPS (Shen *et al.*, 2020). According to Higgins and Novak (1997), the removal of surface PN was most significant than PS in the

deffloculation of microbial aggregates, affecting the flocculation capacity of AS (Wilén *et al.*, 2003). Large amounts of EPS, mainly in the form of LB-EPS, caused a deterioration in cell adhesion and weakened the aggregate structure, resulting in the erosion of the slime flocs cells, for instance, by the medium's turbulence (Li and Yang, 2007). On the other hand, the decrease in the EPS content led to a decrease in the microbial adhesion ability during sludge bulking, which was unfavourable to bacterial cell aggregation (Shen *et al.*, 2020). According to the literature's findings, the relationship between the quantity of an EPS component and bioflocculation is not as simple as it might seem, and individual EPS components play a complex function in the flocculation of microbial aggregates.

Settling ability

So far, there is a non-consensus regarding the effect of EPS on the settling ability of AS. However, many studies have shown that variations in sludge volume index (SVI) are related to variations in EPS concentration due to changes in surface properties of AS flocs. Table 2.2 summarises the main studies presenting a relationship between SVI and EPS. As EPS are negatively charged, a high EPS concentration increases the surface charge of the microorganisms, increasing the repulsive forces between cells and thus contributing to the decrease in the strength of microbial aggregates (Sheng *et al.*, 2010). In this sense, some researchers have demonstrated a positive correlation between the SVI and EPS concentration or EPS components concentration (Table 2.2). According to Liao *et al.* (2001), a higher SVI was associated with a greater amount of total EPS. Li and Yang (2007) concluded that the presence of LB-EPS had a detrimental impact on bioflocculation, settling ability, and dewatering. In accordance, Yang and Li (2009) found that excessive EPS in the form of LB-EPS deteriorated the structure of the flocs, leading to increased cell erosion and poor settling ability. The authors also found a positive correlation between soluble EPS and deterioration of settling ability. Li *et al.* (2011) observed that the SVI increased linearly with EPS content in the sludge. On the other hand, many studies demonstrated the SVI decreased as LB-EPS, TB-EPS, or total EPS increased. For instance, Shen *et al.* (2020) found that total EPS production decreased with a bulking phenomenon. Furthermore, the research work of Melo *et al.* (2021) revealed that, despite the poor floc structure, the rising in EPS content, especially TB-EPS, was the critical point to achieve an AS with good settling properties. In turn, PN and DNA contents in EPS seems to have more significant effects on the settling ability of microbial aggregates, presenting a positive relationship with SVI, not being possible to establish a relationship between PS and SVI (Sheng *et al.*, 2010).

The EPS production or EPS variation in biological WWT, can be affected by many factors, such as, operational conditions (i.e., sludge retention time – SRT) (Liao *et al.*, 2001), type of substrate or organic loading (Geyik *et al.*, 2016), reactor configuration (anoxic, aerobic) (Martinez *et al.*, 2000), temperature (Liao *et al.*, 2011), toxic substances (Zhang *et al.*, 2019), proteins to polysaccharides (PN/PS) ratio. The change in the environment of the microbial aggregates can induce a production of some kind of EPS component, disturbing somehow the forces that govern the interactions between particles and microorganisms, driving the system to a non-steady-state condition. Liao *et al.* (2001), for instance, evaluated the impact of SRT on EPS and found that the most noticeable effect was a change in the proportion of components rather than the total content of EPS. As a consequence, the SVI results were impacted by the change in the EPS. Zhang *et al.* (2019) observed for 200 days AS and sulfate-reducing bacteria (SRB) systems operated under ciprofloxacin (CIP) exposure. CIP induced changes the microbial communities in AS and SRB sludge, and significantly inhibited the family *Nitrosomonadaceae* (ammonia-oxidizing bacteria) and genus *Nitrospira* (nitrite-oxidizing bacteria/complete ammonia oxidizer (comammox)) and the nitrogen removal in AS system. The increase of genera *Zoogloea*, *Acinetobacter* and *Flavobacterium* in AS, and *Zoogloea* and *Acinetobacter* in SRB sludge under CIP exposure promoted EPS production and CIP adsorption for self-protection of biomass against CIP toxicity. Moreover, the increase of genus *Zoogloea-like* organisms favored the production of viscous EPS, increasing the PS EPS content and, hence, significantly reducing the PN/PS ratio. This overproduction of viscous EPS leads to the formation of non-filamentous bulking, with SVI values of 313 ± 12 mL g^{-1} for an influent containing CIP = 5000 μg L^{-1}. Thus, the effect of EPS components on the settling ability of microbial aggregates is still not well understood, and further research is needed.

Table 2.2 – Effect of EPS components on the settling ability of microbial aggregates: the relationship between EPS and SVI.

Relationship	SVI (mL g^{-1})	EPS concentration	EPS units	Reference
Positive Rp = 0.78, p<0.05	≈9.0 to 15	≈5 to 50	PN EPS (mg L^{-1})	(Martinez *et al.*, 2000)
Positive Rp = 0.64, p<0.05	≈40 to 200	≈8 to 30	Total EPS (mg g^{-1}g VSS)	(Liao *et al.*, 2001)
Positive Rp = 0.75, p<0.05	40 to 260	52 to 119	Total EPS (mg g^{-1} MLSS)	(Jin *et al.*, 2003)
Positive Rs = 0.89, p<0.05	≈30 to 50	3.5 to 9.0	LB-EPS (mg TOC g^{-1} SS)	(Li and Yang, 2007)

Positive Rp = 0.57, p<0.002	≈40 to 160	≈110 to 190	HAS EPS (mg g^{-1} VSS)	(Wilén *et al.*, 2008)
Positive Rs = 0.36, p < 0.05	45 to 120 90 to 180	5.2 to 7.1 1.4 to 4.6	LB-EPS (mg TOC g^{-1} SS)	(Yang and Li, 2009)
Positive Without coefficient correlation	≈250 to >1000	115 to 522	Total EPS (mg g^{-1} VSS)	(Li *et al.*, 2011)
Positive Without coefficient correlation	270 (on average)	32 (on average)	TB-EPS (mg g^{-1} MLSS)	(Liao *et al.*, 2011)
Positive correlation Rp = 0.73, p<0.05	≈80 to 460	≈18 to 45	PN LB-EPS (mg g^{-1} SS)	(Ye *et al.*, 2011b)
Positive correlation Rp = 0.37, p<0.05	≈80 to 120	5 to 13	PN LB-EPS (mg g^{-1} SS)	(Ye *et al.*, 2011a)
Linear positive relationship	≈62 to 92	≈60 to 310 ≈50 to 230 ≈10 to 70	Total EPS (mg g^{-1} MLVSS) TB-EPS (mg g^{-1} MLVSS) LB-EPS (mg g^{-1} MLVSS)	(Yu *et al.*, 2019)
Negative Without coefficient correlation	578 to 126	≈5 to ≈130	LB-EPS (mg g^{-1} VSS)	(Li *et al.*, 2011)
Linear positive relationship R^2 = 0.87 R^2 = 0.95	78 to 105 87 to 125	7.5 to 25 6.3 to 10.2	LB-EPS (mg g^{-1} MLSS) PS LB-EPS (mg g^{-1} MLSS)	(Gao *et al.*, 2019)
Negative relationship Without coefficient correlation	222 to 74	84 to 104	Total EPS (mg g^{-1} MLSS)	(Yao *et al.*, 2019)
Negative correlation Rp = -0.9, p<0.05	97 to 667	71 to 40	Total EPS (mg g^{-1}g VSS)	(Shen *et al.*, 2020)

Rp – Pearson coefficient; Rs – Spearman coefficient; R^2 – correlation coefficient.

2.3.4 Relationship between EPS and sludge morphology

Quantitative differences were observed in the composition of EPS in flocs of different sizes. The relationship between floc structure and EPS quantity or EPS type needs to be further explored. The increase in EPS content, changes in the EPS components (PS, PN, HAS), and variation on PN/PS ratio have been reported in the literature (Basuvaraj *et al.*, 2015; Liu *et al.*, 2021; Xu *et al.*, 2021). The increase in EPS content and EPS components during the granulation process indicated that EPS have a vital role in this process (Xu *et al.*, 2021), while insufficient EPS and unbalanced PN/PS compromised

the aerobic granules stability (He *et al.*, 2019). A sharply increase in EPS occurred during the transition from flocs to granules, where EPS remained at high levels during this period. Then EPS followed a decreasing trend during the granules maturation, where EPS established in a lower level (Xu *et al.*, 2021). This behavior that EPS raised remarkably during the granulation process, dropping slightly when granules maturated, was corroborated by McSwain *et al.* (2005) and Adav and Lee (2008). Liu *et al.* (2021) observed that when the aggregate size increased, the EPS content also increased. A comparison between a full-scale system and a lab-scale system has been conducted by Basuvaraj *et al.* (2015) with different aggregate sizes. The authors revealed that in full-scale with predominantly small flocs (diameter < 50 μm), a higher LB-EPS concentration was obtained. In contrast, a higher TB-EPS concentration was reached in lab-scale with predominantly large flocs (diameter > 340 μm). Ye *et al.* (2011a, 2011b) obtained a negative relationship between the LB-EPS and floc size. However, only a weak negative correlation between PN content in LB-EPS and floc size was found.

Beyond the quantities, the distribution of EPS components on flocs plays a significant role in increasing the stability of aggregates. PN EPS has been identified in the core of granules contributing to stability due to increased hydrophobicity and the negative surface charge, promoting cell-to-cell interaction. The outer layer of the aggregates that contain the other EPS components appears to include PS EPS (Basuvaraj *et al.*, 2015; McSwain *et al.*, 2005). Additionally, the granular structure seems to contain a higher portion of PN (PN/PS ratio of 1.4 - 1.6) in its total EPS fraction, whereas higher quantities of PS (PN/PS ratio of 0.5) are present in flocs (Basuvaraj *et al.*, 2015). During the granulation process, the abundance of β-sheets PS secondary structure was extremely coincident with the changes of aggregates size, showing that β-sheets reduced to 20% at the same time that aggregates size decreased (Shi and Liu, 2021). PN EPS content in anammox sludge and large granules was prominently higher than that of small granules and floc sludge, indicating that the concentration of PN EPS increased with increasing aggregates' size (Liu *et al.*, 2021). These results suggest a trend regarding the aggregate size and EPS quantity, following the same order of aggregate sizes (large granules > small granules > flocs).

2.3.5 Role of EPS in removal of micropollutants

EPS might play an important role in the transport and transformation of micropollutants due to abundant functional groups (e.g. hydroxyl, carboxyl, sulfhydryl, phosphate amine groups), therefore interactions between EPS and micropollutants also affect their removal efficiencies (Ahmed *et al.*, 2017; Torresi *et al.*, 2017; Wang *et al.*, 2018). Since EPS can play a crucial role in the adsorption process, a

relevant mechanism for the removal of micropollutants from wastewater, the roles of EPS in biological WWT during the removal of micropollutants has drawn particular attention from researchers over the last two decades (Wang *et al.*, 2018; Yang *et al.*, 2012). Many studies have demonstrated that in the presence of toxic substances, such as pharmaceutical compounds and herbicides, EPS form a protective layer for cells against the adverse external environment (Bitton, 2005; More *et al.*, 2014; Song *et al.*, 2014). Thus, complexes might be formed between EPS and micropollutants through hydrophobic interaction, hydrogen bond or electrostatic interaction, which significantly affects the removal and migration of these micropollutants in biological WWT (Song *et al.*, 2014; Xu *et al.*, 2013). However, there is still a knowledge gap about the structural interactions between EPS and these compounds in biological WWT systems. Some researchers have indicated that under toxic conditions (i.e. increase of toxic substances concentration), the PN EPS far exceeds those systems in normal conditions (Table 2.3) (Li *et al.*, 2015; More *et al.*, 2014) and is the main EPS component that interacts with antibiotics (sulfamethizole), anti-epileptic drugs (carbamazepine), and anti-inflammatory compounds (ibuprofen, naproxen, diclofenac) (Li *et al.*, 2015; Wang *et al.*, 2018). Barret *et al.* (2010) determined through PLS regression a correlation between micropollutants and sludge chemical predictors (PN EPS). It was showed by equilibrium constants $K_{particles}$ and $K_{dissolved\ matter}$ results that PN had a strong influence on micropollutant sorption in sludge. Correlation between $K_{organic\ matter}$ and EPS was also found by Khunjar and Love (2011). Regarding the variation in EPS concentration, it was pointed out that it increased after dosing as a mixture of four pharmaceutical compounds (carbamazepine, diclofenac, ibuprofen and naproxen) (Lay *et al.*, 2012). In addition, an increase in PN content was also observed, which may be a natural microbial response to environmental changes. Another hypothesis presented by the authors was the occurrence of cell lysis and release of intracellular polymers under pharmaceutical stress. Pasquini *et al.* (2013) also investigated the behavior of biomass towards the presence of eight household micropollutants with different concentrations (erythromycin, ofloxacin, triclosan, 4-nonylophenol, perfluoroalkyl acids – PFAAs and ibuprofen). The authors concluded that the impact on bound EPS in AS flocs was micropollutant dependent. Only ibuprofen at 0.1, 1 and 5 mg L^{-1} caused a decrease in bound EPS that was lower than the quantity of EPS in the control sludge, while the other compounds influenced the increase in EPS production (Table 2.3). It should be mentioned that none of these works were able to reveal in detail the particular functional groups of micropollutants involved in interaction with EPS (and other studies with the same approach) because the characterization is mainly based on fractional EPS components such as PN, PS and HAS, through colorimetric methods, without considering their high compositional and structural

heterogeneity. However, to solve the lack of fundamental composition, new instruments and techniques for the characterization of EPS have been used in the last few years, which generated a large amount of information about the structural and functional properties of EPS (Yu, 2020).

Spectroscopy, including Fourier transform infrared spectroscopy (FTIR) (Sheng *et al.*, 2013; Yin *et al.*, 2016), three-dimensional excitation-emission matrix fluorescence spectroscopy (3D-EEM) (Pan *et al.*, 2010; Sheng *et al.*, 2010; Wei *et al.*, 2015), X-ray photoelectron spectroscopy (XPS) (Feng *et al.*, 2018), cross polarisation magic angle spinning (CPMAS) with nuclear magnetic resonance spectroscopy (Meng *et al.*, 2012), and quartz crystal microbalance with dissipation (QCM-D) (Lyu *et al.*, 2021) have been used to give an in-depth insight of the structural binding mechanisms between EPS and micropollutants. In this framework, the influence of different antibiotics on the biological properties of sludge was studied by Avella *et al.* (2010) and Avella *et al.* (2010) through FTIR spectroscopy. An increase of bound EPS in flocs was observed for erythromycin and roxithromycin, while amoxicillin, tetracycline and sulfamethoxazole had no noticeable impact on the increase in bound or soluble EPS. They also found by FTIR analysis that the spectra exhibit the same IR regions in the presence or absence of antibiotics, showing only a global variation in absorbance, which was related to the change in the amount of PN and PS, but not designating which types of interactions occurred between EPS and these compounds (Avella *et al.*, 2010). Likewise, cyclophosphamide and its mean metabolites influenced the production of EPS in the biomass, inducing an increase in soluble EPS in the bulk solution and a lower concentration of bound EPS in the sludge; likewise, FTIR analysis revealed that the soluble species did not appear to undergo any chemical modifications as a result of the presence of cyclophosphamide (Avella *et al.*, 2010). Song *et al.* (2014) also investigated the interaction between tetracycline and EPS, finding additional information regarding the binding mechanisms. PN was identified through FTIR, XPS, nuclear magnetic resonance (NMR) and fluorescence spectroscopy as the dominant active constituent in EPS reaction with tetracycline. They found one binding site during the interaction, and the process is spontaneous in which electrostatic forces play a major role. The authors revealed that the reaction of EPS on tetracycline was a static quenching process, suggesting the formation of a complex. It was also observed that hydroxyl groups were altered during the reaction, reducing the effect of antibiotics and diminishing the inhibitory effect on microorganisms. These results were corroborated by Wang *et al.* (2018) and confirm that EPS have an key role in protecting bacteria. The transport of three antibiotics (sulfamethizole, tetracycline and norfloxacin) in the biofilm suspension from a moving bed biofilm reactor promoted the adsorption of these three antibiotics onto EPS that accounted for 14.5%, 88.2% and 13.1% of total concentration, respectively, at the biodegradation stage.

It was also observed that PN dominated the interactions between EPS and antibiotics (Wang *et al.*, 2018). FTIR results showed that the band intensities at 1340, 1408 and 1600 cm^{-1} decreased as the sulfamethizole concentration increased, suggesting that the major interaction sites for sulfamethizole and EPS were aliphatic C–H, phenolic C–O and C=O stretching in amides. Norfloxacin had a weaker interaction with EPS, and a slighter spectra variation induced by the addition of norfloxacin was observed. Tetracycline resulted in a significant increase in spectral intensity, associated with O–P–O stretching, P=O stretching, P=O asymmetric stretching and COO– symmetric stretching. From 3D-EEM fluorescence spectroscopy, the results suggested that the quenching of fluorescence intensities could be atributed to the formation of EPS-antibiotics complexes (static quenching) rather than dynamic quenching. The quenching constant of three compounds for PN was higher than for HAS, suggesting that PN, in the forms of tryptophan and tyrosine, might be dominant fractions to interact with the biofilm EPS. Hydrophobic interaction played a major role in the binding reaction and contributed to the stability of the sulfamethazine-EPS complex formation by a static quenching mechanism. PN instead of HAS dominated the interaction between EPS and sulfamethazine due to the large proportion and high binding strength. The reason may be that sulfamethazine could enter the internal hydrophobic region of PN. For the authors, the results imply that tryptophan residues were involved in the binding between EPS and sulfamethazine. After binding, the EPS structure was expanded and became loose, favoring mass transfer and capturing pollution (Xu *et al.*, 2013). The authors revealed that at the initial stage of the reactor operation, sulfamethazine was adsorbed mainly by EPS, and in the later stage, the adsorption of sulfamethazine by microorganisms increased, attributed to biodegradation.

Ciprofloxacin, a fluoroquinolone antibiotic, was used to control filamentous bulking and membrane fouling mitigation in membrane bioreactor (MBR) (Meng *et al.*, 2012). The authors found that EPS, including PN and PS, experienced an increase and then a decrease during the operational period. Furthermore, PS seemed to be much more sensitive to the ciprofloxacin exposure than PN, increasing around 50% in the whole experiment (Meng *et al.*, 2012).

Additionally, to understand the structural of EPS, CPMAS with NMR spectroscopy was used to identify the structural difference of EPS between the reactor control and the reactor with ciprofloxacin. Accordingly, six structural groups could be assigned: aliphatic carbon, α-carbon of amino acids, O-alkyl carbon, anomeric carbohydrates, aromatic carbon, and carboxyl carbon. Results showed an increase in PS, favored by the addition of ciprofloxacin, containing a much higher carbon content of anomeric carbohydrate (6%) and O-alkyl carbon (20%) than those in the control reactor (Meng *et al.*, 2012). Moreover, the interaction between ciprofloxacin and PN EPS extracted from an anaerobic-anoxic-aerobic

process (A2O) was pH-dependent, with a strong binding obtained at pH 5, suggesting electrostatic interactions as the dominating binding mechanism. Also, the binding of ciprofloxacin with the extracellular PN followed the pseudo-first-order kinetic equation and Langmuir model (Lyu *et al.*, 2021). Moreover, EPS from the sulfate-reducing bacteria (SRB) process seemed to have a higher capacity to interact with ciprofloxacin than EPS from the sulfur-oxidising bacteria (SOB) process (Zhang *et al.*, 2020). More potential adsorption sites were found in the SRB sludge for ciprofloxacin adsorption than in the SOB sludge, due to the presence of higher PN content, more kinds of aromatic amino acid substances in EPS, higher negative zeta potential and higher numbers of functional groups.

Soluble EPS and bound EPS had a different role in the binding with herbicide dicamba. According to Pan *et al.* (2010), protein-like substances in soluble EPS formed more stable complexes with dicamba than those in bound EPS. Electrostatic forces and hydrophobic interaction forces play a crucial role in the binding of dicamba to EPS, and protein-like substances have a stronger binding capacity for dicamba than humic acid-like substances governed by a fluorescence quenching static process. Another herbicide, the ametryn, had a toxic impact on biomass and affected EPS production during the operation of an MBR under different conditions. After the addition of ametryn, PN was the dominant component, and it reduced from 77.5% to 74.2%, while PS concentration increased from 22.5% to 28.5% (Navaratna *et al.*, 2012).

3D-EEM fluorescence spectroscopy was used to investigate the interaction of soluble and bound EPS with acetamiprid, a neonicotinoid insecticide. The findings suggest that the fluorescence quenching processes of tryptophan-protein for soluble/bound EPS and fulvic acid-like substances for bound EPS by acetamiprid were mainly controlled by a static quenching process rather than a dynamic quenching process, resulting in the formation of acetamiprid-EPS complexes. Furthermore, this study demonstrated through binding constants that soluble EPS had a stronger binding capacity for acetamiprid than bound EPS (Song *et al.*, 2010).

The interactions between micropollutants and EPS are dependent of their hydrophilic and hydrophobic characteristics. Proteins to carbohydrates ratio (P/C) has been used as an indicator of the relative hydrophobicity of macromolecules and the stickiness of EPS (Santschi *et al.*, 2020). Important findings were reported suggesting that the P/C ratio is linked to parameters that are related to biopolymer aggregation propensity, such as relative hydrophobicity, surface activity and surface tension, attachment efficiency, and light-induced chemical crosslinking. In this context, the P/C ratio could be predictive for the relative hydrophobicity of EPS. Also, in unfavorable growth conditions, such as when toxic compounds are present, EPS typically exhibits greater PN/PS ratios, which, as a result of the high

amount of PN, tend to be more hydrophobic, influencing the removal of pollutants (i.e., organic matter, oil and other organic pollutants, including plastics and microplastics) (Santschi *et al.*, 2021).

The main studies found in the literature addressing the effect of micropollutants on EPS are presented in Table 2.3, and the proposed mechanisms of interaction between micropollutants and EPS are presented in Figure 2.5.
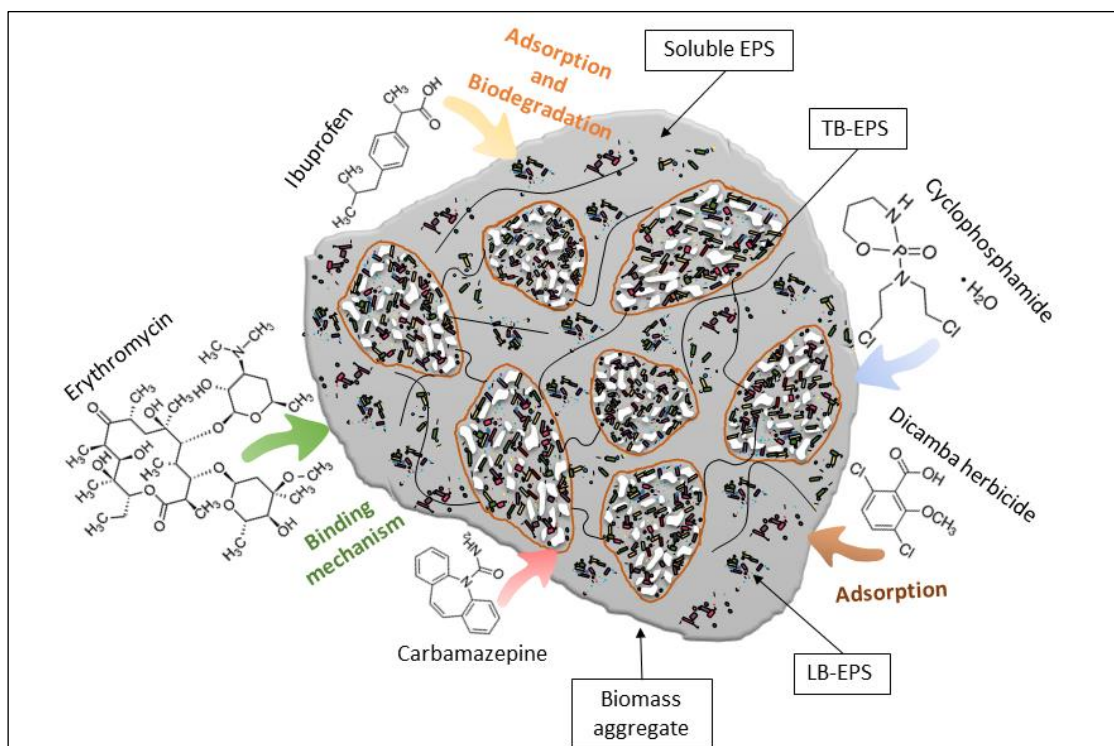
Figure 2.5 – Proposed interaction mechanisms of the microbial EPS in bioaggregates interacting with micropollutants. Complexes formed between EPS and pollutants through hydrophobic interaction, hydrogen bond or electrostatic interaction.

Table 2.3 – Effect of different micropollutants on EPS production and composition.

System	Scale	Micropollutants	Concentration	Results	Reference
AS	Lab-scale	Erythromycin, roxithromycin, amoxicillin, tetracycline, sulfamethoxazole	10 mg L^{-1}	Roxithromycin and erythromycin induced ↑ in bound PN EPS All induced more PN EPS than PS EPS and erythromycin inhibited COD removal All except amoxicillin induced more PS soluble EPS than soluble PN EPS	(Avella *et al.*, 2010)
AS	Lab-scale	Sulfamethazine	500 µg L^{-1}	Slight variation in PN and total EPS	(Xu *et al.*, 2013)
AS	Lab-scale	Erythromycin Ofloxacin	100 µg L^{-1}	Except for ibuprofen, the compounds induced an	(Pasquini *et al.*, 2013)

				increase in bound EPS	
		Triclosan	$10\ \mu g\ L^{-1}$		
		4-nonylphenol	$0.5\ \mu g\ L^{-1}$		
		PFAAs	$5000\ \mu g\ L^{-1}$		
		Ibuprofen	$0.1\ \mu g\ L^{-1}$		
			$100\ \mu g\ L^{-1}$		
AS	Batch experiments	Tetracycline	0 to 50 $\mu mol\ L^{-1}$	PN were the dominant active constituents in the EPS during the interaction with tetracycline	(Song *et al.*, 2014)
SBR	Lab-scale	Ibuprofen	$10\ mg\ L^{-1}$	↑ PN TB-EPS from 38 to 49.7 mg L^{-1}	(Melo *et al.*, 2021)
MBR	Lab-scale	Cyclophosphamide	$5\ \mu g\ L^{-1}$	↑ soluble EPS, PS and soluble PN EPS	(Avella *et al.*, 2010)
				↑ PS EPS and HAS EPS	(Delgado *et al.*, 2010)
MBR	Lab-scale	Ciprofloxacin	$1\ mg\ L^{-1}$	↑ bound and soluble EPS	(Meng *et al.*, 2012)
MBR	Lab-scale	Ametryn	$1\ mg\ L^{-1}$	↑ EPS to MLSS ratio and higher rate of fouling ↑PS EPS from 22.5% to 28.5%, but ↓ PN EPS from 77.5% to 74.2%	(Navaratna *et al.*, 2012)
MBR	Lab-scale	Fluoroquinolone antibiotic	0.9 to 9 mg L^{-1}	Soluble EPS increased from 16.72 to 26.4 mg L^{-1}	(Meng *et al.*, 2015)
MBR	Lab-scale	Carbamazepine	$90\ \mu g\ L^{-1}$	↑ PN EPS from 25 to 35 mg L^{-1}	(Li *et al.*, 2015)
OMBR	Lab-scale	Carbamazepine, diclofenac, ibuprofen, naproxen,	20-25 ppb	↑ soluble PN EPS from 1.1 ± 1.1 to 2.6 ± 2.1 mg g^{-1} SS and soluble PS EPS from 3.3 ± 1.8 to 5.1 ± 0.5 mg g^{-1} SS ↑ PN EPS from 15.6 ± 6.1 to 25.8 ± 9.4 mg g^{-1} SS and PS EPS from 21.0 ± 7.4 to 26.2 ± 5.9 mg g^{-1} SS	(Lay *et al.*, 2012)

AS (activated sludge); SBR (sequencing batch reactor); MBR (membrane bioreactor); OMBR (osmotic membrane bioreactor)

2.4 Respirometry technique

Respirometry stands out among the techniques available to control the AS system. This technique is an indicator of the biological activity of microorganisms based on the respiration rate when they consume the substrate available. Furthermore, this technique is directly related to cell growth, another necessary process that must be controlled (Spanjers *et al.*, 1996).

Traditional methods for characterizing wastewater are generally time-consuming. Although commercial methods are available through probes or cuvette tests (e.g. BOD, COD, nitrate, etc.), the detection of toxic compounds within the system is difficult due to the broad range of these substances, including pesticides and pharmaceuticals. So far, the ecotoxic effect of various micropollutants has been documented using bacterial luminescence inhibition assays with *Vibrio fischeri* (Borowska *et al.*, 2016; Maculewicz *et al.*, 2022; Singh *et al.*, 2018) as well as using *Daphnia magna* and algal tests (Cleuvers, 2004). Microtox and respirometry are common techniques for toxicity assessment of micropollutants present in wastewaters. Microtox is probably the most popular test for assessing wastewater toxicity (Bitton, 2005). However, this bioluminescence test has inherent problems since the single microbial species (*Vibrio fischeri*) does not represent the microbial complexity of the communities present in AS systems (Ricco *et al.*, 2004). Thus, the respirometry technique becomes useful for evaluating toxicity events, since this technique allows the evaluation of the biological activity of microorganisms (Henriques and Love, 2007; Vasiliadou *et al.*, 2018). The advantage of this technique is that wastewater toxicity is measured directly on the active biomass in the biological treatment system, and changes in the respiration rate of microorganisms will indicate changes in wastewater composition (Le Bonté *et al.*, 2005). In addition, performing this technique requires little handling, no reagents or complex apparatus during testing, and is not time-consuming. Many respirometry techniques have been developed in recent decades. Still, these techniques can be classified according to two criteria: (1) the phase at which DO is measured (gas or liquid) and (2) whether or not there is inlet and outlet of gas or liquid in the system (flow or static) (Spanjer *et al.*, 1996). Respirometers based on the measurement of oxygen in the liquid phase use the DO mass balance of the liquid phase. It can be assumed that the concentration of DO in the liquid phase is obtained according to the mass balance presented in equation 2.2,

$$\frac{d(V_L C_L)}{dt} = Q_{in}C_{in} - Q_{out}C_{out} + V_L K_{La}(C_L^* - C_L) - V_L r_{O2} \qquad (2.2)$$

where, C_L is the DO concentration in the liquid phase (mg L^{-1}), C_L^* is the saturation DO concentration in the liquid phase (mg L^{-1}), $C_{L,in}$ is the DO concentration in the liquid phase entering the system (mg L^{-1}), K_{La} is the oxygen mass transfer coefficient, based on liquid volume (h^{-1}), Q_{in} is the flow rate of the liquid entering the system (L h^{-1}), Q_{out} is the flow rate of the liquid leaving the system (L h^{-1}), r_{O2} is the respiration rate of the biomass in the liquid, (mg L^{-1} h^{-1}), and V_L is the volume of the liquid phase (L). The third term represents the transfer of oxygen from the gas phase to the liquid phase. The last term means the respiration rate derived from mass balance. Therefore, C_L must be measured and all other coefficients be known or neglected (Spanjers *et al.*, 1996). One approach to simplifying the respirometry test is to use the method without liquid flow and gas flow, so the first three terms of the equation can be eliminated, which simplifies equation 2.2. Thus only the differential term of the equation needs to be determined to obtain the oxygen uptake rate (OUR).

$$\frac{d(C_L)}{dt} = -r_{O2} \tag{2.3}$$

Hence, only the differential term must be determined to obtain the respiration rate. This can be done by measuring the decrease in DO as a function of time due to respiration (Figure 2.6), which is equivalent to approximating the differential term with a finite-difference term. The consequence of this approach is that the DO becomes depleted after some time, so for each new measurement of r_{O2} a reaeration is needed to raise the DO concentration to a higher level. The disadvantage of the need for reaerations can be eliminated by continuously aerating the biomass. Then, the oxygen mass transfer term ($K_{La}C_L^* - C_L$) must be included in the mass balance. To obtain r_{O2}, the differential and mass transfer terms must be determined. To calculate the latter, the mass transfer coefficient (K_{La}) and the DO saturation concentration (C_L^*) must be known (Spanjers *et al.*, 1996).

In biological WWTP, toxic substances can cause severe disturbances such as inhibition of biomass activity or death. Therefore, determining whether or not a compound is toxic before contact with biomass becomes crucial. The toxicity of a given compound can be assessed using the respirometry technique (Figure 2.6) by comparing the slope value in the DO profile obtained after the addition of a substrate (normal biological biomass activity) to the slope value obtained after the addition of the substrate mixture with the toxic substance (shock condition) (Guisasola *et al.*, 2004).
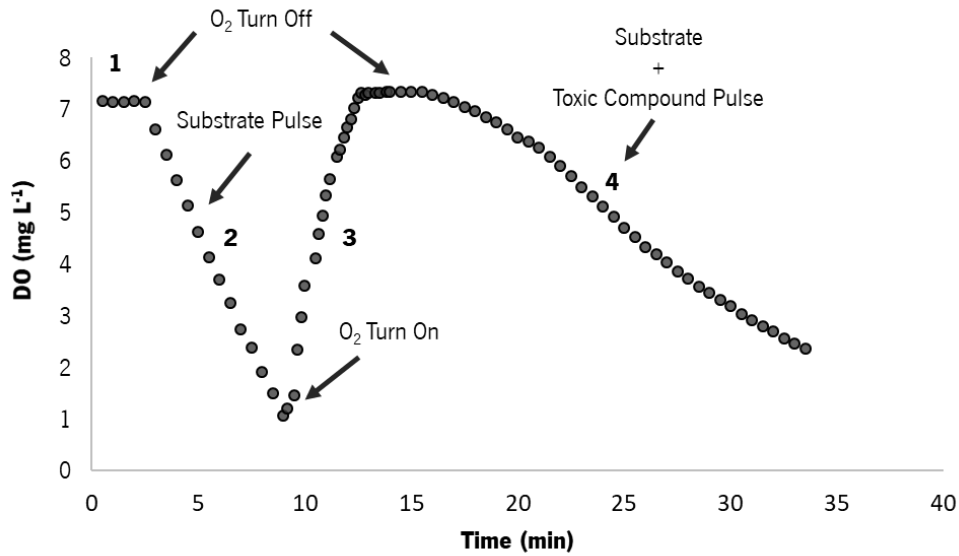
Figure 2.6 – Toxicity assessment comparing the slope value of the DO profile: 1 - DO saturated value; 2 - OUR of the substrate pulse; 3 - Reaeration profile; 4 - OUR of the substrate + toxic compound.

Most of the work on toxicity has been carried out on fish species, planktonic crustaceans and other bacterial cultures (Singh *et al.*, 2018; Vasiliadou *et al.*, 2018). Thus, applying the respirometric test to assess the toxicity of micropollutants in AS is a practical approach.

2.5 Quantitative image analysis (QIA)

The purpose of image analysis is to extract useful information from images. Since modern image analysis allows fast, accurate, and reliable results, it is currently widely used in many areas of research and development (Jung, 2019). QIA is a process of obtaining digitalized images by a microscope connected to a video camera and a frame-grabber or a digital camera or by whole slide scanning to conduct computer-based analyses to extract meaningful information from the images (Riber-Hansen *et al.*, 2012). Image segmentation, object tracking and counting are time-consuming, tedious and error-prone processes when performed manually. Besides, manual annotation is hard to scale for biological images since expert annotators are typically required for correct image interpretation (Berg *et al.*, 2019). Therefore, the aim is to use computational processes to accelerate repetitive tasks while obtaining quantitative results since statistical results are much more compelling, scientifically speaking, than qualitative observations (Schindelin *et al.*, 2015). Image analysis has become a fundamental tool with great application in biological WWT systems. For example, the investigations of AS flocs usually concern the following issues: (i) morphology (size and shape of bioaggregates); (ii) composition of

bioaggregates, such as internal structure (flocs or granules); (iii) the identification of microbial species; (iv) spatial arrangement of microorganisms (Liwarska-Bizukojc, 2005). Microscopy coupled with image analysis has been successfully applied to study AS flocs morphology (Grijspeerdt, 1997), and recognition of metazoa and protozoa species (Ginoris *et al.*, 2007). Furthermore, in AS systems QIA has been applied for a more detailed morphological characterization of microbial flocs, allowing the estimation of many different geometric parameters (Amaral and Ferreira, 2005), and identifying the overgrowth of filamentous bacteria, which is an undesired phenomenon in the AS treatment process (Mesquita *et al.*, 2011). QIA has also been used to monitor and model the full-scale AS process based on features extracted using morphological parameters of flocs obtained through bright-field microscopy from nine full-scale plants (Khan *et al.*, 2018). Moreover, QIA has been demonstrated to be a helpful technique for assessing the impact of low temperature and variation in the operational parameters on AS flocs morphology and filaments content in a full-scale WWTP in Poland (Liwarska-Blzukojc *et al.*, 2019). In addition, morphological changes in aerobic granular sludge during exposure to 17 β-estradiol, 17α-ethinylestradiol and sulfamethoxazole were identified by QIA (Leal *et al.*, 2021).

The SVI has been predicted with a high degree of accuracy using partial least square (PLS) regression employing 69 parameters from QIA directly or indirectly generated by this technique (Silva *et al.*, 2022). In another study, the early detection of filamentous bulking in AS systems was used to predict the changes in SVI using two or three image analysis parameters such as form factor, filamentous length, and reduced gyration radius (Banadda *et al.*, 2003).

2.5.1 QIA methodology

The main steps of image analysis are image capturing, image storage (compression), correcting imaging defects (e.g. non-uniform illumination, electronic noise, glare effect), image enhancement (to make the image easier to visually examine and interpret), segmentation of objects in the image and image measurements (Oberholzer *et al.*, 1996; Russ and Neal, 2018).

Image acquisition is the first and important step in digital image processing (Oberholzer *et al.*, 1996). It starts with capturing an image by the sensor (such as video cameras, CCD cameras or CMOS detectors) and digitized. If the output of the camera or sensor is not digital, then an analogue-to-digital converter (ADC) is used (Russ and Neal, 2018). On the other hand, using digital cameras allows for obtaining digitalized images by a microscope connected to a digital camera (Riber-Hansen *et al.*, 2012).

The numerical information generated in the digitalization consists of the grey values describing the brightness of every point within the image, named a pixel. The information is stored in bits. Eight

bits are summarised in one byte. Therefore, grey values can have a value between 0 and 256. For bright-field (without staining), monochrome images have generally been acquired with the non-uniformity problem of the background illumination (Mesquita *et al.*, 2013), difficulting in recognizing of imagem features (Peng, 2008). Useful image features can correspond to statistical, geometrical, morphological properties and frequency of image pixels and regions, among other temporal and spatial variations (Moen *et al.*, 2019). Thus, for a well-succeeded image processing and analysis procedure, this kind of issue should be eliminated and optimized prior to acquiring the images (Mesquita *et al.*, 2013).

The *processing step* is generally based on image analysis software that processes an object's unique color information and then extracts a color channel of interest from an original color image. A grey channel is most common mainly in the bright field, although R (red), G (green), and B (blue) channels are also used when using staining procedures (Jung, 2019). In this step, the pixel grey values in a digitised image can vary within regions that are uniform in the original scene. Therefore, for optimal discrimination between different objects or features in an image, uniformity of illumination is required to be achieved by subtraction a background image from the original image, pixel per pixel, or dividing the original image by the background image (Oberholzer *et al.*, 1996).

After image enhancement by background elimination, segmentation is performed, consisting of a binarization to convert such a single-color channel image into a binary image that is composed of only black (a value of 0 in an 8-bit image) and white (a value of 255 in an 8-bit image) pixels. Segmentation is one of the most basic processing steps in many (bio)image informatic applications to segment the significant objects of interest in the respective image (Peng, 2008). A simple binarization method by thresholding has been used, which converts the pixel value to zero if it is lower than a threshold value or 255 if it is greater than the threshold. At the end of binarization, a region labelling algorithm is used to detect individual objects for further analysis of the position, size, area, perimeter, and color information, such as an average grey value.

Finally, the last step is the *image analysis* of the images from the processing and segmentation steps. In the image analysis step, the parameters used to describe Euclidean morphology of bioaggregates in AS systems include area, perimeter, equivalent diameter, length, width, compacity, convexity, and eccentricity roundness, among many others (Amaral, 2003). Besides that, determining the length of filamentous bacteria, its numbers, and contents is crucial to comprehend sludge dysfunction events.

2.6 Chemometric techniques

Many different processes happen simultaneously in WWTP, leading to the difficulty of understanding the whole system. In this way, to aid in the interpretative task of the system behavior, several parameters are constantly recorded in WWTP to monitor the performance of the process over time to detect any special events and control the effluent quality. However, the vast amount of registered data requires adequate techniques to extract useful information (Avella *et al.*, 2011).

Many variables are normally measured in an AS WWTP, and some of them are strongly cross-correlated. Considering the complexity and large amount of data obtained during the operation and monitoring of the biological WWT systems, the multivariate data analysis is presented as a valuable technique for data reduction and better interpretation of the correlations between the variables (Teppola *et al.*, 1997).

Principal component analysis (PCA) and partial least squares (PLS) have been widely used in this kind of process, as both can be used with redundant data sets (Mehmood *et al.*, 2012; Teppola *et al.*, 1997). Mujunen *et al.* (1998) used the PLS method with cross-validation to describe WWTP effluent quality parameters. The reduction of COD was predicted for a full-scale WWTP using multivariate statistical methods. Firstly, the PCA method was employed to reduce the dimensionality and remove the collinearity of the data. Then, a fuzzy model was used to build a nonlinear model (Yoo *et al.*, 2003). The multiscale PCA was developed for a wide range of observed changes in full-scale WWTP data (Lennox and Rosen, 2002). Li and Yan (2019) have proposed a novel ensemble process monitoring method based on genetic algorithm for selective diversity of principal components (PC). The genetic algorithm was used to determine a set of PC subspaces with the greatest diversity as the base models. Then, Bayesian inference was adopted to combine the results of base models into a probability index. This approach showed the model's strong generalisation ability in describing the assessed WWTP process.

Principal components analysis (PCA) is a technique that allows the transformation of a given dataset of correlated variables to a new set of uncorrelated (orthogonal) variables, called PC (Amaral *et al.*, 2017). The original data matrix X decomposes into the product of two smaller matrices (equation 2.4),

$$X = P^T + E \tag{2.4}$$

where X is the original data set of size, T is called scores, P is called loadings and E is the model residual (Rosen *et al.*, 2003). The original data matrix is transformed into a new matrix with PC sorted by their variance. Most of the variance is contained in the first PC, decreasing in order of importance, that is, reducing the ability to explain the original dataset (Amaral *et al.*, 2017; Faassen and Hitzmann,

2015). By taking the first principal components, holding almost the whole variance of the data, the dimension of the original data matrix **X** is reduced dramatically. Because often one, two or three PC contain approximately all the variance of the data – and the others represent only noise **E**– the data can be visualized by plotting a so-called score plot, where further interpretations become possible, for example, the identification of different process states (Faassen and Hitzmann, 2015).

PLS has proven to be a very versatile method for multivariate data analysis. As a result, the number of applications is steadily increasing in research fields such as bioinformatics, machine learning, and chemometrics (Mehmood *et al.*, 2012). In PLS the matrix **X** is decomposed into a score matrix **T** and a loading matrix **P**. In a similar way, the matrix **Y** is decomposed into a score matrix **U** and a loading matrix **Q**. The first latent variable is extracted from the matrices **X** and **Y** and explains as much as possible of the variance of matrix **Y** (Teppola *et al.*, 1998). In a similar way, the second latent variable is extracted from the variance in residual matrices, which has not been described by the first latent variable, and so on. The idea behind calculating the latent variables iteratively can be seen as a way of extracting informative features one by one. When the optimal number of latent variables has been con-determined, what remains is considered tributed by noise (Teppola *et al.*, 1998). PLS extracts linear combinations of essential features that model the original data in X and Y; however, it also models the dependence of both data sets. For this reason, PLS is highly suitable for modelling and simulating relationships. The goodness of fit of PLS models is measured by an error of prediction, similarly to ordinary least-squares methods. Via a cross-validation test, the number of significant vectors in **U** and **T** and the prediction error can be determined (Einax *et al.*, 1999). PLS has widely been used to control and monitor AS processes. Several studies have reported the use of this technique to predict: (i) the deterioration of sludge sedimentation properties (Mujunen *et al.*, 1998), (ii) the SVI in WWTP during filamentous bulking phenomenon using QIA parameters (Amaral and Ferreira, 2005), (iii) effluent quality parameters in an aerobic granular sludge system treating industrial wastewater (Costa *et al.*, 2022), and (iv) the bioflocculation and fouling rate in an AS system (Staey *et al.*, 2016).

CHAPTER 3 - MATERIAL AND METHODS

3.1 Experimental set-up

3.1.1 SBR operation and sampling

A sequencing batch reactor (SBR) consisting of a volume of 2 L was operated at room temperature containing AS (initial concentration of ≈3000 mg L^{-1} of mixed liquor suspended solids - MLSS) inoculated from a full-scale WWTP from Portugal. Pumps were used to control the feed and effluent withdrawal of the reactor during the length cycle. The SBR was operated in cycles of 6 h distributed in four stages: filling (40 min), aerobic reaction (240 min), settling (40 min), and effluent withdrawal (40 min). The aeration was controlled with a mass flow controler, and the distribution of the fine air bubbles were supplied through a porous stone at the bottom of the reactor. Timers were used in aeration, feeding and discharge pumps allowing to control the SBR cycles. The experimental set-up of the SBR used during the experiments is presented in Figure 3.1.
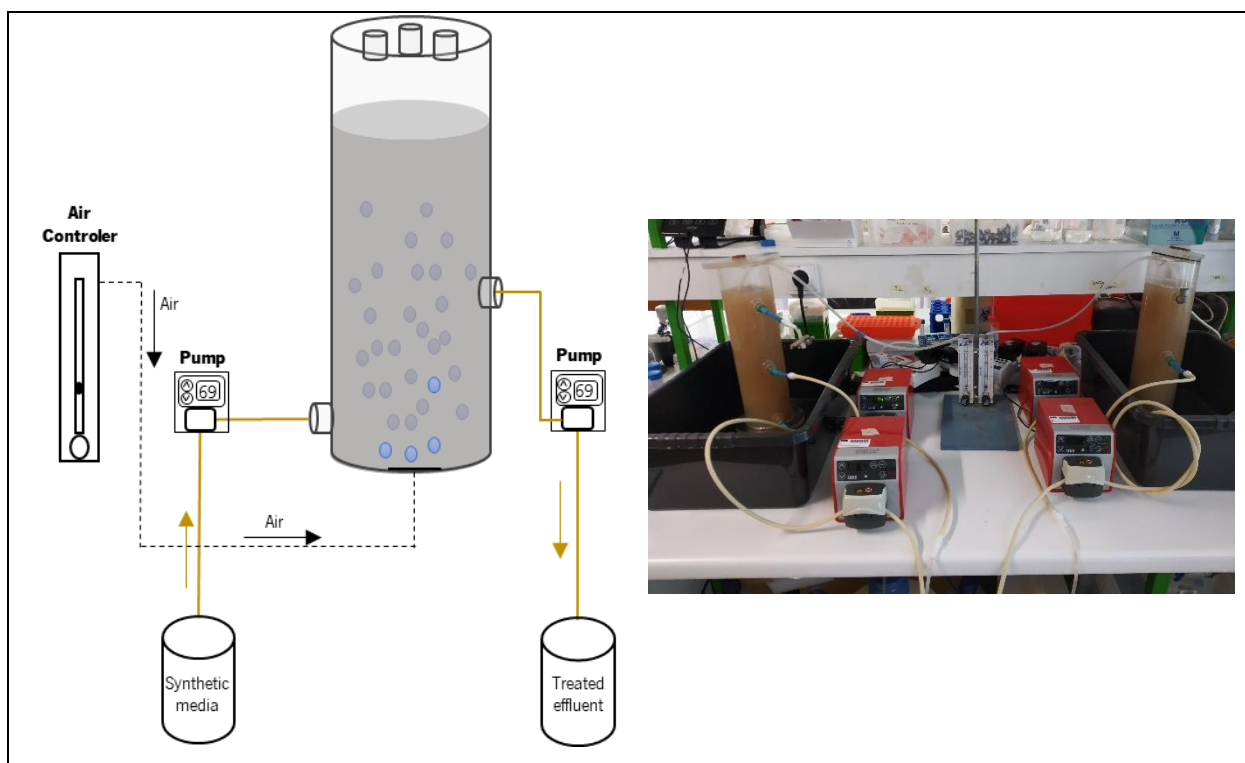
Figure 3.1 – SBR reactor employed to experiments.

A synthetic wastewater containing the following components per litre: 1.450 g sodium acetate ($NaCH_3COO\cdot3H_2O$), 0.120 g NH_4Cl, 0.028 g K_2HPO_4, 0.030 g $MgSO_4\cdot7H_2O$, 0.07 g $CaCl_2\cdot2H_2O$, 0.015 g KCl, and 3.5 mL trace element solution for biomass maintenance, was used (Smolders *et al.*, 1994).

The hydraulic retention time was 12 h with a volumetric exchange ratio of 50%, and the sludge retention time was set at ≈10 days by discharging daily an appropriate amount of suspended sludge.

For physico-chemical characterization of the biomass and SBR performance in terms of organic matter removal (COD, NH_4^+-N, NO_2^--N , NO_3^--N), the reactor was first operated in all experiments without the presence of the selected toxic compounds as a control. The following experiments with selected toxic compounds (IBU, DESL and ATZ) were conducted operating the SBR as described in the next section. Prior to each experiment, the inoculated biomass was acclimatized for a period of 20 days to the synthetic media to reach the steady-state condition. The biomass was sampled three times per week, 5 min before the end of the reaction phase to ensure that samples were collected well mixed, and the treated effluent sampling were taken during effluent withdrawal stage.

Three phases were carried out in the experiment with addition of IBU in the synthetic wastewater. During phase I (day-0 to day-56), the SBR was fed with synthetic wastewater without IBU as a control. From day-57 to day-98 (phase II), IBU (Acros Organics) was added to the synthetic influent media at 10 mg L^{-1} for only the first cycle of the day. Lastly, from day-99 onwards (phase III), the reactor was operated containing 5 mg L^{-1} IBU, following the same operational procedure as in phase II. Phases I, II, and III were sequentially conducted, in which the system was re-inoculated with new biomass to eliminate the effects caused by adding IBU to the system.

For DESL and ATZ experiments, unlike the first experiment with IBU, the inoculated biomass was acclimatized for 20 days to the synthetic media to achieve the steady-state condition, and then DESL was stepwise added to the medium to reach a concentration in the inlet feeding, as indicated in Table 3.1. Finally, the same methodology was employed for the reactor with ATZ in the synthetic influent media, thus making four phases for these two last experiments (Table 3.1).

Table 3.1 – Concentrations at the inlet feeding throughout SBR operation in the experiments with DESL and ATZ.

Phase	Operation days	Inlet concentration (mg L^{-1})	
		DESL	ATZ
I	0 - 34	0	0
II	35 - 69	1	2
III	70 - 105	5	5.5
IV	106 - 139	10	12

3.1.2 Analytical methods

Physicochemical analysis

Chemical oxygen demand (COD), ammonium (NH_4^+-N), nitrite (NO_2^--N), and nitrate (NO_3^--N) concentrations were determined with cell tests on a Hach Lange DR 2800 spectrophotometer (Hach Lange, Dusseldorf, Germany). The pH of synthetic wastewater and temperature of mixed liquor was monitored with a Consort C1010 multiparameter analyzer (Consort, Turnhout, Belgium). Mixed liquor volatile suspended solids (MLVSS), MLSS, and the sludge volume index (SVI_{30}) of a sludge sample were measured according to the Standard Methods (APHA, 1998). The sludge suspension was settled for 30 min, after which the supernatant fraction was collected and measured as effluent suspended solids (ESS). This ESS level indicates the microbial flocculation performance, whereas the SVI value specifies the sludge settleability and compressibility.

UHPLC Analysis

The chromatographic analysis of IBU, DESL and ATZ was performed for the synthetic feeding and for the treated effluent with all collected samples filtered with a 0.2 μm filter prior to HPLC analysis. The analysis was performed using a Shimadzu Corporation apparatus (Shimadzu, Tokyo, Japan) consisting of a Nexera UHPLC equipment with a multi-channel pump (LC-30 CE), an autosampler (SIL-30AC), an oven (CTO-20AC), a diode array detector (M-20A) and a system controller (CBM-20A) with built-in software (LabSolutions), according to (Quintelas *et al.*, 2020, 2019). For the analysis of all the three compounds a Kinetex 5 u EVO C18 column (150×4.6mm i.d.) supplied by Phenomenex, Inc. (CA, USA) was used.

For IBU, the mobile phase, with a flow rate of 1.5 mL min^{-1}, consisted of sodium phosphate (20 mM; pH 2.4) (pump A) and acetonitrile (pump B). The starting mobile phase composition was 80% A, decreasing to 30% A in 10 min and remaining in this percentage for 5 min. The sample was monitored by the diode array detector from 190 to 400 nm, and the chromatograms were extracted at 225 nm. The column oven was set to 40 °C and the volume of injection was 10 μL.

For the quantification of DESL, the mobile phase was potassium dihydrogen phosphate (0.05 M; pH 3) (pump A), acetonitrile (pump B) and methanol (pump C). An isocratic method was employed with 45% A, 48% B and 7% C. The flow rate was 0.8 mL min^{-1}. The samples were monitored by a diode array detector from 190 to 400 nm, and chromatograms were extracted at 247 nm. Column oven was set at 25 °C and the injection volume was 12 μL.

Lastly for the ATZ quantification, the mobile phase was water (pump A) and acetonitrile (pump B). An isocratic method was employed with 15% A and 85% B. The flow rate was 1.0 mL min^{-1}. The samples were monitored by a diode array de-tector from 190 to 400 nm, and chromatograms were extracted at 220 nm. Column oven was set at 25 °C and the injection volume was 30 µL.

3.1.3 EPS extraction and quantification

A heat extraction method (Li and Yang, 2007) was modified to extract the loosely bound EPS (LB-EPS) and tightly bound EPS (TB-EPS) from AS. A sludge suspension was first dewatered by centrifugation (5810 R, Eppendorf) in a 40 mL tube at 8000 g for 5 min. The sludge pellet in the tube was resuspended at its original volume of 40 mL with 100 mM NaCl solution with a similar salinity to the SBR reactor solution. The NaCl solution for dilution was preheated to 70 °C to ensure that the sludge suspension immediately reached 50 °C. Without delay, the sludge suspension was sheared with a vortex mixer for 1 min, followed by centrifugation at 4000 g for 10 min. The organic matter in the supernatant was readily extractable EPS, regarded as the biomass's LB-EPS. For TB-EPS extraction, the sludge pellet left in the centrifuge tube was re-suspended in 100 mM NaCl solution to its original volume of 40 mL. The sludge suspension was heated to 60 °C in a water-bath for 30 min, and the mixture was then centrifuged at 12,000 g for 20 min at 4 °C. The supernatant collected was regarded as the TB-EPS extraction of the sludge. All supernatant samples were filtered through a 0.45 µm acetate cellulose membrane.

Both the LB-EPS and TB-EPS extractions were analysed for PS, PN and HAS. PN and HAS were analysed in triplicate in an UV/VIS spectrophotometer (DR 500 Hach Lange, Dusseldorf, Germany), following the modified Lowry method using bovine serum albumin (BSA) and humic acid as standards, respectively. The PS content was determined in duplicate by the anthrone-sulphuric acid method, using glucose as the standard (Frølund *et al.*, 1995). The sum of PN, HAS and PS content was referred to as the total LB-EPS and TB-EPS. The sum of LB-EPS and TB-EPS was also assessed as the total EPS.

For experiments with DESL and ATZ in the influent, EPS samples previously extracted were also evaluated by 3D-EEM spectra, using a luminescence spectrophotometer (Aqualog, Horiba). The 3D-EEM spectra were collected with subsequent scanning emission spectra from 240 to 600 nm at 5 nm increments by varying the excitation wavelength from 240 to 600 nm at 5 nm sampling intervals. The excitation and emission splits were maintained at 5 nm and 2.5 nm, respectively. The 3D-EEM data were processed using the software Origin 8.0.

The EEM spectrum can be divided into regions based on the specific excitation and emission wavelength pair. The organic substances present in the EPS, such as protein-like and humic acid-like substances, could be depicted by the percent fluorescence response (Pi,n), according to Chen *et al.* (2003), Yang *et al.* (2019), and Qian *et al.* (2021). In the present study excitation and emission boundaries were defined into two regions associated with peaks containing excitation wavelengths of 250- ≈280 nm and emission wavelengths <380 nm for protein-like substances (region A). Peaks with excitation wavelengths >280 nm and longer emission wavelengths (>380 nm) are related to humic acid-like substances (region B).

3.1.4 *Image acquisition processing and analysis*

For the QIA analysis, a 2 mL sample was taken from the middle depth of the SBR during the aeration phase, and then standardized aliquots with a volume of 10 µL were collecte with a sectioned tip to allow the large aggregates pass through. Images were acquired in triplicate of 10 µL air-dried slides through bright-field microscopy with an Olympus BX51 microscope (Olympus, Shinjuku, Japan) at 40× (1360×1024 pixels) and 8-bits, coupled to an Olympus DP72 camera (Olympus, Tokyo, Japan), giving us 150 images per day. The images used for the characterization of aggregates and filaments content were processed by a program developed in Matlab 9.2 (The Mathworks, Inc., Natick, USA) by Amaral and Ferreira (2005). Image processing and analysis information can be seen in the Figure 3.2.

The aggregates and filaments content were measured in terms of the total area per sample volume (TA/Vol), the total filament length per sample volume (TL/Vol), and the total filaments length per MLSS (TL/MLSS). The aggregates size (in equivalent diameter, Deq) was also determined. Aggregates were divided into 3 size classes according to their Deq: small (<25 µm), intermediate (25–250 µm), and large (>250 µm). The aggregate area percentage (%Area) was also determined for the small (sml), intermediate (int), and large (larg) aggregates. These parameters proved adequate to study AS morphology, to monitor settling dysfunctions in conventional AS, evaluating morphological aspects of granular sludge, and predict effluent quality (Arelli *et al.*, 2009; Contreras *et al.*, 2004; Costa *et al.*, 2022; Mesquita *et al.*, 2011; Mujunen *et al.*, 1998; Silva *et al.*, 2022).

Table 3.2 depicts the main parameters acquired using QIA as well as the respective formula (Amaral and Ferreira, 2005). With the purpose of better understanding the role of each parameter in this study, they were divided into four main descriptor groups: (i) filamentous content, (ii) aggregates size, (iii) morphological descriptors, and (iv) aggregates content.

Pre-treatment
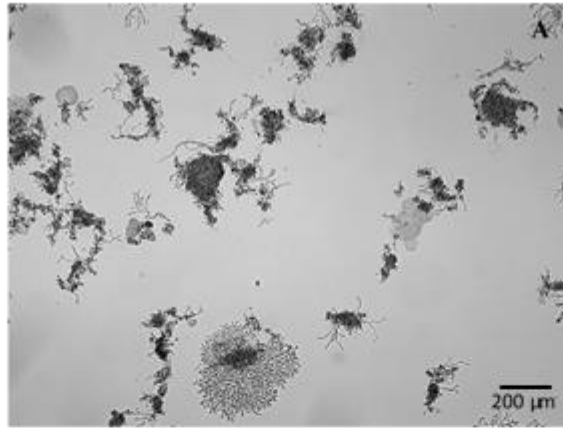
Segmentation
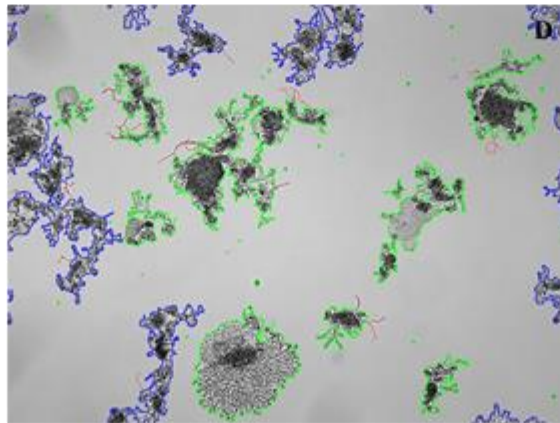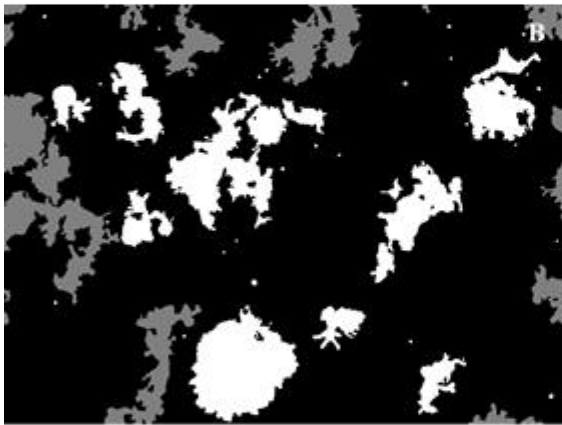
Figure 3.2 – Scheme of bright-field microscopy image processing: (a) original image acquisition and background correction, (b) aggregates binary image, (c) filaments binary image, and (d) aggregates (green and blue) and filaments (red) boundary image. Size bar is equivalent to 200 micrometers.

Table 3.2 – QIA descriptors obtained from samples (adapted from Costa *et al.* (2022)). Detailed definition of each parameter can be found in Amaral (Amaral, 2003).

Main descriptor group	Parameter	Description	Formula
Filamentous bacteria content	TL/Vol	Total filaments length per volume	-
	TL/TA (mm/mm²)	Total filaments length per total area of flocs	$TL/TA = \dfrac{TL}{TA}$
	Nb_{int}/Vol (μL^{-1})	Number of filaments intersections per volume	-
	Nb_{fil}/Vol (flocs/μL)	Number of filaments per volume	-
	Nb_{thn}/Vol (μL^{-1})	Pixel sum of each thinned filament per volume	-
Aggregates morphology (size)	Deq (μm)	Aggregate equivalent diameter	$D_{eq} = 2F_{Cal}\sqrt{\dfrac{A}{\pi}}$
	Per (μm)	Aggregate perimeter	$P = N_{Per} \times 1.1222 \times F_{Cal}$
	Length (μm)	Aggregate length	$Length = F_{max} \times F_{Cal}$
	Width (μm)	Aggregate width	$Width = F_{min} \times F_{Cal}$
	Area (μm^2)	Aggregate area	$A = N_{Obj} \times F_{Cal}$
Aggregates morphology	FF	Aggregate form factor	$FF = \dfrac{P^2}{4\pi A}$
	Conv	Aggregate convexity	$Conv = \dfrac{P_{Conv}}{P}$
	Comp	Aggregate compactness	$Comp = \dfrac{\sqrt{\dfrac{4}{\pi}A}}{F_{max}}$
	Round	Aggregate roundness	$Round = \dfrac{4\pi A}{P_{Conv}^2}$
	Sol	Aggregate solidity	$Sol = \dfrac{A}{A_{Conv}}$
	Ext	Aggregate extent	$Ext = \dfrac{A}{W_{BB} \times L_{BB}}$
	Ecc	Aggregate eccentricity	$Ecc = (4\pi^2)\,(M_{2x} - M_{2y})^2 + 4M_{2xy}^2$
	Rob	Aggregate robustness	$Rob = \dfrac{2er_{obj}}{\sqrt{A}}$
	LrgC	Aggregate largest concavity	$LrgC = \dfrac{2er_{comp}}{\sqrt{A}}$

	RelArea	Flocs ratio between hole and object area	$\text{RelArea} = \dfrac{A_h}{A}$
Number of aggregates content	TA/Vol (mm²/μL)	Total area of aggregates per volume	-
	A_i/Vol	Area of aggregates per volume	-
	Nb/Vol	Total number of aggregates per volume	-
	%Nb_i	Number percentage of the aggregates	$\%Nb_i = \dfrac{\sum_{i=1}^{Nclass} Nbi}{TA}$
	%A_i	Area percentage of the aggregates	$\%A_i = \dfrac{\sum_{i=1}^{Nclass} Ai}{TA}$

i subscript represents each size class of aggregates: small, intermediate and large.

*$L = (N_{Thn} + N_{Int}) \times 1.1222 \times F_{Cal}$; F_{Cal} is the calibration factor (μm per pixel); N_{Per} is the pixel sum of the aggregate boundary; P is the aggregate perimeter; F_{max} is the aggregate maximum Feret Diameter; F_{min} is the aggregate minimum Feret Diameter; N_{obj} is the aggregate pixel sum; A is the aggregate area; P_{Conv} is the aggregate Convex Envelope perimeter; A_{Conv} is the aggregate Convex Envelope area; W_{BB} is the aggregate Bounding Box width; L_{BB} is the aggregate Bounding Box length; M_{2X} and M_{2Y} are the aggregate central second moments with respect to x-axis and y-axis respectively; M_{2XY} is the aggregate second horizontal and vertical order moment; er_{obj} is the number of erosions needed to delete the aggregate; er_{comp} is the number of erosions needed to delete the complement of the aggregate in relation to its convex envelope; A_h is the aggregate holes area; A_i is area of each aggregate belonging to the i size class; Nb_i is number of each aggregate belonging to the i size class; Nb is the total number of aggregates; L is the filament length; Nb_{thn} is the pixel sum of each thinned filament; N_{Int} is the number of filaments intersections; 1.1222 is used in order to homogenize the different angles of filaments.

3.1.5 Data analysis

Statistical Analysis

Statistical analysis were applied for data to characterize the control phase and highlight the main impacts of the selected toxic compounds on SBR performance and biomass physicochemical charateristics. The efficiency removal of the compounds was assessed by the following equation,

$$\%\text{Compound removal} = \frac{(\text{Concentration,influent} - \text{Concentration,efluent})}{\text{Concentration,influent}} * 100 \tag{3.1}$$

Significant differences were determined by analysis of variance (ANOVA), using Tukey's post-hoc test in SPSS 26.0 to verify whether there was a significant difference in the removal of COD, NH_4^+-N, NO_2^--N, and NO_3^--N and selected toxic compounds IBU, DESL and ATZ between the phases, and to investigate whether there were differences in the concentration of EPS and its components.

For experiment with IBU, statistical analysis was used for phase I (17 samples), phase II (17 samples), and phase III (23 samples), while for DESL and ATZ experiments, 15 samples in each phase were collected. For all experiments the results are given as mean and one standard deviation.

Spearman rank-order correlation coefficient was used to identify the strength of the relationship between EPS and its components and ESS, SVI, and QIA parameters for the IBU experiment. The values of the correlation coefficients vary between +1.00 and −1.00. Both extremes represent perfect relationships between the variables, and 0.00 indicates no relationship.

Principal Component Analysis

For experiments with DESL and ATZ, the principal component analysis (PCA) was performed for the SBR physicochemical parameters, EPS and its components, and the main QIA morphological parameters, as shown in Table 3.3. A total of 60 observations and 19 variables were used to compose the dataset matrix. The goal of the employed PCA was to establish key interrelationships between the parameters that compose the dataset matrix and found clusters that describe each stage of the experimental period. The PCA was performed with Matlab 8.5 software (The MathWorks, Inc. Natick, USA).

Table 3.3 – Parameters used in the PCA analysis for experiments with DESL and ATZ.

| N | PARAMETER | |
	DESL	ATZ
1	SVI_{30}	SVI_{30}
2	MLSS	PN/PS LB-EPS
3	PS LB-EPS	PN/PS TB-EPS
4	PN LB-EPS	PN/PS EPS
5	HAS LB-EPS	PS LB-EPS
6	LB-EPS	PN LB-EPS
7	PS TB-EPS	LB-EPS
8	PN TB-EPS	PS TB-EPS
9	HAS TB-EPS	PN TB-EPS
10	TB-EPS	TB-EPS
11	Total EPS	Total EPS
12	TL/Vol	TL/Vol

13	TL/MLSS	TL/MLSS
14	Deq_{sml}	Deq_{sml}
15	Deq_{int}	Deq_{int}
16	Deq_{larg}	Deq_{larg}
17	$\%A_{sml}$	$\%A_{sml}$
18	$\%A_{int}$	$\%A_{int}$
19	$\%A_{larg}$	$\%A_{larg}$

Partial least square regression

In the current study, the explanatory variables dataset (matrix X) was composed only of the QIA data (Table 3.4) to assess the PS and PN LB-EPS, PS and PN TB-EPS, LB-EPS, TB-EPS, and total EPS that formed the response matrix Y. For PLS1, it was used 60 samples (global data), and for PLS2, it was used 15 samples (samples per phase) to perform each PLS regression. The variable importance in PLS projections (VIP) was used as the method for variable selection. It is generally accepted that a variable should be selected if the VIP value is greater than one (Gosselin *et al.*, 2010); however, it has been found that the most relevant variables that influence PLS results can have VIP values slightly below one (Chong and Jun, 2005), in such wise, the main variables were selected for VIP > 0.80. The maximum number of latent variables (LV) allowed for each PLS1 model was set to half of the training model observations (n). In contrast, for PLS2, the maximum number of LV was set as the number of training model observations (n) of PLS2, and finally, in both PLS models, cross-validation was used for selecting the optimal LV. The PLS models were iteratively computed at 5 thousand using random samples divided into 2/3 for the training dataset (67% of the observations to calibrate the models) and 1/3 for the validation dataset (33% of the observations to validate the final model).

Furthermore, the goodness of model fit (R^2 coefficient) was measured between observed and predicted Y values for the overall set. The number of variables of matrix X was reduced according to the methodology adopted by Costa *et al.* (2022). The best model was selected considering the R^2 of the different datasets (training, validation, and overall), the root mean squared error of prediction (RMSEP) and residual prediction deviation (RPD) of the predictive model for the overall (training and validation) dataset. All these multivariate statistical analyses were performed in Matlab 9.2 (The Mathworks, Natick, MA).

Table 3.4 – Morphological parameters obtained in the QIA technique and used to predict EPS content.

Main descriptor group	Parameter	Description	Matrix
Filamentous bacteria content	TL/Vol	Total filaments length per volume	Predictor (X)
	TL/TA	Total filaments length per total area of flocs	
	TL/MLSS	Total filaments length per mixed liquor suspended solids	
	Nb_{int}/Vol	Number of filaments intersections per volume	
	Nb_{fil}/Vol	Number of filaments per volume	
	Nb_{thn}/Vol	Pixel sum of each thinned filament per volume	
Aggregates morphology (size)	Deq_{sml}	Equivalent diameter of small aggregates	
	Deq_{int}	Equivalent diameter of intermediate aggregates	
	Deq_{larg}	Equivalent diameter of large aggregates	
	Per_{sml}	Perimeter of small aggregates	
	Per_{int}	Perimeter of intermediate aggregates	
	Per_{larg}	Perimeter of large aggregates	
	$Length_{sml}$	Length of small aggregates	
	$Length_{int}$	Length of intermediate aggregates	
	$Length_{larg}$	Length of large aggregates	
	$Width_{sml}$	Width of small aggregates	
	$Width_{int}$	Width of intermediate aggregates	
	$Width_{larg}$	Width of large aggregates	
	$Area_{sml}$	Area of small aggregates	
	$Area_{int}$	Area of intermediate aggregates	
	$Area_{larg}$	Area of large aggregates	
Aggregates morphology	FF_{sml}	Form factor of small aggregates	
	FF_{int}	Form factor of intermediate aggregates	
	FFlarg	Form factor large aggregates	
	$Conv_{sml}$	Convexity of small aggregates	
	$Conv_{int}$	Convexity of intermediate aggregates	
	$Conv_{larg}$	Convexity large aggregates	
	$Comp_{sml}$	Compactness of small aggregates	
	$Comp_{int}$	Compactness of intermediate aggregates	
	$Comp_{larg}$	Compactness large aggregates	
	$Round_{sml}$	Roundness of small aggregates	

	Round$_{int}$	Roundness of intermediate aggregates	
	Round$_{larg}$	Roundness large aggregates	
	Sol$_{sml}$	Solidity of small aggregates	
	Sol$_{int}$	Solidity of intermediate aggregates	
	Sol$_{larg}$	Solidity large aggregates	
	Ext$_{sml}$	Extent of small aggregates	
	Ext$_{int}$	Extent of intermediate aggregates	
	Ext$_{larg}$	Extent of large aggregates	
	Ecc$_{sml}$	Eccentricity of small aggregates	
	Ecc$_{int}$	Eccentricity of intermediate aggregates	
	Ecc$_{larg}$	Eccentricity of large aggregates	
	Rob$_{sml}$	Robustness of small aggregates	
	Rob$_{int}$	Robustness of intermediate aggregates	
	Rob$_{larg}$	Robustness of large aggregates	
	LrgC$_{sml}$	Largest concavity of small aggregates	
	LrgC$_{int}$	Largest concavity of intermediate aggregates	
	LrgC$_{larg}$	Largest concavity of large aggregates	
	RelArea$_{sml}$	Flocs ratio between hole and object area of small aggregates	
	RelArea$_{int}$	Flocs ratio between hole and object area of intermediate aggregates	
	RelArea$_{larg}$	Flocs ratio between hole and object area of large aggregates	
Number of aggregates content	TA/Vol	Total area of aggregates per volume	
	Area/Vol$_{sml}$	Area of small aggregates per volume	
	Area/Vol$_{int}$	Area of intermediate aggregates per volume	
	Area/Vol$_{larg}$	Area of large aggregates per volume	
	Nb/Vol$_{sml}$	Total number of small aggregates per volume	
	Nb/Vol$_{int}$	Total number of intermadiate aggregates per volume	
	Nb/Vol$_{larg}$	Total number of large aggregates per volume	
	%Nb$_{sml}$	Number percentage of small aggregates	
	%Nb$_{int}$	Number percentage of intermadiate aggregates	
	%Nb$_{larg}$	Number percentage of large aggregates	
	%A$_{sml}$	Area percentage of small aggregates	

	%A$_{int}$	Area percentage of intermadiate aggregates	
	%A$_{larg}$	Area percentage of large aggregates	
Extracellular polymeric substances	PS LB-EPS	Polyssacharide of loosely bound extracellular polymeric substances	Response (Y)
	PN LB-EPS	Protein of loosely bound extracellular polymeric substances	
	PS TB-EPS	Polyssacharide of tightly bound extracellular polymeric substances	
	PN TB-EPS	Protein of tightly bound extracellular polymeric substances	
	LB-EPS	Loosely bound extracellular polymeric substances	
	TB-EPS	Tightly bound extracellular polymeric substances	
	Total EPS	Total extracellular polymeric substances	

CHAPTER 4 - EFFECT OF IBUPROFEN ON EXTRACELLULAR POLYMERIC SUBSTANCES (EPS) PRODUCTION AND COMPOSITION, AND ASSESSMENT OF MICROBIAL STRUCTURE BY QUANTITATIVE IMAGE ANALYSIS

4.1 Introduction

AS system is the most common biological process found in WWTP worldwide. Meanwhile, in this system, the removal of some micropollutants is not fully achieved as in the particular case of IBU (Ternes, 1998). Furthermore, IBU has been associated with decrease in microbial activity, hence lowering the capacity of AS systems to remove organic matter and nutrients (Jia *et al.*, 2020; Pasquini *et al.*, 2013). Previous studies have investigated the ability of biological processes to degrade IBU under different conditions (Amariei *et al.*, 2017; Zupanc *et al.*, 2013). However, the impact of long-term IBU exposure on EPS production and composition, as well as on the AS floc structure, remains unexplored.

As EPS clearly play a significant role in AS by contributing to flocculation, settling, dewatering and metal binding (Liu and Fang, 2003; More *et al.*, 2014; Song *et al.*, 2014), and also plays an important role in protecting aggregated biomass against environmental disturbances (e.g. toxic compounds), investigations encompassing IBU effects on EPS yield and microbial aggregate structure are of considerable importance.

Secretion of EPS by bacteria under pharmaceutical compounds exposure can delay or prevent toxicants reaching microbes (Sheng *et al.*, 2010; Tian *et al.*, 2019). However, it is uncertain how microbial aggregation properties change when exposed to IBU. Therefore, these changes require further investigation, as also their effect on the performance of biological systems. AS systems are often affected by common dysfunctions related to the overproduction of EPS, including zoogleal (or viscous) bulking, making the density of AS aggregates closer to that of the surrounding water, thus decreasing settling ability (Jenkins *et al.*, 2003).

Microscopy examination coupled to QIA is particularly essential in monitoring and controlling AS systems. As a result, this technique is becoming widespread for the characterization of the morphology of AS microbial aggregates and the evaluation of AS status. QIA has recently allowed the identification of different types of bulking (Mesquita *et al.*, 2011), demonstrating the usefulness of this methodology as a fast, simple and effective way of detecting deviating conditions in AS.

Taking the above into consideration, the main goal of this chapter was to investigate the response of AS to IBU exposure. Additionally, to clarify the EPS protection role towards pharmaceutical compounds, EPS composition and production was assessed, as well as the properties of the microbial aggregates. This work brings a new insight into the effects of IBU on AS floc structure (as assessed by QIA methodologies). Moreover, the relationship between the morphology of aggregates and the type and composition of EPS is of major interest and can contribute to timely decisions in AS treating pharmaceutical compounds, which includes IBU.

4.2 Results and discussion

This subsection presents the results of an SBR with AS operated with synthetic wastewater containing IBU to investigate the biomass stress-responses under long-term IBU exposure. There were 3 different phases: phase I as the control without IBU for 56 days; phase II (40 days); and phase III (60 days) containing IBU at 10 and 5 mg L^{-1} each. The overall performance of the SBR as well as the EPS in terms of PS, PN, and HAS were estimated. In addition, morphological parameters of microbial aggregates in the presence of IBU (phase II and phase III) were assessed by QIA.

4.2.1 SBR performance

Through phase I, the effluent COD was <40 mg L^{-1} (Figure 4.1a), which means that COD removal efficiency was stable and reached an average of 96% (SI - Table S4.1). With IBU (phase II), the effluent COD ranged from 40 to 600 mg L^{-1}, and from 95 to 646 mg L^{-1} in phase III, where the COD average removal efficiency decreased on average to 71 and 65%, respectively (SI - Table S4.1).

Ammonium ions (NH_4^+-N) were almost completely oxidized in phase I, with concentrations in the effluent of <1.6 mg L^{-1} (Figure 4.1b), and therefore removal efficiencies of 99% were obtained (SI - Table S4.1). In phases II and III, higher NH_4^+-N effluent concentrations (Figure 4.1b) and accordingly lower removal efficiencies (SI - Table S4.1) of 77 and 71% were obtained, respectively. Nitrite (NO_2^--N) concentrations remained almost unchanged throughout the experiments (Figure 4.1b) due to rapid transformation to nitrate (NO_3^--N). However, NO_2^--N concentration increased on average from 0.1 mg L^{-1} during phase I to 0.7 mg L^{-1} during phase II and III (SI - Table S4.1). Regarding effluent NO_3^--N concentration (Figure 4.1b), a decreasing trend occurred throughout the entire experiment, with higher concentrations being obtained in the absence of IBU (phase I), ranging from around 7 to 3 mg L^{-1}. On average, effluent NO_3^--N concentration was 4.6 mg L^{-1} in phase I, i.e. twice the concentration for phase II and 10 fold the concentration obtained for phase III (SI - Table S4.1).

Statistical results (ANOVA and Tukey HSD test) also indicated that COD and NH_4^+-N removal efficiencies were significantly different in phase I from both phase II and III (SI - Table S4.2 and S4.3). IBU at concentrations of 10 and 5 mg L^{-1} significantly affected (p < 0.05) the metabolism of

heterotrophic microorganisms, ammonia-oxidizing bacteria (AOB) and nitrite-oxidizing bacteria (NOB), with a decrease of both organic matter removal and ammonia oxidation.

The ability of the biomass to remove IBU from the liquid phase was also investigated, and effluent IBU concentrations of <5 mg L^{-1} (phase II) and 4 mg L^{-1} (phase III) were achieved (Figure 4.1c). Consequently, average removal efficiencies of 58 and 50% were accomplished (SI - Table S4.1). In this case, statistical results indicated that IBU removal efficiencies were not significantly different between phase II and III (SI - Tables S4.2 and S4.3).

We have found that the removal efficiencies of COD and NH_4^+-N during phases with IBU feeding decreased significantly compared with the control phase without IBU feeding, indicating that the selected IBU concentration significantly inhibits SBR biomass activity. Accumulation of NO_2^--N and the decrease of NO_3^--N during phases II and III also indicated that IBU disturbs the biomass in the nitrification process. These findings are consistent with previous works that gave similar removal data for both COD and NH_4^+-N, where SBR systems operated in the presence of 5 and 1 mg L^{-1} IBU (Jia *et al.*, 2020; Pasquini *et al.*, 2013). Additionally, similar results of decreasing NO_3^--N concentration were seen by Roh *et al.* (2009) in a nitrifying AS system with IBU exposure. Accordingly, it seems reasonable to infer that IBU is responsible for dysfunction in nitrification, hindering both AOB and NOB activity.

The removal efficiencies achieved during these investigations agree with those obtained in the operation of an SBR with AS during treatment with 500 µg L^{-1} IBU (Peng *et al.*, 2019). Moreover, IBU removal in AS systems has been shown to be particularly influenced by the microbial community (Men *et al.*, 2017; Peng *et al.*, 2019). Additionally, once a long-term exposure to IBU triggers the development of IBU degrading microorganisms (Cy *et al.*, 2020; Zhou *et al.*, 2019), one can explain the higher biodegradation ability of IBU in phase II (10 mg L^{-1}). Many investigations show the role of heterotrophic and AOB from AS system in degrading IBU; these reports suggest that AOB is not involved in IBU biodegradation, and it seems that heterotrophic microorganisms play a crucial role (Jia *et al.*, 2020; Roh *et al.*, 2009; Men *et al.*, 2017).
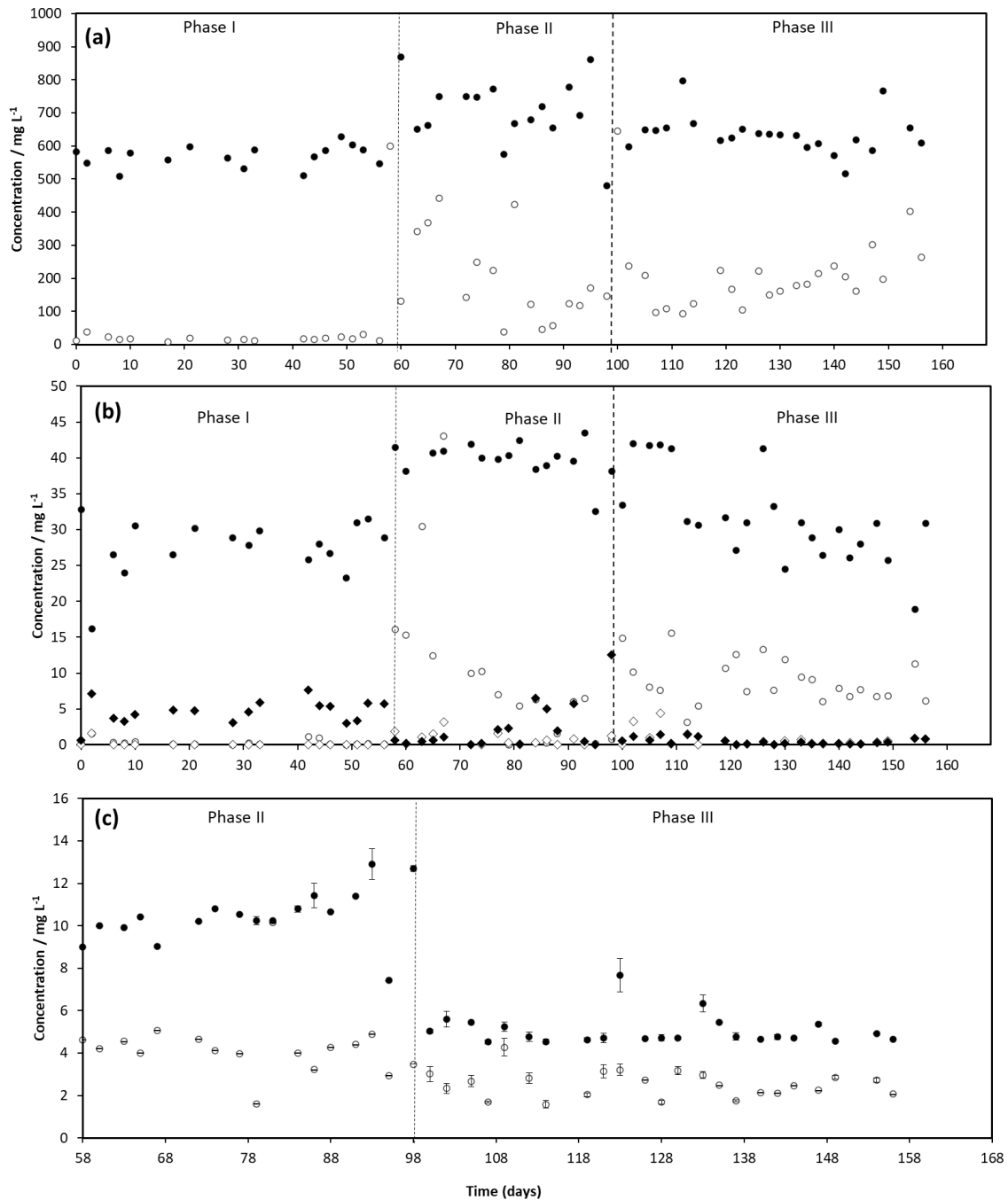
Figure 4.1 – (a) COD concentration (mg L^{-1}) in SBR along phases I-III. COD concentration (mg L^{-1}) in the inlet feeding (●), and in the effluent (o); (b) NH$_4^+$-N, NO$_2^-$-N, and NO$_3^-$-N concentration profile along phases I-III. NH$_4^+$-N concentration (mg L^{-1}) in the inlet feeding (●), in the effluent (o), NO$_2^-$-N in the effluent (◇), and NO$_3^-$-N in the effluent (◆); (c) IBU concentration (mg L^{-1}) in SBR along phases II and III. IBU concentration (mg L^{-1}) in the inlet feeding (●), and in the effluent (o).

4.1.1 Effect of IBU on EPS production and composition

The phase I had an average LB-EPS content of 138.30 mg EPS g_{MLVSS}^{-1}, whereas phase II had an average of 20.02 mg EPS g_{MLVSS}^{-1}, and phase III 38.92 mg EPS g_{MLVSS}^{-1} (Figure 4.2a, SI - Table S4.4), indicating that LB-EPS content decreased as IBU concentration increased, which suggests a negative action on LB-EPS content production. Accordingly, LB-EPS content was significantly different ($p < 0.05$) in phase I (SI - Tables S4.5 and S4.6). Regarding TB-EPS content, similar results were obtained during phase I and II (average of 88.49 mg g_{MLVSS}^{-1} and 92.37 mg g_{MLVSS}^{-1}, respectively), and a lower content during phase III (average 39.16 mg EPS g_{MLVSS}^{-1}) (Figure 4.2a, SI - Table S4.4), thus showing a significant ($p < 0.05$) difference between only phase II and phase III (SI - Tables S4.5 and S4.6). During phases II and III, IBU affected the biomass by varying the amount of EPS produced. Increase of TB-EPS content in phase II (Figure 4.2a) may be assigned to the high relative abundance of large aggregates related to the overproduction of EPS (An *et al.*, 2016; Zhang *et al.*, 2019). For phase III, a decrease in TB-EPS occurred compared with phase I, suggesting that IBU directly interferes with AS metabolic activity (Figure 4.2a). Similar results were reported by Pasquini *et al.* (2013) with concentrations varying from 0.1 to 5 mg L^{-1}, and a reduction in the TB-EPS production was also observed.

Regarding LB-EPS content, HAS represented 53 and 58% for phase I and III, respectively, followed by PN (with 41 and 36%, respectively), and PS at a small proportion (6%) for both phases (Figure 4.2b, SI - Table S4.4). PN was the larger component in phase II, representing on average 50%, followed by HAS and PS (averages of 43 and 7%, respectively; Figure 4.2b, SI - Table S4.4). A significant difference ($p < 0.05$) was recorded for PS, PN, and HAS in the presence of IBU. Nevertheless, the content of PS, PN, and HAS did not change significantly ($p < 0.05$) between phase II and phase III (SI - Tables S4.5 and S4.6).

TB-EPS components showed the same behavior as LB-EPS components (Figure 4.2c). Although TB-EPS components concentration changed in all phases, no significant difference ($p < 0.05$) was found for PS (SI - Tables S4.5 and S4.6). A significant difference was obtained for HAS just between phase I and phase III. PN gave the highest content when IBU has been added in phase II (Figure 4.2c, SI - Table S4.4), and its significant increase ($p < 0.05$) (SI - Tables S4.5 and S4.6) could probably be explained as a strategy of microorganisms defence against harsh conditions (Kong *et al.*, 2017; Zhou *et al.*, 2019). For phase III, a decrease in TB-EPS occurred compared with phase I, suggesting that IBU directly interferes with AS metabolic activity - similar results had been obtained by Pasquini *et al.*, 2013)

when concentrations varying from 0.1 to 5 mg L^{-1} were tested, and a reduction in the TB-EPS production was also observed.

There was a trend regarding the EPS components concerning the concentration of HAS> PN> PS for phases I and III, and for phase II of PN> HAS> PS. Previously it has been suggested that PN and PS are the major components of EPS (Frølund *et al.*, 1996); however, recent works have found greater amounts of PN and HAS in biological systems (Oliveira *et al.*, 2020; Wilén *et al.*, 2003). Indeed, different designs and operational conditions of AS result in different EPS levels. The EPS composition difference can also be attributed to the type of extraction procedure (which strongly affects the yield) and the quantification method to evaluate the extracted EPS chemical composition. In the presence of toxic substances, an increase in EPS production can be considered as a defence mechanism for microorganisms. Accordingly, Zhou *et al.* (2019) found an increase in EPS production for IBU at levels varying from 1 to 5 mg L^{-1}. However, some toxic substances inhibit EPS production; Badireddy *et al.* (2008) found a significant reduction of EPS when *Brevundimonas diminuta* was exposed to bismuth dimercaptopropanol. Besides, the proportion of PN/PS, which is generally used to indicate hydrophobicity, had a higher value (PN/PS = 6.4) for phase II compared to the other two phases (PN/PS = 4.3 for phase I and PN/PS = 2.9 for phase III), suggesting stronger hydrophobicity and the possibility of having more sites for IBU adsorption (Zhang *et al.*, 2019).
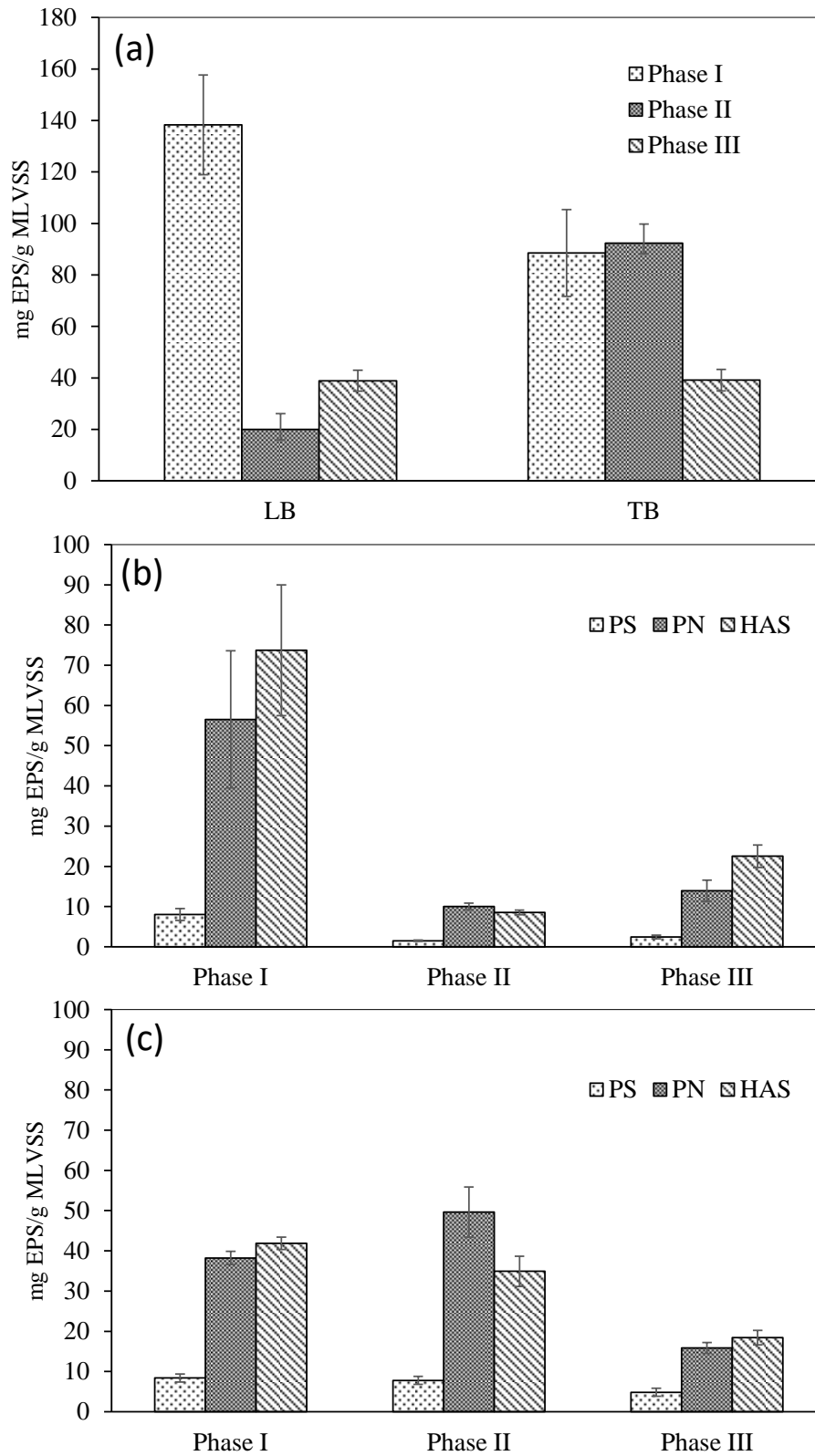
Figure 4.2 – (a) LB-EPS and TB-EPS for different phases of SBR operation. Quantities of LB-EPS and TB-EPS in terms of PS and PN, and HAS content; (b) PS, PN, and HAS content of the LB-EPS; (c) PS, PN, and HAS content of the TB-EPS.

4.1.2 Settling ability and morphological properties

The aggregate area distribution analysis clarifies the nature of aggregates within the biomass (Figure 4.3). During phase I, there was an expected predominance of intermediate aggregates and residual percentages of large aggregates (data not shown), agreeing with the results of Mesquita *et al.* (2011). The significant presence of intermediate aggregates (%Area$_{int}$ ranging from 77 to 47%) until day 77 of phase II, concerning the small (%Area$_{sml}$ ranging from 3 to 7%) and large aggregates (%Area$_{larg}$ ranging from 20 to 46%), indicated the predominance of normal aggregates structures (despite the decreasing trend). From day 77 until day 91, there was a predominance of large aggregates in the system (%Area$_{larg}$ of around 61% on average). These results are also associated at this point to the sharp increase of both MLSS (from 2.3 to 4.5 g L^{-1}) and TA/Vol (from 2.6 to 9.2 mm^2 μL^{-1}) in the same period of operation (data not shown), previously reported as commonly coupled to the growth of large aggregates (Mesquita *et al.*, 2011). From day 84 onwards, the aggregates were accompanied by a significant number of protruding filaments as visualized by microscopy (Figure 4.4c and d), disturbing the image acquisition process.

In phase III, aggregate area distribution analysis showed the same trend as phase II for intermediate and large aggregates, although large aggregates were never predominant in the biological system throughout the experimental period (with the exception of the last samples). A decrease in intermediate aggregates (%Area$_{int}$ from 88 to 45%) and an increase in the large aggregates (%Area$_{larg}$ from 7 to 43%) occurred from day 105 to day 119, pointing to a global trend to form larger structures (Figure 4.3). This behavior was accompanied by a sharp decrease of MLSS (from 3.3 to 1.7 g L^{-1}), indicating a washout phenomenon and a minor decrease of TA/Vol (from 2.6 to 2.0 mm^2 μL^{-1}), due to the low representation of large aggregates in the system (data not shown). Despite this abrupt change, from day 119 until the end of phase III, and in general, intermediate aggregates dominated in the biological system (%Area$_{int}$ of ≈49% on average), with a high contribution of large structures (%Area$_{larg}$ of ≈37% on average). Again, microscopy showed that the aggregates were accompanied by a significant proliferation of protruding filaments (Figure 4.5c-d).
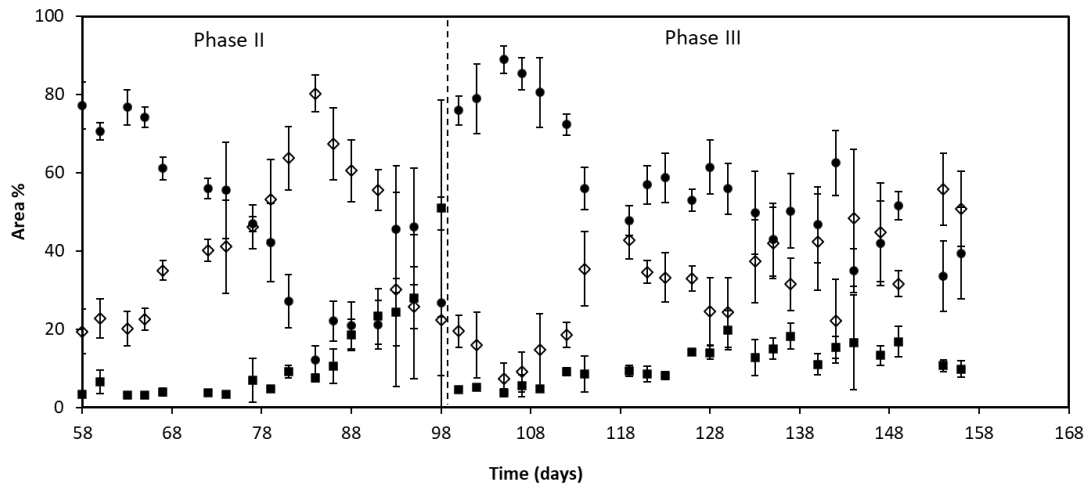
Figure 4.3 – Area percentage behavior for phases II and III for small aggregates (■); intermediate (●); and large aggregates (◇).
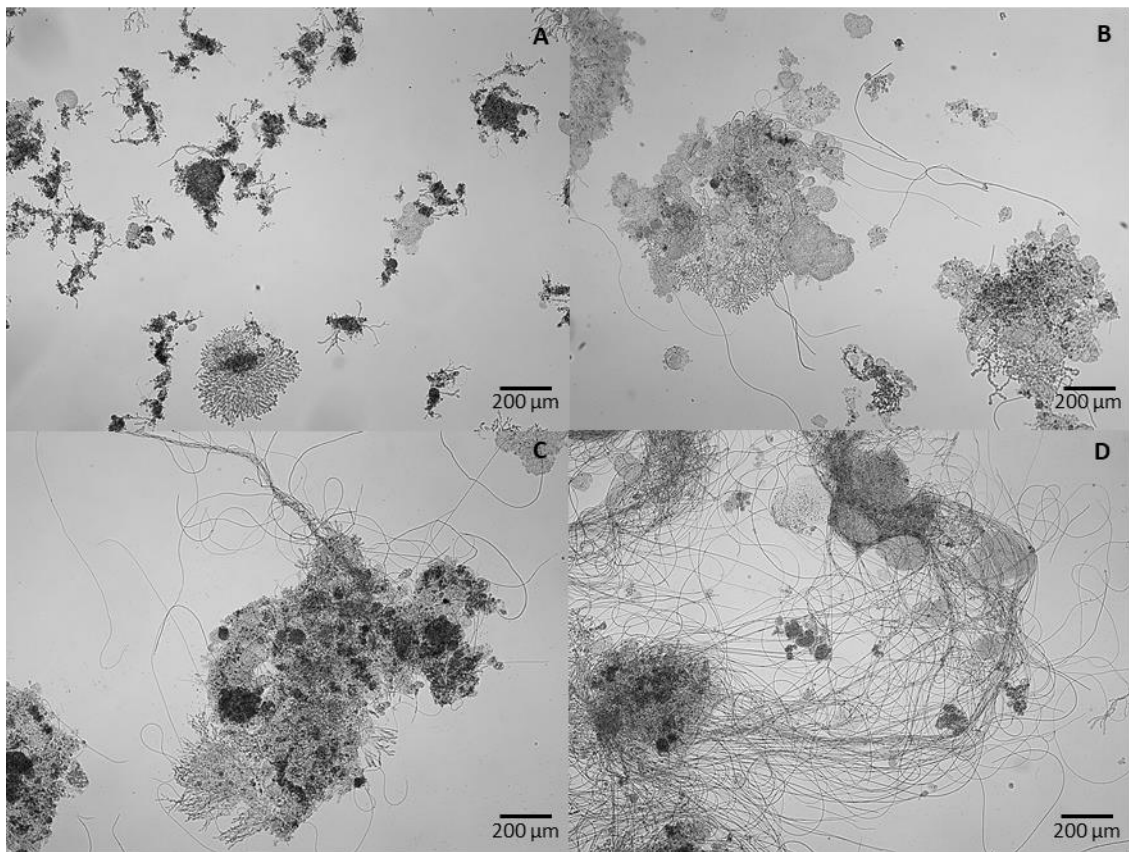
Figure 4.4 – Microscopic view of aerobic sludge during reactor operation along phase II (a) Day 58, (b) Day 77, (c) Day 84 – dilution 1:4 and (d) Day 91. Size bar is equivalent to 200 micrometers.
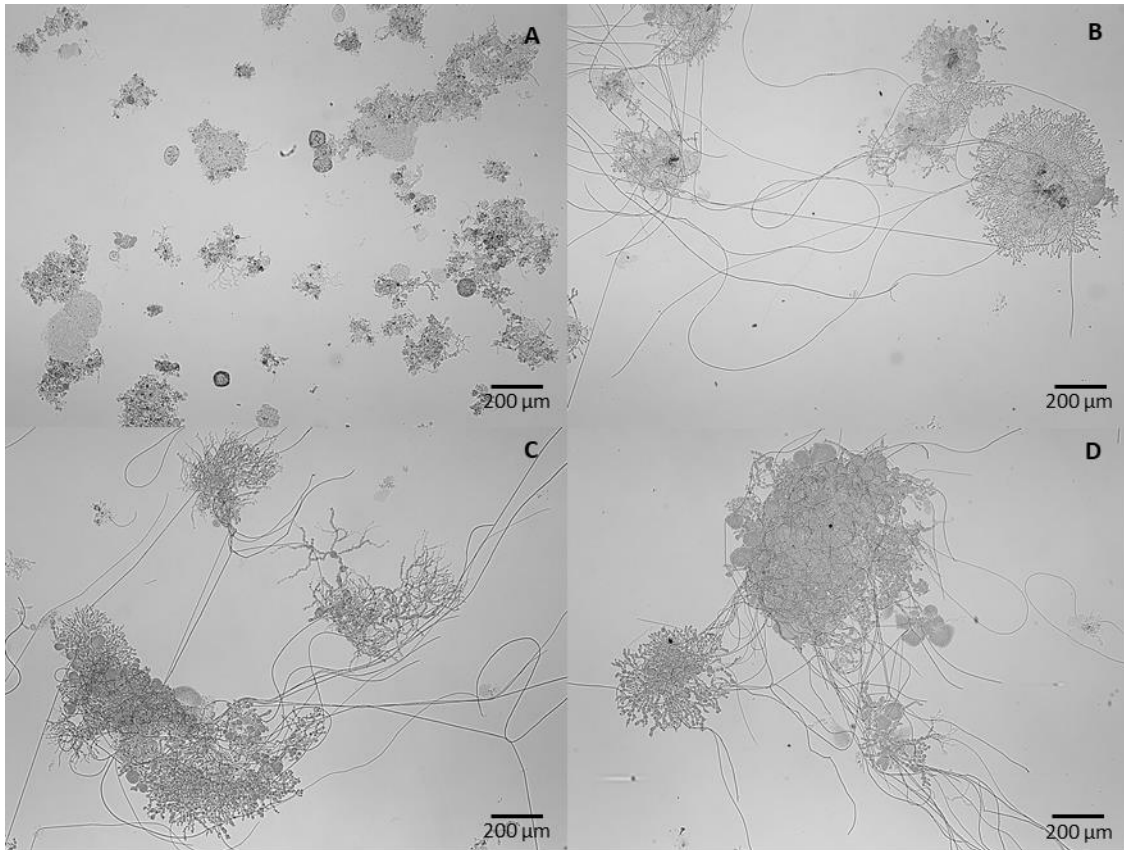
Figure 4.5 – Microscopic view of aerobic sludge during reactor operation along phase III (a) Day 100, (b) Day 119 – dilution 1:4, (c) Day 133 – dilution 1:10, and (d) Day 156 – dilution 1:10. Size bar is equivalent to 200 micrometers.

The SVI results during phase I were consistently lower than 150 mL g^{-1} (data not shown), the threshold for filamentous bulking, as proposed by Jenkins *et al.* (2003). In the presence of IBU, and at the beginning of phase II and III, the SVI values (Figure 4.6) were lower or close to the threshold considered for filamentous bulking, where combining this information with microscopic inspection (Figure 4.4a and Figure 4.5a) excluded this phenomenon. TL/Vol and the TL/MLSS were also included in this evaluation due to their importance in predicting the SVI (Amaral and Ferreira, 2005). Accordingly, the presence of a filamentous bulking condition was established for values >10 mm µL^{-1} for TL/Vol and 10,000 mm mg^{-1} for TL/MLSS (Jenkins *et al.*, 2003; Amaral and Ferreira, 2005). Regarding Figure 4.6, the values obtained for TL/Vol and TL/MLSS at the beginning of phase II and phase III were lower than the established limits. QIA results corroborated a severe bulking problem (Figure 4.6) from day 84 until the end of phase II (TL/MLSS of 46,000 mm mg^{-1}, and TL/Vol of 195 mm µL^{-1} on average), and from day 119 until the end of phase III (TL/MLSS of 55,000 mm mg^{-1}, and TL/Vol of 64 mm µL^{-1} on average).

Throughout phase II and III, SVI were >150 mL g^{-1} and the existence of a filamentous bulking problem with the development of protruding filamentous bacteria (Figures 4.4 and 4.5) has been verified. These results agree with previous studies reporting bulking problems and morphological dysfunctions in AS systems (Amaral and Ferreira 2005; Mesquita *et al.* 2011). Interestingly, SVI values at the end of phase II decreased again to <150 mL g^{-1}, despite the larger values of TL/Vol and TL/MLSS. This can be attributed to the presence of intermediate and large structures that can settle well, despite their poor structure (combined with high amounts of protruding filaments Figure 4.4c, d). Thus, this is a clear indicator that other factors, such as chemical make-up or colloidal properties, are important in the settling of sludge, as well as EPS composition (Wilén *et al.*, 2008), which will be further discussed. Accordingly, the biomass was no longer accurately assessed by QIA, and thus the long-term IBU exposure at 10 mg L^{-1} led to AS system collapse. On the other hand, at the end of phase III, SVI was always higher than the threshold limit, even with a balance of intermediate and large aggregates in the system (Figure 4.3), demonstrating the strong influence of protruding filamentous bacteria in reducing the sludge settling ability (Figure 4.5c-d).

Statistical analysis based on Spearman's correlation coefficients between SVI, ESS, EPS composition, and image analysis parameters during phases II and III, are shown in Figure 4.7. The heat map shows positive correlation in the blue gradient and negative correlation in the red gradient between these variables. In the supplementary material (SI - Tables S4.7 and S4.8), it is possible to observe the specific values of Spearman's correlation coefficients and their corresponding p-values.
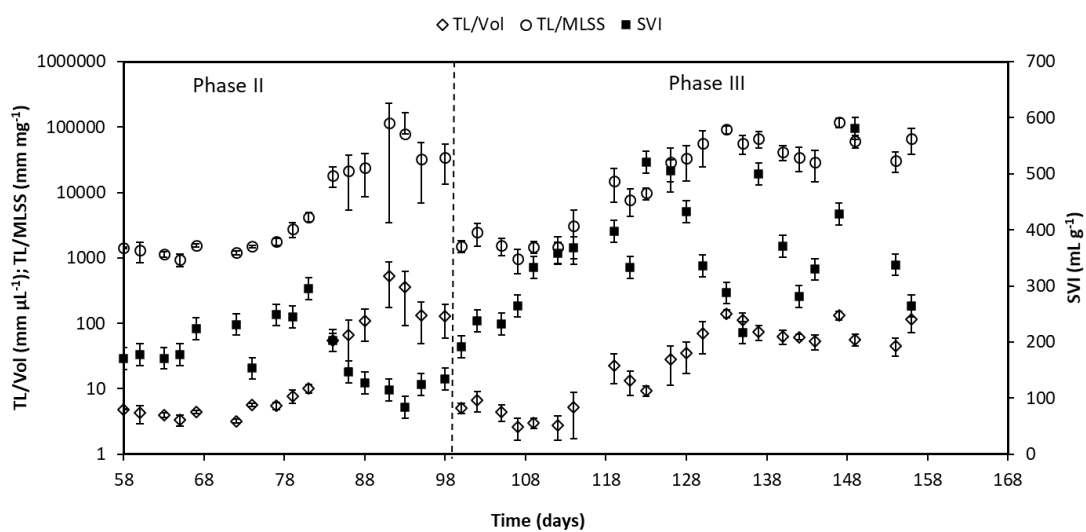
Figure 4.6 – Experimental behavior of TL/Vol (◇); TL/MLSS (○); and SVI (■) for phases II and III.

As previously observed during phase II, high quantities of TB-EPS were obtained, especially PN, which suggest that chemical properties change in the surface of AS. Thus, these variations in EPS may also have influenced the SVI results rather than QIA parameters (as shown in Figure 4.7a). Furthermore, a slight increase in the ESS during phase II occurred. It is likely that large and intermediate aggregates settle faster than small aggregates, which may contribute to the decrease in SVI. The faster settling of the larger flocs associated with a higher concentration of MLSS could also contribute to the low SVI values at the end of phase II (Figure 4.6).

Our results suggest that EPS and its components influence the structure of the aggregates. For phase II, a significant positive correlation was found between intermediate aggregates and HAS LB-EPS and Total LB-EPS (Figure 4.7a and SI - Table S4.7). A trend to large aggregates formation and aggregates with large amounts of filaments was seen that suggest an open floc structure with poor compressibility (Figure 4.4) (Jin *et al.*, 2003). Large aggregate formation can be associated with the high levels of biopolymers produced by biomass since they were positively correlated with the PN-TB, HAS-TB, TB-EPS, and total EPS quantity (Figure 4.7a and SI - Table S4.7). Thus, these results indicate that intermediate and large aggregates contain higher EPS concentrations than small aggregates. Oliveira *et al.* (2020) also observed that EPS had a significant effect on the size distribution of aerobic granular sludge in a full-scale WWTP, with small granules being positively correlated to PN concentration in EPS.

The results suggest that during phase III, the PN TB-EPS level probably had a greater negative influence than other EPS contents regarding dysfunction in bioflocculation (ESS) of the biomass (Figure 4.7b and SI - Table S4.8). PN impacted bioflocculation since they are mainly created by hydrophobic R groups in amino acids promoting flocculation. PN proved to be the main factor determining the aggregation ability of anammox (Hou *et al.*, 2015). PN was also found to play a crucial role in granule formation and stability (McSwain *et al.*, 2005). Higgins and Novak (1997) found that microbial aggregates tend to deflocculate after removing their surface PN. No correlation was found between image analysis parameters and LB-EPS and TB-EPS for phase III (Figure 4.7b and SI - Table S4.8). Nevertheless, a positive correlation was seen only between PS LB-EPS and %Area$_{sml}$. A negative correlation was seen between PS LB-EPS and %Area$_{int}$, suggesting that PS influenced the microbial aggregation properties (Higgins and Novak, 1997).

Due to their physicochemical properties, EPS are involved in microbial aggregates structure through complex interactions, which make this biopolymer bond electrostatically and physically to microbial surfaces. However, the influence of individual EPS components on microbial aggregates

flocculation is complex (Chen *et al.*, 2007; McSwain *et al.*, 2005; Wilén *et al.*, 2008; Hou *et al.*, 2015). Therefore, can be supposed that IBU at 10 mg L^{-1} creates a greater change in the aggregates' structure, instead of IBU at 5 mg L^{-1}. Regarding Figures 4.7a and b, these changes may be associated with the high production of EPS, especially TB-EPS. The correlations suggest that EPS and its components significantly influence aggregates parameters. These findings agree with those of Quintelas *et al.* (2020), showing that a change in the biomass structure occurs when IBU is added at 1, 10, and 20 mg L^{-1}.

Figure 4.7 and SI - Tables S4.7 and S4.8, show that EPS and their components (PS, PN, and HAS) have a critical role in the sludge settleability than the aggregates' morphological structure. The results of our research agree with previous studies demonstrating a positive relationship between SVI content and the content of LB-EPS and TB-EPS (Li and Yang, 2007; Liao *et al.*, 2011). However, the effects of the main components of EPS on the sludge settleability remains unclear, and the results were inconsistent with previous studies. Martinez *et al.* (2000) found that SVI content increased with the PN EPS content, whereas Jin *et al.* (2003) reported that the quantities of PN and PS in EPS were significantly correlated with the SVI, which is in accordance with the results we have obtained. According to Liao *et al.* (2011), EPS can differ in molecular weight and composition, mainly when produced under different conditions by microorganisms in biological systems. Thus, the difference in the concentration EPS components (PS, PN, and HAS) might explain the AS difference in settleability behavior between phases II and III.
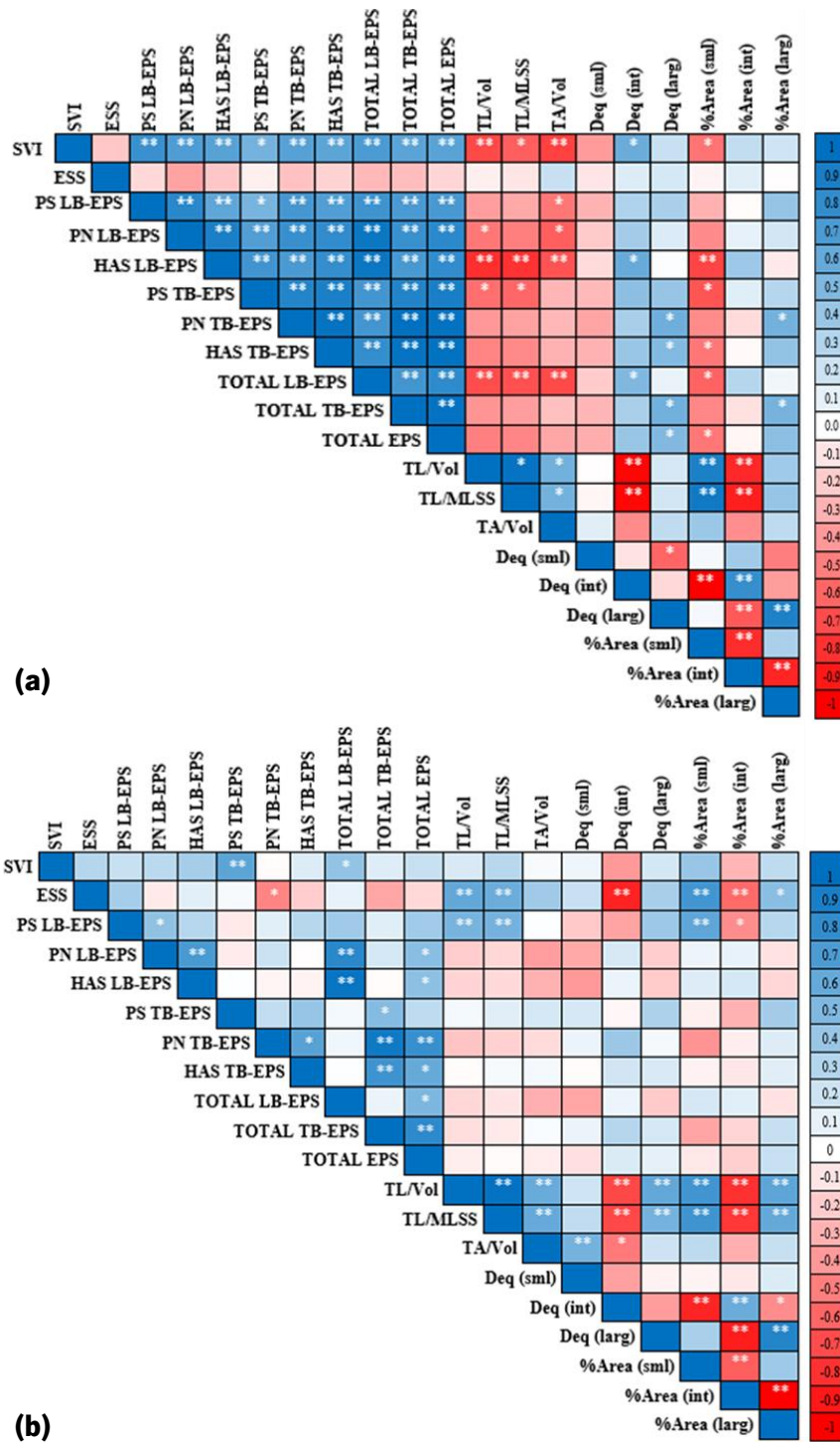
Figure 4.7 – Heat map of Spearman correlation coefficients computed between SVI, ESS, EPS composition, and morphological parameters during (a) phase II (n = 17) and (b) phase III (n = 23). The correlation coefficients' values and directions are displayed according to the colour key: positive correlations as blue gradients from 0 to 1 and negative correlations as red gradients from 0 to -1. Significance of p-values are as followed: $p < 0.01$ represented as **, and $p < 0.05$ represented as *.

4.2 Conclusions

A significant reduction in heterotrophic bacteria activity occured, with a reduced COD removal efficiency and substantial inhibitory effect in the nitrification process, when AS is exposed to IBU during phases II and III. Regarding the removal of IBU in the liquid phase, a reduction in the concentration of 58 and 50% for phases II and III, respectively, was achieved.

A decrease of LB-EPS concentration occurred with increasing IBU concentration. The higher concentration of PN in phase II may be associated with a greater impact on the microbial composition due to the introduction of IBU at 10 mg L^{-1}. The results of PN concentrations and the increase in the PN/PS ratio indicate that PN greatest production in TB-EPS was probably for cellular protection against IBU. EPS plays a significant role in sludge properties, and a significant correlation ($p < 0.05$) was found between SVI and all EPS contents for phase II, which may be associated with a major change in the biomass structure. For phase III, bioflocculation had a significant negative correlation ($p < 0.05$) with PN LB-EPS, and a significant positive correlation was found for sedimentation, ($p < 0.01$) with PS TB-EPS and ($p < 0.05$) with total LB-EPS.

Finally, QIA gave some insight into the changes in the biomass structure correlating well with EPS components. This relationship demonstrates that both LB-EPS and TB-EPS and/or their components (PS, PN, HAS) significantly influence the microbial aggregates' structure.

CHAPTER 5 - EFFECTS OF DESLORATADINE ON ACTIVATED SLUDGE: BEHAVIOR OF EPS AND SLUDGE PROPERTIES

5.1 Introduction

It is known that under toxic conditions, microorganisms in AS can vary the EPS concentration, hence influencing the performance of the biological process (Avella *et al.*, 2010). Thus, it is suggested that EPS can contribute to pharmaceutical compounds' removal from aqueous environments and in the sludge biosorption process, due to abundant functional groups and binding sites (Sheng *et al.*, 2010). However, so far, little information has been available in terms of EPS in AS biomass under DESL exposure.

Beyond traditional techniques to assess the EPS composition, 3D-EEM fluorescence spectroscopy is a rapid, selective and sensitive technique, that offers useful information regarding the fluorescence characteristics of compounds such as protein-like fluorophores and humic-like fluorophores in EPS (Zhu *et al.*, 2015). Furthermore, the composition of EPS has been widely characterized by 3D-EEM spectroscopy since fluorescence characteristics can be applied to elucidate the functional groups and element composition in EPS samples (Miao *et al.*, 2017).

Although the presence and removal of pharmaceutical compounds in WWT systems has been intensively investigated in the last two decades, there is scarce information in the literature on the impact and removal of DESL in AS systems.

In such wise, QIA has proven to be a suitable tool for monitoring biological treatment systems (Amaral *et al.*, 2004), as well as the structural assessment of biological aggregates in AS, including the identification of AS dysfunctions, namely filamentous bulking and non-filamentous bulking phenomenon (Mesquita *et al.*, 2011). Furthermore, methodologies of multivariate statistics, such as principal component analysis (PCA), have become increasingly important in improving biological processes analysis, in organizing and extracting relevant information from such comprehensive datasets (Leal *et al.*, 2021).

Considering the above, the purpose of this chapter is to provide deep insights regarding the impact of DESL on AS systems performance, including the production and composition of EPS. DESL was used in a range of concentrations present in pharmaceutical industry and in hospital wastewaters. QIA and multivariate statistical analysis were applied to improve the biological process evaluation.

5.2 Results and discussion

In this subsection, the overall performance, EPS production, and sludge properties were assessed in a SBR with AS during 139 days, under the presence of DESL (1, 5, and 10 mg L^{-1}). In

addition to chemical methods, the EPS were also analysed by 3D-EEM fluorescence spectroscopy, and PCA were employed to emphasise the relationship between EPS and QIA results.

5.2.1 SBR performance

The concentrations of COD, NH_4^+-N, NO_2^--N, and NO_3^--N during the SBR operation are shown in Figure 5.1a,b. In the absence of DESL (phase I), the COD at the outlet was < 25 mg L^{-1} (Figure 5.1a), with a COD removal efficiency of 96% (on average) (SI - Table S5.1). During phase II and phase III, the COD removal efficiency slightly decreased, on average, to 88 and 87%, respectively (SI - Table S5.1). During phase IV (feeding with 10 mg L^{-1} of DESL), the average COD removal efficiency decreased significantly (p < 0.05) to 78% (SI - Table S5.1-S5.3). The concentration of NH_4^+-N in the effluent was very low during phases I-III (Figure 5.1b), indicating high removal efficiencies around 94-100% (SI - Table S5.1). Higher NH_4^+-N effluent concentrations were found in phase IV, decreasing significantly (p < 0.05) the NH_4^+-N removal efficiency to 71% (on average) (SI - Table S5.1-S5.3). Throughout phases I-II, NO_2^--N concentrations in the effluent were at residual levels, and increased during phases III-IV (Figure 5.1b, SI - Table S5.1). Concerning the NO_3^--N profile in the effluent, an increasing trend occurred along phases I-III and reduced during phase IV (Figure 5.1b, SI - Table S5.1). The present results seem to demonstrate that DESL had a negative impact on biomass activity, which are in agreement with previous works that assessed the effect of pharmaceutical compounds in biological systems, mainly in the organic matter removal (Pasquini *et al.*, 2013), and in nitrification processes (Jia *et al.*, 2020; Peng *et al.*, 2019).

Figure 5.1c shows the profile of DESL concentration and removal efficiency along SBR operation. On average, average removal efficiencies of 75%, 73% and 63% were obtained for DESL during phase II, III and IV, respectively (SI - Table S5.1). In addition, DESL removal efficiencies in phase IV were significantly different (p < 0.05) from phases II-III (SI - Tables S5.2 and S5.3).

71
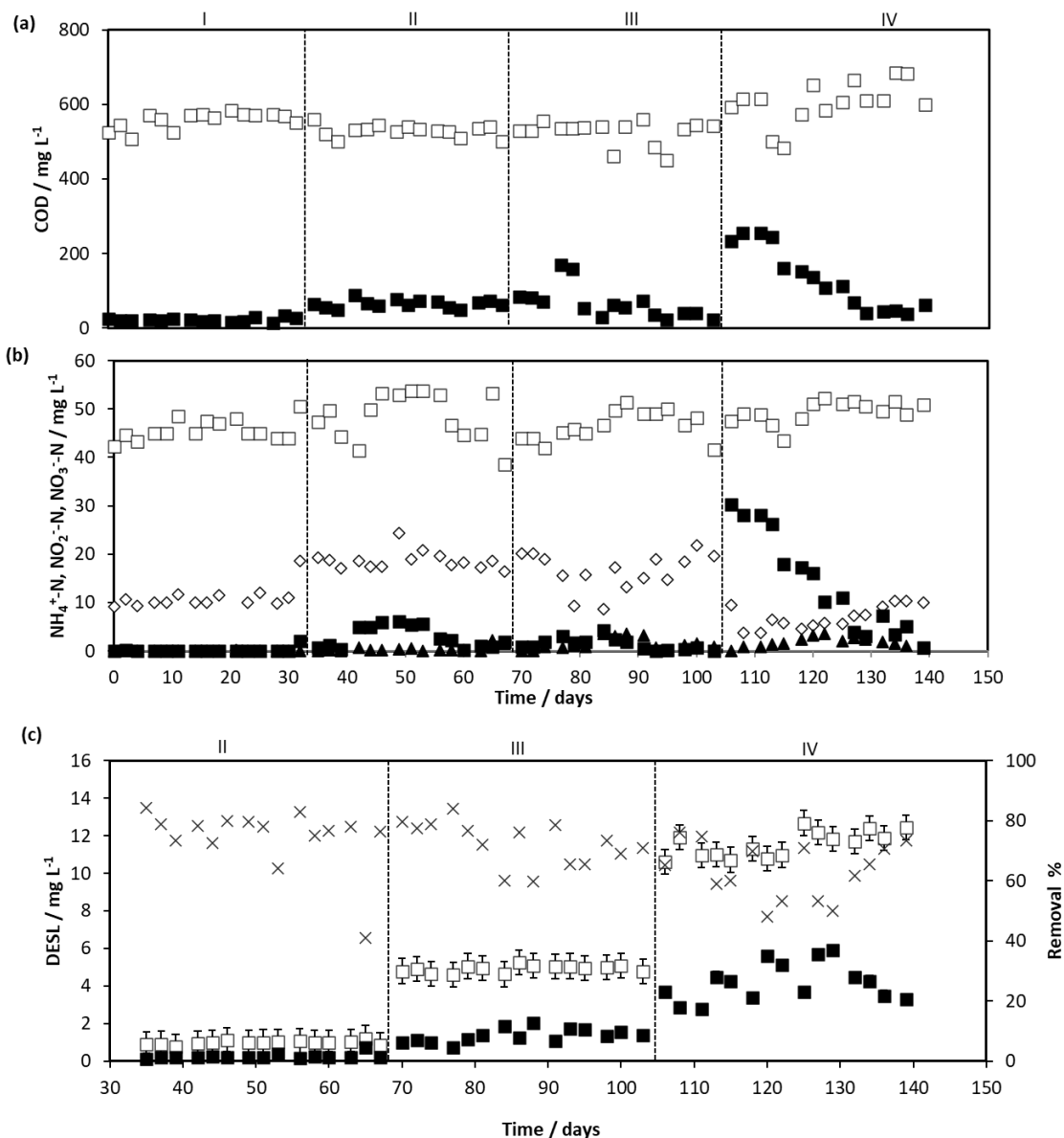
Figure 5.1 – SBR performance profile in terms of COD, NH_4^+-N, NO_2^--N, NO_3^--N and DESL concentration. (a) COD in the inlet feeding (mg L^{-1}) ($\square$), and in the effluent ($\blacksquare$); (b) NH_4^+-N in the inlet feeding (mg L^{-1}) ($\square$), and in the effluent ($\blacksquare$), NO_2^--N in the effluent ($\blacktriangle$), and NO_3^--N in the effluent ($\lozenge$); (c) DESL in the inlet feeding ($\square$), in the effluent ($\blacksquare$), and efficiency removal ($\times$).

DESL has proven to be toxic for organisms of the aquatic trophic chain (Iesce *et al.*, 2019). It was investigated the acute and chronic ecotoxicity of DESL in green alga *Pseudokirchneriella subcapitata*, in planktonic rotifer *Brachionus calyciflorus* abundant in freshwaters, in anostracan crustacean *Thamnocephalus platyurus*, highly sensitive in acute toxicity testing and in cladoceran crustacean *Ceriodaphnia dubia*, often employed in acute and chronic toxicity testing. The results revealed the occurrence of toxic effect in both acute and chronic assays. Regarding acute toxicity testing, DESL was

able to cause 50% of mortality in *B. calyciflorus* at 1.21 mg L^{-1} and *C. dubia* at 1.52 mg L^{-1}, differently from the effects found in *T. platyurus*, requiring a much higher concentration (6.22 mg L^{-1}). On the other hand, chronic toxicity results revealed that DESL was chronically active compound both in *C. dubia*, with a median effective concentration of 9.4 µg L^{-1}, and in the green alga *P. subcapitata* (EC50= 220.2 µg L^{-1}). Accordingly, as AS is composed by a mixed microbial culture, 10 mg L^{-1} of DESL could affect some specific microorganisms, which might explain the decrease in the DESL removal during phase IV. This result corroborates studies where the removal of other antihistamines and psychiatric drugs decreased over time (Boehler *et al.*, 2012; Henning *et al.*, 2019; Kosonen and Kronberg, 2009; Li *et al.*, 2015; Li *et al.*, 2011). The loss of pharmaceutical compounds removal could be attributed to a bacterial shift in the biological process.

5.2.2 EPS production and composition, and assessment by 3D-EEM

Figure 5.2a shows LB-EPS and TB-EPS concentrations. LB-EPS concentration of 49.5 mg g$_{MLVSS}^{-1}$ was achieved during phase I, whereas 100.0, 96.2, and 74.9 mg g$_{MLVSS}^{-1}$ were obtained, on average, for phase II, III and IV, respectively (Figure 5.2a, SI - Table S5.4). Accordingly, LB-EPS content showed significant differences (p < 0.05) between phase I and phases II-III (SI - Tables S5.5, S5.6). During phase IV, LB-EPS decreased, suggesting that 10 mg L^{-1} of DESL can influence the contents of LB-EPS by affecting the metabolism of the microorganisms. Li *et al.* (2011) reported similar results of LB-EPS in SBR when copper Cu(II) was added during a long-term period. LB-EPS increased after adding Cu(II) and then decreased slightly. For these authors, the increase in LB-EPS content indicated a microbial response to relieve the sudden exposure to Cu(II). Indeed, LB-EPS is regarded as the primary surface for contact and interaction with toxic compounds (Ma *et al.*, 2013). Also, according to Miao *et al.* (2017) the increase in toxicity caused by copper oxide (CuO) nanoparticles stimulated the production of EPS, especially LB-EPS, due to their presence in the upper layers of biofilm, and may have functioned as the primary surface for contact and interaction with CuO (Miao *et al.*, 2017). In this way, the decrease of LB-EPS can be attributed to the rise of larger aggregates, leading to the increase of TB-EPS content during phase IV.

From phase I to phase IV, an increase in the TB-EPS content was obtained, reaching 149.5 mg g$_{MLVSS}^{-1}$ in phase IV (Figure 5.2a, SI -Table S5.4). Significant differences (p < 0.05) were found between phase I and phase III-IV (SI - Tables S5.5, S5.6). The increase in TB-EPS production can be considered

a defence mechanism for microorganisms in the presence of toxic substances (Kong *et al.*, 2017; Li *et al.*, 2015; Song *et al.*, 2014; Zhou *et al.*, 2019). As along phases II-IV, an increase in TB-EPS content occurred, it can be concluded that DESL directly interferes with AS metabolic activity. Consequently, the increase in TB-EPS content during SBR operation may have contributed to a high relative abundance of large aggregates (An *et al.*, 2016; Melo *et al.*, 2021; Zhang *et al.*, 2019).

The LB-EPS components from phase I to phase IV are shown in Figure 5.2b. For PS the results obtained during phase I and III were similar, and the concentration increased significantly ($p < 0.05$) in phase II and IV (SI – Tables S5.5, S5.6). PN in phases II-III increased to the highest levels, statistically different ($p < 0.05$) from phase I (Figure 5.2b, SI - Tables S5.5, S5.6). During phase IV, PN decreased to levels close to phase I. In this way, PN showed significant differences ($p < 0.05$) between phases I-IV and phases II-III. For HAS, a significant difference ($p < 0.05$) was solely observed between phase I and phases II-III (Figure 5.2b, SI Tables S5.5, S5.6). The TB-EPS components from phase I to phase IV are shown in Figure 5.2c. For PS, a significant difference ($p < 0.05$) was found between phase I and phases II-IV (SI - Tables S5.5, S5.6). For PN, a significant change was obtained between phase I and phases III-IV. HAS content increased from phase I to phase IV.

The proportions of PS and PN for each experimental phase have changed as a result of the addition of DESL. Changes in the operating parameters (pH, temperature, toxic compounds, etc.) may have an impact on the yield and composition of the different fractions of EPS produced by microorganisms, according to a number of studies (Li *et al.*, 2021; Tian *et al.*, 2019). In the present work, LB- and TB-EPS contained a large portion of proteins (PN/PS ratio = 1.0 – 2.5, and 1.6 – 3.6, respectively). Interestingly, from the middle to the end of phase III, PN/PS ratio presented the highest values (3.7 and 3.8) for LB- and TB-EPS, respectively, which likely influenced the rise of large aggregates. This finding supports a prior work by Xu *et al.* (2021), which found that the production of large aggregates (during the granulation phase) was dependent on an increase in the PN/PS ratio because of the hydrophobic (PN) and hydrophilic (PS) properties of EPS components (Santschi *et al.*, 2021). It has been also reported that a sharp increase in PN was recognized to be crucial for the long-term stability of AS (Basuvaraj *et al.*, 2015). The results found in the present work revealed that pharmaceutical compounds (especially antihistamines), favoured the increase in EPS production for bacterial self-defense, especially TB-EPS.
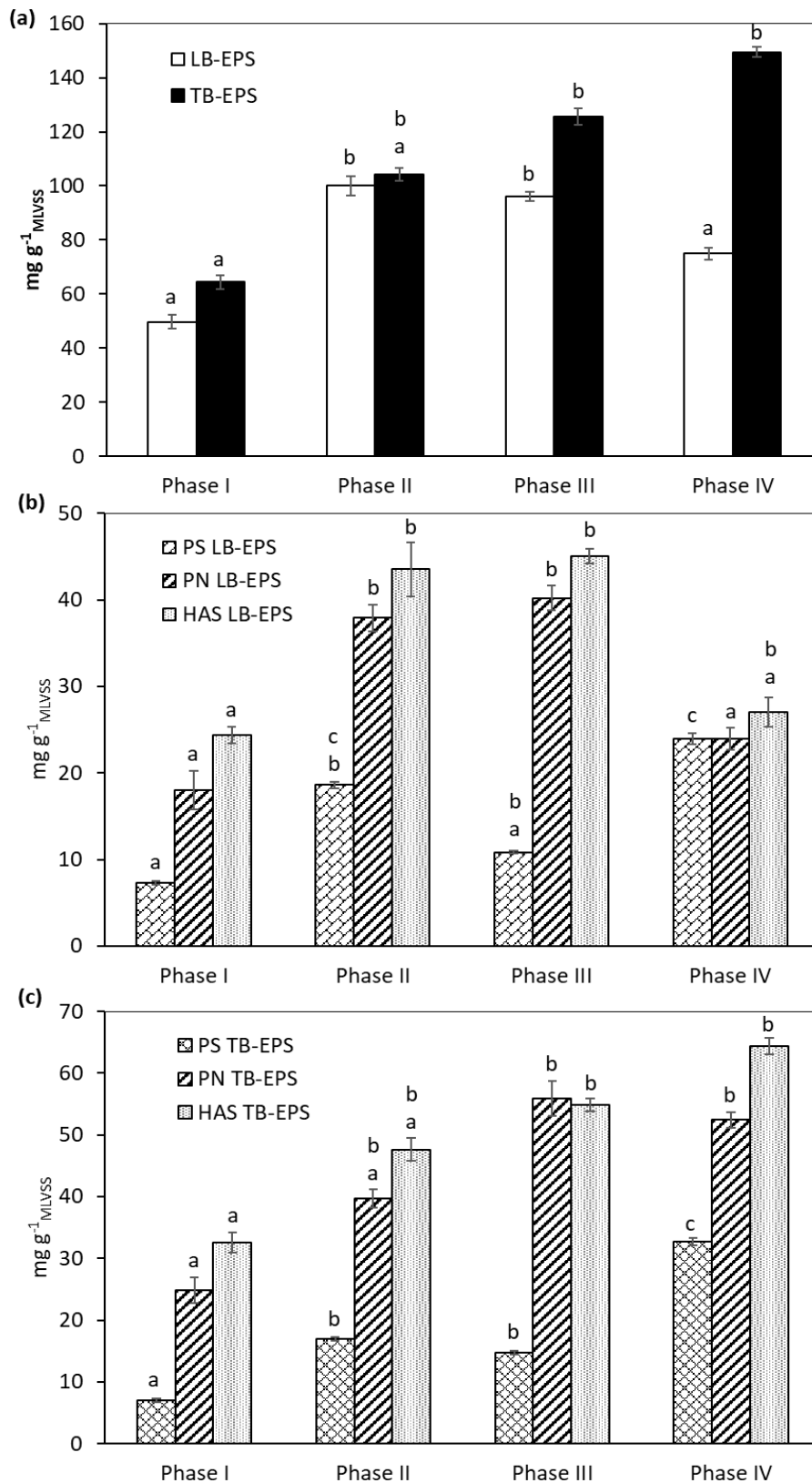
Figure 5.2 – (a) LB-EPS and TB-EPS for different phases of SBR operation; (b) PS, PN, and HAS content of the LB-EPS; (c) PS, PN, and HAS content of the TB-EPS. The error bars represent the standard deviation. Bars with different letters present statistically significant differences (p < 0.05).

Figures 5.3 and 5.4 present 3D-EEM results of sludge EPS at the beginning, middle and end for each phase, and peaks fluorescence intensity are displayed in Table 5.1. Samples were analysed by 3D-EEM fluorescence spectroscopy to characterize changes in the organic compounds present in the EPS which have fluorescent characteristics, such as protein-like, humic acid-like and fulvic acid-like substances (Guo *et al.*, 2014; Sheng and Yu, 2006). The 3D-EEM fluorescence spectra of LB-EPS and TB-EPS under DESL exposure revealed relationships between the characteristic peaks' intensities and the EPS components. The shifts of the fluorescence peaks can provide information on the chemical structural changes of the EPS, being related to the change of some enzyme activities, the biosynthetic and metabolic pathways of the organics and the redistribution of the metabolic flux with the increase of DESL concentration (Wang *et al.*, 2013).

Four peaks could be detected from the 3D-EEM fluorescence results. Peak A and peak B representing protein-like substances (peak A, Ex/Em = 270-275/300-305; peak B, Ex/Em = 270-275/370-375), peak C for fulvic acid-like substances (peak C, Ex/Em = 297-303/420-445), and finally peak D representing humic acid-like substances (peak D, Ex/Em = 320-360/414-451).

In the beginning of phase I (day 0), LB-EPS was composed mainly of proteins-like substances (peak B) (Figure 5.3a). After that, LB-EPS composition slightly increased humic (peak D) and fulvic acid-like substances (peak C) on day 32. During phase II, the fluorescence intensity of the peaks C and D from day 35 till day 67 increased (Figure 5.3b). Additionally, the fluorescence intensity of peak B, representing the protein-like substances, had similar behavior during phases I and II. During phases III and IV (Figure 5.3c-d), peaks C and D showed a decreasing trend from day 70 onwards and protein-like substances prevailed (peaks A and B).

For TB-EPS, the chemical composition of EPS did not change significantly during phases I and II, mainly consisted of protein-like substances (peaks A and B) (Figure 5.4a,b). Proteins-like substances displayed an increase in fluorescence intensity at the end of phase II (Figure 5.4b), suggesting an increase in some functional groups, such as carboxyl, amino, hydroxyl and carbonyl (Chen *et al.*, 2002). After that, EPS composition increased humic and fulvic acid-like on day 86. The move of peak positions indicated chemical changes in the EPS components. The appearance and transformation of peak C and peak D during phase III (Figure 5.4c), indicated chemical changes in the EPS components, probably by a complex formation between EPS and DESL. The study of Almutairi *et al.* (2021) demonstrated that the fluorescence intensity of glycoproteins is quenched by loratadine (parent compound of DESL). The Gibb's free energy change was found to be negative for the interaction of loratadine with acid glycoprotein, indicating that the binding process is spontaneous. These authors also

observed that hydrogen bonding and hydrophobic interactions were the main bonding forces between glycoproteins–loratadine. The additional peaks further confirmed that the presence of 10 mg L^{-1} of DESL could promote the secretion of EPS with different functional groups (proteins, humic acids and fulvic acids substances) by bacteria. During phase III and phase IV, a decrease in fluorescence intensity in the 3D-EEM spectra was obtained, which accounted for the reduction of some functional groups, such as aromatic ring and conjugated bond in chain structures (Świetlik *et al.*, 2004). These findings are consistent with previous work that gave similar shifts of fluorescence intensity and peak location, indicating chemical changes of the EPS components when biofilm was exposed to CuO nanoparticles (Miao *et al.*, 2017). All location shifts of the fluorescence peaks could provide spectral information on the chemical structural changes, indicating the functional group changes of EPS during DESL exposure (Liu *et al.*, 2011; Zhu *et al.*, 2012).

It was further calculated (Table 5.2) that the percent fluorescence response of region A decreased, on average, from 73.1% to 56.5% for LB-EPS and from 56.4% to 40.7% for TB-EPS. For region B, the percent fluorescence response increased from 26.9% to 43.5% for LB-EPS and from 43.6% to 59.3% for TB-EPS, on average. It was evident that the percent fluorescence response of protein-like substances (region A) decreased in phases with DESL, implying that protein-like substances, instead humic acid-like substances, were quenched in the presence of DESL. Thus, these results propose that proteins-like substances played a specific role in removing DESL, probably by giving sites to DESL adsorption and forming a complex DESL-PN EPS and then decreasing the percent fluorescence response, which is in accordance with previous literature (Almutairi *et al.*, 2021).

Table 5.1 – Peak fluorescence intensity of samples at beginning, middle and end of each phase.

LB-EPS	Peak Intensity				TB-EPS	Peak Intensity			
Day	A	B	C	D	Day	A	B	C	D
0	-	6600	-	-	0	-	7000	-	-
16	-	2000	-	-	16	-	2400	2000	-
32	-	4200	700	2500	32	-	900	800	-
35	-	1900	1000	1800	35	-	1000	700	900
51	-	4100	-	-	51	2000	2000	-	-
67	-	3300	1500	5500	67	5600	5100	-	-
70	-	4700	1800	3300	70	8200	9200	-	-
86	3900	5800	1300	1400	86	-	4400	2100	1200
103	-	3400	1200	1200	103	-	1900	1800	1800
106	-	2700	-	2500	106	-	4400	3700	4200
122	2500	2500	-	600	122	-	6600	2400	1600
139	-	5400	800	1500	139	-	2400	2200	1200

Table 5.2 – Average percentage of fluorescence response [Pi,n (%)] of LB-EPS and TB-EPS under different DESL concentration for each phase.

LB-EPS	Pi,n (%) Region A	Pi,n (%) Region B	TB-EPS	Pi,n (%) Region A	Pi,n (%) Region B
Phase I	73.06	26.94	Phase I	56.44	43.56
Phase II	51.12	48.88	Phase II	66.91	33.09
Phase III	51.31	48.69	Phase III	53.44	46.56
Phase IV	56.52	43.48	Phase IV	40.71	59.29
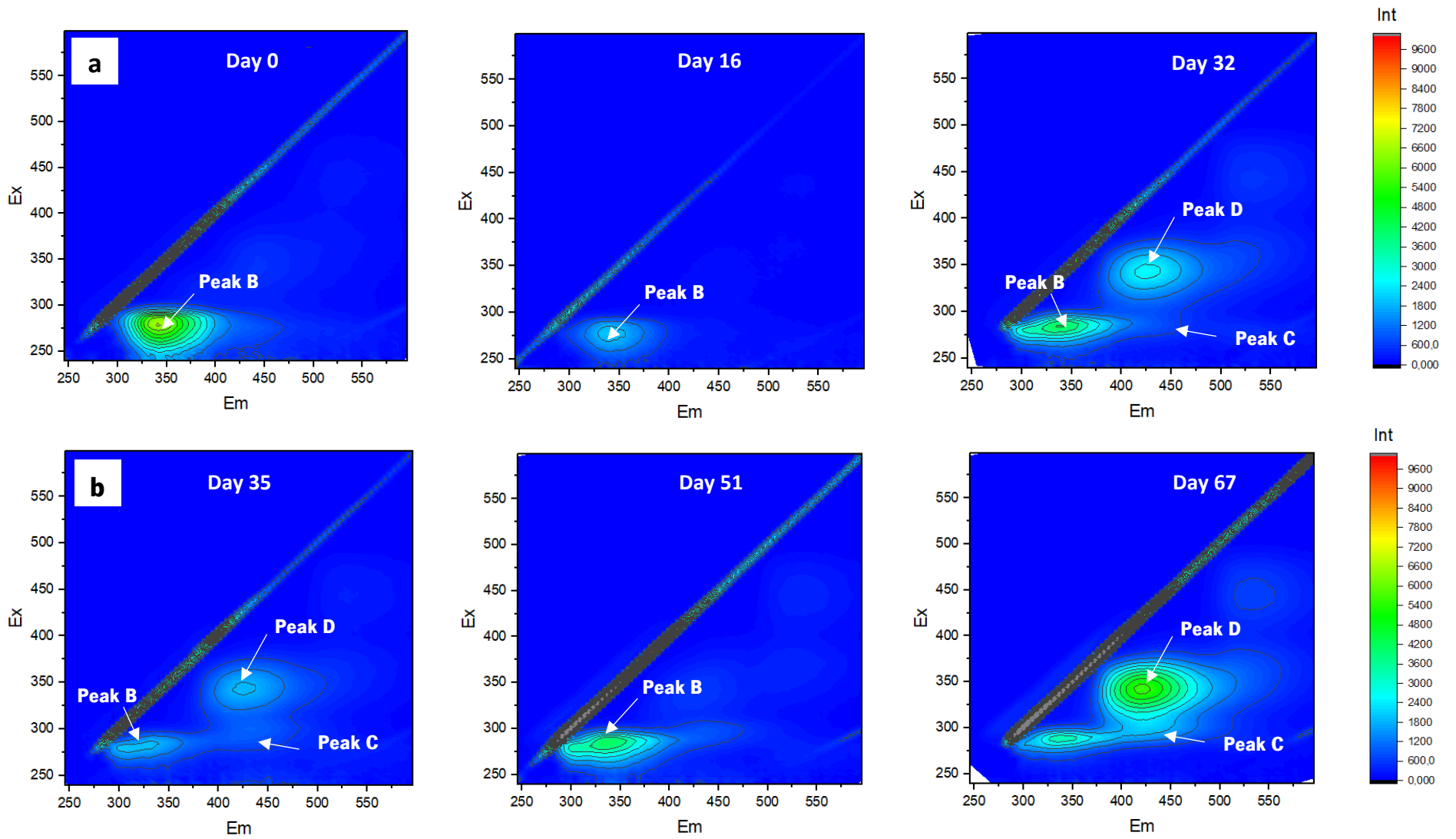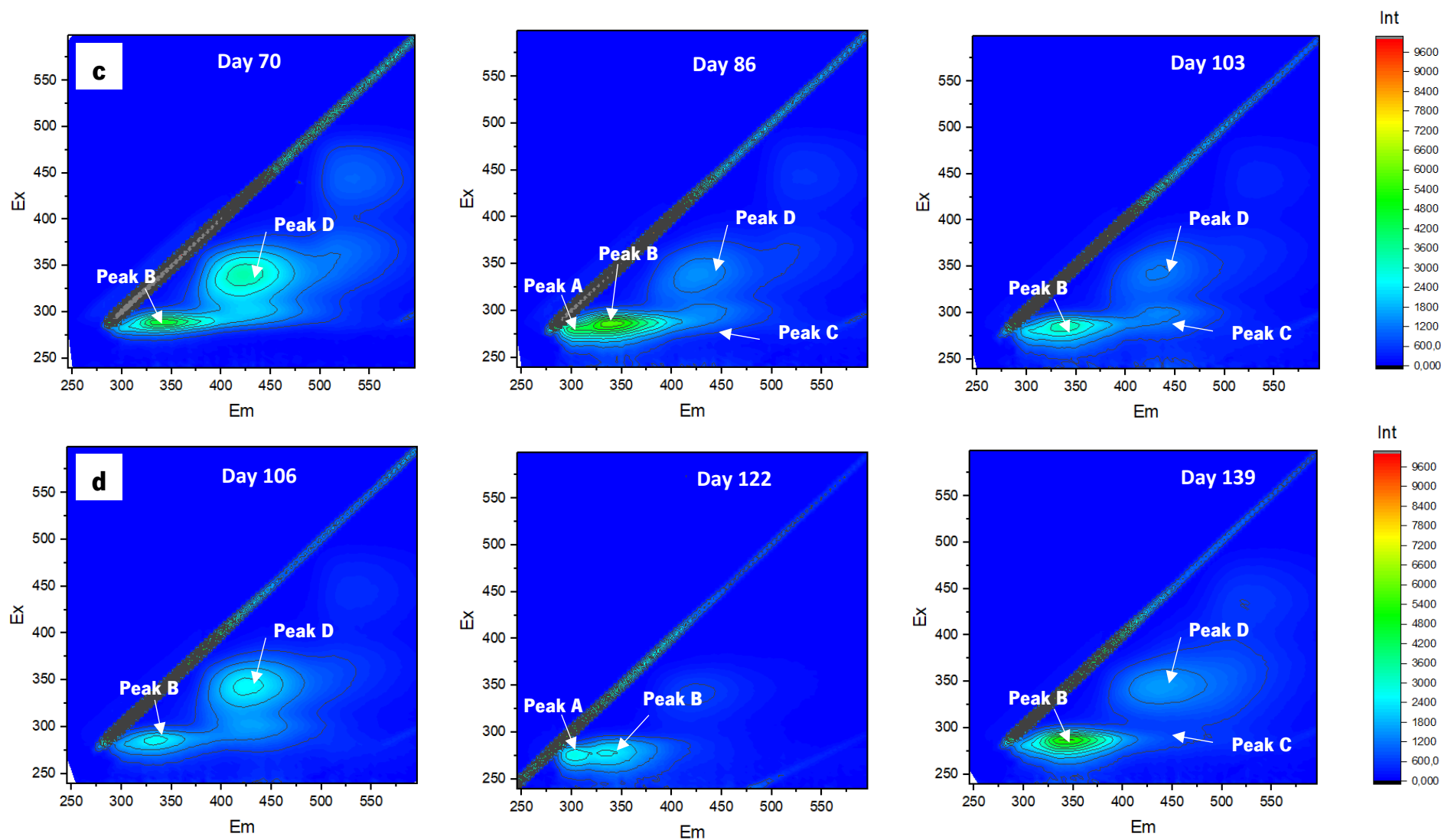
Figure 5.3 – 3D-EEM fluorescence spectra of LB-EPS under different DESL concentration: (a) phase I (0 mg L^{-1}); (b) phase II (1 mg L^{-1}); (c) phase III (5 mg L^{-1}); (d) phase IV (10 mg L^{-1}).
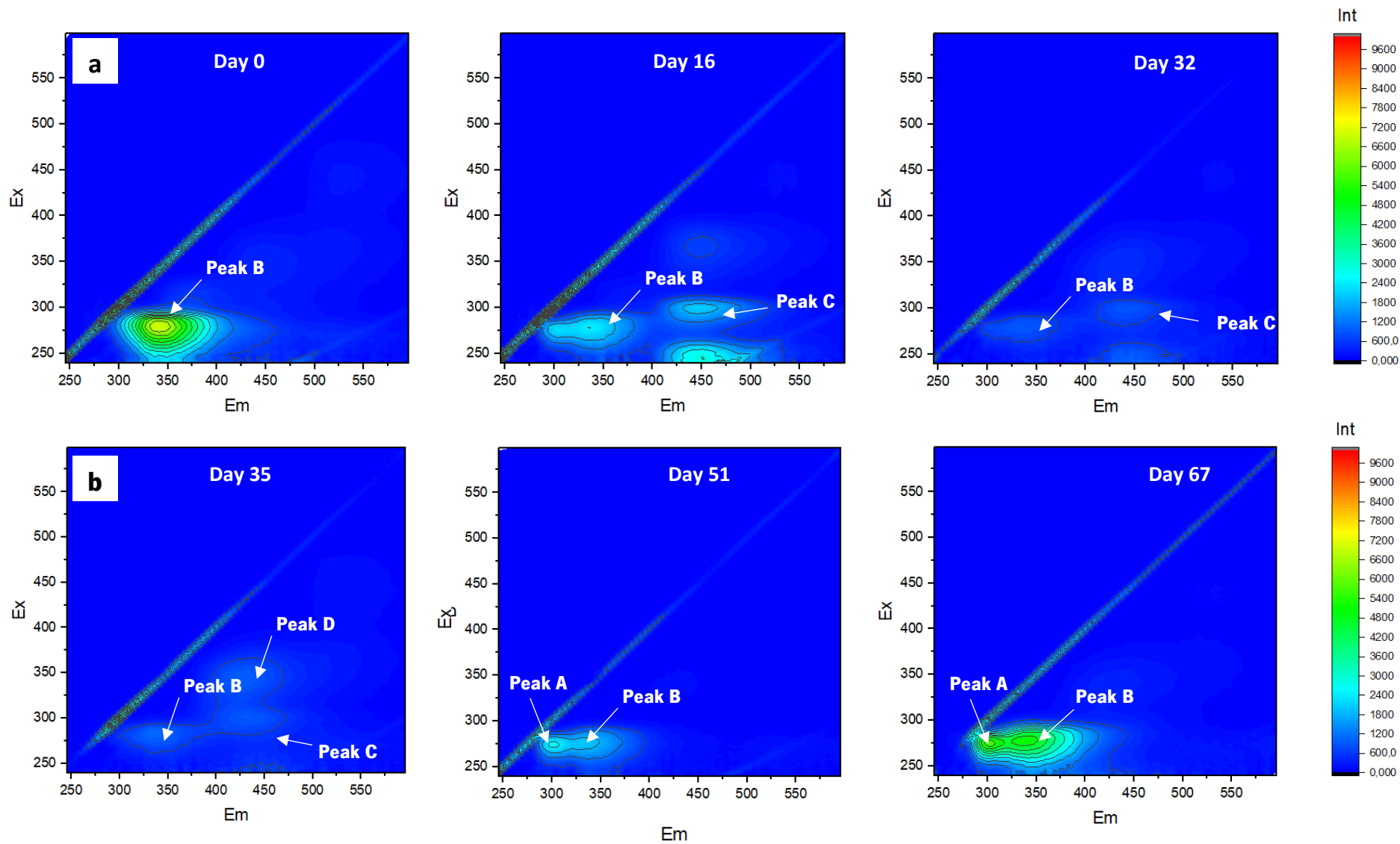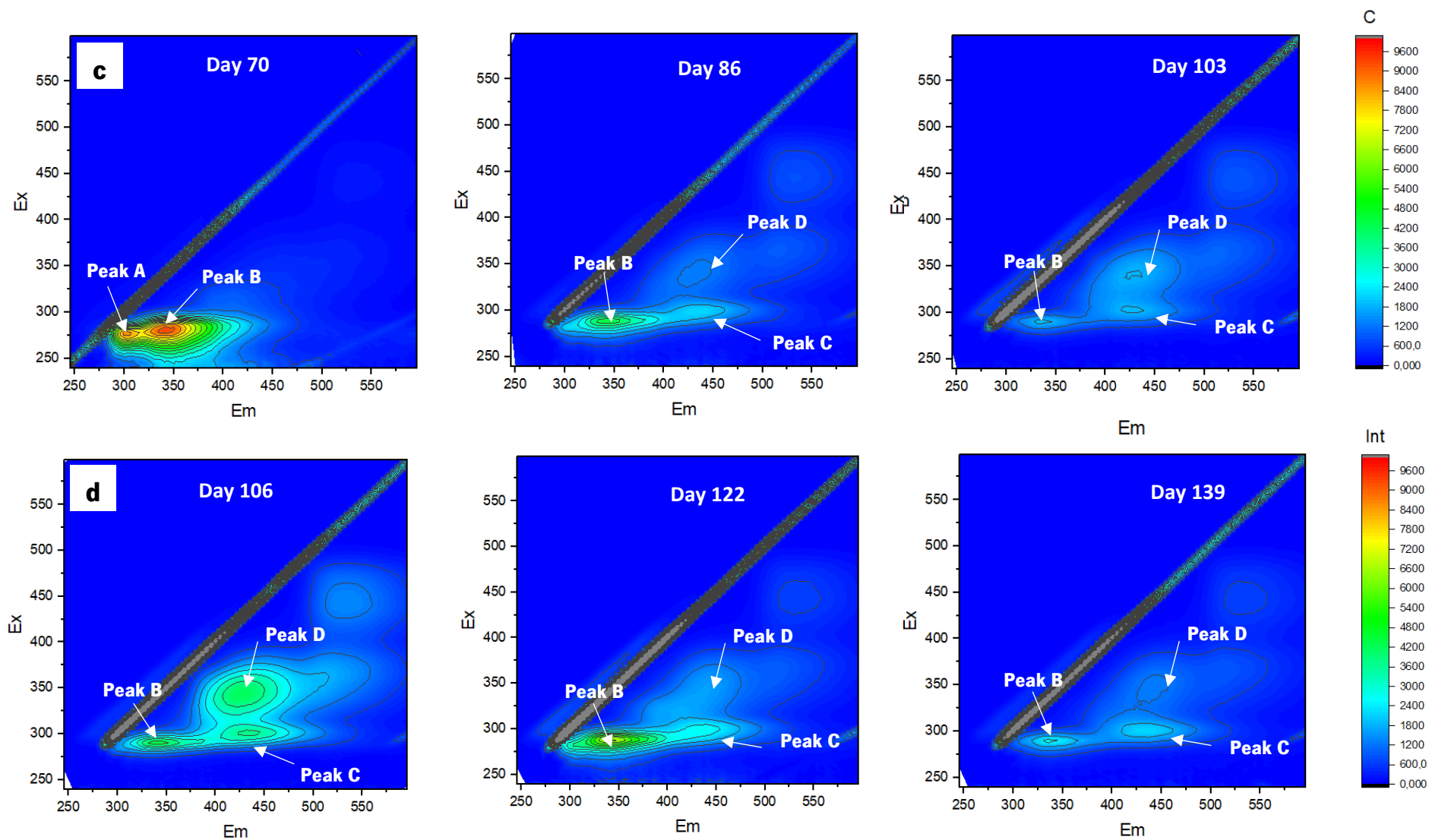
Figure 5.4 – 3D-EEM fluorescence spectra of TB-EPS under different DESL concentration: (a) phase I (0 mg L^{-1}); (b) phase II (1 mg L^{-1}); (c) phase III (5 mg L^{-1}); (d) phase IV (10 mg L^{-1}).

5.2.3 Structural characterization

Figure 5.5a shows the aggregates area percentage along phases I-IV. During phase I, a normal aggregates structure was found, with a considerable presence of intermediate aggregates (%Area$_{int}$ of 81%, on average). A significant increase in large aggregates (%Area$_{larg}$ from 40% to 67%) occurred during phases III and IV, pointing to a global trend to form larger structures as visualized by microscopy (Figures 5.6-5.9). The increase in large aggregates, especially during phases III and IV, had a close relationship with TB-EPS production, suggesting that the increase in DESL concentration induced the production of more TB-EPS leading to larger aggregates. In fact, the EPS are involved in the structure of microbial aggregates and in interactions between cells as well. Treating the same wastewater, a full-scale system with predominantly pinpoint flocs (diameter < 50 μm) had more LB-EPS than a lab-scale system with predominantly large flocs (diameter > 340 μm) with more TB-EPS content (Basuvaraj *et al.*, 2015).

The SVI and MLSS results along operation are shown in Figure 5b and Figure 5c shows the total filament length per volume (TL/Vol), and the total filaments length per MLSS (TL/MLSS). During phase I, the SVI values were < 150 mL g^{-1}, although close to the threshold limit (Figure 5.5b). TL/MLSS was < 10,000 mm mg^{-1} and TL/Vol was < 10 mm μL^{-1} throughout the SBR operation (Figure 5.5c). The present results corroborate previous studies where good settling ability was obtained for sludge with SVI, TL/Vol and TL/MLSS lower than 150 mL g^{-1}, 10 mm μL^{-1} and 10,000 mm mg^{-1}, respectively (Amaral and Ferreira, 2005; Melo *et al.*, 2021; Yao *et al.*, 2019). Regarding phase II, SVI results were > 150 mL g^{-1}, and the sludge demonstrated meagre settling ability. However, microscope inspection (Figure 5.7) did not show any evidence that the low settling ability was due to filamentous bulking since the TL/MLSS and TL/Vol were less than the threshold limits (Figure 5.5c). In fact, these results corroborate the findings of Jin *et al.* (2003) and Melo *et al.* (2021), revealing that the dysfunction on sludge settling ability can be governed by different sludge characteristics, such as EPS. Therefore, low settling ability may be associated with floccular sludge surrounded by large contents of LB-EPS during phase II (Figure 2a, SI – Table S5.4), which likely retained water in the sludge flocs structure producing poorly settling and poorly compacting sludge. At the end of phase II, SVI decreased to values quite lower than the threshold limit, demonstrating the strong influence of chemical properties of AS aggregates surface in influencing the sludge settling ability. Thus, the difference in the concentration of EPS components (PS, PN, and HAS) might explain the settling ability along phase II. In fact, looking at data from the start of phase II until day 49 (SVI of 227 mL g^{-1}), a positive correlation between LB-EPS

(chiefly PN and HAS) and SVI was found (SI – Table S5.7). In addition, during phase II, the LB-EPS concentration was quite close to the TB-EPS, which increased the LB/TB EPS ratio, suggesting that when LB-EPS and TB-EPS concentrations are similar, a dysfunction on the settling ability occurs. On the other hand, from the middle to the end of phase II, the SVI decreased to values lower than the threshold limit and presented a negative correlation with TB-EPS, mainly PN and HAS components. During phases III and IV, the biomass presented the best settling ability with values of SVI < 100 mL g^{-1}. Interestingly, the aggregates become larger (Figure 5.5a), containing quite compact structures without free filamentous bacteria (Figure 5.8, 5.9). This behavior was accompanied by a sharp increase of MLSS (from 3.0 to 4.8 g L^{-1}) at the beginning of phase IV. Also, our results imply that the fluctuation of MLSS during the experiment did not influence the biomass settling ability (Figure 5.5b) since, for the same concentration of MLSS, different SVI results were found. This fact clearly demonstrates the contribution of aggregates structure to the settling ability quality. It can be reasonable to assume that other factors, such as chemical properties of AS aggregates, probably influenced by the change in the EPS composition and concentration, especially TB-EPS, had a key role to microbial aggregates become larger during phases III and IV. These results agree with previous studies reporting the influence of EPS on aggregates size (Basuvaraj *et al.*, 2015; Xu *et al.*, 2021).
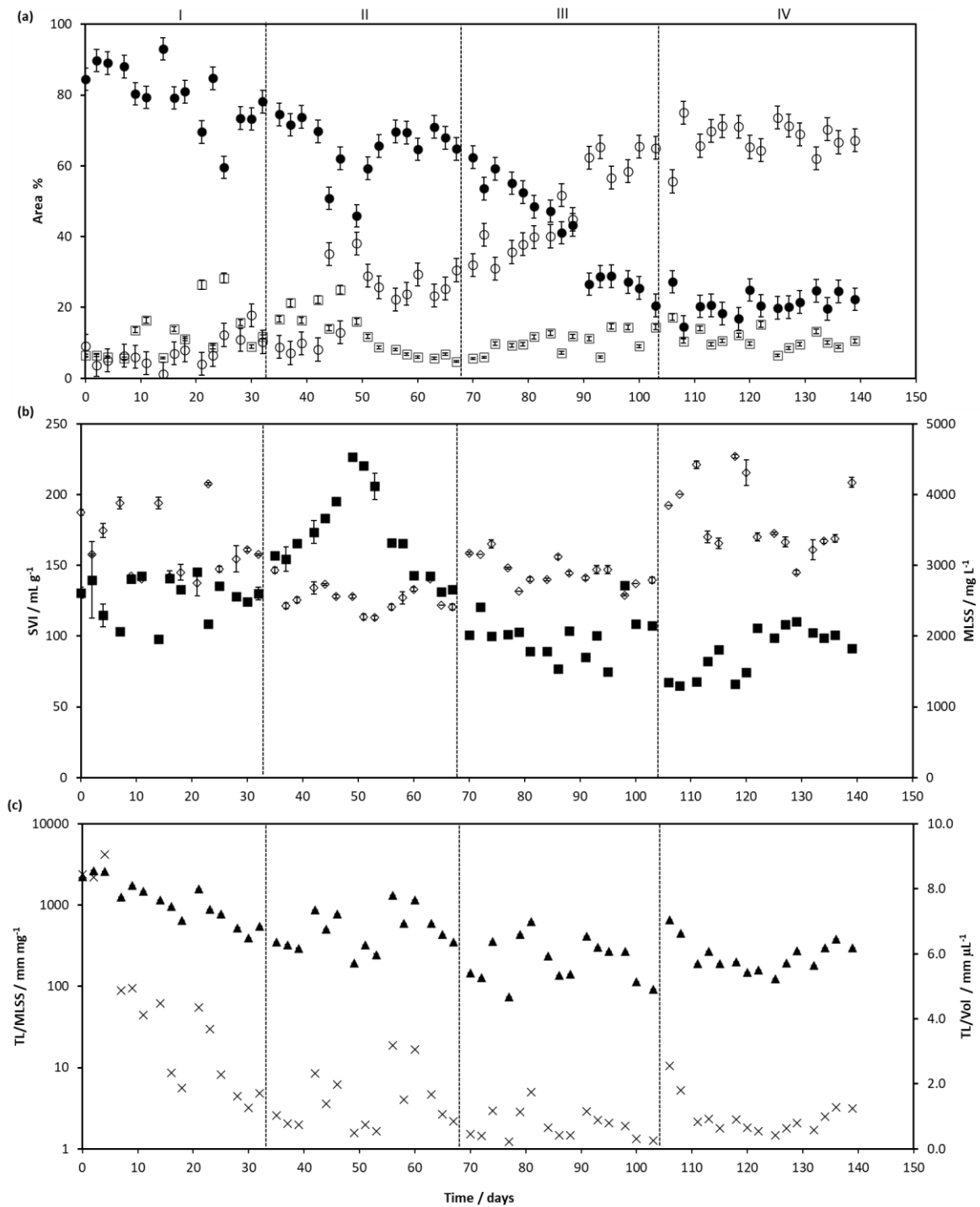
Figure 5.5 – (a) Area percentage behavior for small (sml) (□); intermediate (int) (●); and large (larg) aggregates (○); (b) SVI (■) and MLSS (◇); total filaments length per MLSS (TL/MLSS) (▲) and total filament length per volume (TL/Vol) (×). Results obtained along experimental phases (I–IV).
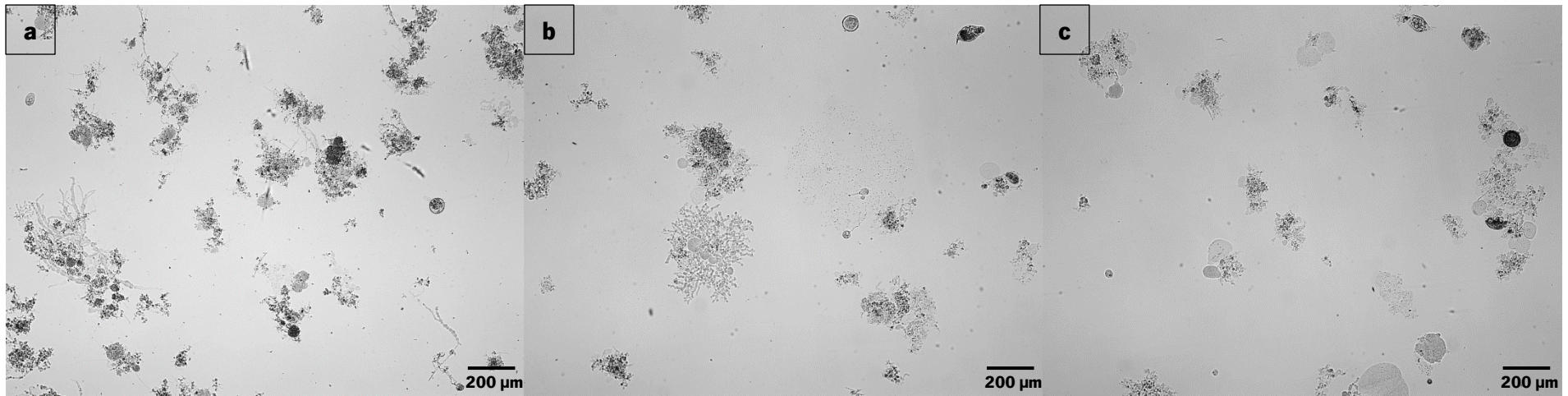
Figure 5.6 – Microscopic view of aerobic sludge during reactor operation along phase I (a) Day 0, (b) Day 16 – dilution 1:4, and (d) Day 32 – dilution 1:4. Size bar is equivalent to 200 micrometers.
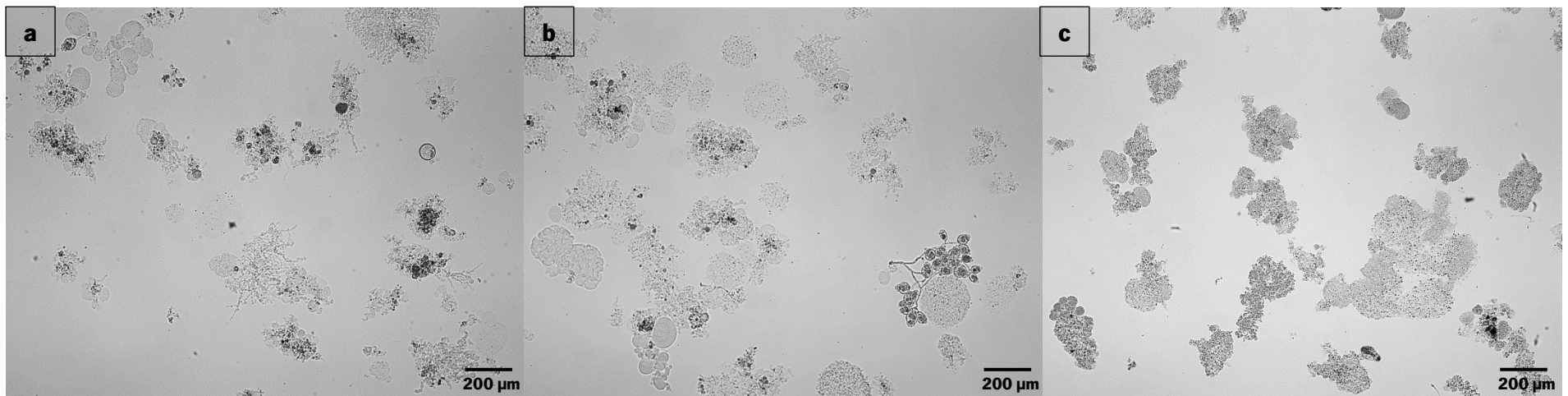
Figure 5.7 – Microscopic view of aerobic sludge during reactor operation along phase II (a) Day 35, (b) Day 51, and (c) Day 67. Dilution 1:4 for all samples. Size bar is equivalent to 200 micrometers.
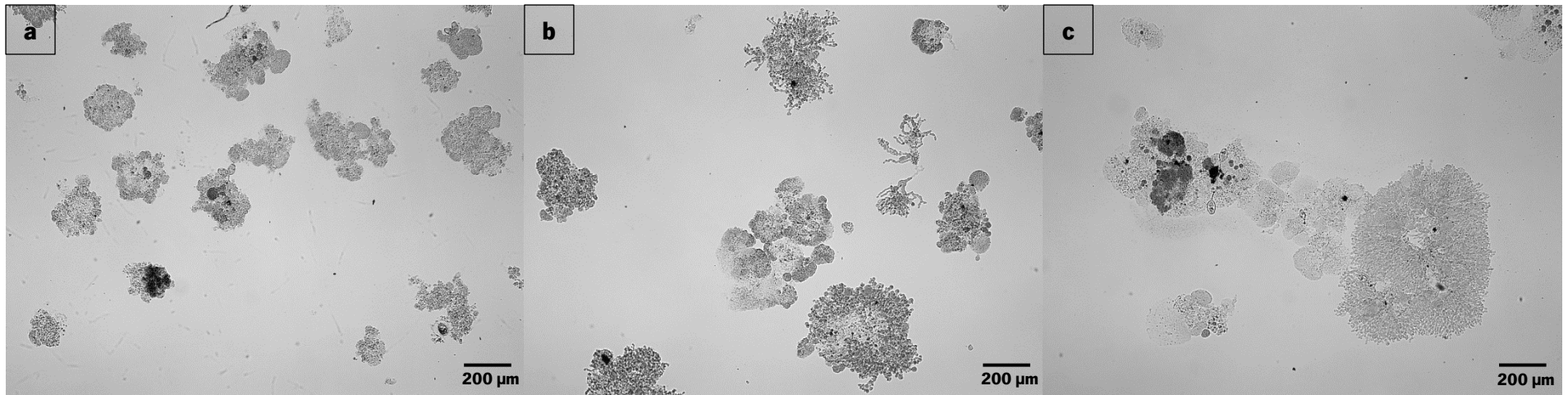
Figure 5.8 – Microscopic view of aerobic sludge during reactor operation along phase III (a) Day 70, (b) Day 86 – dilution 1:4, and (c) Day 103 – dilution 1:4. Size bar is equivalent to 200 micrometers.
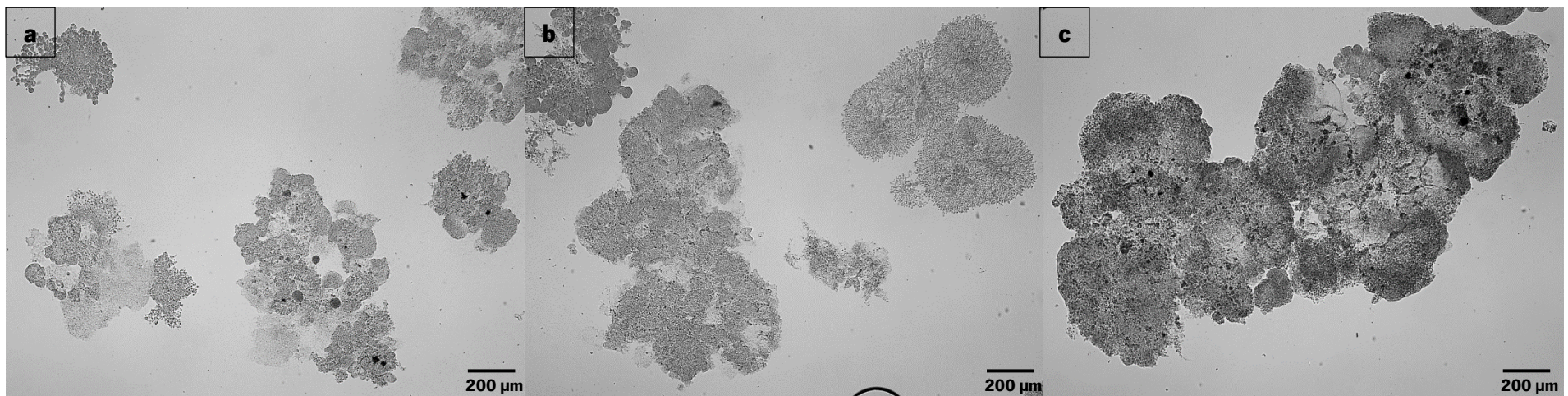
Figure 5.9 – Microscopic view of aerobic sludge during reactor operation along phase IV (a) Day 106 – dilution 1:4, (b) Day 122 – dilution 1:5, and (c) Day 139 – dilution 1:5.   Size   bar   is   equivalent   to   200   micrometers.

5.2.4 *Principal component analysis*

The PCA encompassed the QIA parameters (TL/MLSS, TL/Vol, Deq and %Area), biomass properties (MLVSS and SVI), and EPS and its components. PC1 and PC2 explained 36% and 21% of the original dataset variance, respectively, and were used in this analysis. Each operational phase was clearly identified in Figure 5.10a. Phase I was characterized by presenting positive PC1 values and mainly negative PC2 values. On the other hand, positive values for PC2 could be inferred for the phases II and III. Moreover, both operational periods differed in terms of PC1 values, being phase II on the positive side and phase III on the negative side. In addition, in the bottom left quadrant, phase IV was characterized by negative values for both PC1 and PC2.

With respect to the variable's importance shown in Figure 5.11, it should be stressed that PC1 (Figure 5.11a) was positively influenced by the $Area_{int}$), Deq_{sml}, filamentous bacteria content (TL/Vol and TL/MLSS), and SVI. Negative values for PC1 were severely influenced by the overall EPS content, mainly TB-EPS components, MLVSS and large aggregates characteristics (Deq_{larg} and $\%Area_{larg}$). On the other hand, PC2 (Figure 5.11b) was positively influenced by the Total EPS, LB-EPS and its components, Deq_{int}, and SVI. Negative values for PC2 were influenced by the MLVSS, filamentous bacteria content (TL/MLSS, TL/Vol) and $\%Area_{larg}$, TB-EPS and its components.

Concerning the variable loadings presented in Figure 5.10b, the SVI showed a close relationship with TL/MLSS and TL/Vol, Deq_{sml}, and $\%Area_{int}$. Furthermore, the results showed a strong relationship of AS aggregates (Deq_{larg} and $\%Area_{larg}$) with the total EPS and TB-EPS and its components (PS, PN and HAS). Additionally, a close relationship was found between Deq_{int} and LB-EPS and its components (PN and HAS).

Differences observed in clusters (Figure 5.10a) from PCA results are in accordance with the evolution of biomass behavior. Phase I differed significantly from phases II, III and IV where the lowest values for overall EPS and the highest filamentous bacteria content were achieved. In addition, the difference between phase II and phase III could be explained by the increase of LB-EPS content (mainly HAS, PN and LB-EPS). In fact, these results could be explained by a somewhat similar biomass behavior in terms of LB-EPS and its components content during both operational periods (PC2) and different aggregate's structure (PC1), mainly $\%Area_{int}$ versus $\%Area_{larg}$ with an accentuated change in the middle of phase III. Phase IV was totally opposite from other phases, being influenced by TB-EPS content, lowest values of filamentous content (TL/Vol and TL/MLSS), and large aggregates structure (Deq_{larg}, $\%Area_{larg}$).

As previously observed, during phases II and III, high LB-EPS concentrations were obtained, especially PN and HAS components, which positively influenced the variation in PC2 suggesting chemical properties change in the surface of AS. EPS can differ in molecular weight and composition, mainly when produced under different conditions by microorganisms in biological systems (Liao *et al.*, 2011). Thus, these variations in LB-EPS can be related with the biomass response to DESL addition along phases II and III since LB-EPS content decreased again during phase IV (as shown in Figure 5.2a).

Summarizing, our results suggest that TB-EPS and its components influence the structure of the aggregates, which can be positively related to the large aggregates (Deq_{larg}, $\%Area_{larg}$) and negatively related to the small and intermediate aggregates (Deq_{int}, $\%Area_{sml}$, $\%Area_{int}$). Hence, large aggregates formation can be associated with the high levels of EPS produced by biomass, supporting previous findings (Xu *et al.*, 2021). Beyond these results, aggregates were found with a large structure where cells were compactly packed during phases III and IV (Figures 5.8 and 5.9).This might explain the good settling ability during these phases. In fact, these results are in accordance with previous studies that found EPS as key players in granules formation and stability (Adav *et al.*, 2008; Hou *et al.*, 2015; Xu *et al.*, 2021). Nevertheless, the LB-EPS and its components (PS, PN and HAS) correlated positively only with the Deq_{int}. Globally, we can infer that TB-EPS forms have a more critical role in aggregates' structure than LB-EPS components.
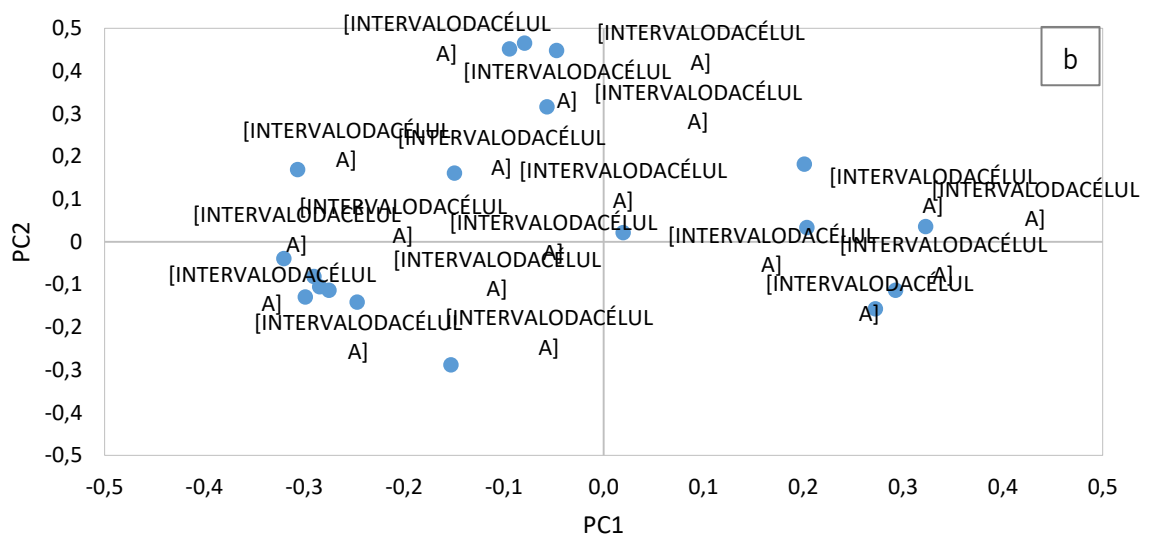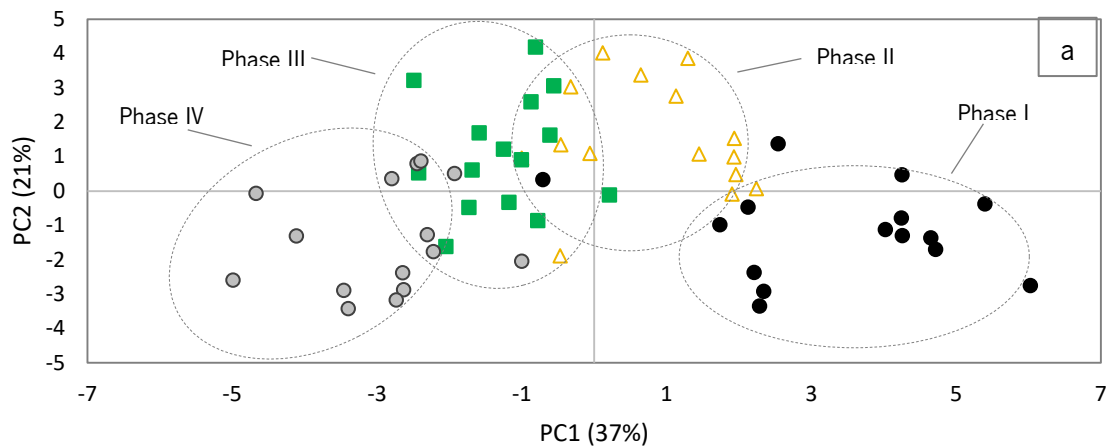
Figure 5.10 – PCA scores plot of the SBR operational parameters, EPS and QIA dataset for PC1 versus PC2. (a) phase I (●); phase II (△); phase III (■); and phase IV (●). (b) Variables loadings plot of PC1 and PC2.
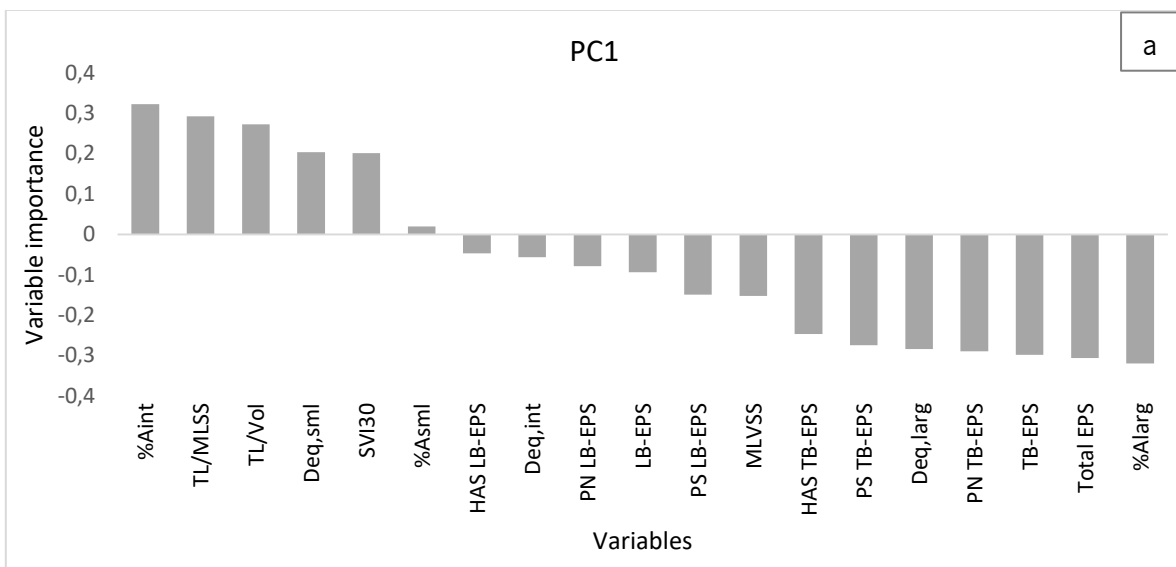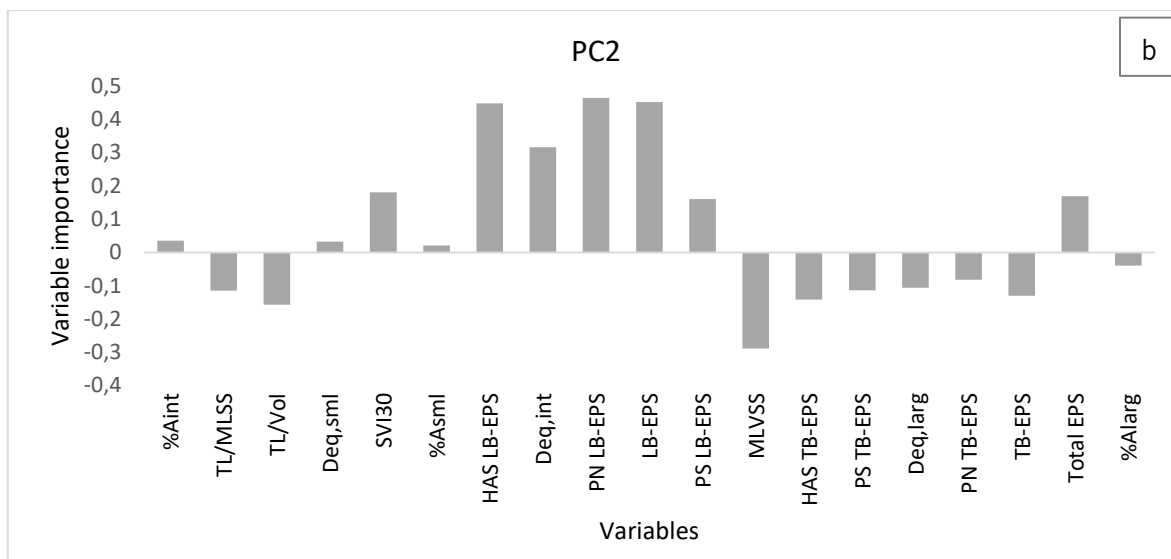
Figure 5.11 – Variable importance for PC1 and PC2, regarding the PCA analysis of Figure 8. (a) Variable importance for PC1; (b) Variable importance for PC2.

5.3   Conclusion

COD and ammonium efficiency decreased, on average, from phase II to IV in the presence of DESL. Concerning the removal of DESL, just for the highest concentration (10 mg L^{-1}), the biomass significantly reduced its capacity compared to phases II and III. An increase in LB-EPS concentration during phases II and III with a subsequent reduction in phase IV, suggests that this variation could be a response of the biomass in SBR to DESL exposure. For TB-EPS, an increasing trend was observed, indicating a self-defence behavior of the microorganisms in SBR towards DESL exposure. The 3D-EEM spectral analysis indicated that the primary components of LB-EPS and TB-EPS were protein-like substances, humic acid-like substances, and fulvic acid-like substances. Protein-like fluorophores were the key components in the sludge, which probably contributed to the formation and structural stability of large aggregates. QIA was valuable in understanding the changes in biomass properties over the experimental phases, demonstrating, for instance, that during phase II the low settling ability was unrelated to the filamentous bacteria content. Finally, PCA results suggest that EPS, especially TB-EPS, significantly influenced aggregates structural parameters rather than LB-EPS.

CHAPTER 6 - ASSESSING EXTRACELLULAR POLYMERIC SUBSTANCES IN ACTIVATED SLUDGE UNDER ATRAZINE EXPOSURE

6.1 Introduction

In AS, EPS fractions act differently toward the change in the surrounding environment of microorganisms (Hou *et al.*, 2013; Wang *et al.*, 2013; Wang *et al.*, 2014). Moreover, different roles can be attributed to EPS components (PN, PS, HAS, etc.) influencing the chemical properties of the aggregate surface (Sivasubramanian *et al.*, 2021; Wang *et al.*, 2018). Also, the PN/PS ratio has been reported in the literature as an indicator of hydrophobicity, where PN is considered a major contributor to this property (Santschi *et al.*, 2020; Wilén *et al.*, 2003; Xu *et al.*, 2011). By interacting with hazardous compounds like ATZ through their functional groups, EPS' unique properties make them suited to be used in the biosorption process, allowing bacterial cells to degrade these substances (Yu *et al.*, 2019).

Chemical methods are typically used to determine EPS since they are more widely available and well-established than more sophisticated approaches. However, the chemical quantification of EPS is a time-consuming procedure and leads to chemical residues. Finding a eco-friendlier methodology that can accurately assess the content and forms of EPS is thus necessary.

Therefore, the main objective of this chapter is to demonstrate the feasibility of combining the aggregates properties with chemometrics, to improve AS process monitoring, focusing on the assessment of EPS content and forms in a more economical and environmentally friendly manner.

6.2 Results and discussion

In this subsection, the overall performance, EPS production, and sludge properties were assessed by QIA in a SBR wastewater treatment process with AS for 139 days: phase I (32 days) without ATZ, phase II (32 days), phase III (33 days), and phase IV (33 days) containing ATZ at 2, 5.5 and 12 mg L^{-1} each. In addition to chemical methods, EPS were also analyzed by 3D-EEM fluorescence spectroscopy. Chemometric methods were employed to support the interpretation of the dataset, with PCA highlighting the close relationship between variables that influenced the SBR operation and PLS regression employed to assess the EPS content.

6.2.1 SBR performance

The main results of SBR monitoring regarding organic matter, nitrogen, ATZ as well as removal percentages are presented in Figure 6.1 and SI - Tables S6.1-S6.3. In phase I, the COD removal efficiency was stable and reached an average of 95% (SI - Table S6.1). Due to the inhibitory impact of

ATZ on biomass, the removal efficiency of COD dropped with the addition of ATZ to 89, 80, and 77% during phases II, III, and IV, respectively (SI - Table S6.1). This result was quite similar to that of (Derakhshan *et al.*, 2018a), who noted an impact of ATZ at concentrations of 10 mg L^{-1} and 5.5 mg L^{-1}, reaching COD removal efficiencies of 86.9 and ≈80%, respectively. In addition, in phases I and II, NH_4^+-N removal efficiencies of 99.9 and 95%, respectively were found. On the other hand, in phases III and IV, with the increase in ATZ concentration, NH_4^+-N removal efficiencies decreased significantly ($p < 0.05$) to 62 and 63%, respectively (SI - Tables S6.1-S6.3). Effluent NO_2^--N concentrations increased significantly ($p < 0.05$) on average to 2.07 mg L^{-1} solely during phase IV (SI - Tables S6.1-S6.3). Regarding effluent NO_3^--N (SI - Table S6.1), low concentration (4.82 mg L^{-1}, on average) was obtained through phase IV, showing a significant effect ($p < 0.05$) of ATZ on reducing the activity of NOB (SI - Tables S6.1-S6.3). Zhou *et al.* (2017) previously found that ATZ at 4 mg L^{-1} inhibited the activity of AOB and NOB, decreasing the NH_4^+-N removal rate and promoting NO_2^--N accumulation (Zhou *et al.*, 2017).

As shown in Figure 6.1c and Table S6.1, ATZ removal from the liquid phase slightly varied during the experiment, ranging on average from 41% in phase II to 51% in phase IV. Although the results were quite close from phase II to IV, statistical results indicated that ATZ removal was significantly different between phase II and phases III-IV (SI - Table S6.1-6.3). These results may be attributed to the fact that microorganisms achieved the maximum biodegradation of ATZ (Derakhshan *et al.*, 2018b). In this context, microorganisms involved in ATZ biodegradation may prevailed in the system. Thus, phase II was likely a period of microbial adaptation, which helped to slightly boost the removal effectiveness of ATZ during phase III. Furthermore, the removal efficiency remained unchanged when the ATZ content rose in phase IV, showing that the capacity of the microorganisms to degrade this chemical has been reached.

Up to now, some studies have shown that several microbial species and bacterial strains isolated from different areas are involved in ATZ biodegradation, especially when they become acclimated and subsequently acquire the capacity to degrade the compound (Nsabimana *et al.*, 1996; Singh *et al.*, 2018). More specifically, a culture of *Raoultella planticola* was isolated from the sludge of a wastewater treatment facility and incubated with stepwise addition of the ATZ concentrations ranging from 7 to 30 ppm. The culture was then inoculated into the sludge, and it was observed that complete ATZ degradation occurred in the supernatant within 3 h. Without the addition of acclimated *Raoultella planticola* bacteria cells, degradation of ATZ occurred only after 4 days (Swissa *et al.*, 2014).

Furthermore, a recent report indicates a high rate of ATZ degradation after 8 h, using self-immobilized biomixture with pellets of *Aspergillus niger* Y3 and *Arthrobacter* sp ZXY-2 (Yu *et al.*, 2019). In addition, other studies have shown that some bacterial strains can degrade ATZ as the sole carbon source, such as *Pseudomonas*, (Yanze-Kontchou and Gschwind, 1994) and as nitrogen source (Mandelbaum *et al.*, 1995; Yang *et al.*, 2010).
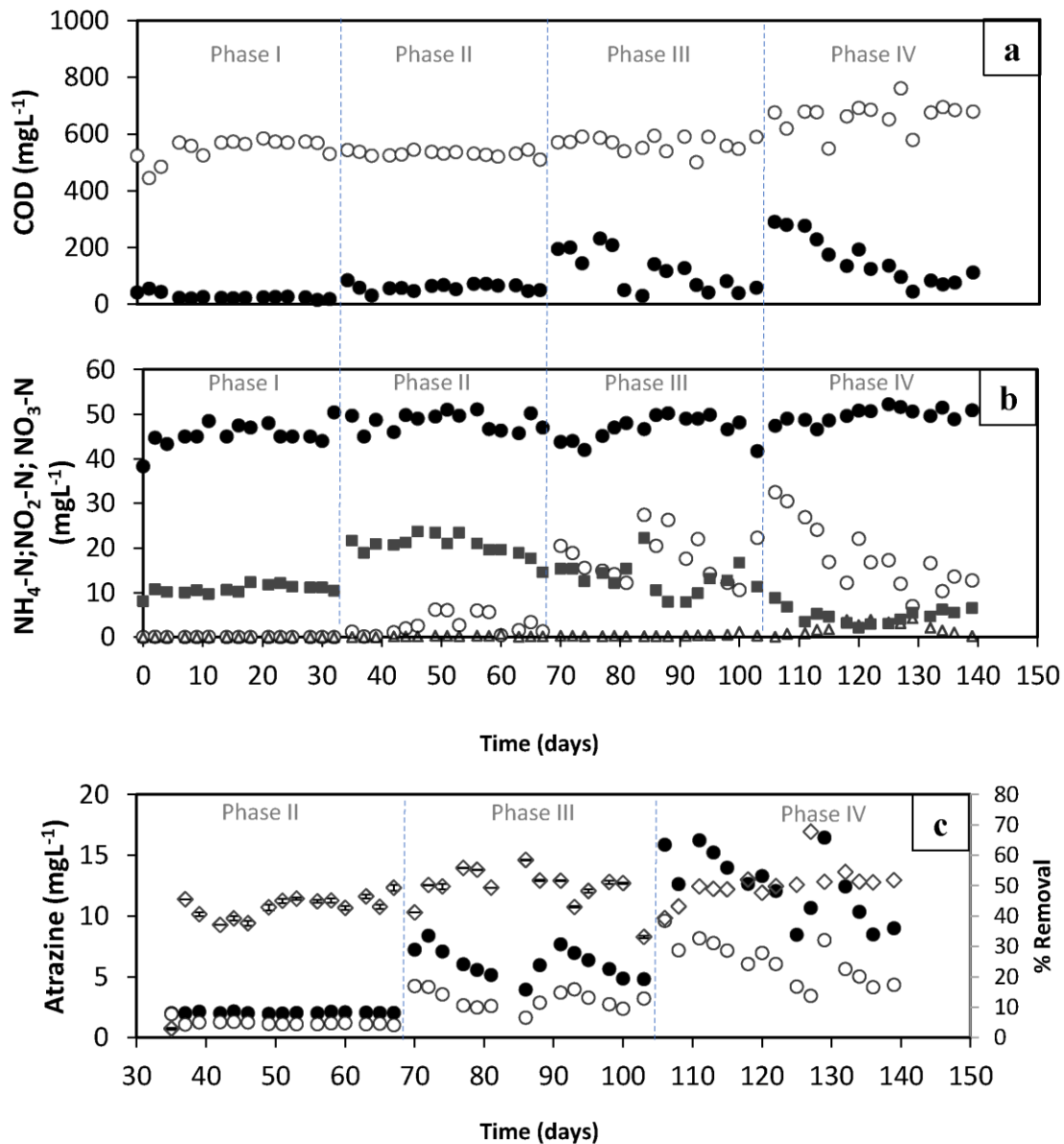
Figure 6.1 — SBR performance profile in terms of COD, NH_4^+-N, NO_2^--N, and NO_3^--N concentration along phases I-IV. (a) COD concentration (mg L^{-1}) in the inlet feeding (o), and in the effluent (●); (b) NH_4^+-N concentration (mg L^{-1}) in the inlet feeding (●), in the effluent (o), NO_2^--N in the effluent (Δ), and NO_3^--N in the effluent (■); (c) ATZ concentration (mg L^{-1}) in SBR along phases II-IV. ATZ concentration (mg L^{-1}) in the inlet feeding (●), in the effluent (o), and efficiency removal (◇).

6.2.2 Oxygen Uptake Rate (OUR)

Since the COD removal efficiency in AS system decreased with increasing ATZ concentration (Figure 6.1a), the effect of ATZ in AS system, was evaluated in respirometric experiments with 0, 1, 5, 10, and 20 mg L^{-1} of ATZ. Figure S6.2 shows an example of the OUR profiles obtained, clearly demonstrating the reduction in biomass activity. The inhibitory effect was further confirmed by the decrease in the amount of O_2 consumed for the different concentrations of ATZ during the OUR assays (Figure S6.3 and Table S6.4). Furthermore, the OUR_{Max} for assays without ATZ was higher (0.83 mg O_2 g^{-1} MLVSS min^{-1}) than the OUR_{Max} in assays with different ATZ concentrations (SI - Table S6.4), also confirming that the biomass activity was affected by the presence of ATZ. These findings are in agreement with those made by Sanchis *et al.* (2014), who observed that when bioassays were conducted with ATZ at 30 mg L^{-1}, the respirometric profile revealed a progressive decline of the specific OUR values, indicating toxicity that impacted the activity of the biomass. In addition, these authors also found that unacclimated AS was unable to remove the herbicide ATZ. Respirometric tests have been used during the past few years as a more suited tool to detect inhibitory effects of toxic or hazardous compounds in detrimental of conventional assays (Polo *et al.*, 2011; Vasiliadou *et al.*, 2018). For realistic knowledge of the behavior of a chemical upon biological treatment in a wastewater plant, experiments should be carried out with its own AS and in similar operating conditions since, otherwise, the standard tests (e.g. Microtox®, Zahn-Wellens test) could provide unrealistic predictions (Polo *et al.*, 2011).

6.2.3 EPS production, composition, PN/PS ratio, and assessment by 3D-EEM

Figure 6.2 shows LB-EPS and TB-EPS concentrations. It was found that during phase I, LB-EPS concentration was 17.7 mg EPS g^{-1}_{MLVSS}, on average, and increased during phases II, III and IV to 49.3 mg EPS g^{-1}_{MLVSS}, 37.1 mg EPS g^{-1}_{MLVSS}, and 44.7 mg EPS g^{-1}_{MLVSS}, respectively (Figure 6.2a and SI - Table S6.4). In phase I, LB-EPS concentration was significantly different (p < 0.05) from phases II-IV (SI - Tables S6.5-S6.6). For TB-EPS, the lowest concentration was obtained during phase I, (average of 34.1 mg EPS g^{-1}_{MLVSS}), followed by a slight increase during phase II (average of 46.5 mg EPS g^{-1}_{MLVSS}). Phases III and IV presented higher concentrations, significantly different (p < 0.05) from phase I and phase II.

On average, 57.3 mg EPS g_{MLVSS}^{-1} and 66.4 mg EPS g_{MLVSS}^{-1} for phase III and phase IV were obtained, respectively (SI - Table S6.4). The results suggest that AS exposure to ATZ influenced the EPS contents (LB- and TB-EPS) by affecting the metabolism of the microorganisms. As it is known, the presence of toxic substances might intensify the production of EPS contents to diminish the damage of these substances in microbial activity (Kong *et al.*, 2017; Zhang *et al.*, 2014; Zhou *et al.*, 2019). In this respect, it was found that LB and TB-EPS might interact differently with herbicide compounds, as reported by Pan *et al.* (2010). These authors found that the fluorescence of the peaks of protein (aromatic amino acids and tryptophan) for LB-EPS and fluorescence of the peak of aromatic amino acids for TB-EPS were markedly quenched by the herbicide dicamba at different experimental temperatures, whereas the fluorescence of the peaks of tryptophan and HAS for TB-EPS was quenched only at 298 K. In addition, protein-like substances in LB-EPS formed more stable complexes with dicamba than those in TB-EPS, and protein-like substances have stronger binding capacity for dicamba than HAS.

As the interaction of micropollutants and EPS depends on their hydrophobic and hydrophilic characteristics, the PN/PS ratio has been used as an indicator of the relative hydrophobicity of the EPS content (Santschi *et al.*, 2021; Zhang *et al.*, 2019). Regarding PN/PS for total EPS content (Figure 6.2a), the increase observed after the addition of ATZ indicates that the hydrophobicity in the surface sludge increased mainly due to changes in the PN content. Moreover, the microorganisms ability to adapt to toxic compounds probably contributed to changes not only in PN content but also in EPS composition (Shiu *et al.*, 2020). This indicates that such a variation could have had an impact on the biomass aggregates' stability and structure (Wang *et al.*, 2014).

Figure 6.2b shows the LB-EPS components. The results demonstrated quite similar PS content for phases I and III and for phases II and IV. However, during phases with ATZ addition, PN significantly increased compared to phase I. The PN/PS ratio of LB-EPS rised from 2.14 to 6.74 (phases I-III) and then decreased to 3.51 in phase IV. The highest value of PN/PS for LB-EPS during phase III was mainly influenced by the lower PS concentration.

The PS TB-EPS had the same tendency as PN, except for phase IV, slightly decreasing compared with phase III (Figure 6.2c). Consequently, the PN/PS of TB-EPS increased to 3.74 during phase II due to rising PN content and unchanged concentration of PS. However, in phase III, both PS and PN increased, decreasing the PN/PS to 2.34. In phase IV, the PN/PS content raised, reaching the highest value of 4.13. On the other hand, the PN TB-EPS gradually increased from phase I to phase IV, probably due to the protective response of bacteria under ATZ exposure, producing PN with

hydrophobic characteristics. Indeed, oxidative stress (Singh *et al.*, 2018) is one of the reported adverse effects of ATZ in microorganisms, being observed significant changes in the metabolism of microorganisms in response to ATZ stress (Szewczyk *et al.*, 2020).

The overall results for LB- and TB-EPS components suggest that the addition of ATZ favored the increase of hydrophobic regions in EPS (Geyik *et al.*, 2016; Santschi *et al.*, 2021; Xu *et al.*, 2021) since PN/PS ratio results were more remarkable in phases with addition of ATZ than in phase I. Indeed, PN might dominate the interaction between ATZ and EPS due to the presence of more potential adsorption sites for ATZ adsorption than PS. Furthermore, PN contains more functional groups than PS, such as aromatic amino acid substances, favoring the ATZ-EPS complex's formation (Tao *et al.*, 2019).
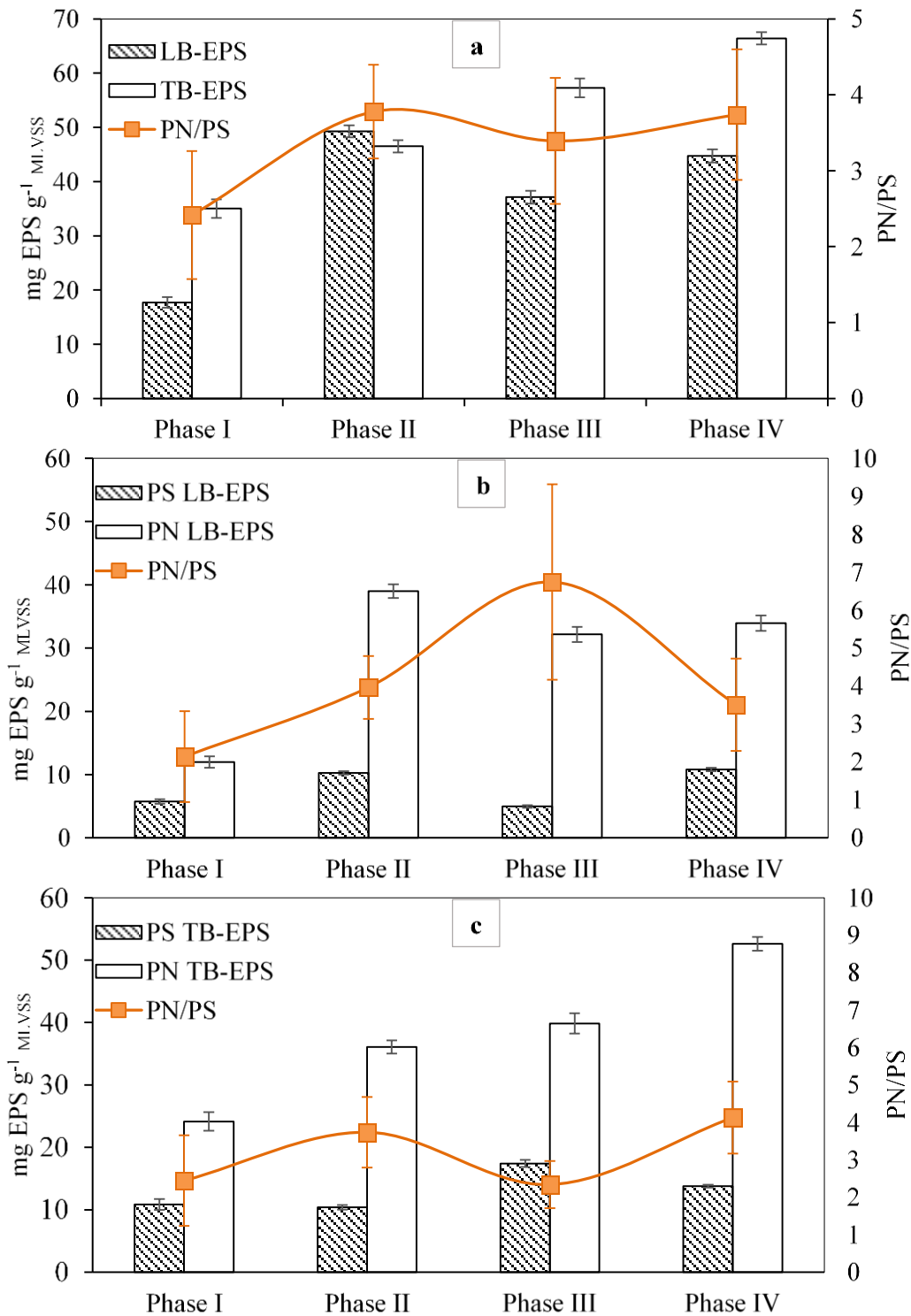
Figure 6.2 – LB-EPS and TB-EPS concentrations, and PN/PS ratios. (a) LB-, TB-EPS and total PN/PS ratio for different phases of SBR operation; (b) PS, PN, and PN/PS ratio of the LB-EPS; (c) PS, PN, and PN/PS ratio of the TB-EPS.

The 3D-EEM spectra of LB- and TB-EPS at the end of each phase are displayed in Figure 6.3. For LB, two fluorescence peaks were observed prior to ATZ exposure, and for TB-EPS, three fluorescence

peaks were observed that were smoother than those in LB-EPS. The fluorescence spectral position and intensity of fluorescence are summarized in Table 6.1. The identified peaks indicated that LB- and TB-EPS were composed mainly of tryptophan-containing proteins (peaks A and B), humic acid-like substances (peak D) and lastly, fulvic acid-like substances (peak C) (Figure 6.3). It was found that during ATZ exposure, the fluorescence intensities of peak B increased in both LB- and TB-EPS. On one hand, in LB-EPS, humic acid-like substances slightly varied during the experimental phases, with a decrease in the fluorescence intensity and being absent in phase III (Table 6.1, Figure 6.3a). On the other hand, in TB-EPS, humic acid-like substances were present with quite low fluorescence intensities throughout phases I, III and IV (Table 6.1, Figure 6.3b). Fluorescence intensities results suggest that protein was the main component in the interaction with ATZ in both LB- and TB-EPS.

The variation of 3D-EEM fluorescence spectra of LB- and TB-EPS under ATZ exposure revealed relationships between the peaks' intensities and the EPS components. Furthermore, the changes in the fluorescence peaks and increase in the fluorescence intensity of tryptophan-containing proteins highlight their role during the interaction between ATZ and EPS and provide information on the chemical structure changes of the EPS components (Chen *et al.*, 2002). Tao *et al.* (2019) found that the interaction between ATZ and EPS was mainly governed by the static fluorescence quenching process, suggesting the formation of an ATZ-EPS complex. These authors found a remarkable fluorescence decrease for protein-like substances from 8966 to 3011 when a fixed concentration of EPS was combined with a different concentration of ATZ. At the same time, static quenching indicates that EPS can bind to ATZ, which facilitates the entry of ATZ into the cells of degrading bacteria. Similar results were observed by Yu *et al.* (2019), reporting that EPS had an important influence on the adsorption of ATZ by biofilm, allowing cells to degrade ATZ. Tao *et al.* (2019) revealed that there was a slight shift in fluorescence spectra emission, likely because EPS protein was placed in a more hydrophobic environment after the addition of ATZ, which is in agreement with previous works (Szewczyk *et al.*, 2020; Xu *et al.*, 2013).
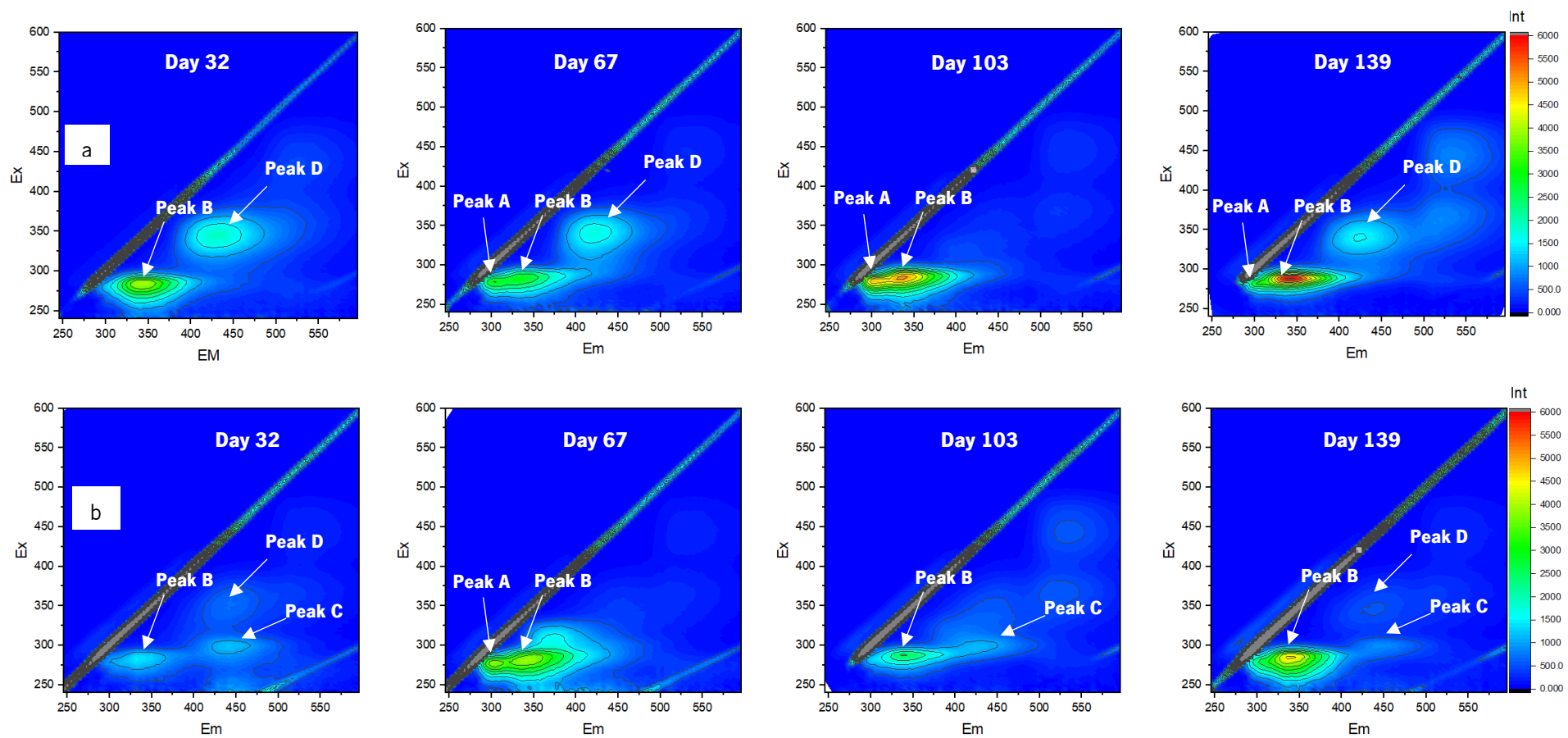
Figure 6.3 – EEM fluorescence spectra of LB-EPS and TB-EPS under different ATZ concentrations: (a) LB-EPS at the end of each phase; and (b) TB-EPS at the end of each phase.

Table 6.1 – Peak fluorescence intensity of samples at beginning, middle and end of each phase.

LB-EPS	Peak Intensity				TB-EPS	Peak Intensity			
Day	A	B	C	D	Day	A	B	C	D
32	-	3957	-	1867	32	-	1452	1200	675
67	3200	2970	-	1715	67	3790	3900	-	-
103	4815	5130	-	-	103	-	2540	4732	-
139	3000	6000	-	1525	139	-	4600	880	515

It was further calculated that the percent fluorescence response of region A (protein-like substances) remained almost stable for phases I, II and IV, increasing during phase III for LB-EPS and decreasing for TB-EPS (Table 6.2). In the presence of ATZ, it is possible to observe that the percent fluorescence response values of region A, only for TB-EPS, were consistently below the values obtained without ATZ, suggesting that protein-like substances were quenched in the presence of ATZ. Moreover, the results obtained for LB-EPS indicate that this fraction of the biopolymers did not interact with ATZ, which explains the increase in the percent fluorescence response in phase III. For region B (humic acid-like and fulvic acid-like substances), the lower percent fluorescence response suggests that these compounds had a minimum role in forming a complex of ATZ-EPS. Indeed, our results propose that proteins-like substances played a specific role in removing ATZ, probably by giving sites to ATZ adsorption and forming a complex ATZ-PN TB-EPS and then decreasing the percent fluorescence response, which follows previous literature (Tao *et al.*, 2019).

Table 6.2 – Average percentage of fluorescence response [Pi,n (%)] of LB-EPS and TB-EPS under different ATZ concentration for each phase.

LB-EPS	Pi,n (%) Region A	Pi,n (%) Region B	TB-EPS	Pi,n (%) Region A	Pi,n (%) Region B
Phase I	63.61	36.39	Phase I	71.12	28.88
Phase II	63.48	36.52	Phase II	70.99	29.01
Phase III	75.28	22.08	Phase III	65.02	34.83
Phase IV	63.58	36.42	Phase IV	69.40	24.09

6.2.4 Structural characterization

The TL/MLSS is a valuable parameter allowing the determination of the relationship between the presence of free filamentous bacteria and aggregates (Amaral, 2003). According to Jenkins *et al.* (2003), TL/MLSS larger than 10,000 mm mg^{-1} indicates the existence of filamentous bulking. From Figure 6.4, TL/MLSS decreased throughout the experimental phases, with values consistently below the threshold (<10,000 mm mg^{-1} MLSS), excluding the filamentous bulking phenomenon.

The AS had different compaction and settling properties throughout the experiment, with SVI varying from 167 to 68 mL g^{-1}. The sludge demonstrated deficient settling ability for SVI higher and close to 150 mL g^{-1}. This behavior was observed mainly during phase I until the middle of phase II as shown in Figure 6.4. This result suggests that beyond filamentous content, other characteristics influenced the sludge settling properties (Chen *et al.*, 2010). Afterwards, the SVI values decreased, obtaining the lowest value (68 mL g^{-1} MLSS) during phase IV. The obtained results indicate that the decrease in filaments content, changes in the EPS content and AS morphology, positively influenced the settling ability of AS, as will be discussed later. In fact, the present research follows previous studies that demonstrate the impact of AS aggregates' surface chemical properties, such as different EPS forms (PS, PN, LB-EPS, TB-EPS and PN/PS ratios), influencing the sludge settling ability (Chen *et al.*, 2010; Gao *et al.*, 2019; Shen *et al.*, 2020).
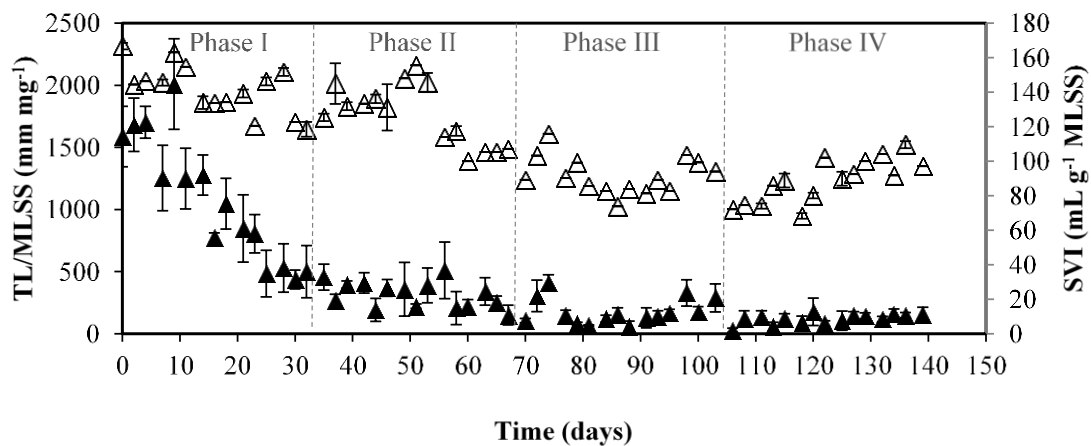
Figure 6.4 – TL/MLSS (▲) and SVI (Δ) behavior along experimental phases.

The aggregates area distribution presented in Figure 6.5 demonstrates during phase I, a significant presence of intermediate aggregates was found (%Area$_{int}$ ranging from 72 to 88%), concerning the small aggregates (%Area$_{sml}$ ranging from ≈5 to 24%) and large aggregates (%Area$_{larg}$

ranging from ≈2 to 11%). In phase II, an opposite behavior was observed for large and intermediate aggregates; while %Area$_{int}$ decreased from 80 to 52%, the %Area$_{larg}$ simultaneously increased from ≈16 to 42%. From the beginning of phase III (day 74) until the end of phase IV, a remarkable formation of larger aggregates (%Area$_{larg}$ from ≈48 to 68%) occurred (Figure 6.6). The rise of large aggregates, especially during phases III and IV, exposed to higher concentrations of ATZ, seems to be closely related to the increase of TB-EPS and total EPS production.
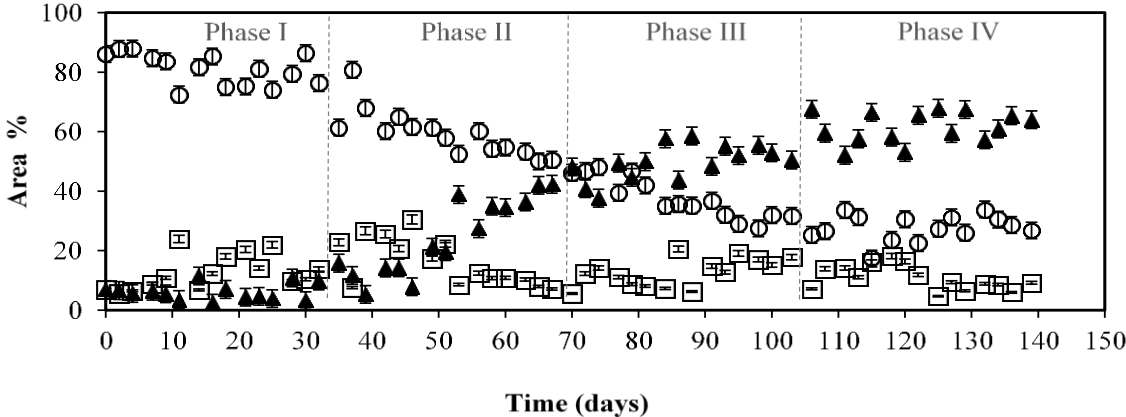
Figure 6.5 – Area percentage behavior for small (sml) (□), intermediate (int) (○), and large (larg) aggregates (▲) along experimental phases.
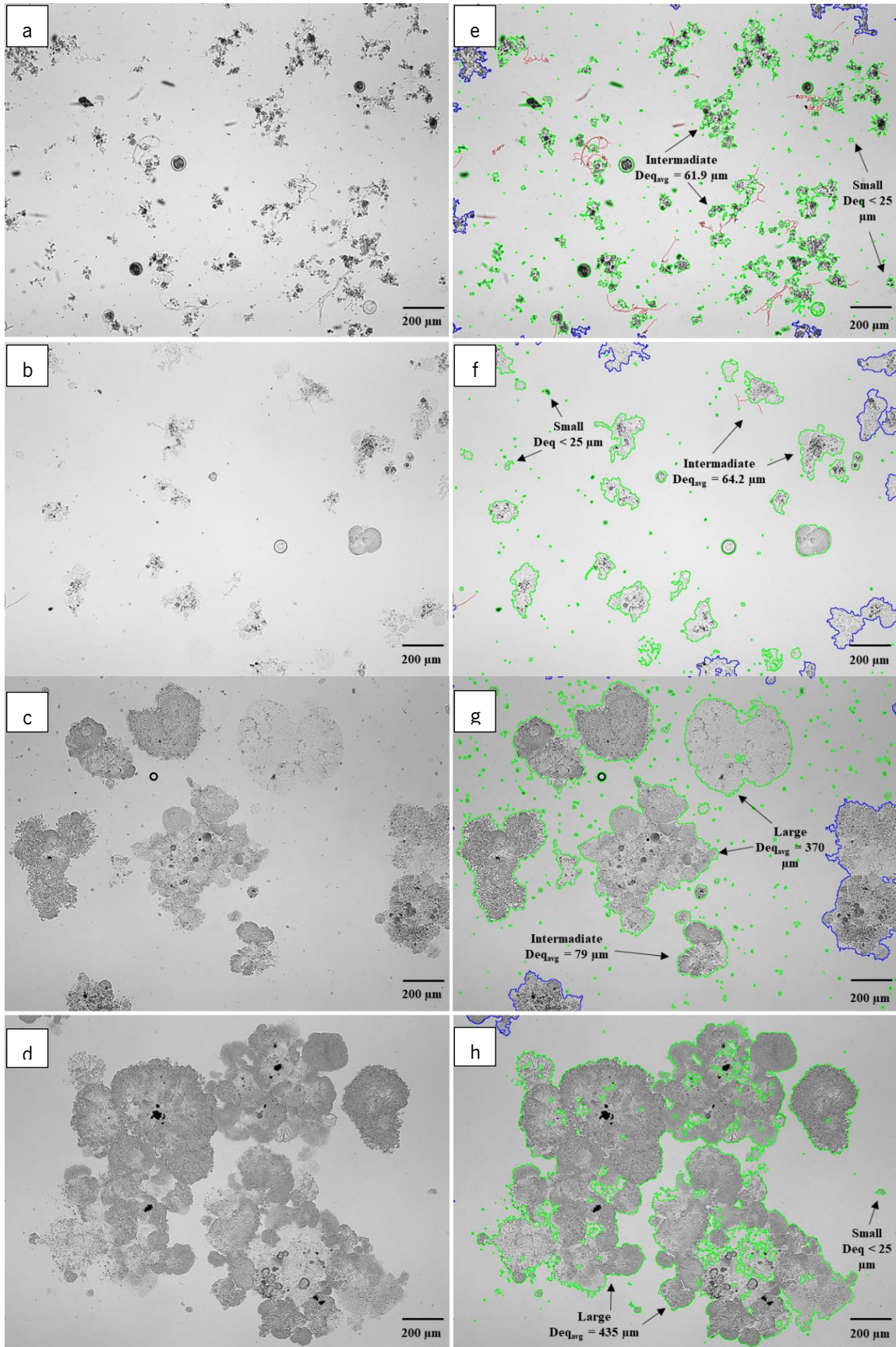
Figure 6.6 – Microscopic view of aerobic sludge during reactor operation. Image correspond to the beginning of each phase: (a) phase I, day-0; (b) phase II, day 35; (c) phase III, day 72; and (d) phase IV, day 106. Recognition of the aggregates by the image analysis software for the corresponding days in letters from (e) to (h). Size bar is

equivalent to 200 micrometers and diameter equivalent is presented in average values (Deq$_{avg}$) for that specific day. Dilution 1:4 for samples in phases II, III and IV.

In addition, a morphological characterization was performed related with the exposure to ATZ based on the evaluation of eccentricity, solidity and convexity (Figure 6.7). In general, intermediate aggregates exhibited compact, elongated structures and regular boundaries (high solidity, eccentricity, convexity values, respectively) along phases I-IV. During the experimental phases, large aggregates presented variable eccentricity values (ranging from elongated and circular structures). Finally, along phases I-IV, large aggregates became more compact (solidity values increased from 0.57 to 0.84) and presented irregular boundaries (low convexity values) due to ATZ exposure.
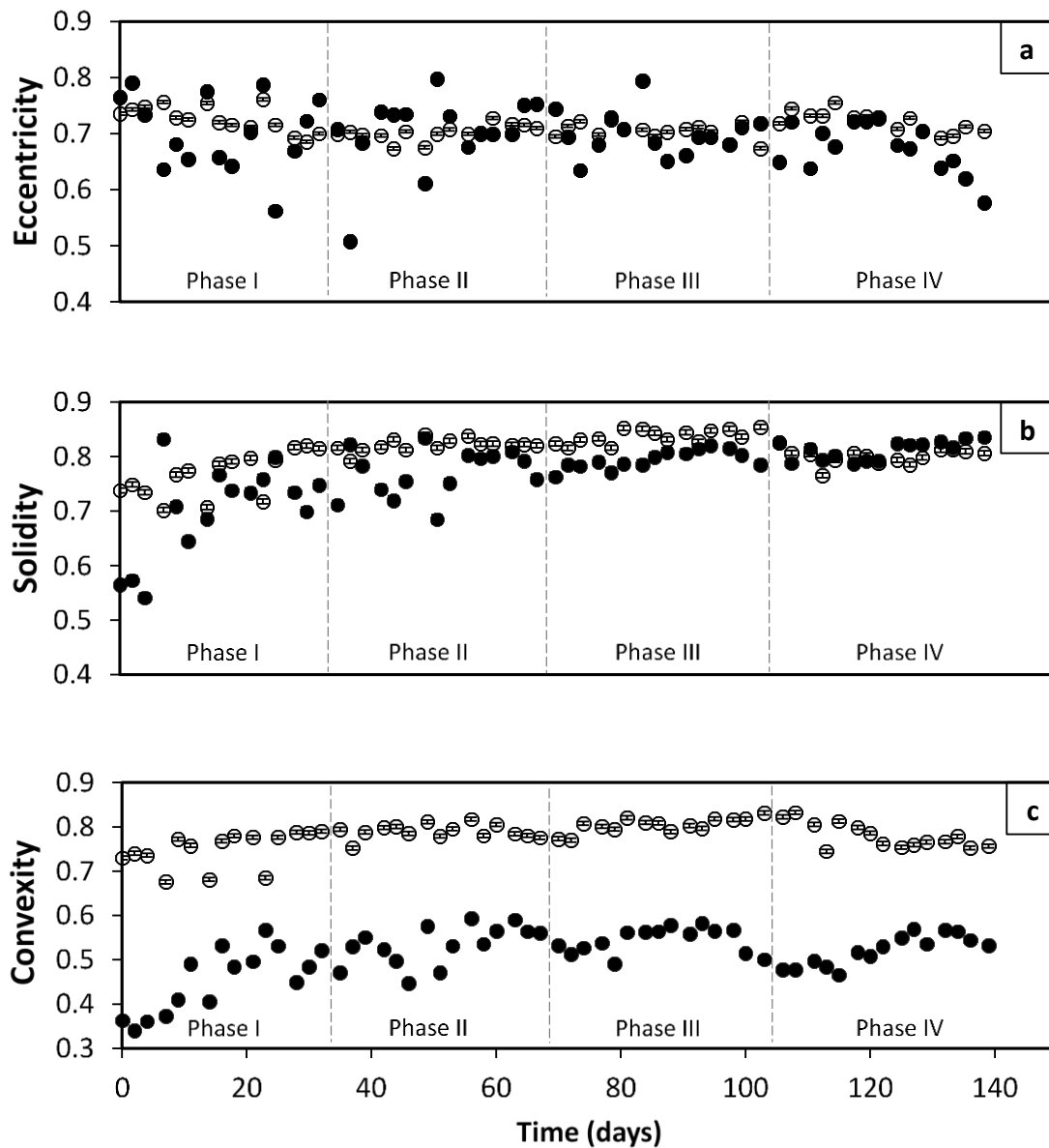
Figure 6.7 – The eccentricity (a), solidity (b) and convexity (c) for intermediate (o) and large (●) aggregates along phases I-IV.

6.2.5 Principal component analysis

The PCA addressed the QIA parameters (TL/MLSS, TL/Vol, Deq and %Area), SVI, and complete forms of EPS, including PN/PS ratios (Figures 6.8-6.10). PC1 explains 41% and PC2 explains 15% of the original dataset variance.

Concerning Figure 6.8a, phase I differed from phases II, III and IV, where the samples with the lowest values for total EPS and the highest filaments content were achieved on the positive side of PC1. Analyzing the variable's importance, shown in Figure 6.10a, the $\%Area_{int}$, Deq_{sml}, TL/Vol, TL/MLSS, and SVI positively influenced samples from phase I. In addition, the difference between phase I and phase II could be explained by the increase in all forms of EPS content (especially in LB-EPS forms) and an accentuated decrease in filaments content (TL/Vol and TL/MLSS), which contributed to the phase II samples being positioned in the middle of Figure 6.8a. On the other hand, phases III and IV showed a higher EPS content and its components, large aggregates size and fraction area (Deq_{larg}, $\%Area_{larg}$), located on the left side of PC1 and both quadrants. Regarding phases III and IV, samples from the end of phase III and from the beginning of phase IV (days 98 to 115) are located with negative scores of PC1 due to the higher content of EPS and large aggregate formation, while samples from day 118 through day 132 presented a lower concentration of EPS and moved toward the center of Figure 6.8a, staying close to most phase III samples. Figure 6.8b shows a correlation between the variables of $\%Area_{Larg}$, Deq_{int}, Deq_{larg}, the fraction TB-EPS and EPS in the left-bottom quadrant, which were the main variables that severely contributed to the negative values for PC1 and PC2 (Figure 6.10a-b). Moreover, the upper left quadrant revealed a correlation between the LB-EPS fractions and the PN/PS ratios (Figure 6.8b), with these variables being the primary influences on the displacement of samples to the upper left quadrant (Figure 6.10b). In addition, samples from days 98, 100 and 125 were placed in the left-bottom quadrant, being mainly influenced by the TB-EPS fractions, including PS and PN (Figure 6.10b).
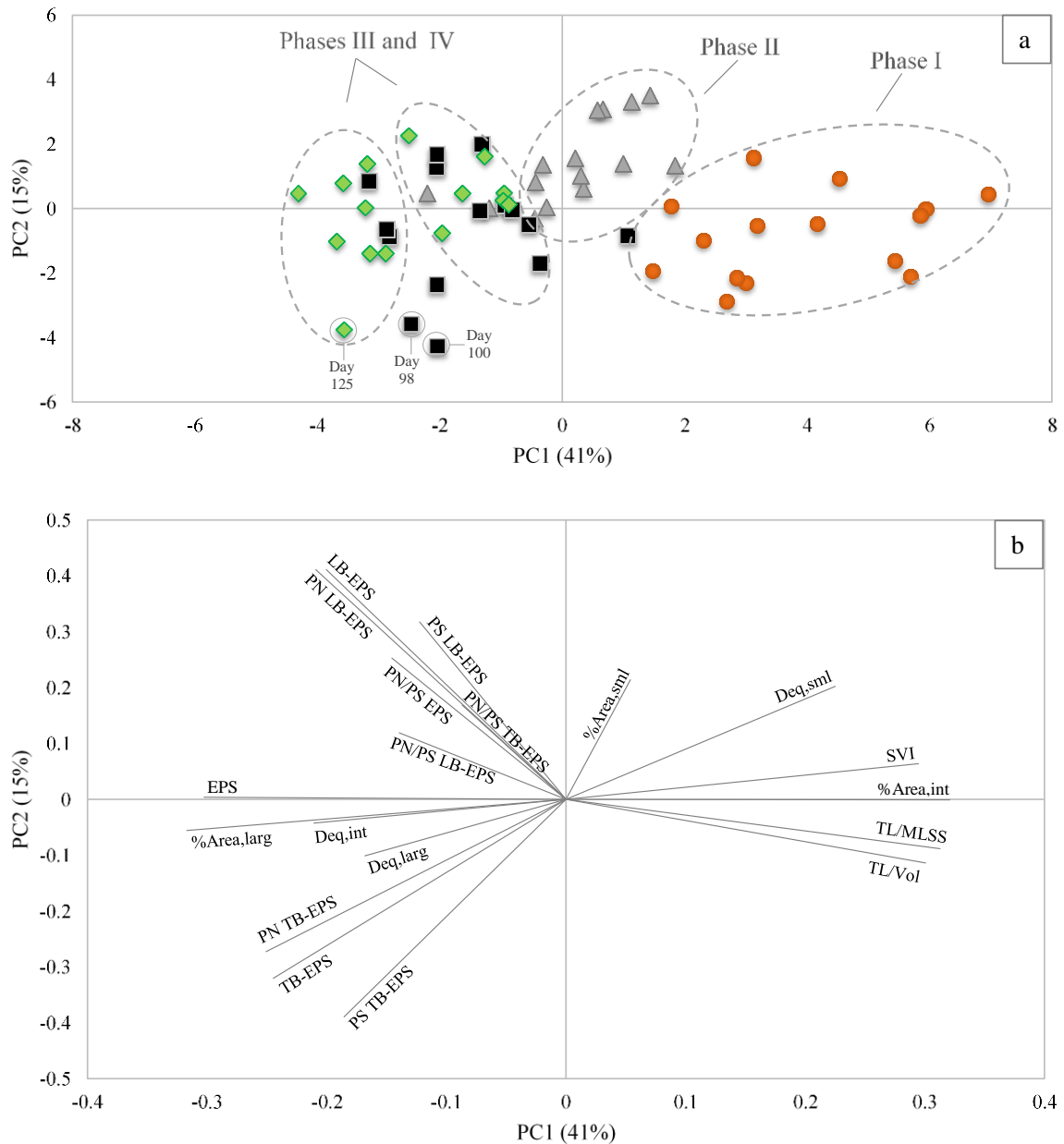
Figure 6.8 – PCA scores plot of the SBR operational parameters, EPS and QIA dataset for PC1 versus PC2. (a) phase I (●); phase II (▲); phase III (■); and phase IV (◆). (b) Variables loadings plot of PC1 and PC2.

The addition of the PC3 explaining 12% of the variance of the original dataset was evaluated in Figure 6.9. Phase III presented similar behavior for most samples being placed in the left-bottom quadrant, as showed in Figure 6.9a, except at the end of this phase (days 98 to 103). Regarding phase IV, part of the samples was influenced by the Deq_{int}, PN/PS ratio of total EPS and PN/PS LB-EPS, and part of the samples was most influenced by the different content of EPS (Figure 6.10c). Figure 6.9b shows a close relationship between $\%Area_{larg}$, Deq_{int} and the PN/PS ratios of all EPS forms in the left-bottom quadrant and a positive relationship between Deq_{larg} and all forms of EPS. These relationships

contributed to form a more defined cluster for phase III, with samples located in the left-bottom quadrant (Figure 6.9a). In contrast, for phase IV, two clusters were identified, one in the upper left quadrant, including samples with higher EPS concentration, and one in the left-bottom quadrant, with samples that showed higher values for the PN/PS ratios.
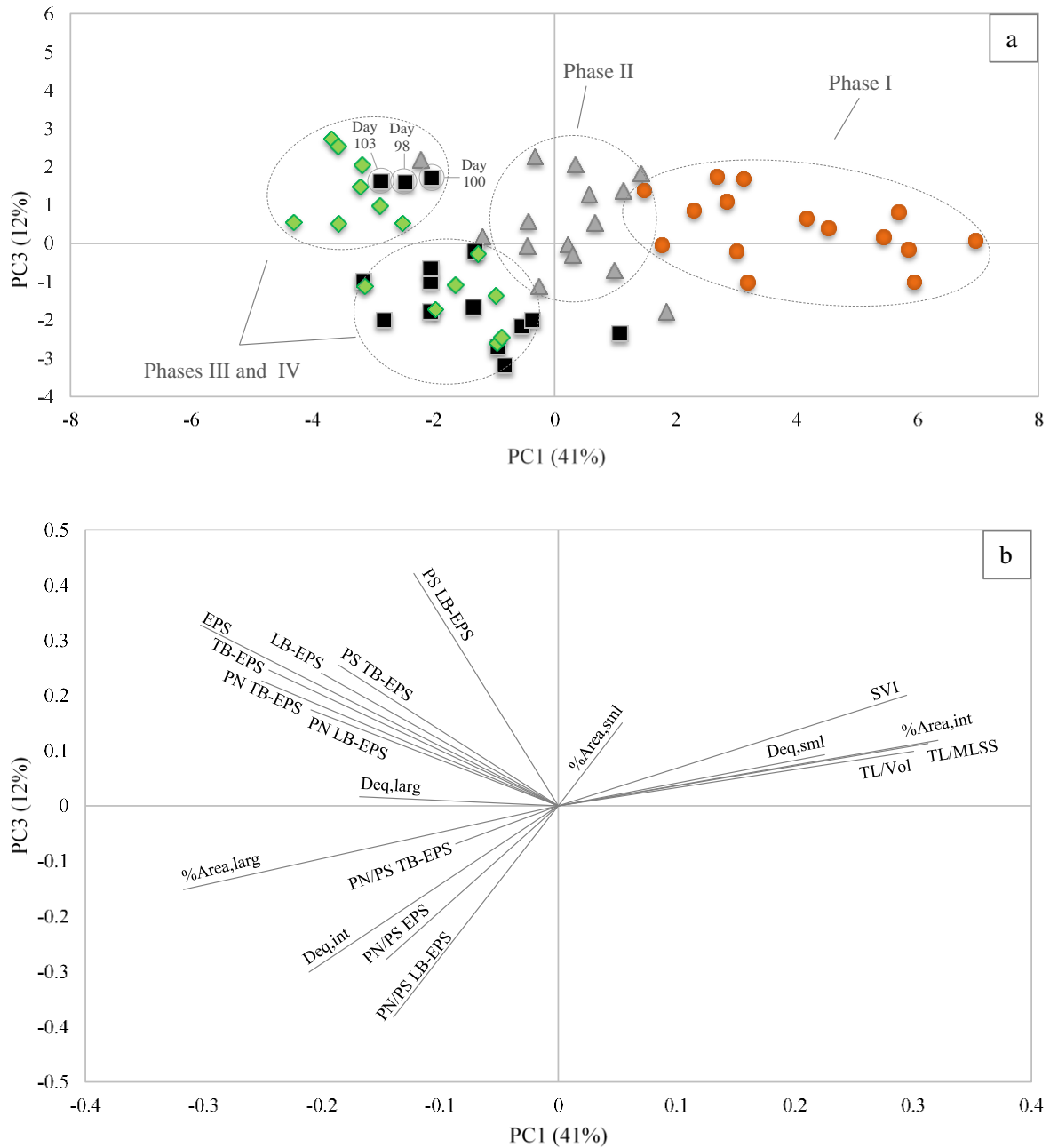
Figure 6.9 – PCA scores plot of the SBR operational parameters, EPS and QIA dataset for PC1 versus PC3. (a) phase I (●); phase II (▲); phase III (■); and phase IV (◆). (b) Variables loadings plot of PC1 and PC3.
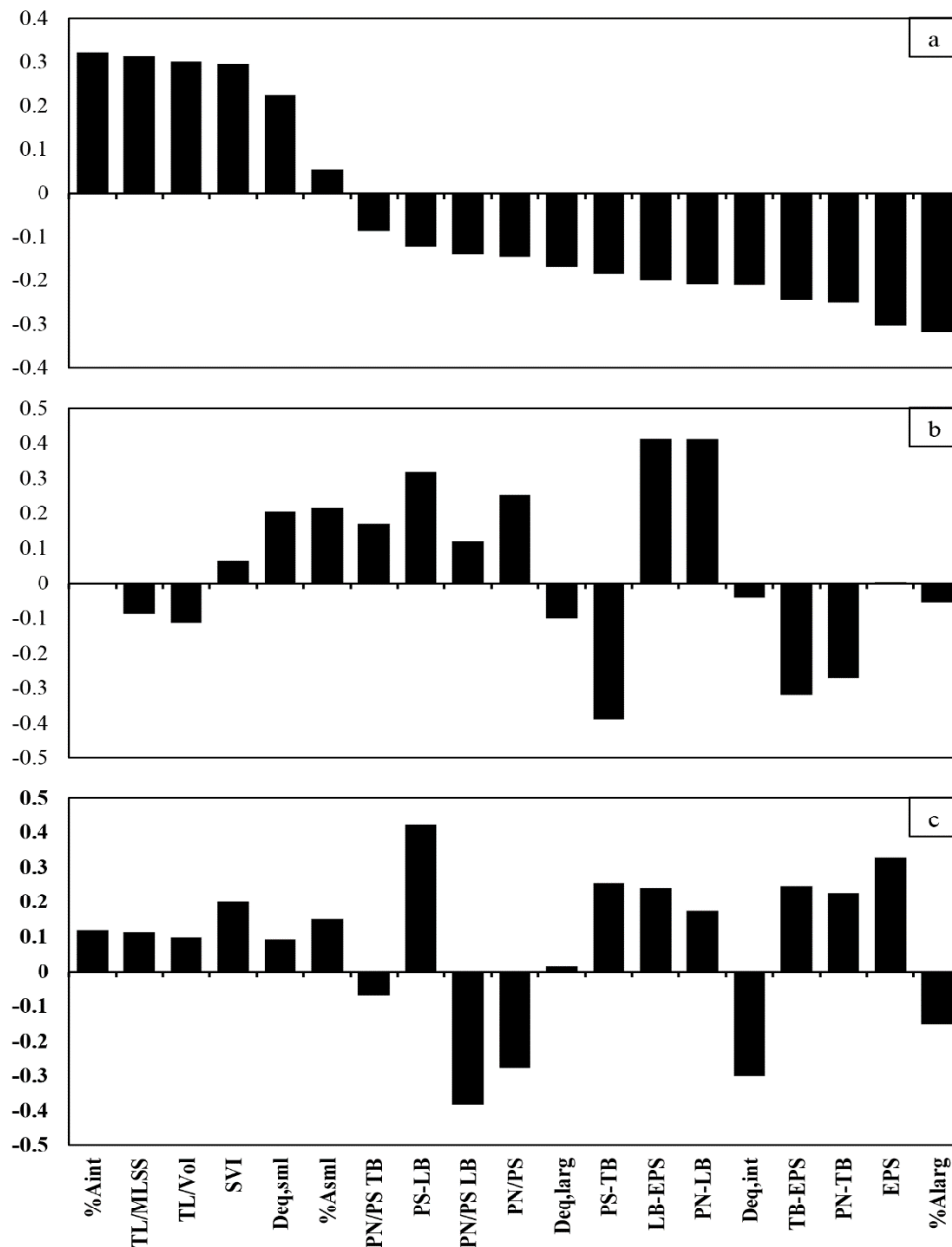
Figure 6.10 – Variable importance for PC1, PC2, and PC3 regarding the PCA analysis of Figures 6.8-6.9. (a) variable importance for PC1; (b) variable importance for PC2; and (c) variable importance for PC3.

These results support earlier findings (An *et al.*, 2016; Guo *et al.*, 2016) by showing that the increase in EPS content and TB-EPS forms over the operational period (Figure 6.2) may have had some impact on the noticeable emergence of large aggregates. The development of biomass from intermediate to large aggregates shows that the EPS content variation and the rise in the PN/PS ratios had an impact on the stability of the aggregates (as previously mentioned and shown in Figure 6.7), which is consistent with the findings of He *et al.* (2019). Furthermore, the present results corroborate the findings that EPS and its components play an essential role in the formation of granules during the

110

granulation process (Feng *et al.*, 2019; Hou *et al.*, 2015; Xu *et al.*, 2021). Furthermore, Basuvaraj *et al.* (2015) found that PN contributed to granules stability due to increased hydrophobicity and negative surface charge, favoring cell interaction. On the other hand, the abundance of β-sheet PS secondary structure was highly correlated with the variations in aggregates size during the granulation process (Shi and Liu, 2021), suggesting that the EPS components play different roles in the morphology and stability of the aggregates. Thus, the increase in the PN/PS ratio values under ATZ exposure suggests a change in the surface of the AS, in which the environment probably became more hydrophobic (Czaczyk and Myszka, 2007; Feng *et al.*, 2019; Wang *et al.*, 2005) since more PN were produced during these phases (Figure 6.2), and PS only presented a slight variation. Hence, in our study, alterations in the chemical characteristics of the AS surface affected the morphology of the aggregates, resulting in an improvement in settling ability throughout phases III and IV.

6.2.6   *Partial least square regression*

In this work, PLS was used to perform the analysis of the QIA dataset (Table 3.4) to predict PS and PN LB-EPS, PS and PN TB-EPS, LB-EPS, TB-EPS and total EPS. For this, two studies were developed, PLS1 considering all experiment observations (n = 60) and PLS2 considering each phase as an independent model (n = 15). Tables 6.3-6.4 present the selected variables and VIP values for each PLS model describing the different EPS types.

The first step employed for modelling EPS concentrations was the PLS analysis using a raw dataset containing all QIA variables. Then, the variables were sorted by the highest VIP values, and afterwards, the cross-correlation technique was performed to eliminate one variable for each pair representing a correlation factor above 0.9. The second step was to perform the PLS analysis again and select the latent variables with the highest VIP values (Costa *et al.*, 2022).

In PLS 1, the main variables (VIP > 0.80) for modelling all EPS forms are those related to morphological descriptors, which appeared most frequently for all PLS models (PS and PN LB-EPS, PS and PN TB-EPS, LB-EPS, TB-EPS, and total EPS) as described in Table 6.3. Following morphological descriptors, aggregates contents are the second variable group that most contributed to the PLS models with 3 to 5 variables. Interestingly, the number percentage per aggregate (%Nbi) contributed in all PLS models with VIP values greater than 0.90. For PN LB-EPS and LB-EPS, the %Nbi variable had the highest importance in contributing to the model with VIP of 1.43 and 1.44, respectively. Regarding the descriptor group of filamentous bacteria, TL/MLSS was the variable that most contributed to build the PLS regression models of PN LB-EPS, PS TB-EPS, PN TB-EPS, and TB-EPS. For PS LB-EPS and LB-EPS,

the number of filaments per volume (Nb_{fil}/Vol) with a VIP of 1.03 and 1.44, respectively, was the variable from the filamentous bacteria content descriptor group contributing the most for the PLS regression models. TL/TA with a VIP of 0.98 was the variable from the filamentous bacteria content descriptor group that contributed to the total EPS PLS model.

In PLS 2, variables related to filamentous bacteria content descriptor group were selected for the PLS regression models describing the individual EPS components (PS and PN), LB-EPS, TB-EPS and total EPS (Table 6.4). This descriptor group showed more influence for PN TB-EPS, being present in phases I, II and IV. In phase I with the variable TL/MLSS and TL/TA, in phase II with Nb_{thn}/Vol, and finally in phase IV with Nb_{fil}/Vol, all variables containing VIP > 0.80. For LB- and TB-EPS, Nb_{fil}/Vol appeared in phase IV with VIP of 1.25 and 1.21, respectively. Variables that presented less importance were TL/TA and TL/MLSS for LB-EPS (phase IV) and TL/MLSS for TB-EPS (phase I). Lastly, for total EPS, Nb_{int}/Vol had VIP of 1.74 and 1.59 for phases I and II, respectively.

For all models, aggregates morphology and content were the main descriptor groups that influenced the prediction of EPS content. Analyzing each PLS model, it is possible to observe that the descriptor group of morphological characteristics was the one that most frequently influenced the PLS regression. Indeed, this descriptor group presented between 5 to 8 variables with the highest VIP values (VIP > 0.80) for each PLS model (Table 6.4).

Regarding the aggregates content descriptor group, 6 variables presented VIP > 0.80 for PS LB-EPS models: Nb/Vol, $\%A_{int}$, Nb/Vol_{int} and Area/Vol_{int} for phase I; Nb/Vol_{larg} for phase II; $\%A_{larg}$ and $\%A_{int}$ for phase III; and Area/Vol_{int} for phase IV. For PN LB-EPS models, the variables with VIP > 0.80 that most contribute were $\%Nb_{larg}$ in phase III, Area/Vol_{larg} and Nb/Vol_{int} in phase IV. For PN LB-EPS models (all phases), aggregates morphological and size descriptor groups showed greater relevance standing out 18 variables with VIP > 0.80 (Table 6.4). Concerning the PLS analysis for LB-EPS fraction, parameters pertaining to aggregates content descriptor group appeared in phases II and IV (see Table 6.4). However, in phases I-IV, some morphological parameters (Ecc, LrgC, Comp, Conv and Rob) and parameters describing the aggregates size (Area and Deq) were more relevant in predicting LB-EPS content.

The aggregates content descriptor group influenced the models for phase IV, especially TB-EPS forms where for PN TB-EPS 4 variables (Nb/Vol_{int}, $\%Nb_{sml}$, Nb_{fil}/Vol, and $\%Nb_{larg}$), presented VIP > 0.80 and for PS TB-EPS, 3 variables ($\%Nb_{larg}$, $\%Nb_{int}$, and Nb/Vol_{int}), showed VIP > 0.80. Relatively to the TB-EPS fraction, 6 variables from the aggregates content descriptor group (Nb_{fil}/Vol, Nb_{int}/Vol, Nb/Vol,

TA/Vol, %Area, and %Nb) appeared throughout phases I-IV having a specific contribution in the PLS model. The remaining variables were related to aggregates morphology and size descriptor groups, with the Ecc, LrgC, Comp, Conv and Rob standing out again between variables, in addition to Round, Ext, and FF, and also aggregates size variables (Length, Width, Area, Per and Deq) appeared for TB-EPS assessment.

Regarding the PLS in what the total EPS is concerned (Table 6.4) from phase I to phase IV, aggregates morphology descriptors group were the most suited for representing EPS content. The small aggregates fraction only occurred among the variables in phases I-III. Furthermore, aggregate size descriptor group influenced the prediction of EPS content mainly in phase I, with VIP higher than 1 for Area$_{larg}$ and Width$_{larg}$.

By analyzing the PLS models, it was possible to observe the role of the different descriptor groups. For example, regarding PLS2 (best results), the descriptor group of filamentous bacteria content appeared in a few PLS models aiming to predict the EPS content. Considering all EPS forms and experiment phases, this descriptor group appeared in 9 models out of 28, with VIP higher than 0.80 but no more than 2 variables per model, while the descriptor group of morphological characteristics and aggregates content predominated among all PLS models with more variables having VIP greater than 0.80.

So far, it is known that EPS play an essential role in the floc formation, hydrophobic interaction and binding of the various floc constituents and may therefore be associated with the morphological characteristics of aggregates (Jin *et al.*, 2003). Besides, a higher amount of EPS was associated with large flocs (Sodhi *et al.*, 2022), and EPS are reported to participate in the granulation processes and benefit the maintenance of granules structure, which means that EPS are involved in changes in aggregates size (Shi and Liu, 2021). In addition, a significant role of specific EPS components rather than EPS amount determines the difference in the sludge morphology (Liu *et al.*, 2021; Shi *et al.*, 2022; Shi and Liu, 2021).

In this sense, PN was reported to affect microbial cell aggregation through changing hydrophobic interactions between microbial cells (Yin *et al.*, 2015). Accordingly, Shi and Liu (2021) found that PN, mainly β-sheets, was crucial in sludge size changes along with the sludge granulation process. Furthermore, relatively hydrophobicity, generally appointed as PN/PS ratio, has also been reported to interfere with the aggregation process, contributing to shifting in the morphology of the bioaggregates (Shi and Liu, 2021; Zhang *et al.*, 2020). In accordance, Wang *et al.* found that after TB-EPS extraction, the free energy (ΔG) of sludge samples increased, indicating that the sludge hydrophobicity decreased

significantly, and the adsorption capacity between sludge and water molecules increased. Besides, with the granulation process, the variation of ΔG before and after extraction of TB-EPS increased from 9.43 mJ/m^2 to 61.45 mJ/m^2. It indicated that TB-EPS was the main driver of sludge granulation because of its increasing adsorption on sludge cells and promoting cell aggregation (Wang *et al.*, 2021).

Taking the above into consideration, different forms of EPS have distinct physical and chemical properties that cause various effects on sludge properties, influencing the morphology of the aggregates (Wang *et al.*, 2021; Wang *et al.*, 2005). Hence, this fact can explain the predominance of aggregates morphology descriptors in matrix X with higher VIP (Tables 6.3 and 6.4) to assess PS, PN, LB-EPS, TB-EPS and total EPS content (matrix Y) during this work. In addition, the present results imply that a higher concentration of ATZ resulted in an increment of EPS, governed by large aggregates during phases III-IV. Furthermore, by modelling, mostly large and intermediate morphological descriptors represented the principal part of variables in assessing the different EPS forms.

Table 6.3 – Selected variables and VIP values for PS and PN LB-EPS, PS and PN TB-EPS, LB-EPS, TB-EPS, and total EPS for the global PLS regression models.

GLOBAL DATA

PS LB-EPS	VIP	PN LB-EPS	VIP	PS TB-EPS	VIP	PN TB-EPS	VIP	LB-EPS	VIP	TB-EPS	VIP	TOTAL EPS	VIP
Ecc_{int}	1.60	$\%Nb_{int}$	1.43	Deq_{sml}	1.45	$Width_{int}$	1.49	$\%Nb_{int}$	1.44	$Length_{int}$	1.44	$Area/Vol_{int}$	1.43
Deq_{int}	1.36	$LrgC_{sml}$	1.34	$RelArea_{larg}$	1.25	Sol_{larg}	1.48	$Length_{int}$	1.43	$Area/Vol_{larg}$	1.37	$\%Nb_{larg}$	1.35
$Comp_{larg}$	1.27	Sol_{sml}	1.27	$Length_{sml}$	1.24	$\%Nb_{larg}$	1.28	Ecc_{int}	1.38	Sol_{larg}	1.32	Sol_{larg}	1.34
Ext_{sml}	1.15	$Round_{larg}$	1.24	Rob_{sml}	1.22	$RelArea_{larg}$	1.26	FF_{sml}	1.33	$Area_{sml}$	1.29	$Length_{int}$	1.33
$LrgC_{larg}$	1.12	$\%A_{int}$	1.15	$Area/Vol_{int}$	1.15	$Width_{sml}$	1.23	Sol_{int}	1.22	$RelArea_{larg}$	1.19	$Area/Vol_{larg}$	1.24
Rob_{int}	1.10	$TL/MLSS$	1.14	Rob_{larg}	1.11	$Area/Vol_{int}$	1.11	Per_{sml}	1.19	$Area/Vol_{int}$	1.17	$\%Nb_{int}$	1.21
Nb_{fil}/Vol	1.03	$LrgC_{int}$	1.08	Ext_{int}	1.07	$TL/MLSS$	1.11	$Area/Vol_{larg}$	1.06	$Length_{sml}$	1.12	FF_{sml}	1.16
$Area_{sml}$	1.01	Per_{sml}	1.06	Sol_{larg}	1.04	Rob_{larg}	1.07	$LrgC_{sml}$	0.98	$TL/MLSS$	1.11	$RelArea_{int}$	1.02
$Width_{larg}$	1.00	Nb/Vol_{larg}	0.95	FF_{larg}	1.01	$Length_{sml}$	1.00	$RelArea_{int}$	0.95	$\%Nb_{larg}$	1.07	FF_{int}	1.01
TA/Vol	0.98	Ecc_{int}	0.94	$Conv_{int}$	1.00	Nb/Vol_{larg}	0.98	Nb_{fil}/Vol	0.91	Ecc_{larg}	0.99	TL/TA	0.98
$LrgC_{sml}$	0.93	FF_{int}	0.92	$TL/MLSS$	0.98	$\%Nbi_{int}$	0.92	$Area/Vol_{int}$	0.88	Ext_{sml}	0.92	Ecc_{int}	0.93
$\%Nb_{larg}$	0.93	$\%Nb_{larg}$	0.90	$Area/Vol_{larg}$	0.96	TA/Vol	0.90	Sol_{larg}	0.86	Deq_{larg}	0.81	$LrgC_{sml}$	0.89
$\%Ai_{int}$	0.92	Nb/Vol_{int}	0.89	$\%Nb_{larg}$	0.91	$Area_{larg}$	0.80	FF_{larg}	0.82	$RelArea_{int}$	0.80	Ecc_{larg}	0.87
Per_{int}	0.90	$Conv_{larg}$	0.86	Ext_{sml}	0.86	FF_{larg}	0.78	$Conv_{larg}$	0.75	Per_{larg}	0.77	Ecc_{sml}	0.86
$RelArea_{larg}$	0.72	Rob_{sml}	0.82	$Length_{int}$	0.83	Per_{larg}	0.73	Rob_{sml}	0.75	Ecc_{larg}	0.71	FF_{larg}	0.69
Rob_{sml}	0.72	$RelArea_{int}$	0.79	Per_{larg}	0.75	FF_{sml}	0.67	TA/Vol	0.73	$Length_{larg}$	0.66	$Conv_{int}$	0.66
Nb/Vol_{int}	0.71	TA/Vol	0.78	Ecc_{int}	0.74	$\%Ai_{sml}$	0.64	Ecc_{larg}	0.72	Ecc_{int}	0.65	Ecc_{larg}	0.60
Rob_{larg}	0.69	Rob_{larg}	0.66	Ecc_{larg}	0.68	Ecc_{sml}	0.64	$Comp_{larg}$	0.72	FF_{larg}	0.64	$RelArea_{larg}$	0.58
Per_{larg}	0.68	$Width_{sml}$	0.63	$Width_{larg}$	0.64	$LrgC_{sml}$	0.58	$\%Nb_{larg}$	0.60	Ext_{larg}	0.63	$Area_{larg}$	0.50
FF_{larg}	0.59	FF_{larg}	0.63	$Conv_{larg}$	0.62	Rob_{int}	0.52	$Length_{larg}$	0.49	Rob_{sml}	0.58	Per_{larg}	0.43

115

Table 6.4 – Selected variables and VIP values for PS and PN LB-EPS, PS and PN TB-EPS, LB-EPS, TB-EPS, and total EPS for the PLS regressions for phases I-IV.

PS LB-EPS							
Phase I		**Phase II**		**Phase III**		**Phase IV**	
Parameters	VIP	Parameters	VIP	Parameters	VIP	Parameters	VIP
$LrgC_{larg}$	1.66	Rob_{sml}	1.48	Ecc_{sml}	1.36	Ecc_{larg}	1.60
$Comp_{larg}$	1.16	TL/Vol	1.42	$Width_{larg}$	1.10	$Area/Vol_{int}$	1.28
Nb/Vol	1.11	Nb/Vol_{larg}	1.29	$\%A_{larg}$	1.07	$Conv_{int}$	1.09
$Length_{int}$	1.00	$LrgC_{int}$	0.95	$\%A_{int}$	1.07	Rob_{larg}	1.02
$\%A_{int}$	0.88	$Length_{larg}$	0.93	Sol_{larg}	1.05	TL/TA	1.01
Nb/Vol_{int}	0.86	Nb_{thn}/Vol	0.85	$RelArea_{larg}$	0.90	$LrgC_{int}$	0.91
$Area/Vol_{int}$	0.85	TL/TA	0.72	$LrgC_{larg}$	0.89	$RelArea_{int}$	0.72
$Area/Vol_{larg}$	0.76	FF_{sml}	0.64	Ecc_{int}	0.87	$Conv_{larg}$	0.71
Ecc_{larg}	0.71	$RelArea_{int}$	0.62	Rob_{larg}	0.79	TA/Vol	0.70
$Area_{int}$	0.58	Deq_{larg}	0.53	Per_{larg}	0.75	$LrgC_{larg}$	0.49
PN LB-EPS							
Phase I		**Phase II**		**Phase III**		**Phase IV**	
Parameters	VIP	Parameters	VIP	Parameters	VIP	Parameters	VIP
Ecc_{int}	1.89	$LrgC_{int}$	1.46	Sol_{sml}	1.38	FF_{sml}	1.47
Ecc_{larg}	1.47	$RelArea_{int}$	1.23	$LrgC_{larg}$	1.37	Ecc_{larg}	1.05
$RelArea_{larg}$	0.94	Deq_{larg}	1.20	Ecc_{int}	1.28	FF_{larg}	1.05
Deq_{larg}	0.92	Rob_{sml}	1.11	$\%Nb_{larg}$	0.92	$Area/Vol_{larg}$	1.04
$RelArea_{int}$	0.87	$LrgC_{sml}$	0.91	$RelArea_{larg}$	0.87	Nb/Vol_{int}	0.99
Per_{larg}	0.73	$Length_{int}$	0.90	$Conv_{larg}$	0.86	Nb_{fil}/Vol	0.99
$Conv_{larg}$	0.69	Rob_{int}	0.87	Per_{larg}	0.80	Ext_{larg}	0.98
$\%A_{int}$	0.58	Nb/Vol_{larg}	0.79	$Length_{larg}$	0.76	Per_{larg}	0.85
$Area/Vol_{sml}$	0.58	$Conv_{larg}$	0.67	Ext_{int}	0.73	$Conv_{int}$	0.75
Rob_{larg}	0.27	TA/Vol	0.47	$Area_{larg}$	0.70	$Width_{larg}$	0.62
PS TB-EPS							
Phase I		**Phase II**		**Phase III**		**Phase IV**	
Parameters	VIP	Parameters	VIP	Parameters	VIP	Parameters	VIP
$\%Nb_{larg}$	1.48	Ecc_{sml}	1.43	$Conv_{larg}$	1.62	FF_{larg}	1.31
$TL/MLSS$	1.47	$Width_{sml}$	1.26	$Conv_{int}$	1.41	Per_{larg}	1.29
Ecc_{larg}	1.40	$Width_{larg}$	1.11	$Round_{sml}$	1.10	Deq_{sml}	1.24
Rob_{larg}	1.18	Nb/Vol_{larg}	1.10	$\%A_{larg}$	0.97	$\%Nb_{larg}$	1.14
$Area_{sml}$	1.13	Sol_{sml}	1.04	$\%Ai_{int}$	0.94	$\%Nb_{int}$	1.00
$RelArea_{int}$	0.53	$\%Ai_{int}$	0.95	Rob_{sml}	0.88	Nb/Vol_{int}	0.87
$Conv_{sml}$	0.51	$\%Ai_{larg}$	0.88	Per_{larg}	0.76	Ecc_{sml}	0.82
TA/Vol	0.50	Ecc_{larg}	0.68	Ext_{int}	0.63	$Length_{sml}$	0.68
$Width_{sml}$	0.45	$LrgC_{int}$	0.67	$Area_{larg}$	0.56	TA/Vol	0.66
$Width_{int}$	0.16	Per_{larg}	0.50	$Length_{larg}$	0.54	TL/TA	0.65

116

PN TB-EPS

Phase I		Phase II		Phase III		Phase IV	
Parameters	VIP	Parameters	VIP	Parameters	VIP	Parameters	VIP
$Width_{int}$	1.61	$Width_{sml}$	1.46	$Conv_{int}$	1.70	Nb/Vol_{int}	1.34
$RelArea_{int}$	1.57	Nb/Vol_{larg}	1.18	$Round_{sml}$	1.33	$Length_{sml}$	1.27
$TL/MLSS$	1.19	$Width_{larg}$	1.13	$LrgC_{sml}$	1.06	$\%Nbi_{sml}$	1.15
$\%Ai_{larg}$	0.94	$Comp_{sml}$	1.10	Ecc_{larg}	0.97	Nb_{fil}/Vol	1.03
TL/TA	0.89	FF_{sml}	1.03	Rob_{sml}	0.96	Deq_{sml}	1.02
$LrgC_{sml}$	0.81	Nb_{thn}/Vol	0.88	TA/Vol	0.86	FF_{larg}	0.96
$Conv_{sml}$	0.70	$Conv_{larg}$	0.84	$Area/Vol_{larg}$	0.81	$\%Nbi_{larg}$	0.80
$\%Nb_{larg}$	0.54	Sol_{sml}	0.78	$Area_{larg}$	0.66	$Conv_{larg}$	0.78
Rob_{larg}	0.48	$Comp_{int}$	0.74	$Conv_{larg}$	0.59	$Area/Vol_{larg}$	0.72
Nb/Vol_{larg}	0.48	TL/TA	0.54	Per_{larg}	0.42	$\%Ai_{larg}$	0.68

LB-EPS

Phase I		Phase II		Phase III		Phase IV	
Parameters	VIP	Parameters	VIP	Parameters	VIP	Parameters	VIP
Ecc_{int}	1.63	$LrgC_{int}$	1.39	Ecc_{int}	1.55	FF_{sml}	1.38
$Area_{sml}$	1.26	$Comp_{int}$	1.23	$Conv_{larg}$	1.09	$Area_{larg}$	1.36
$Area_{larg}$	1.21	Rob_{sml}	1.02	Sol_{larg}	1.09	Nb_{fil}/Vol	1.25
Rob_{sml}	0.99	Rob_{int}	1.01	Sol_{sml}	1.07	$Width_{larg}$	1.22
$RelArea_{larg}$	0.99	Deq_{larg}	0.98	Ext_{int}	1.06	$Area_{int}$	0.94
Ecc_{larg}	0.80	Nb_{larg}	0.98	$Length_{larg}$	0.96	Ecc_{larg}	0.93
$Conv_{larg}$	0.75	$Conv_{larg}$	0.94	$Area_{larg}$	0.87	Rob_{larg}	0.85
$Comp_{larg}$	0.68	$Length_{sml}$	0.92	$LrgC_{larg}$	0.75	TL/TA	0.58
$LrgC_{sml}$	0.64	TA/Vol	0.73	Ecc_{sml}	0.67	$TL/MLSS$	0.51
Rob_{larg}	0.54	$LrgC_{sml}$	0.54	$Width_{sml}$	0.50	Ext_{larg}	0.35

TB-EPS

Phase I		Phase II		Phase III		Phase IV	
Parameters	VIP	Parameters	VIP	Parameters	VIP	Parameters	VIP
$RelArea_{int}$	1.37	$Width_{sml}$	1.59	$Conv_{int}$	1.65	FF_{int}	1.25
Ecc_{larg}	1.35	$Width_{larg}$	1.41	$Round_{sml}$	1.14	$\%Nb_{sml}$	1.23
$Area_{larg}$	1.29	Ecc_{sml}	1.20	Ext_{int}	1.10	Nb_{fil}/Vol	1.21
Rob_{larg}	1.09	$LrgC_{sml}$	0.99	$\%Area_{larg}$	0.91	Deq_{sml}	1.16
$Comp_{larg}$	1.03	Ext_{sml}	0.97	$LrgC_{larg}$	0.90	FF_{sml}	1.16
TA/Vol	0.98	Nb_{int}/Vol	0.93	$Conv_{larg}$	0.88	$Length_{sml}$	0.84
$TL/MLSS$	0.77	Rob_{larg}	0.69	$LrgC_{sml}$	0.85	Per_{int}	0.82
Nb/Vol_{larg}	0.59	Per_{sml}	0.59	Rob_{sml}	0.84	$\%Nb_{larg}$	0.76
$Width_{int}$	0.53	$Conv_{larg}$	0.53	$Area_{larg}$	0.71	Ecc_{sml}	0.72
$Conv_{sml}$	0.46	$LrgC_{larg}$	0.39	TA/Vol	0.66	$\%Area_{larg}$	0.52

Total EPS							
Phase I		**Phase II**		**Phase III**		**Phase IV**	
Parameters	VIP	Parameters	VIP	Parameters	VIP	Parameters	VIP
Nb_{int}/Vol	1.74	Nb_{int}/Vol	1.59	$RelArea_{larg}$	1.58	FF_{larg}	1.31
$Area/Vol_{larg}$	1.19	$Round_{sml}$	1.48	$\%Area_{int}$	1.11	Nb/Vol_{int}	1.26
Rob_{Larg}	1.10	Ecc_{int}	1.36	Ecc_{int}	1.08	Ext_{larg}	1.26
$Width_{larg}$	1.07	$Width_{sml}$	1.01	$\%Area_{larg}$	1.07	$Comp_{larg}$	1.23
$\%Area_{int}$	1.01	Ecc_{larg}	0.87	$Round_{sml}$	1.07	$Conv_{int}$	1.16
$LrgC_{sml}$	0.80	$LrgC_{int}$	0.82	$Area_{larg}$	1.04	$Area_{larg}$	0.94
$\%Nb_{larg}$	0.76	$LrgC_{sml}$	0.58	Sol_{larg}	0.85	Ecc_{larg}	0.69
Per_{larg}	0.73	$Width_{larg}$	0.57	Nb/Vol_{larg}	0.61	FF_{int}	0.67
Nb/Vol_{larg}	0.68	$Round_{int}$	0.45	Rob_{sml}	0.61	$Area_{int}$	0.60
$Conv_{sml}$	0.34	Per_{larg}	0.32	$Comp_{sml}$	0.52	Nb/Vol_{larg}	0.31

For each PLS result, the regression equation, coefficient of determination (R^2), RMSEP and RPD values were determined, as well as the limits of applicability of the models (minimum and maximum) values for each studied parameter. The regression equation, RMSEP and RPD values are presented for the global (training + validation) dataset, whereas the R^2 values are presented for the global, training and validation dataset (Table 6.5). An RPD parameter, i.e. the ratio between the standard deviation of the observed values and the prediction standard error (RMSEP), larger than 3 is recommended for screening purposes (Cozzolino *et al.*, 2004; Quintelas *et al.*, 2020).

For PLS 1, PLS models obtained do not fit well with the measured data (matrix Y). For example, the RMSEP values ranged from 12.4 for PN LB-EPS to 19.8 for total EPS model, and the lowest values were obtained for PS LB-EPS (4.1) and PS TB-EPS (6.0) (Table 6.5). Furthermore, considering RPD for all global models, the values were always <3 for the global set (training + validation), which indicated that these PLS regression models do not present a good ability to predict the matrix Y. Moreover, R^2 values ranging from 0.42 for PS LB-EPS to 0.74 for total EPS were achieved (Table 6.5 and Figure 6.11).

For PLS 2, the methodology adopted allowed for an adequate assessment for all EPS forms. Regarding EPS components (PS and PN), lower values for RMSEP were obtained ranging from 0.3 (PS LB-EPS) to 2.2 (PN TB-EPS), while for LB-EPS, RMSEP values ranging from under 1 to 3.6, 1.1 to 4.0 for TB-EPS, and from 2.8 to slightly above 7 for total EPS. Also, the PLS assessment ability analysis revealed that all the EPS forms presented RPD values > 3 for all the PLS regression models (Table 6.5) for the global set (training + validation). Also, regression analysis presented reasonable assessment abilities for PS LB-EPS phase I (R^2 of 0.86, Figure 6.12), LB-EPS phase III (R^2 of 0.88, Figure 6.14) and

TB-EPS phase I (R^2 of 0.88, Figure 6.14). For all other models, the assessment ability presented good capacity ($R^2 > 0.9$) in determining the EPS content (Figures 6.12-6.14).

In overview, the implemented strategy considering the characteristics inherent to each phase can produce satisfactory PLS models with a very high level of accuracy of assessment than PLS models considering the whole global data (Asensi *et al.*, 2019). Furthermore, the selection of samples by phases for the elaboration of each PLS calibration model could apparently minimize the influence of the effects of ATZ on the morphology of the aggregates since the samples from phases III and IV completely differ from phases I and II (Figures 6.6, 6.8 and 6.9). Thus, the adopted strategy of using more than one PLS model to predict particular features in a system with high data variability may produce more accurate model (Lourenço *et al.*, 2010; Sampson *et al.*, 2013). Finally, our findings demonstrated that QIA parameters allowed assessing EPS content through PLS models, being a suitable time-saving and environmentally friendly methodology minimizing the need of chemicals.

Table 6.5 – Regression equation, R^2, RMSEP and RPD values for each studied EPS form (glb – global, trn – training set, and val – validation set).

Matrix (Y)	PLS	Phase	Regression Equation glb	R^2 glb	R^2 trn	R^2 val	RMSEP	RPD	Mín	Máx
PS-LB EPS	PLS1	global	Y = 0.69 x + 3.00	0.42	0.75	0.11	4.1	1.2	1.10	20.32
	PLS2	I	Y = 0.99 x + 0.74	0.86	0.97	0.89	0.8	4.7	1.10	14.73
		II	Y = 1.01 x – 0.17	0.96	0.98	0.95	0.3	10.2	2.85	15.00
		III	Y = 1.00 x – 0.10	0.96	0.98	0.93	0.3	9.8	1.18	10.39
		IV	Y = 0.93 x + 0.32	0.92	0.91	0.96	0.8	7.0	2.98	20.32
PN-LB EPS	PLS1	global	Y = 0.66 x + 10.23	0.56	0.66	0.58	12.4	1.4	0.69	58.36
	PLS2	I	Y = 1.00 x + 0.00	0.92	0.96	0.86	1.3	7.0	0.69	31.41
		II	Y = 0.95 x + 2.00	0.96	0.98	0.90	1.0	10.9	18.2	54.94
		III	Y = 0.96 x + 0.50	0.97	0.99	0.97	1.4	12.3	9.11	58.36
		IV	Y = 1.00 x – 0.01	0.96	0.98	0.93	1.5	10.2	14.55	56.04
PS-TB EPS	PLS1	global	Y = 0.80 x + 2.54	0.51	0.78	0.24	6.0	1.2	2.17	38.12
	PLS2	I	Y = 1.00 x + 0.80	0.93	0.99	0.95	0.9	6.6	2.17	22.01
		II	Y = 1.00 x + 0.01	0.92	0.96	0.92	0.6	8.9	5.25	22.60
		III	Y = 1.00 x + 0.54	0.96	0.98	0.95	0.9	9.6	9.93	38.12
		IV	Y = 1.01 x – 0.41	0.93	0.96	0.93	0.9	7.5	5.66	27.04
PN-TB EPS	PLS1	global	Y = 0.73 x + 10.12	0.58	0.66	0.53	13.1	1.4	3.47	83.49
	PLS2	I	Y = 0.97 x + 0.67	0.95	0.94	0.97	1.9	9.2	3.47	50.60
		II	Y = 0.98 x – 0.21	0.91	0.96	0.79	1.8	6.5	16.99	52.64
		III	Y = 0.97 x – 0.57	0.95	0.98	0.91	2.2	8.4	14.7	71.85
		IV	Y = 0.94 x + 3.40	0.97	0.99	0.95	1.6	12.2	25.25	83.49
LB-EPS	PLS1	global	Y = 0.95 x + 2.06	0.52	0.80	0.43	18.5	1.1	1.79	73.83
	PLS2	I	Y = 1.03 x – 0.62	0.97	0.99	0.94	1.0	12.2	1.79	46.14
		II	Y = 0.99 x + 1.33	0.98	1.00	0.94	0.9	14.9	21.05	69.94
		III	Y = 1.01 x + 1.04	0.88	0.94	0.91	3.6	5.3	10.48	66.28
		IV	Y = 1.01 x + 1.31	0.94	0.98	0.94	2.7	7.5	18.92	73.83

TB-EPS	PLS1	global	Y = 0.79 x + 10.22	0.63	0.74	0.54	16.3	1.6	5.78	109.97
	PLS2	I	Y = 0.99 x + 2.59	0.88	0.80	0.99	4.0	5.5	5.78	72.61
		II	Y = 1.01 x + 0.00	0.98	0.99	0.96	1.1	14.8	22.24	71.63
		III	Y = 0.99 x + 1.15	0.97	0.98	0.93	2.1	12.7	26.41	109.97
		IV	Y = 0.99 x – 1.05	0.93	0.98	0.71	3.6	7.2	32.20	109.69
Total EPS	PLS1	global	Y = 1.00 x – 1.24	0.74	0.86	0.72	19.8	1.7	23.36	154.78
	PLS2	I	Y = 1.00 x – 0.32	0.93	0.94	0.94	2.8	7.8	23.36	95.60
		II	Y = 0.99 x + 1.01	0.92	0.93	0.91	3.1	6.8	55.1	141.57
		III	Y = 0.99 x + 2.19	0.94	0.97	0.88	7.3	4.1	48.73	141.68
		IV	Y = 0.91 x + 5.99	0.90	0.96	0.86	5.6	5.9	60.34	154.78
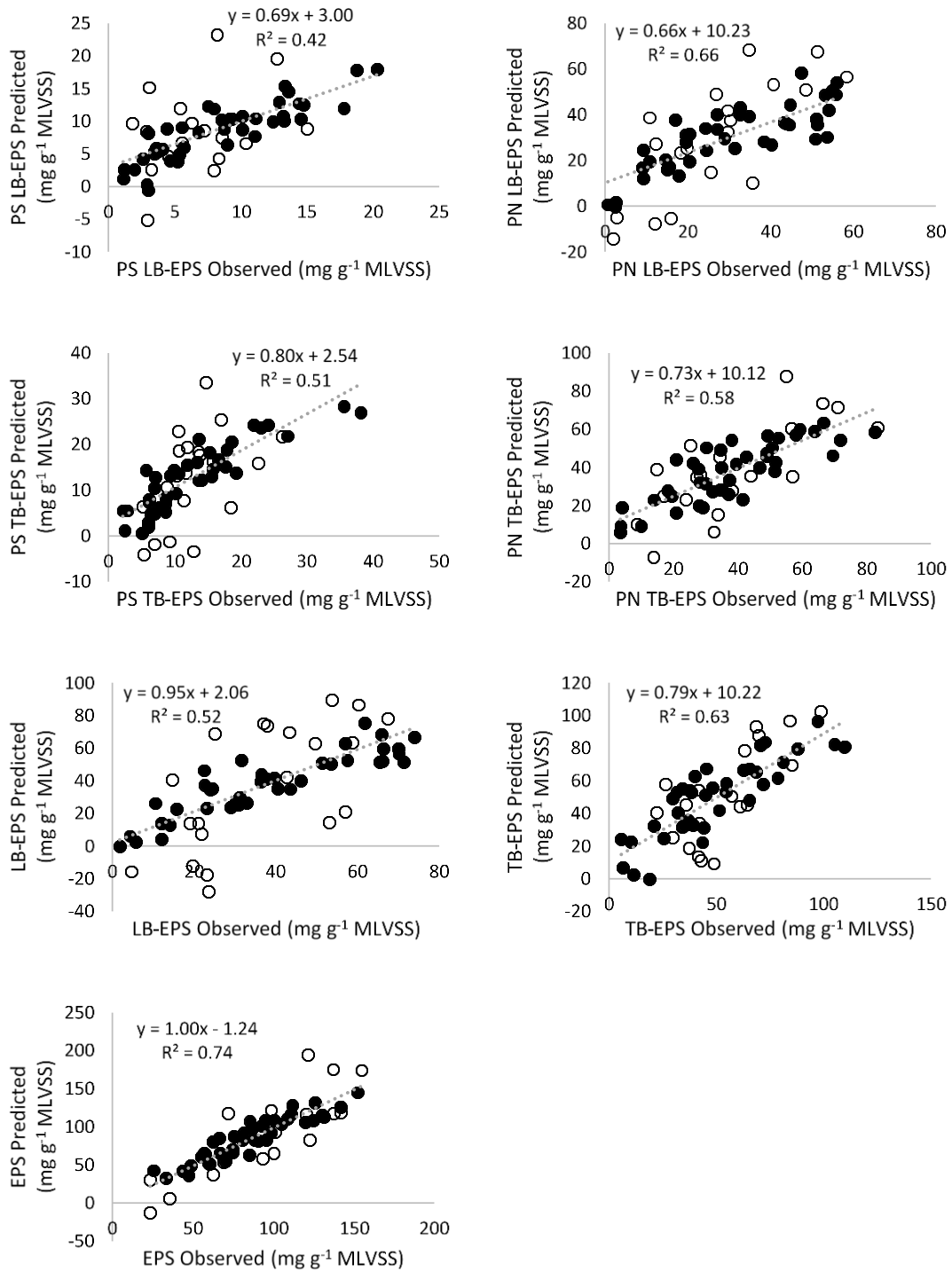
Figure 6.11 – PLS regression models for the overall LB-, TB-EPS and total EPS predictions. The black dots (●) represent the training set, and white dots (○) represent the validation set.
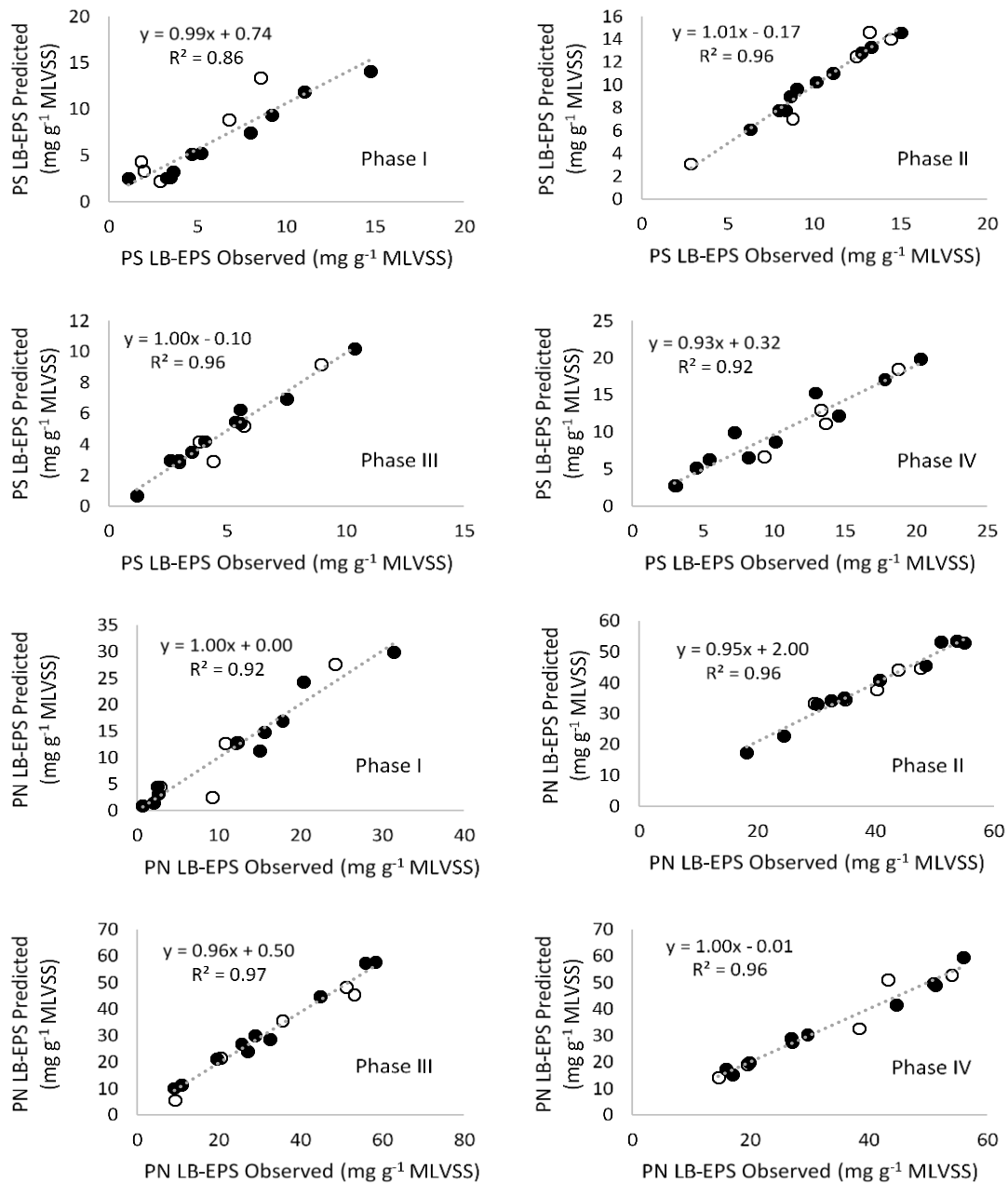
Figure 6.12 – PLS regression models for the PS and PN LB-EPS predictions for phases I-IV. The black dots (●) represent the training set, and white dots (○) represent the validation set.
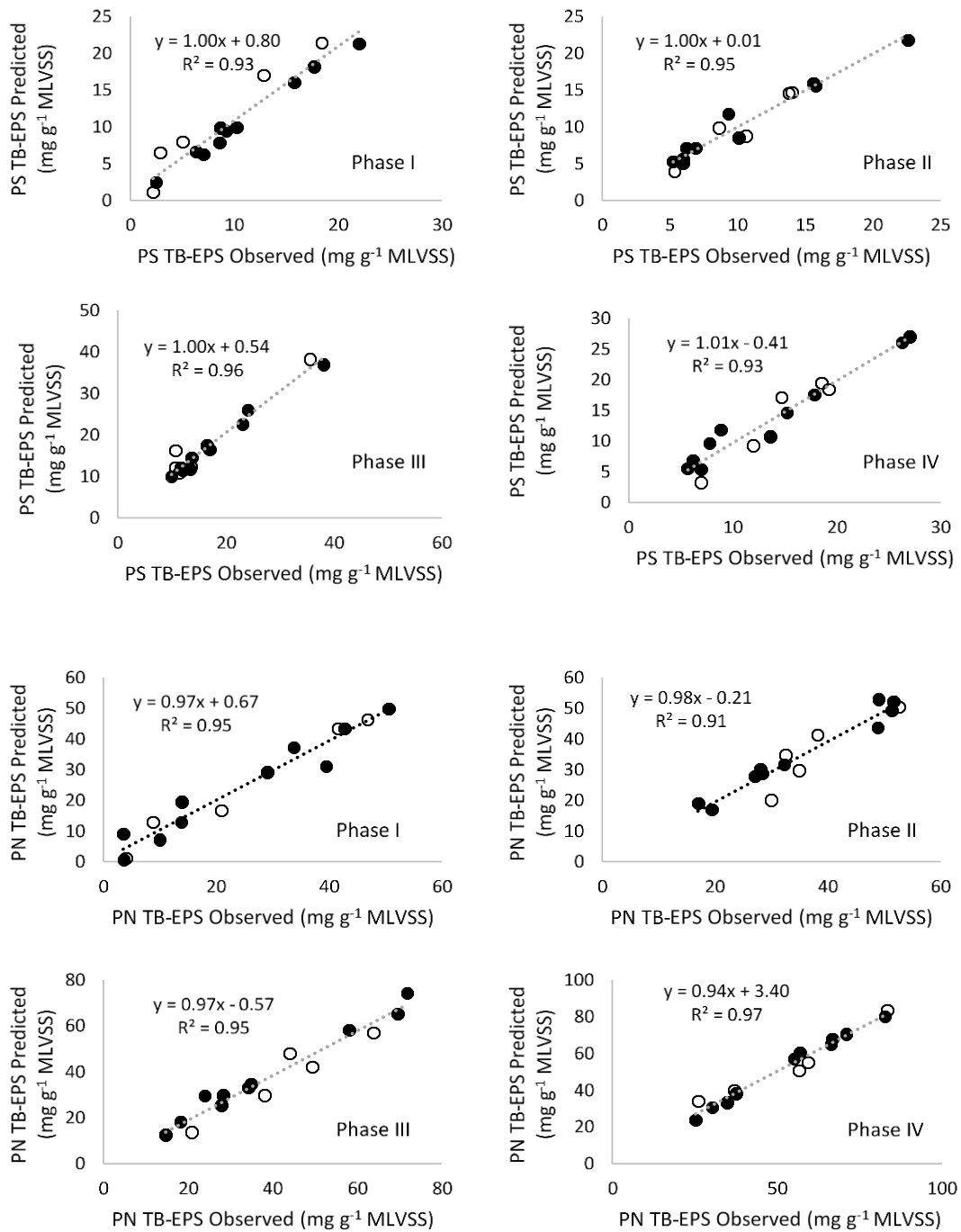
Figure 6.13 – PLS regression models for the PS and PN TB-EPS predictions for phases I-IV. The black dots (●) represent the training set, and white dots (○) represent the validation set.
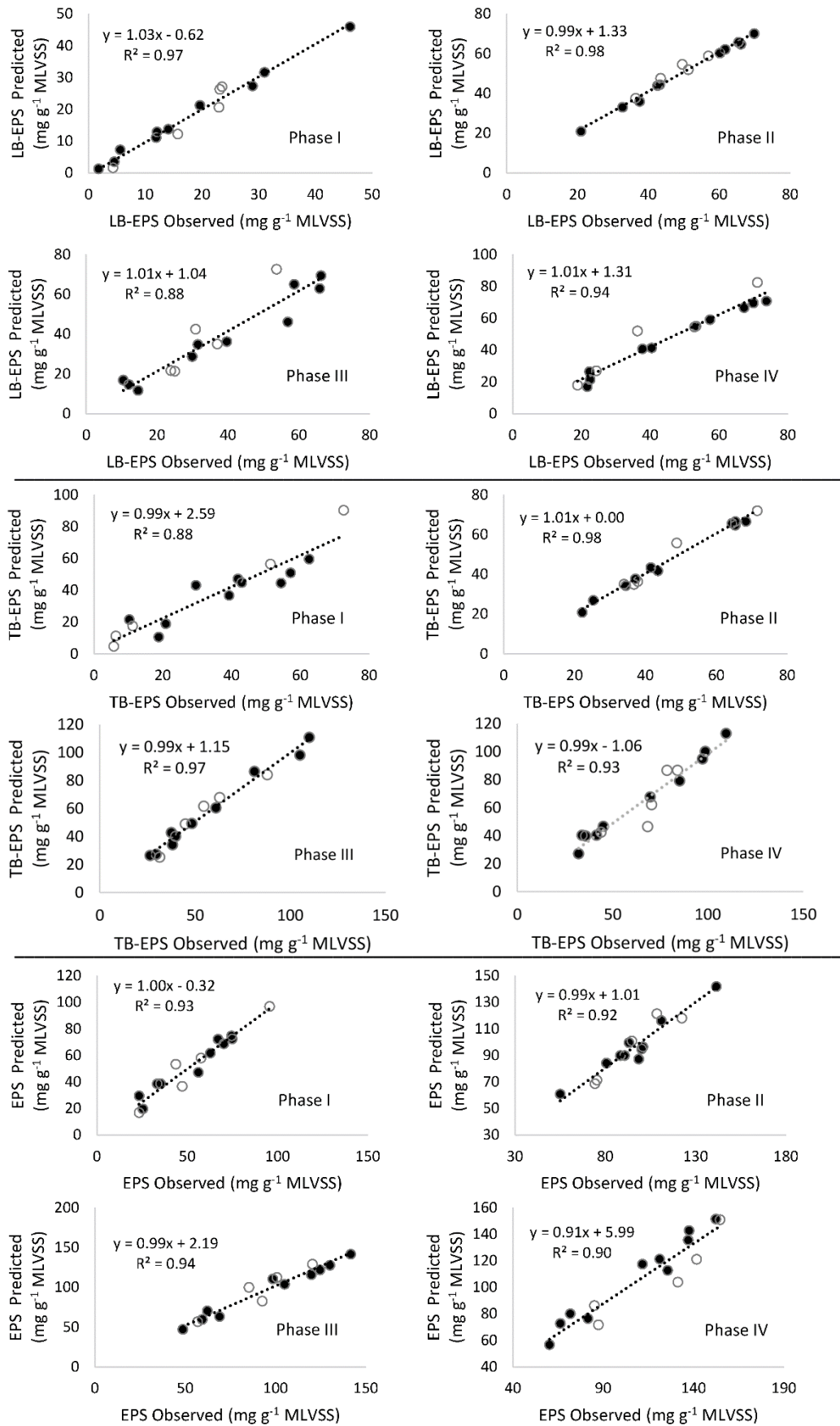
Figure 6.14 — PLS regression models for the LB, TB and total EPS predictions for phases I-IV. The black dots (●) represent the training set, and white dots (○) represent the validation set.

125

6.3   Conclusions

Our results indicated that ATZ at the highest concentrations caused a significant reduction in heterotrophic bacteria activity and the nitrification process. This was further proven through OUR results that the microbial activity decreased significantly with increasing ATZ concentration. Furthermore, ATZ efficiency removal increased along the experiment, suggesting that phase II was probably a period for acclimation of some microorganisms degrading ATZ, which gradually enhanced its removal during phase III. In phase IV, no change in removal efficiency of ATZ was observed, suggesting that the microorganisms reached their maximum capacity to degrade the micropollutant. TB-EPS might be involved in interaction with ATZ. The 3D-EEM spectral analysis confirmed that the primary components of LB-EPS and TB-EPS were protein-like substances, and humic acid-like substances presented smooth fluorescence peaks, demonstrating that the protein was the key component in the sludge contributing to the development and structural stability of large aggregates. Furthermore, PCA encompassing QIA and EPS data revealed that total EPS and TB-EPS significantly contributed to changes in aggregates morphology rather than LB-EPS forms. Finally, PLS2 models allowed EPS forms assessment, which is a crucial strategy to reduce the time spent during EPS chemical determination, making the PLS regression a suitable technique for EPS estimation.

CHAPTER 7 - CONCLUSION AND FUTURE PERSPECTIVES

7.1 General conclusions

This thesis analysed the impact of different classes of micropollutants in the AS system operated in a SBR. The effect of IBU, DESL, and ATZ on biomass activity was measured regarding organic matter removal and and nitrification process. It was observed that, with the presence of these compounds, there was a reduction in the activity of heterotrophic and autotrophic bacteria (AOB and NOB) due to the reduction in removal of organic matter, NH_4^+ and accumulation of NO_2^--N and reduction of NO_3^--N concentrations during the experiments. In terms of IBU, DESL, and ATZ removal, the results showed that the biomass was less able to remove IBU and ATZ (by 50%) compared to DESL, which ranged from 67 to 80%.

The effects of selected compounds were also evaluated in terms of EPS production. In general, greater production of EPS was observed in the form of TB-EPS as a protective mechanism for microorganisms against the effects caused by IBU, DESL, and ATZ. In chapter 4, for IBU at 10 mg L^{-1}, an overproduction of EPS was observed, especially PN TB-EPS. Interestingly, the biomass developed large aggregates and presented a jelly-like consistence associated with the overproduction of EPS. On the other hand, for IBU at 5 mg L^{-1}, a decrease in EPS production compared to the control phase was observed, both for LB- and TB-EPS, which may indicate that IBU acted as a selector for some groups of EPS-producing bacteria. Regarding the production of EPS in the experiment with DESL, the TB-EPS form consistently increased its concentration throughout the experiment, mainly PN. The LB-EPS form had a variation, with an increase in concentration in phases II and III, and in phase IV decreasing EPS production to values similar to those of the control phase. These findings reinforce the idea that TB-EPS is expelled to alleviate the toxicity caused by DESL. Furthermore, similar results were obtained in the ATZ experiment, with EPS production gradually increasing throughout phases I-IV. However, in phase II, the concentration of LB-EPS was slightly higher than that of TB-EPS, implying that each compound affected the biomass in a particular way.

For chapters 5 and 6, the 3D-EEM technique helped clarify the main functional groups present in the LB-EPS and TB-EPS forms. The main substances found were proteins, humic acid and fulvic acid-like substances. Furthermore, through the percent fluorescence response, it was possible to establish that the EPS had an important role in interacting with these compounds. The results for DESL propose that proteins-like substances in both LB- and TB-EPS were quenched by DESL, while the results for ATZ propose that only the protein-like substances in TB-EPS were quenched. These finds mean that EPS

played a specific role in removing DESL and ATZ, probably by giving sites for the adsorption of these compounds and forming a complex between DESL-PN (LB and TB-EPS) and ATZ-PN TB-EPS.

The QIA technique was essential to clarify the impacts of the compounds in terms of the morphological structure of the aggregates. The most notable changes imposed by the presence of IBU were the development of filamentous bacteria and the formation of large flocs interconnected by filaments, which caused a negative effect on sludge settling ability. On the other hand, for the experiments with DESL and ATZ, the filamentous content decreased throughout the phases. Large flocs with better morphological structures were formed, implying a greater settling ability capacity to biomass. Besides, the PN/PS ratio results suggest an increase in hydrophobicity on the surface of the flocs due to the change in EPS concentrations, which could have contributed to the increase in the content of larger aggregates in detrimental of intermediate and small ones.

PCA was employed in chapters 5 and 6 to analyze the complex interactions between the most important variables, including the settling ability (SVI) of the biomass, EPS forms and morphological parameters. Thus, PCA allowed visualizing the interrelationship between EPS and QIA parameters, indicating that the formation of the large aggregates was closely related to an increase in the amount of TB-EPS forms and total EPS content. Furthermore, our finds demonstrate that with the rise in the PN/PS ratios, which is an indicator of hydrophobicity, the SVI decreased due to the development of aggregates with good settling characteristics. Also, PCA allowed distinguishing different clusters regarding the operational periods, evidencing the difference in phases with toxic compounds and control phases. In addition, for the ATZ experiment, the PCA score plot revealed that phases III and IV did not distinguish between them, indicating that ATZ concentration in upper phase III was irrelevant.

Finally, using a PLS technique further allowed to model the prediction of the EPS contents based on the AS ensemble morphological and structural parameters for flocs in the presence of ATZ. For strategy of PLS2, reasonable to good coefficients of determination were obtained for the PS LB-EPS (0.86 - 0.96) and PN LB-EPS (0.92 - 0.97); PS TB-EPS (0.92 - 0.96) and PN TB-EPS (0.91 - 0.97); LB-EPS (0.88 - 0.97); TB-EPS (0.88 - 0.98); and total EPS (0.90 - 0.94).

7.2 Future perspectives

The work presented in this thesis significantly broadened the role of EPS in AS process toward toxic compounds by using conventional chemical methods and advanced techniques such as 3D-EEM and QIA methodology. Although the different roles of EPS and its components in biological WWT under toxic compounds have yet to be fully discovered, visible progress has been made on this subject; however, there are still several challenges to overcome the entire interaction of EPS in a dynamic

environment like biological WWT. Therefore, further research is essential to improve the knowledge about EPS on biological WWT systems. Future perspectives and recommendations resulting from this thesis include:

- Further research on molecular microbial community identification must be performed to elucidate the microorganisms developed after adding these toxic compounds could bring new insights into bacteria involved in EPS production. In addition, further studies regarding the viability assessment of sludge (e.g., Live Dead fluorescent staining) would be of interest in micropollutants' presence in AS regarding EPS production. These techniques should increase the knowledge of how micropollutants selectively affect different bacteria in sludge aggregates.

- The use of more sensitive analytical techniques, such as Liquid Chromatography coupled to Mass Spectrometry (LC-MS), that could be employed for IBU, DESL, and ATZ determination in the lowerest ranges (ng L^{-1} and µg L^{-1}) could improve the monitoring ability and consequently, broaden the knowledge about the studied compounds' behavior in EPS-producing microorganisms, and also including the analysis of metabolites and parent compounds contribution in the EPS variation.

- The impact of these compounds in terms of EPS production and composition in different biological systems (granular activated sludge, attached biomass and anaerobic systems) or even different operational strategies (anoxic and aerobic) and operation in multiple reactors in parallel for control purposes, could be another approach for assessing the behavior of these systems in comparison with AS. Furthermore, the evaluation of different toxic compounds, both standing alone and in the mixture, could also contribute to the scientific knowledge addressing the EPS production and effects on biological system performance under micropollutants' presence.

- Further assessment in terms of molecular structure and interactions between EPS components and micropollutants could be of great interest. For that purpose, the use of other advanced techniques such as Fourier-transform infrared spectroscopy, X-ray photoelectron spectroscopy, scanning electronic microscopy with the classic microbiology techniques, and the integration of different fields are considered fundamental for increasing the knowledge on EPS composition, function, structure, and applications in different areas. Furthermore, the use of these techniques could improve the knowledge about the main EPS components involved in the

interaction with target compounds and also elucidate which kind of binding mechanisms prevailed during chemical bonding.

REFERENCES

Adav, S.S., Lee, D.-J., 2008. Extraction of extracellular polymeric substances from aerobic granule with compact interior structure. J. Hazard. Mater. 154, 1120–1126. https://doi.org/10.1016/j.jhazmat.2007.11.058

Adav, S.S., Lee, D.-J., Tay, J.-H., 2008. Extracellular polymeric substances and structural stability of aerobic granule. Water Res. 42, 1644–1650. https://doi.org/10.1016/j.watres.2007.10.013

Ahmed, M.B., Zhou, J.L., Hao, H., Guo, W., Thomaidis, N.S., Xu, J., 2017. Progress in the biological and chemical treatment technologies for emerging contaminant removal from wastewater : A critical review. J. Hazard. Mater. 323, 274–298. https://doi.org/10.1016/j.jhazmat.2016.04.045

Al-Rekabi, W.S., Qiang, H., Qiang, W.W., 2006. Review on Sequencing Batch Reactors. Pakistan J. Nutr. 6, 11–19. https://doi.org/10.3923/pjn.2007.11.19

Al Aukidy, M., Verlicchi, P., Jelic, A., Petrovic, M., Barcelò, D., 2012. Monitoring release of pharmaceutical compounds: Occurrence and environmental risk assessment of two WWTP effluents and their receiving bodies in the Po Valley, Italy. Sci. Total Environ. 438, 15–25. https://doi.org/10.1016/j.scitotenv.2012.08.061

Alavanja, M.C.R., 2009. Introduction: Pesticides Use and Exposure, Extensive Worldwide. Rev. Environ. Health 24, 303–309. https://doi.org/10.1515/REVEH.2009.24.4.303

Almutairi, F.M., Ajmal, M.R., Siddiqi, M.K., Alalawy, A.I., Khan, R.H., 2021. On the binding reaction of loratadine with human serum acute phase protein alpha 1-acid glycoprotein. J. Biomol. Struct. Dyn. 0, 1–8. https://doi.org/10.1080/07391102.2021.1930164

Amaral, A.L., 2003. Image analysis in biotechnological processes: applications to wastewater treatment. Univ. Minho. University of Minho.

Amaral, A.L., Abreu, H., Leal, C., Mesquita, D.P., Castro, L.M., Ferreira, E.C., 2017. Quantitative image analysis of polyhydroxyalkanoates inclusions from microbial mixed cultures under different SBR operation strategies. Environ. Sci. Pollut. Res. 24, 15148–15156. https://doi.org/10.1007/s11356-017-9132-0

Amaral, A.L., Da Motta, M., Pons, M.N., Vivier, H., Roche, N., Mota, M., Ferreira, E.C., 2004. Survey of Protozoa and Metazoa populations in wastewater treatment plants by image analysis and discriminant analysis. Environmetrics 15, 381–390. https://doi.org/10.1002/env.652

Amaral, A.L., Ferreira, E.C., 2005. Activated sludge monitoring of a wastewater treatment plant using image analysis and partial least squares regression. Anal. Chim. Acta 544, 246–253. https://doi.org/10.1016/j.aca.2004.12.061

Amariei, G., Boltes, K., Rosal, R., Letón, P., 2017. Toxicological interactions of ibuprofen and triclosan on biological activity of activated sludge. J. Hazard. Mater. 334, 193–200. https://doi.org/10.1016/j.jhazmat.2017.04.018

An, W., Guo, F., Song, Y., Gao, N., Bai, S., Dai, J., Wei, H., Zhang, L., Yu, D., Xia, M., Yu, Y., Qi, M.,

Tian, C., Chen, H., Wu, Z., Zhang, T., Qiu, D., 2016. Comparative genomics analyses on EPS biosynthesis genes required for floc formation of Zoogloea resiniphila and other activated sludge bacteria. Water Res. 102, 494–504. https://doi.org/10.1016/j.watres.2016.06.058

APHA, 1998. Standard methods for the examination of water and wastewater: 20th ed, American P. ed, American Public Health Association, Washington, DC.

Araújo, R. dos S., Bernardes, R.C., Martins, G.F., 2021. A mixture containing the herbicides Mesotrione and Atrazine imposes toxicological risks on workers of Partamona helleri. Sci. Total Environ. 763. https://doi.org/10.1016/j.scitotenv.2020.142980

Arelli, A., Luccarini, L., Madoni, P., 2009. Application of image analysis in activated sludge to evaluate correlations between settleability and features of flocs and filamentous species. Water Sci. Technol. 59, 2029–2036. https://doi.org/10.2166/wst.2009.119

Asensi, E., Zambrano, D., Alemany, E., Aguado, D., 2019. Effect of the addition of precipitated ferric chloride on the morphology and settling characteristics of activated sludge flocs. Sep. Purif. Technol. 227, 115711. https://doi.org/10.1016/j.seppur.2019.115711

Ashton, D., Hilton, M., Thomas, K. V., 2004. Investigating the environmental transport of human pharmaceuticals to streams in the United Kingdom. Sci. Total Environ. 333, 167–184. https://doi.org/10.1016/j.scitotenv.2004.04.062

Avella, A.C., Delgado, L.F., Görner, T., Albasi, C., Galmiche, M., de Donato, P., 2010. Effect of cytostatic drug presence on extracellular polymeric substances formation in municipal wastewater treated by membrane bioreactor. Bioresour. Technol. 101, 518–526. https://doi.org/10.1016/j.biortech.2009.08.057

Avella, A. C., Essendoubi, M., Louvet, J.N., Görner, T., Sockalingum, G.D., Pons, M.N., Manfait, M., De Donato, P., 2010. Activated sludge behaviour in a batch reactor in the presence of antibiotics: Study of extracellular polymeric substances. Water Sci. Technol. 61, 3147–3155. https://doi.org/10.2166/wst.2010.924

Avella, A.C., Görner, T., Yvon, J., Chappe, P., Guinot-Thomas, P., de Donato, P., 2011. A combined approach for a better understanding of wastewater treatment plants operation: Statistical analysis of monitoring database and sludge physico-chemical characterization. Water Res. 45, 981–992. https://doi.org/10.1016/j.watres.2010.09.028

Badireddy, A.R., Chellam, S., Gassman, P.L., Engelhard, M.H., Lea, A.S., Rosso, K.M., 2010. Role of extracellular polymeric substances in bioflocculation of activated sludge microorganisms under glucose-controlled conditions. Water Res. 44, 4505–4516. https://doi.org/10.1016/j.watres.2010.06.024

Badireddy, A.R., Chellam, S., Yanina, S., Gassman, P., Rosso, K.M., 2008. Bismuth dimercaptopropanol (BisBAL) inhibits the expression of extracellular polysaccharides and proteins by Brevundimonas diminuta: Implications for membrane microfiltration. Biotechnol. Bioeng. 99, 634–643. https://doi.org/10.1002/bit.21615

Bala Subramanian, S., Yan, S., Tyagi, R.D., Surampalli, R.Y., 2010. Extracellular polymeric substances (EPS) producing bacterial strains of municipal wastewater sludge: Isolation, molecular

identification, EPS characterization and performance for sludge settling and dewatering. Water Res. 44, 2253–2266. https://doi.org/10.1016/j.watres.2009.12.046

Banadda, E.N., Jenne, R., Smets, I.Y., Van Impe, J.F., 2003. Predicting the onset of filamentous bulking in biological wastewater treatment systems by exploiting image analysis information, in: 2003 European Control Conference (ECC). IEEE, pp. 2935–2940. https://doi.org/10.23919/ECC.2003.7086486

Barret, M., Carrère, H., Latrille, E., Wisniewski, C., Patureau, D., 2010. Micropollutant and sludge characterization for modeling sorption equilibria. Environ. Sci. Technol. 44, 1100–1106. https://doi.org/10.1021/es902575d

Basuvaraj, M., Fein, J., Liss, S.N., 2015. Protein and polysaccharide content of tightly and loosely bound extracellular polymeric substances and the development of a granular activated sludge floc. Water Res. 82, 104–117. https://doi.org/10.1016/j.watres.2015.05.014

Berg, S., Kutra, D., Kroeger, T., Straehle, C.N., Kausler, B.X., Haubold, C., Schiegg, M., Ales, J., Beier, T., Rudy, M., Eren, K., Cervantes, J.I., Xu, B., Beuttenmueller, F., Wolny, A., Zhang, C., Koethe, U., Hamprecht, F.A., Kreshuk, A., 2019. ilastik: interactive machine learning for (bio)image analysis. Nat. Methods 16, 1226–1232. https://doi.org/10.1038/s41592-019-0582-9

Bitton, G., 2005. Wastewater Microbiology, Third Edit. ed, Wastewater Microbiology. John Wiley & Sons, Inc., Hoboken, NJ, USA. https://doi.org/10.1002/0471717967

Boehler, M., Zwickenpflug, B., Hollender, J., Ternes, T., Joss, A., Siegrist, H., 2012. Removal of micropollutants in municipal wastewater treatment plants by powder-activated carbon. Water Sci. Technol. 66, 2115–2121. https://doi.org/10.2166/wst.2012.353

Boleij, M., Pabst, M., Neu, T.R., Van Loosdrecht, M.C.M., Lin, Y., 2018. Identification of Glycoproteins Isolated from Extracellular Polymeric Substances of Full-Scale Anammox Granular Sludge. Environ. Sci. Technol. 52, 13127–13135. https://doi.org/10.1021/acs.est.8b03180

Borowska, E., Bourgin, M., Hollender, J., Kienle, C., McArdell, C.S., von Gunten, U., 2016. Oxidation of cetirizine, fexofenadine and hydrochlorothiazide during ozonation: Kinetics and formation of transformation products. Water Res. 94, 350–362. https://doi.org/10.1016/j.watres.2016.02.020

Buser, H.R., Poiger, T., Muller, M.D., 1999. Occurrence and environmental behavior of the chiral pharmaceutical drug ibuprofen in surface waters and in wastewater. Environ. Sci. Technol. 33, 2529–2535. https://doi.org/10.1021/es981014w

Camenzuli, L., Scheringer, M., Hungerbühler, K., 2016. Local organochlorine pesticide concentrations in soil put into a global perspective: supplementary material. Environ. Pollut. 217, 11–18. https://doi.org/10.1016/j.envpol.2015.08.028

Campbell, K., Wang, J., Daniels, M., 2019. Assessing activated sludge morphology and oxygen transfer performance using image analysis. Chemosphere 223, 694–703. https://doi.org/10.1016/j.chemosphere.2019.02.088

Campo, J., Masiá, A., Blasco, C., Picó, Y., 2013. Occurrence and removal efficiency of pesticides in

sewage treatment plants of four Mediterranean River Basins. J. Hazard. Mater. 263, 146–157. https://doi.org/10.1016/j.jhazmat.2013.09.061

Chará-Serna, A.M., Epele, L.B., Morrissey, C.A., Richardson, J.S., 2019. Nutrients and sediment modify the impacts of a neonicotinoid insecticide on freshwater community structure and ecosystem functioning. Sci. Total Environ. 692, 1291–1303. https://doi.org/10.1016/j.scitotenv.2019.06.301

Chaturvedi, P., Shukla, P., Giri, B.S., Chowdhary, P., Chandra, R., Gupta, P., Pandey, A., 2021. Prevalence and hazardous impact of pharmaceutical and personal care products and antibiotics in environment: A review on emerging contaminants. Environ. Res. 194, 110664. https://doi.org/10.1016/j.envres.2020.110664

Chen, H., Zhou, S., Li, T., 2010. Impact of extracellular polymeric substances on the settlement ability of aerobic granular sludge. Environ. Technol. 31, 1601–1612. https://doi.org/10.1080/09593330.2010.482146

Chen, J., Gu, B., LeBoeuf, E.J., Pan, H., Dai, S., 2002. Spectroscopic characterization of the structural and functional properties of natural organic matter fractions. Chemosphere 48, 59–68. https://doi.org/10.1016/S0045-6535(02)00041-3

Chen, M.-Y., Lee, D.-J., Tay, J.-H., Show, K.-Y., 2007. Staining of extracellular polymeric substances and cells in bioaggregates. Appl. Microbiol. Biotechnol. 75, 467–474. https://doi.org/10.1007/s00253-006-0816-5

Chen, W., Westerhoff, P., Leenheer, J.A., Booksh, K., 2003. Fluorescence Excitation-Emission Matrix Regional Integration to Quantify Spectra for Dissolved Organic Matter. Environ. Sci. Technol. 37, 5701–5710. https://doi.org/10.1021/es034354c

Chen, Y., Yang, H., Gu, G., 2001. Effect of acid and surfactant treatment on activated sludge dewatering and settling. Water Res. 35, 2615–2620. https://doi.org/10.1016/S0043-1354(00)00565-0

Chong, I.-G., Jun, C.-H., 2005. Performance of some variable selection methods when multicollinearity is present. Chemom. Intell. Lab. Syst. 78, 103–112. https://doi.org/10.1016/j.chemolab.2004.12.011

Cleuvers, M., 2004. Mixture toxicity of the anti-inflammatory drugs diclofenac, ibuprofen, naproxen, and acetylsalicylic acid. Ecotoxicol. Environ. Saf. 59, 309–315. https://doi.org/10.1016/S0147-6513(03)00141-6

Commission Decision of 10 March 2004 concerning the non-inclusion of atrazine in Annex I to Council Directive 91/414/EEC and the withdrawal of authorisations for plant protection products containing this active substance. Off.J. Eur., 2004.

Contreras, E.M., Giannuzzi, L., Zaritzky, N.E., 2004. Use of image analysis in the study of competition between filamentous and non-filamentous bacteria. Water Res. 38, 2621–2630. https://doi.org/10.1016/j.watres.2004.03.022

Costa, J.G., Paulo, A.M.S., Amorim, C.L., Amaral, A.L., Castro, P.M.L., Ferreira, E.C., Mesquita, D.P.,

2022. Quantitative image analysis as a robust tool to assess effluent quality from an aerobic granular sludge system treating industrial wastewater. Chemosphere 291, 132773. https://doi.org/10.1016/j.chemosphere.2021.132773

Cozzolino, D., Kwiatkowski, M.., Parker, M., Cynkar, W.., Dambergs, R.., Gishen, M., Herderich, M.., 2004. Prediction of phenolic compounds in red wine fermentations by visible and near infrared spectroscopy. Anal. Chim. Acta 513, 73–80. https://doi.org/10.1016/j.aca.2003.08.066

Cy, H., Lh, F., Mh, S., Cf, H., Jp, W., Hw, K., 2020. Ibuprofen biodegradation by hospital, municipal, and distillery activated sludges. Environ. Technol. (United Kingdom) 41, 171–180. https://doi.org/10.1080/09593330.2018.1493146

Czaczyk, K., Myszka, K., 2007. Biosynthesis of Extracellular Polymeric Substances (EPS) and Its Role in Microbial Biofilm Formation. Polish J. Environ. Stud. 16, 799–806.

Delgado, L.F., Faucet-Marquis, V., Schetrite, S., Pfohl-Leszkowicz, A., Paranthoen, S., Albasi, C., 2010. Effect of cytostatic drugs on the sludge and on the mixed liquor characteristics of a cross-flow membrane bioreactor: Consequence on the process. J. Memb. Sci. 347, 165–173. https://doi.org/10.1016/j.memsci.2009.10.020

Derakhshan, Z., Ehrampoush, M.H., Mahvi, A.H., Dehghani, M., Faramarzian, M., Ghaneian, M.T., Mokhtari, M., Ebrahimi, A.A., Fallahzadeh, H., 2018a. Evaluation of a moving bed biofilm reactor for simultaneous atrazine, carbon and nutrients removal from aquatic environments: Modeling and optimization. J. Ind. Eng. Chem. 67, 219–230. https://doi.org/10.1016/j.jiec.2018.06.032

Derakhshan, Z., Mahvi, A.H., Ghaneian, M.T., Mazloomi, S.M., Faramarzian, M., Dehghani, M., Fallahzadeh, H., Yousefinejad, S., Berizi, E., Ehrampoush, M.H., Bahrami, S., 2018b. Simultaneous removal of atrazine and organic matter from wastewater using anaerobic moving bed biofilm reactor: A performance analysis. J. Environ. Manage. 209, 515–524. https://doi.org/10.1016/j.jenvman.2017.12.081

Ding, Z., Bourven, I., Guibaud, G., van Hullebusch, E.D., Panico, A., Pirozzi, F., Esposito, G., 2015. Role of extracellular polymeric substances (EPS) production in bioaggregation: application to wastewater treatment. Appl. Microbiol. Biotechnol. 99, 9883–9905. https://doi.org/10.1007/s00253-015-6964-8

Directive 2000/60/EC of the European Parliament and of the Council of 23 October 2000 establishing a framework for Community action in the field of water policy (OJ L 327, 22.12.2000, p. 1), 2000., 2000.

Du, B., Haddad, S.P., Luek, A., Scott, W.C., Saari, G.N., Burket, S.R., Breed, C.S., Kelly, M., Broach, L., Rasmussen, J.B., Chambliss, C.K., Brooks, B.W., 2016. Bioaccumulation of human pharmaceuticals in fish across habitats of a tidally influenced urban bayou. Environ. Toxicol. Chem. 35, 966–974. https://doi.org/10.1002/etc.3221

Einax, J.W., H. W. Zwanziger, Geis, S., 1999. Chapter 14 Chemometrics in environmental analysis, in: Comprehensive Analytical Chemistry. pp. 747–833. https://doi.org/10.1016/S0166-526X(99)80016-6

Faassen, S.M., Hitzmann, B., 2015. Fluorescence Spectroscopy and Chemometric Modeling for

Bioprocess Monitoring 10271–10291. https://doi.org/10.3390/s150510271

Falås, P., Wick, A., Castronovo, S., Habermacher, J., Ternes, T.A., Joss, A., 2016. Tracing the limits of organic micropollutant removal in biological wastewater treatment. Water Res. 95, 240–249. https://doi.org/10.1016/j.watres.2016.03.009

Feng, L.-J., Wang, J.-J., Liu, S.-C., Sun, X.-D., Yuan, X.-Z., Wang, S.-G., 2018. Role of extracellular polymeric substances in the acute inhibition of activated sludge by polystyrene nanoparticles. Environ. Pollut. 238, 859–865. https://doi.org/10.1016/j.envpol.2018.03.101

Feng, Q., Tai, X., Sun, Y., Li, M., 2019. Influence of turbulent mixing on the composition of extracellular polymeric substances (EPS) and aggregate size of aerated activated sludge. Chem. Eng. J. 378, 122123. https://doi.org/10.1016/j.cej.2019.122123

Fick, J., Söderström, H., Lindberg, R.H., Phan, C., Tysklind, M., Larsson, D.G.J., 2009. Contamination of surface, ground, and drinking water from pharmaceutical production. Environ. Toxicol. Chem. 28, 2522. https://doi.org/10.1897/09-073.1

Filella, M., Buffle, J., Parthasarathy, N., 2005. HUMIC AND FULVIC COMPOUNDS, in: Encyclopedia of Analytical Science. Elsevier, pp. 288–298. https://doi.org/10.1016/B0-12-369397-7/00260-0

Fischer, K., Majewsky, M., 2014. Cometabolic degradation of organic wastewater micropollutants by activated sludge and sludge-inherent microorganisms. Appl. Microbiol. Biotechnol. 98, 6583–6597. https://doi.org/10.1007/s00253-014-5826-0

Foster, G.D., Lippa, K.A., Miller, C. V., 2000. Seasonal concentrations of organic contaminants at the fall line of the Susquehanna River basin and estimated fluxes to northern Chesapeake Bay, USA. Environ. Toxicol. Chem. 19, 992–1001. https://doi.org/10.1002/etc.5620190428

Frølund, B., Griebe, T., Nielsen, P.H., 1995. Enzymatic activity in the activated-sludge floc matrix. Appl. Microbiol. Biotechnol. 43, 755–761. https://doi.org/10.1007/BF00164784

Frølund, B., Palmgren, R., Keiding, K., Nielsen, P.H., 1996. Extraction of extracellular polymers from activated sludge using a cation exchange resin. Water Res. 30, 1749–1758. https://doi.org/10.1016/0043-1354(95)00323-1

Gao, M., Liu, R., Li, B., Wei, W., Zhang, Y., 2019. Characteristics of extracellular polymeric substances and soluble microbial products of activated sludge in a pulse aerated reactor. Environ. Technol. (United Kingdom) 0, 1–10. https://doi.org/10.1080/09593330.2019.1573849

Gerardi, M.H., 2010. Troubleshooting the Sequencing Batch Reactor, Troubleshooting the Sequencing Batch Reactor. John Wiley & Sons, Inc., Hoboken, NJ, USA. https://doi.org/10.1002/9780470649633

Geyik, A.G., Kılıç, B., Çeçen, F., 2016. Extracellular polymeric substances (EPS) and surface properties of activated sludges: effect of organic carbon sources. Environ. Sci. Pollut. Res. 23, 1653–1663. https://doi.org/10.1007/s11356-015-5347-0

Ginoris, Y.P., Amaral, A.L., Nicolau, A., Coelho, M.A.Z., Ferreira, E.C., 2007. Development of an image analysis procedure for identifying protozoa and metazoa typical of activated sludge system. Water

Res. 41, 2581–2589. https://doi.org/10.1016/j.watres.2007.02.006

Golovko, O., Kumar, V., Fedorova, G., Randak, T., Grabic, R., 2014. Seasonal changes in antibiotics, antidepressants/psychiatric drugs, antihistamines and lipid regulators in a wastewater treatment plant. Chemosphere 111, 418–426. https://doi.org/10.1016/j.chemosphere.2014.03.132

Gosselin, R., Rodrigue, D., Duchesne, C., 2010. A Bootstrap-VIP approach for selecting wavelength intervals in spectral imaging applications. Chemom. Intell. Lab. Syst. 100, 12–21. https://doi.org/10.1016/j.chemolab.2009.09.005

Grijspeerdt, K., 1997. Image analysis to estimate the settleability and concentration of activated sludge. Water Res. 31, 1126–1134. https://doi.org/10.1016/S0043-1354(96)00350-8

Guasch, H., Muñoz, I., Rosés, N., Sabater, S., 1997. Changes in atrazine toxicity throughout succession of stream periphyton communities. J. Appl. Phycol. 9, 137–146. https://doi.org/10.1023/A:1007970211549

Guisasola, A., Baeza, J.A., Carrera, J., Casas, C., Lafuente, J., 2004. An off-line respirometric procedure to determine inhibition and toxicity of biodegradable compounds in biomass from an industrial WWTP. Water Sci. Technol. 48, 267–275. https://doi.org/10.2166/wst.2004.0858

Guo, J., Li, Z., Ranasinghe, P., Bonina, S., Hosseini, S., Corcoran, M.B., Smalley, C., Kaliappan, R., Wu, Y., Chen, D., Sandy, A.L., Wang, Y., Rockne, K.J., Sturchio, N.C., Giesy, J.P., Li, A., 2016. Occurrence of Atrazine and Related Compounds in Sediments of Upper Great Lakes. Environ. Sci. Technol. 50, 7335–7343. https://doi.org/10.1021/acs.est.6b00706

Guo, L., Lu, M., Li, Q., Zhang, J., Zong, Y., She, Z., 2014. Three-dimensional fluorescence excitation-emission matrix (EEM) spectroscopy with regional integration analysis for assessing waste sludge hydrolysis treated with multi-enzyme and thermophilic bacteria. Bioresour. Technol. 171, 22–28. https://doi.org/10.1016/j.biortech.2014.08.025

Guo, X., Wang, X., Liu, J., 2016. Composition analysis of fractions of extracellular polymeric substances from an activated sludge culture and identification of dominant forces affecting microbial aggregation. Sci. Rep. 6, 1–9. https://doi.org/10.1038/srep28391

Harman, C., Reid, M., Thomas, K. V., 2011. In Situ Calibration of a Passive Sampling Device for Selected Illicit Drugs and Their Metabolites in Wastewater, And Subsequent Year-Long Assessment of Community Drug Usage. Environ. Sci. Technol. 45, 5676–5682. https://doi.org/10.1021/es201124j

Hayes, T.B., Khoury, V., Narayan, A., Nazir, M., Park, A., Brown, T., Adame, L., Chan, E., Buchholz, D., Stueve, T., Gallipeau, S., 2010. Atrazine induces complete feminization and chemical castration in male African clawed frogs (Xenopus laevis). Proc. Natl. Acad. Sci. 107, 4612–4617. https://doi.org/10.1073/pnas.0909519107

He, Q., Zhang, J., Gao, S., Chen, L., Lyu, W., Zhang, W., Song, J., Hu, X., Chen, R., Wang, H., Yu, J., 2019. A comprehensive comparison between non-bulking and bulking aerobic granular sludge in microbial communities. Bioresour. Technol. 294, 122151. https://doi.org/10.1016/j.biortech.2019.122151

Heeb, F., Singer, H., Pernet-Coudrier, B., Qi, W., Liu, H., Longrée, P., Müller, B., Berg, M., 2012. Organic Micropollutants in Rivers Downstream of the Megacity Beijing: Sources and Mass Fluxes in a Large-Scale Wastewater Irrigation System. Environ. Sci. Technol. 46, 8680–8688. https://doi.org/10.1021/es301912q

Henning, N., Falås, P., Castronovo, S., Jewell, K.S., Bester, K., Ternes, T.A., Wick, A., 2019. Biological transformation of fexofenadine and sitagliptin by carrier-attached biomass and suspended sludge from a hybrid moving bed biofilm reactor. Water Res. 167, 115034. https://doi.org/10.1016/j.watres.2019.115034

Henriques, I.D.S., Love, N.G., 2007. The role of extracellular polymeric substances in the toxicity response of activated sludge bacteria to chemical toxins. Water Res. 41, 4177–4185. https://doi.org/10.1016/j.watres.2007.05.001

Higgins, M.J., Novak, J.T., 1997. Characterization of exocellular protein and its role in bioflocculation. J. Environ. Eng. 123, 479–485. https://doi.org/10.1061/(ASCE)0733-9372(1997)123:5(479)

Holt, J.S., 2013. Herbicides, in: Encyclopedia of Biodiversity. Elsevier, pp. 87–95. https://doi.org/10.1016/B978-0-12-384719-5.00070-8

Hou, W., Ma, Z., Sun, L., Han, M., Lu, J., Li, Z., Mohamad, O.A., Wei, G., 2013. Extracellular polymeric substances from copper-tolerance Sinorhizobium meliloti immobilize Cu2+. J. Hazard. Mater. 261, 614–620. https://doi.org/10.1016/j.jhazmat.2013.06.043

Hou, X., Liu, S., Zhang, Z., 2015. Role of extracellular polymeric substance in determining the high aggregation ability of anammox sludge. Water Res. 75, 51–62. https://doi.org/10.1016/j.watres.2015.02.031

Hutchings, M., Truman, A., Wilkinson, B., 2019. Antibiotics: past, present and future. Curr. Opin. Microbiol. https://doi.org/10.1016/j.mib.2019.10.008

Iesce, M.R., Lavorgna, M., Russo, C., Piscitelli, C., Passananti, M., Temussi, F., DellaGreca, M., Cermola, F., Isidori, M., 2019. Ecotoxic effects of loratadine and its metabolic and light-induced derivatives. Ecotoxicol. Environ. Saf. 170, 664–672. https://doi.org/10.1016/j.ecoenv.2018.11.116

Irvine, R.L., Ketchum, L.H., Asano, T., 1989. Sequencing batch reactors for biological wastewater treatment. Crit. Rev. Environ. Control 18, 255–294. https://doi.org/10.1080/10643388909388350

Jayaraj, R., Megha, P., Sreedev, P., 2016. Review Article. Organochlorine pesticides, their toxic effects on living organisms and their fate in the environment. Interdiscip. Toxicol. 9, 90–100. https://doi.org/10.1515/intox-2016-0012

Jenkins, D., Richard, M.G., Daigger, G.T., 2003. Manual on the Causes and Control of Activated Sludge Bulking, Foaming, and Other Solids Separation Problems, Manual on the Causes and Control of Activated Sludge Bulking, Foaming, and Other Solids Separation Problems. CRC Press. https://doi.org/10.1201/9780203503157

Jia, Y., Yin, L., Khanal, S.K., Zhang, H., Oberoi, A.S., Lu, H., 2020. Biotransformation of ibuprofen in

biological sludge systems: Investigation of performance and mechanisms. Water Res. 170, 115303. https://doi.org/10.1016/j.watres.2019.115303

Jin, B., Wilén, B.M., Lant, P., 2003. A comprehensive insight into floc characteristics and their impact on compressibility and settleability of activated sludge. Chem. Eng. J. 95, 221–234. https://doi.org/10.1016/S1385-8947(03)00108-6

Joss, A., Zabczynski, S., Göbel, A., Hoffmann, B., Löffler, D., McArdell, C.S., Ternes, T.A., Thomsen, A., Siegrist, H., 2006. Biological degradation of pharmaceuticals in municipal wastewater treatment: Proposing a classification scheme. Water Res. 40, 1686–1696. https://doi.org/10.1016/j.watres.2006.02.014

Jung, S.-K., 2019. A Review of Image Analysis in Biochemical Engineering. Biotechnol. Bioprocess Eng. 24, 65–75. https://doi.org/10.1007/s12257-018-0372-8

Kalyabina, V.P., Esimbekova, E.N., Kopylova, K. V, Kratasyuk, V.A., 2021. Pesticides: formulants, distribution pathways and effects on human health – a review. Toxicol. Reports 8, 1179–1192. https://doi.org/10.1016/j.toxrep.2021.06.004

Kasprzyk-Hordern, B., Dinsdale, R.M., Guwy, A.J., 2009. The removal of pharmaceuticals, personal care products, endocrine disruptors and illicit drugs during wastewater treatment and its impact on the quality of receiving waters. Water Res. 43, 363–380. https://doi.org/10.1016/j.watres.2008.10.047

Khan, M.B., Nisar, H., Ng, C.A., Lo, P.K., Yap, V.V., 2018. Generalized classification modeling of activated sludge process based on microscopic image analysis. Environ. Technol. (United Kingdom) 39, 24–34. https://doi.org/10.1080/09593330.2017.1293166

Khunjar, W.O., Love, N.G., 2011. Sorption of carbamazepine, 17α-ethinylestradiol, iopromide and trimethoprim to biomass involves interactions with exocellular polymeric substances. Chemosphere 82, 917–922. https://doi.org/10.1016/j.chemosphere.2010.10.046

Kim, S.D., Cho, J., Kim, I.S., Vanderford, B.J., Snyder, S.A., 2007. Occurrence and removal of pharmaceuticals and endocrine disruptors in South Korean surface, drinking, and waste waters. Water Res. 41, 1013–1021. https://doi.org/10.1016/j.watres.2006.06.034

Klamerth, N., Rizzo, L., Malato, S., Maldonado, M.I., Agüera, A., Fernández-Alba, A.R., 2010. Degradation of fifteen emerging contaminants at µg L-1 initial concentrations by mild solar photo-Fenton in MWTP effluents. Water Res. 44, 545–554. https://doi.org/10.1016/j.watres.2009.09.059

Kong, Q., He, X., Feng, Y., Miao, M. sheng, Wang, Q., Du, Y. da, Xu, F., 2017. Pollutant removal and microorganism evolution of activated sludge under ofloxacin selection pressure. Bioresour. Technol. 241, 849–856. https://doi.org/10.1016/j.biortech.2017.06.019

Kosonen, J., Kronberg, L., 2009. The occurrence of antihistamines in sewage waters and in recipient rivers. Environ. Sci. Pollut. Res. 16, 555–564. https://doi.org/10.1007/s11356-009-0144-2

Kristofco, L.A., Brooks, B.W., 2017. Global scanning of antihistamines in the environment: Analysis of occurrence and hazards in aquatic systems. Sci. Total Environ. 592, 477–487.

https://doi.org/10.1016/j.scitotenv.2017.03.120

Larsson, D.G.J., de Pedro, C., Paxeus, N., 2007. Effluent from drug manufactures contains extremely high levels of pharmaceuticals. J. Hazard. Mater. 148, 751–755. https://doi.org/10.1016/j.jhazmat.2007.07.008

Lay, W.C.L., Zhang, Q., Zhang, J., McDougald, D., Tang, C., Wang, R., Liu, Y., Fane, A.G., 2012. Effect of Pharmaceuticals on the Performance of a Novel Osmotic Membrane Bioreactor (OMBR). Sep. Sci. Technol. 47, 543–554. https://doi.org/10.1080/01496395.2011.630249

Le Bonté, S., Potier, O., Pons, M.-N., 2005. Toxic event detection by respirometry and adaptive principal components analysis. Environmetrics 16, 589–601. https://doi.org/10.1002/env.724

Leal, C.S., Lopes, M., Val del Río, A., Quintelas, C., Castro, P.M.L., Ferreira, E.C., Amaral, A.L., Mesquita, D.P., 2021. Assessment of an aerobic granular sludge system in the presence of pharmaceutically active compounds by quantitative image analysis and chemometric techniques. J. Environ. Manage. 289. https://doi.org/10.1016/j.jenvman.2021.112474

Lee, H.B., Peart, T.E., Svoboda, M.L., 2005. Determination of endocrine-disrupting phenols, acidic pharmaceuticals, and personal-care products in sewage by solid-phase extraction and gas chromatography-mass spectrometry. J. Chromatogr. A 1094, 122–129. https://doi.org/10.1016/j.chroma.2005.07.070

Lee, J.W., Yeomans, W.G., Allen, A.L., Deng, F., Gross, R.A., Kaplan, D.L., 1999. Biosynthesis of novel exopolymers by Aureobasidium pullulans. Appl. Environ. Microbiol. 65, 5265–5271. https://doi.org/10.1128/aem.65.12.5265-5271.1999

Lennox, J., Rosen, C., 2002. Adaptive multiscale principal components analysis for online monitoring of wastewater treatment. Water Sci. Technol. 45, 227–235. https://doi.org/10.2166/wst.2002.0593

Li, C., Cabassud, C., Reboul, B., Guigui, C., 2015. Effects of pharmaceutical micropollutants on the membrane fouling of a submerged MBR treating municipal wastewater: Case of continuous pollution by carbamazepine. Water Res. 69, 183–194. https://doi.org/10.1016/j.watres.2014.11.027

Li, J., Liu, X., Liu, Y., Ramsay, J., Yao, C., Dai, R., 2011. The effect of continuous exposure of copper on the properties and extracellular polymeric substances (EPS) of bulking activated sludge. Environ. Sci. Pollut. Res. 18, 1567–1573. https://doi.org/10.1007/s11356-011-0492-6

Li, W.W., Zhang, H.L., Sheng, G.P., Yu, H.Q., 2015. Roles of extracellular polymeric substances in enhanced biological phosphorus removal process. Water Res. 86, 85–95. https://doi.org/10.1016/j.watres.2015.06.034

Li, X.Y., Yang, S.F., 2007. Influence of loosely bound extracellular polymeric substances (EPS) on the flocculation, sedimentation and dewaterability of activated sludge. Water Res. 41, 1022–1030. https://doi.org/10.1016/j.watres.2006.06.037

Li, Y., Xin, M., Xie, D., Fan, S., Ma, J., Liu, K., Yu, F., 2021. Variation in Extracellular Polymeric Substances from Enterobacter sp. And Their Pb2+ Adsorption Behaviors. ACS Omega 6, 9617–

9628. https://doi.org/10.1021/acsomega.1c00185

Li, Z., Yan, X., 2019. Ensemble model of wastewater treatment plant based on rich diversity of principal component determining by genetic algorithm for status monitoring. Control Eng. Pract. 88, 38–51. https://doi.org/10.1016/j.conengprac.2019.04.008

Liao, B.Q., Allen, D.G., Droppo, I.G., Leppard, G.G., Liss, S.N., 2001. Surface properties of sludge and their role in bioflocculation and settleability. Water Res. 35, 339–350. https://doi.org/10.1016/S0043-1354(00)00277-3

Liao, B.Q., Lin, H.J., Langevin, S.P., Gao, W.J., Leppard, G.G., 2011. Effects of temperature and dissolved oxygen on sludge properties and their role in bioflocculation and settling. Water Res. 45, 509–520. https://doi.org/10.1016/j.watres.2010.09.010

Lienert, J., Bürki, T., Escher, B.I., 2007. Reducing micropollutants with source control: substance flow analysis of 212 pharmaceuticals in faeces and urine. Water Sci. Technol. 56, 87–96. https://doi.org/10.2166/wst.2007.560

Lin, Y., Reino, C., Carrera, J., Pérez, J., van Loosdrecht, M.C.M., 2018. Glycosylated amyloid-like proteins in the structural extracellular polymers of aerobic granular sludge enriched with ammonium-oxidizing bacteria. Microbiologyopen 7, 1–13. https://doi.org/10.1002/mbo3.616

Lin, Y.M., Sharma, P.K., van Loosdrecht, M.C.M., 2013. The chemical and mechanical differences between alginate-like exopolysaccharides isolated from aerobic flocculent sludge and aerobic granular sludge. Water Res. 47, 57–65. https://doi.org/10.1016/j.watres.2012.09.017

Liu, H., Fang, H.H.P., 2002. Extraction of extracellular polymeric substances (EPS) of sludges. J. Biotechnol. 95, 249–256. https://doi.org/10.1016/S0168-1656(02)00025-1

Liu, T., Chen, Z. lin, Yu, W. zheng, You, S. jie, 2011. Characterization of organic membrane foulants in a submerged membrane bioreactor with pre-ozonation using three-dimensional excitation-emission matrix fluorescence spectroscopy. Water Res. 45, 2111–2121. https://doi.org/10.1016/j.watres.2010.12.023

Liu, X., Liu, J., Deng, D., Li, R., Guo, C., Ma, J., Chen, M., 2021. Investigation of extracellular polymeric substances (EPS) in four types of sludge: Factors influencing EPS properties and sludge granulation. J. Water Process Eng. 40, 101924. https://doi.org/10.1016/j.jwpe.2021.101924

Liu, Y., Fang, H.H.P., 2003. Influences of Extracellular Polymeric Substances (EPS) on Flocculation, Settling, and Dewatering of Activated Sludge. Crit. Rev. Environ. Sci. Technol. 33, 237–273. https://doi.org/10.1080/10643380390814479

Liwarska-Bizukojc, E., 2005. Application of Image Analysis Techniques in Activated Sludge Wastewater Treatment Processes. Biotechnol. Lett. 27, 1427–1433. https://doi.org/10.1007/s10529-005-1303-2

Liwarska-Blzukojc, E., Andrzejczak, O., Solecka, M., 2019. Study on activated sludge flocs morphology and composition in a full-scale wastewater treatment plant in Poland. Isr. Explor. J. 69, 69–82. https://doi.org/10.5277/epe190205

Loos, R., Gawlik, B.M., Locoro, G., Rimaviciute, E., Contini, S., Bidoglio, G., 2009. EU-wide survey of polar organic persistent pollutants in European river waters. Environ. Pollut. 157, 561–568. https://doi.org/10.1016/j.envpol.2008.09.020

Loos, R., Wollgast, J., Huber, T., Hanke, G., 2007. Polar herbicides, pharmaceutical products, perfluorooctanesulfonate (PFOS), perfluorooctanoate (PFOA), and nonylphenol and its carboxylates and ethoxylates in surface and tap waters around Lake Maggiore in Northern Italy. Anal. Bioanal. Chem. 387, 1469–1478. https://doi.org/10.1007/s00216-006-1036-7

López-Serna, R., Jurado, A., Vázquez-Suñé, E., Carrera, J., Petrović, M., Barceló, D., 2013. Occurrence of 95 pharmaceuticals and transformation products in urban groundwaters underlying the metropolis of Barcelona, Spain. Environ. Pollut. 174, 305–315. https://doi.org/10.1016/j.envpol.2012.11.022

Loraine, G.A., Pettigrove, M.E., 2006. Seasonal variations in concentrations of pharmaceuticals and personal care products in drinking water and reclaimed wastewater in Southern California. Environ. Sci. Technol. 40, 687–695. https://doi.org/10.1021/es051380x

Lourenço, N.D., Paixão, F., Pinheiro, H.M., Sousa, A., 2010. Use of Spectra in the Visible and Near-Mid-Ultraviolet Range with Principal Component Analysis and Partial Least Squares Processing for Monitoring of Suspended Solids in Municipal Wastewater Treatment Plants. Appl. Spectrosc. 64, 1061–1067. https://doi.org/10.1366/000370210792434332

Luo, Y., Guo, W., Hao, H., Duc, L., Ibney, F., Zhang, J., Liang, S., Wang, X.C., 2014. A review on the occurrence of micropollutants in the aquatic environment and their fate and removal during wastewater treatment. Sci. Total Environ. 473–474, 619–641. https://doi.org/10.1016/j.scitotenv.2013.12.065

Lyu, Y., Yu, J., Guo, M., Wang, K., Yu, Z., Zhang, L., Zhang, Y., Chen, L., 2021. New insights into interaction of proteins in extracellular polymeric substances of activated sludge with ciprofloxacin using quartz crystal microbalance with dissipation. Chemosphere 263, 128044. https://doi.org/10.1016/j.chemosphere.2020.128044

Ma, J., Quan, X., Si, X., Wu, Y., 2013. Responses of anaerobic granule and flocculent sludge to ceria nanoparticles and toxic mechanisms. Bioresour. Technol. 149, 346–352. https://doi.org/10.1016/j.biortech.2013.09.080

Maculewicz, J., Kowalska, D., Świacka, K., Toński, M., Stepnowski, P., Białk-Bielińska, A., Dołżonek, J., 2022. Transformation products of pharmaceuticals in the environment: Their fate, (eco)toxicity and bioaccumulation potential. Sci. Total Environ. 802. https://doi.org/10.1016/j.scitotenv.2021.149916

Mahlalela, L.C., Casado, C., Marugán, J., Septien, S., Ndlovu, T., Dlamini, L.N., 2021. Coupling biological and photocatalytic treatment of atrazine and tebuthiuron in aqueous solution. J. Water Process Eng. 40. https://doi.org/10.1016/j.jwpe.2021.101918

Mandelbaum, R.T., Allan, D.L., Wackett, L.P., 1995. Isolation and Characterization of a Pseudomonas sp. That Mineralizes the s-Triazine Herbicide Atrazine. Appl. Environ. Microbiol. 61, 1451–1457. https://doi.org/10.1128/aem.61.4.1451-1457.1995

Martinez, F., Favela-Torres, E., Gomez, J., 2000. Oscillations of exopolymeric composition and sludge volume index in nitrifying flocs. Appl. Biochem. Biotechnol. - Part A Enzym. Eng. Biotechnol. 87, 177–188. https://doi.org/10.1385/ABAB:87:3:177

McSwain, B.S., Irvine, R.L., Hausner, M., Wilderer, P.A., 2005. Composition and distribution of extracellular polymeric substances in aerobic flocs and granular sludge. Appl. Environ. Microbiol. 71, 1051–1057. https://doi.org/10.1128/AEM.71.2.1051-1057.2005

Mehmood, T., Liland, K.H., Snipen, L., Sæbø, S., 2012. A review of variable selection methods in Partial Least Squares Regression. Chemom. Intell. Lab. Syst. 118, 62–69. https://doi.org/10.1016/j.chemolab.2012.07.010

Melo, A., Costa, J., Quintelas, C., Ferreira, E.C., Mesquita, D.P., 2021. Effect of ibuprofen on extracellular polymeric substances (EPS) production and composition, and assessment of microbial structure by quantitative image analysis. J. Environ. Manage. 293, 112852. https://doi.org/10.1016/j.jenvman.2021.112852

Men, Y., Achermann, S., Helbling, D.E., Johnson, D.R., Fenner, K., 2017. Relative contribution of ammonia oxidizing bacteria and other members of nitrifying activated sludge communities to micropollutant biotransformation. Water Res. 109, 217–226. https://doi.org/10.1016/j.watres.2016.11.048

Meng, F., Gao, G., Yang, T.T., Chen, X., Chao, Y., Na, G., Ge, L., Huang, L.N., 2015. Effects of fluoroquinolone antibiotics on reactor performance and microbial community structure of a membrane bioreactor. Chem. Eng. J. 280, 448–458. https://doi.org/10.1016/j.cej.2015.06.025

Meng, F., Wang, Z., Li, Y., 2012. Cure of filament-caused MBR fouling in the presence of antibiotics: Taking ciprofloxacin exposure as an example. Ind. Eng. Chem. Res. 51, 13784–13791. https://doi.org/10.1021/ie301401a

Mesquita, D.P., Amaral, A.L., Ferreira, E.C., 2013. Activated sludge characterization through microscopy: A review on quantitative image analysis and chemometric techniques. Anal. Chim. Acta 802, 14–28. https://doi.org/10.1016/j.aca.2013.09.016

Mesquita, D.P., Amaral, A.L., Ferreira, E.C., 2011. Identifying different types of bulking in an activated sludge system through quantitative image analysis. Chemosphere 85, 643–652. https://doi.org/10.1016/j.chemosphere.2011.07.012

Metcalf & Eddy, I., 2003. Wastewater Engineering: Treatment and Reuse, 4th ed. McGraw-Hill, New York, NY.

Miao, L., Wang, C., Hou, J., Wang, P., Ao, Y., Li, Y., Yao, Y., Lv, B., Yang, Y., You, G., Xu, Y., Gu, Q., 2017. Response of wastewater biofilm to CuO nanoparticle exposure in terms of extracellular polymeric substances and microbial community structure. Sci. Total Environ. 579, 588–597. https://doi.org/10.1016/j.scitotenv.2016.11.056

Miqueleto, A.P., Dolosic, C.C., Pozzi, E., Foresti, E., Zaiat, M., 2010. Influence of carbon sources and C/N ratio on EPS production in anaerobic sequencing batch biofilm reactors for wastewater treatment. Bioresour. Technol. 101, 1324–1330.

https://doi.org/10.1016/j.biortech.2009.09.026

Moen, E., Bannon, D., Kudo, T., Graf, W., Covert, M., Van Valen, D., 2019. Deep learning for cellular image analysis. Nat. Methods 16, 1233–1246. https://doi.org/10.1038/s41592-019-0403-1

Montiel-León, J.M., Munoz, G., Vo Duy, S., Do, D.T., Vaudreuil, M.A., Goeury, K., Guillemette, F., Amyot, M., Sauvé, S., 2019. Widespread occurrence and spatial distribution of glyphosate, atrazine, and neonicotinoids pesticides in the St. Lawrence and tributary rivers. Environ. Pollut. 250, 29–39. https://doi.org/10.1016/j.envpol.2019.03.125

More, T.T., Yadav, J.S.S., Yan, S., Tyagi, R.D., Surampalli, R.Y., 2014. Extracellular polymeric substances of bacteria and their potential environmental applications. J. Environ. Manage. 144, 1–25. https://doi.org/10.1016/j.jenvman.2014.05.010

Moreno-González, R., Rodriguez-Mozaz, S., Gros, M., Barceló, D., León, V.M., 2015. Seasonal distribution of pharmaceuticals in marine water and sediment from a mediterranean coastal lagoon (SE Spain). Environ. Res. 138, 326–344. https://doi.org/10.1016/j.envres.2015.02.016

Mujunen, S.P., Minkkinen, P., Teppola, P., Wirkkala, R.S., 1998. Modeling of activated sludge plants treatment efficiency with PLSR: A process analytical case study. Chemom. Intell. Lab. Syst. 41, 83–94. https://doi.org/10.1016/S0169-7439(98)00025-2

Navaratna, D., Elliman, J., Cooper, A., Shu, L., Baskaran, K., Jegatheesan, V., 2012. Impact of herbicide Ametryn on microbial communities in mixed liquor of a membrane bioreactor (MBR). Bioresour. Technol. 113, 181–190. https://doi.org/10.1016/j.biortech.2011.12.018

Nielsen, P.H., Frølund, B., Keiding, K., 1996. Changes in composition of extracellular polymeric subtances in activated sludge during anaerobic storage. Appl. Microbiol. Biotechnol. 44, 823–830.

Nouha, K., Yan, S., Tyagi, R.D., Surampalli, R.Y., 2016. EPS producing microorganisms from municipal wastewater activated sludge. J. Pet. Environ. Biotechnol. 2016, 1–13. https://doi.org/10.4172/2157-7463.1000255

Nsabimana, E., Bohatier, J., Belan, A., Pepirr, D., Charles, L., 1996. Effects of the herbicide atrazine on the activated sludge process: microbiology and functional views. Chemosphere 33, 479–494. https://doi.org/10.1016/0045-6535(96)00182-8

Oberholzer, M., Östreicher, M., Christen, H., Brühlmann, M., 1996. Methods in quantitative image analysis. Histochem. Cell Biol. 105, 333–355. https://doi.org/10.1007/BF01463655

Oliveira, A.S., Amorim, C.L., Ramos, M.A., Mesquita, D.P., Inocêncio, P., Ferreira, E.C., Van Loosdrecht, M., Castro, P.M.L., 2020. Variability in the composition of extracellular polymeric substances from a full-scale aerobic granular sludge reactor treating urban wastewater. J. Environ. Chem. Eng. 8, 104156. https://doi.org/10.1016/j.jece.2020.104156

Oluah, M., Obiezue, R., Ochulor, A., Onuoha, E., 2010. Toxicity and histopathological effect of atrazine (Herbicide) on the earthworm Nsukkadrilus mbae under laboratory conditions. Anim. Res. Int. 7, 1287–1293.

Ortiz de García, S.A., Pinto Pinto, G., García-Encina, P.A., Irusta-Mata, R., 2014. Ecotoxicity and environmental risk assessment of pharmaceuticals and personal care products in aquatic environments and wastewater treatment plants. Ecotoxicology 23, 1517–1533. https://doi.org/10.1007/s10646-014-1293-8

Palma, P., Köck-Schulmeyer, M., Alvarenga, P., Ledo, L., Barbosa, I.R., López de Alda, M., Barceló, D., 2014. Risk assessment of pesticides detected in surface water of the Alqueva reservoir (Guadiana basin, southern of Portugal). Sci. Total Environ. 488–489, 208–219. https://doi.org/10.1016/j.scitotenv.2014.04.088

Pan, X., Liu, J., Zhang, D., Chen, X., Song, W., Wu, F., 2010. Binding of dicamba to soluble and bound extracellular polymeric substances (EPS) from aerobic activated sludge: A fluorescence quenching study. J. Colloid Interface Sci. 345, 442–447. https://doi.org/10.1016/j.jcis.2010.02.011

Pasquini, L., Merlin, C., Hassenboehler, L., Munoz, J., Pons, M., Görner, T., 2013. Impact of certain household micropollutants on bacterial behavior. Toxicity tests/study of extracellular polymeric substances in sludge. Sci. Total Environ. 463–464, 355–365. https://doi.org/10.1016/j.scitotenv.2013.06.018

Patel, M., Kumar, R., Kishor, K., Mlsna, T., Pittman, C.U., Mohan, D., 2019. Pharmaceuticals of Emerging Concern in Aquatic Systems: Chemistry, Occurrence, Effects, and Removal Methods. Chem. Rev. 119, 3510–3673. https://doi.org/10.1021/acs.chemrev.8b00299

Peng, H., 2008. Bioimage informatics: A new area of engineering biology. Bioinformatics 24, 1827–1836. https://doi.org/10.1093/bioinformatics/btn346

Peng, J., Wang, X., Yin, F., Xu, G., 2019. Characterizing the removal routes of seven pharmaceuticals in the activated sludge process. Sci. Total Environ. 650, 2437–2445. https://doi.org/10.1016/j.scitotenv.2018.10.004

Petrie, B., Barden, R., Kasprzyk-Hordern, B., 2015. A review on emerging contaminants in wastewaters and the environment: Current knowledge, understudied areas and recommendations for future monitoring. Water Res. 72, 3–27. https://doi.org/10.1016/j.watres.2014.08.053

Polo, A.M., Tobajas, M., Sanchis, S., Mohedano, A.F., Rodríguez, J.J., 2011. Comparison of experimental methods for determination of toxicity and biodegradability of xenobiotic compounds. Biodegradation 22, 751–761. https://doi.org/10.1007/s10532-010-9448-7

Qian, J., He, X., Wang, P., Xu, B., Li, K., Lu, B., Jin, W., Tang, S., 2021. Effects of polystyrene nanoplastics on extracellular polymeric substance composition of activated sludge: The role of surface functional groups. Environ. Pollut. 279, 116904. https://doi.org/10.1016/j.envpol.2021.116904

Quintana, J.B., Weiss, S., Reemtsma, T., 2005. Pathways and metabolites of microbial degradation of selected acidic pharmaceutical and their occurrence in municipal wastewater treated by a membrane bioreactor. Water Res. 39, 2654–2664. https://doi.org/10.1016/j.watres.2005.04.068

Quintelas, C., Melo, A., Costa, M., Mesquita, D.P., Ferreira, E.C., Amaral, A.L., 2020. Environmentally-friendly technology for rapid identification and quantification of emerging pollutants from

wastewater using infrared spectroscopy. Environ. Toxicol. Pharmacol. 80, 103458. https://doi.org/10.1016/j.etap.2020.103458

Quintelas, C., Mesquita, D.P., Ferreira, E.C., Amaral, A.L., 2019. Quantification of pharmaceutical compounds in wastewater samples by near infrared spectroscopy (NIR). Talanta 194, 507–513. https://doi.org/10.1016/j.talanta.2018.10.076

Ramanathan, R., Alvarez, N., Su, A.D., Chowdhury, S., Alton, K., Stauber, K., Patrick, J., 2005. Metabolism and excretion of loratadine in male and female mice, rats and monkeys. Xenobiotica 35, 155–189. https://doi.org/10.1080/00498250500038906

Ramanathan, R., Reyderman, L., Kulmatycki, K., Su, A.-D., Alvarez, N., Chowdhury, S.K., Alton, K.B., Wirth, M.A., Clement, R.P., Statkevich, P., Patrick, J.E., 2007. Disposition of loratadine in healthy volunteers. Xenobiotica 37, 753–769. https://doi.org/10.1080/00498250701463317

Rani, L., Thapa, K., Kanojia, N., Sharma, N., Singh, S., Grewal, A.S., Srivastav, A.L., Kaushal, J., 2021. An extensive review on the consequences of chemical pesticides on human health and environment. J. Clean. Prod. 283, 124657. https://doi.org/10.1016/j.jclepro.2020.124657

Riber-Hansen, R., Vainer, B., Steiniche, T., 2012. Digital image analysis: A review of reproducibility, stability and basic requirements for optimal results. APMIS. https://doi.org/10.1111/j.1600-0463.2011.02854.x

Ricart, M., Guasch, H., Barceló, D., Brix, R., Conceição, M.H., Geiszinger, A., Alda, M.J.L. de, López-Doval, J.C., Muñoz, I., Postigo, C., Romaní, A.M., Villagrasa, M., Sabater, S., 2010. Primary and complex stressors in polluted mediterranean rivers: Pesticide effects on biological communities. J. Hydrol. 383, 52–61. https://doi.org/10.1016/j.jhydrol.2009.08.014

Ricco, G., Tomei, M.C., Ramadori, R., Laera, G., 2004. Toxicity assessment of common xenobiotic compounds on municipal activated sludge: Comparison between respirometry and Microtox®. Water Res. 38, 2103–2110. https://doi.org/10.1016/j.watres.2004.01.020

Rodriguez-Narvaez, O.M., Peralta-hernandez, J.M., Goonetilleke, A., Bandala, E.R., 2017. Treatment technologies for emerging contaminants in water : A review. Chem. Eng. J. 323, 361–380. https://doi.org/10.1016/j.cej.2017.04.106

Roh, H., Subramanya, N., Zhao, F., Yu, C.P., Sandt, J., Chu, K.H., 2009. Biodegradation potential of wastewater micropollutants by ammonia-oxidizing bacteria. Chemosphere 77, 1084–1089. https://doi.org/10.1016/j.chemosphere.2009.08.049

Rosen, C., Röttorp, J., Jeppsson, U., 2003. Multivariate on-line monitoring: Challenges and solutions for modern wastewater treatment operation. Water Sci. Technol. 47, 171–179. https://doi.org/10.2166/wst.2003.0113

Rott, E., Pittmann, T., Wasielewski, S., Kugele, A., Minke, R., 2017. Detoxification of pesticide-containingwastewater with FeIII, activated carbon and fenton reagent and its control using three standardized bacterial inhibition tests. Water (Switzerland) 9. https://doi.org/10.3390/w9120969

Russ, J.C., Neal, F.B., 2018. The Image Processing Handbook, Number by Colors. CRC Press, New

York, NY. https://doi.org/10.1201/b18983

Ryu, J., Oh, J., Snyder, S.A., Yoon, Y., 2014. Determination of micropollutants in combined sewer overflows and their removal in a wastewater treatment plant (Seoul , South Korea) 3239–3251. https://doi.org/10.1007/s10661-013-3613-5

Sacher, F., Lange, F.T., Brauch, H.-J., Blankenhorn, I., 2001. Pharmaceuticals in groundwaters: Analytical methods and results of a monitoring program in Baden-Wurttemberg, Germany. J. Chromatogr. A 938, 199–210. https://doi.org/10.1016/S0021-9673(01)01266-3

Sahar, E., David, I., Gelman, Y., Chikurel, H., Aharoni, A., Messalem, R., Brenner, A., 2011. The use of RO to remove emerging micropollutants following CAS/UF or MBR treatment of municipal wastewater. Desalination 273, 142–147. https://doi.org/10.1016/j.desal.2010.11.004

Sampson, P.D., Richards, M., Szpiro, A.A., Bergen, S., Sheppard, L., Larson, T. V, Kaufman, J.D., 2013. A regionalized national universal kriging model using Partial Least Squares regression for estimating annual PM2.5 concentrations in epidemiology. Atmos. Environ. 75, 383–392. https://doi.org/10.1016/j.atmosenv.2013.04.015

Sanchis, S., Polo, A.M., Tobajas, M., Rodriguez, J.J., Mohedano, A.F., 2014. Strategies to evaluate biodegradability: Application to chlorinated herbicides. Environ. Sci. Pollut. Res. 21, 9445–9452. https://doi.org/10.1007/s11356-013-2130-y

Santos, J.L., Aparicio, I., Alonso, E., 2007. Occurrence and risk assessment of pharmaceutically active compounds in wastewater treatment plants. A case study: Seville city (Spain). Environ. Int. 33, 596–601. https://doi.org/10.1016/j.envint.2006.09.014

Santos, L.H.M.L.M., Araújo, A.N., Fachini, A., Pena, A., Delerue-Matos, C., Montenegro, M.C.B.S.M., 2010. Ecotoxicological aspects related to the presence of pharmaceuticals in the aquatic environment. J. Hazard. Mater. 175, 45–95. https://doi.org/10.1016/j.jhazmat.2009.10.100

Santos, L.H.M.L.M., Gros, M., Rodriguez-Mozaz, S., Delerue-Matos, C., Pena, A., Barceló, D., Montenegro, M.C.B.S.M., 2013. Contribution of hospital effluents to the load of pharmaceuticals in urban wastewaters: Identification of ecologically relevant pharmaceuticals. Sci. Total Environ. 461–462, 302–316. https://doi.org/10.1016/j.scitotenv.2013.04.077

Santos, T.G., Martinez, C.B.R., 2012. Atrazine promotes biochemical changes and DNA damage in a Neotropical fish species. Chemosphere 89, 1118–1125. https://doi.org/10.1016/j.chemosphere.2012.05.096

Santschi, P.H., Chin, W.C., Quigg, A., Xu, C., Kamalanathan, M., Lin, P., Shiu, R.F., 2021. Marine gel interactions with hydrophilic and hydrophobic pollutants. Gels 7, 1–14. https://doi.org/10.3390/gels7030083

Santschi, P.H., Xu, C., Schwehr, K.A., Lin, P., Sun, L., Chin, W.C., Kamalanathan, M., Bacosa, H.P., Quigg, A., 2020. Can the protein/carbohydrate (P/C) ratio of exopolymeric substances (EPS) be used as a proxy for their 'stickiness' and aggregation propensity? Mar. Chem. 218, 103734. https://doi.org/10.1016/j.marchem.2019.103734

Schindelin, J., Rueden, C.T., Hiner, M.C., Eliceiri, K.W., 2015. The ImageJ ecosystem: An open

platform for biomedical image analysis. Mol. Reprod. Dev. 82, 518–529. https://doi.org/10.1002/mrd.22489

Sesay, M.L., Özcengiz, G., Dilek Sanin, F., 2006. Enzymatic extraction of activated sludge extracellular polymers and implications on bioflocculation. Water Res. 40, 1359–1366. https://doi.org/10.1016/j.watres.2006.01.045

Sharma, A., Kumar, V., Shahzad, B., Tanveer, M., Sidhu, G.P.S., Handa, N., Kohli, S.K., Yadav, P., Bali, A.S., Parihar, R.D., Dar, O.I., Singh, K., Jasrotia, S., Bakshi, P., Ramakrishnan, M., Kumar, S., Bhardwaj, R., Thukral, A.K., 2019. Worldwide pesticide usage and its impacts on ecosystem. SN Appl. Sci. 1, 1446. https://doi.org/10.1007/s42452-019-1485-1

Shen, Y., Huang, D.M., Chen, Y.P., Yan, P., Gao, X., 2020. New insight into filamentous sludge bulking during wastewater treatment: Surface characteristics and thermodynamics. Sci. Total Environ. 712, 135795. https://doi.org/10.1016/j.scitotenv.2019.135795

Sheng, G.-P., Xu, J., Li, W.-H., Yu, H.-Q., 2013. Quantification of the interactions between Ca^2, Hg^{2+} and extracellular polymeric substances (EPS) of sludge. Chemosphere 93, 1436–1441. https://doi.org/10.1016/j.chemosphere.2013.07.076

Sheng, G.-P., Yu, H.-Q., Li, X.-Y., 2010. Extracellular polymeric substances (EPS) of microbial aggregates in biological wastewater treatment systems: A review. Biotechnol. Adv. 28, 882–894. https://doi.org/10.1016/j.biotechadv.2010.08.001

Sheng, G.P., Xu, J., Luo, H.W., Li, W.W., Li, W.H., Yu, H.Q., Xie, Z., Wei, S.Q., Hu, F.C., 2013. Thermodynamic analysis on the binding of heavy metals onto extracellular polymeric substances (EPS) of activated sludge. Water Res. 47, 607–614. https://doi.org/10.1016/j.watres.2012.10.037

Sheng, G.P., Yu, H.Q., 2006. Characterization of extracellular polymeric substances of aerobic and anaerobic sludge using three-dimensional excitation and emission matrix fluorescence spectroscopy. Water Res. 40, 1233–1239. https://doi.org/10.1016/j.watres.2006.01.023

Sheng, G.P., Yu, H.Q., Yue, Z., 2006. Factors influencing the production of extracellular polymeric substances by Rhodopseudomonas acidophila. Int. Biodeterior. Biodegrad. 58, 89–93. https://doi.org/10.1016/j.ibiod.2006.07.005

Shi, H.X., Wang, J., Liu, S.Y., Guo, J.S., Fang, F., Chen, Y.P., Yan, P., 2022. New insight into filamentous sludge bulking: Potential role of AHL-mediated quorum sensing in deteriorating sludge floc stability and structure. Water Res. 212, 118096. https://doi.org/10.1016/j.watres.2022.118096

Shi, Y., Liu, Y., 2021. Evolution of extracellular polymeric substances (EPS) in aerobic sludge granulation: Composition, adherence and viscoelastic properties. Chemosphere 262, 128033. https://doi.org/10.1016/j.chemosphere.2020.128033

Shiu, R.F., Chiu, M.H., Vazquez, C.I., Tsai, Y.Y., Le, A., Kagiri, A., Xu, C., Kamalanathan, M., Bacosa, H.P., Doyle, S.M., Sylvan, J.B., Santschi, P.H., Quigg, A., Chin, W.C., 2020. Protein to carbohydrate (P/C) ratio changes in microbial extracellular polymeric substances induced by oil and Corexit. Mar. Chem. 223, 103789. https://doi.org/10.1016/j.marchem.2020.103789

Shu, C., Lung, M., 2004. Effect of pH on the production and molecular weight distribution of exopolysaccharide by Antrodia camphorata in batch cultures 39, 931–937. https://doi.org/10.1016/S0032-9592(03)00220-6

Silva, S.A., Val del Río, A., Amaral, A.L., Ferreira, E.C., Madalena Alves, M., Mesquita, D.P., 2022. Monitoring morphological changes from activated sludge to aerobic granular sludge under distinct organic loading rates and increasing minimal imposed sludge settling velocities through quantitative image analysis. Chemosphere 286. https://doi.org/10.1016/j.chemosphere.2021.131637

Simons, F.E.R., Simons, K.J., 2011. Histamine and H1-antihistamines: Celebrating a century of progress. J. Allergy Clin. Immunol. 128, 1139-1150.e4. https://doi.org/10.1016/j.jaci.2011.09.005

Singh, S., Kumar, V., Chauhan, A., Datta, S., Wani, A.B., Singh, N., Singh, J., 2018. Toxicity, degradation and analysis of the herbicide atrazine. Environ. Chem. Lett. 16, 211–237. https://doi.org/10.1007/s10311-017-0665-8

Sivasubramanian, R., Chen, G. hao, Mackey, H.R., 2021. Shock effects of monovalent cationic salts on seawater cultivated granular sludge. J. Hazard. Mater. 403, 123646. https://doi.org/10.1016/j.jhazmat.2020.123646

Smolders, G.J.F., van der Meij, J., van Loosdrecht, M.C.M., Heijnen, J.J., 1994. Model of the anaerobic metabolism of the biological phosphorus removal process: Stoichiometry and pH influence. Biotechnol. Bioeng. 43, 461–470. https://doi.org/10.1002/bit.260430605

Sobeck, D.C., Higgins, M.J., 2002. Examination of three theories for mechanisms of cation-induced bioflocculation. Water Res. 36, 527–538. https://doi.org/10.1016/S0043-1354(01)00254-8

Sodhi, V., Bansal, A., Jha, M.K., 2022. Effect of extracellular polymeric compositions on in-situ sludge minimization performance of upgraded activated sludge treatment for industrial wastewater. J. Environ. Manage. 306, 114516. https://doi.org/10.1016/j.jenvman.2022.114516

Song, C., Sun, X.F., Xing, S.F., Xia, P.F., Shi, Y.J., Wang, S.G., 2014. Characterization of the interactions between tetracycline antibiotics and microbial extracellular polymeric substances with spectroscopic approaches. Environ. Sci. Pollut. Res. 21, 1786–1795. https://doi.org/10.1007/s11356-013-2070-6

Song, W., Mu, G., Zhang, D., Pan, X., 2010. Interaction of acetamiprid with extracellular polymeric substances (EPS) from activated sludge: A fluorescence study. African J. Biotechnol. 9, 7667–7673. https://doi.org/10.5897/AJB09.1539

Song, Y., Zheng, G., Huo, M., Zhao, B., Zhou, L., 2014. Extracellular polymeric substances and bound water drastically affect bioleached sludge dewaterability at low temperature. Environ. Technol. (United Kingdom) 35, 2538–2545. https://doi.org/10.1080/09593330.2014.911755

Spanjers, H., Peter, V., Olsson, G., Dold, P., 1996. Respirometry in control of the activated sludge process. Water Sci. Technol. 34, 117–126. https://doi.org/10.1016/0273-1223(96)84211-9

Staey, G. Van De, Gins, G., Smets, I., 2016. Bioflocculation and Activated Sludge Separation: A PLS

Case Study. IFAC-PapersOnLine 49, 1151–1156. https://doi.org/10.1016/j.ifacol.2016.07.358

Sutherland, I.W., 2001. Microbial polysaccharides from Gram-negative bacteria. Int. Dairy J. 11, 663–674. https://doi.org/10.1016/S0958-6946(01)00112-1

Świetlik, J., Dąbrowska, A., Raczyk-Stanisławiak, U., Nawrocki, J., 2004. Reactivity of natural organic matter fractions with chlorine dioxide and ozone. Water Res. 38, 547–558. https://doi.org/10.1016/j.watres.2003.10.034

Swissa, N., Nitzan, Y., Langzam, Y., Cahan, R., 2014. Atrazine biodegradation by a monoculture of Raoultella planticola isolated from a herbicides wastewater treatment facility. Int. Biodeterior. Biodegrad. 92, 6–11. https://doi.org/10.1016/j.ibiod.2014.04.003

Szewczyk, R., Różalska, S., Mironenka, J., Bernat, P., 2020. Atrazine biodegradation by mycoinsecticide Metarhizium robertsii: Insights into its amino acids and lipids profile. J. Environ. Manage. 262. https://doi.org/10.1016/j.jenvman.2020.110304

Tadkaew, N., Hai, F.I., McDonald, J.A., Khan, S.J., Nghiem, L.D., 2011. Removal of trace organics by MBR treatment: The role of molecular properties. Water Res. 45, 2439–2451. https://doi.org/10.1016/j.watres.2011.01.023

Tao, Y., Hu, S., Han, S., Shi, H., Yang, Y., Li, H., Jiao, Y., Zhang, Q., Akindolie, M.S., Ji, M., Chen, Z., Zhang, Y., 2019. Efficient removal of atrazine by iron-modified biochar loaded Acinetobacter lwoffii DNS32. Sci. Total Environ. 682, 59–69. https://doi.org/10.1016/j.scitotenv.2019.05.134

Teppola, P., Mujunen, S.-P., Minkkinen, P., 1998. A combined approach of partial least squares and fuzzy c-means clustering for the monitoring of an activated-sludge waste-water treatment plant. Chemom. Intell. Lab. Syst. 41, 95–103. https://doi.org/10.1016/S0169-7439(98)00026-4

Teppola, P., Mujunen, S.-P., Minkkinen, P., 1997. Partial least squares modeling of an activated sludge plant: A case study. Chemom. Intell. Lab. Syst. 38, 197–208. https://doi.org/https://doi.org/10.1016/S0169-7439(97)00055-5

Ternes, T.A., 1998. Occurrence of drugs in German sewage treatment plants and rivers. Water Res. 32, 3245–3260. https://doi.org/10.1016/S0043-1354(98)00099-2

Tian, X., Shen, Z., Han, Z., Zhou, Y., 2019. The effect of extracellular polymeric substances on exogenous highly toxic compounds in biological wastewater treatment : An overview. Bioresour. Technol. Reports 5, 28–42. https://doi.org/10.1016/j.biteb.2018.11.009

Tomita, R.K., Park, S.W., Sotomayor, O.A.Z., 2002. Analysis of activated sludge process using multivariate statistical tools—a PCA approach. Chem. Eng. J. 90, 283–290. https://doi.org/10.1016/S1385-8947(02)00133-X

Torquetti, C.G., Guimarães, A.T.B., Soto-Blanco, B., 2021. Exposure to pesticides in bats. Sci. Total Environ. 755, 142509. https://doi.org/10.1016/j.scitotenv.2020.142509

Torresi, E., Polesel, F., Bester, K., Christensson, M., Smets, B.F., Trapp, S., Andersen, H.R., Plósz, B.G., 2017. Diffusion and sorption of organic micropollutants in biofilms with varying thicknesses. Water Res. 123, 388–400. https://doi.org/10.1016/j.watres.2017.06.027

Tran, N.H., Urase, T., Ta, T.T., 2014. A Preliminary Study on the Occurrence of Pharmaceutically Active Compounds in Hospital Wastewater and Surface Water in Hanoi, Vietnam. CLEAN - Soil, Air, Water 42, 267–275. https://doi.org/10.1002/clen.201300021

Triassi, M., Montuori, P., Provvisiero, D.P., De Rosa, E., Di Duca, F., Sarnacchiaro, P., Díez, S., 2022. Occurrence and spatial-temporal distribution of atrazine and its metabolites in the aquatic environment of the Volturno River estuary, southern Italy. Sci. Total Environ. 803, 149972. https://doi.org/10.1016/j.scitotenv.2021.149972

Tu, X., Song, Y., Yu, H., Zeng, P., Liu, R., 2012. Fractionation and characterization of dissolved extracellular and intracellular products derived from floccular sludge and aerobic granules. Bioresour. Technol. 123, 55–61. https://doi.org/10.1016/j.biortech.2012.07.075

Vasiliadou, I.A., Molina, R., Martinez, F., Melero, J.A., Stathopoulou, P.M., Tsiamis, G., 2018. Toxicity assessment of pharmaceutical compounds on mixed culture from activated sludge using respirometric technique: The role of microbial community structure. Sci. Total Environ. 630, 809–819. https://doi.org/10.1016/j.scitotenv.2018.02.095

Verenitch, S.S., Lowe, C.J., Mazumder, A., 2006. Determination of acidic drugs and caffeine in municipal wastewaters and receiving waters by gas chromatography-ion trap tandem mass spectrometry. J. Chromatogr. A 1116, 193–203. https://doi.org/10.1016/j.chroma.2006.03.005

Waller, S.A., Paul, K., Peterson, S.E., Hitti, J.E., 2010. Agricultural-related chemical exposures, season of conception, and risk of gastroschisis in Washington State. Am. J. Obstet. Gynecol. 202, 241.e1-241.e6. https://doi.org/10.1016/j.ajog.2010.01.023

Wang, B.-B., Liu, X.-T., Chen, J.-M., Peng, D.-C., He, F., 2018. Composition and functional group characterization of extracellular polymeric substances (EPS) in activated sludge: the impacts of polymerization degree of proteinaceous substrates. Water Res. 129, 133–142. https://doi.org/10.1016/j.watres.2017.11.008

Wang, B. Bin, Chang, Q., Peng, D.C., Hou, Y.P., Li, H.J., Pei, L.Y., 2014. A new classification paradigm of extracellular polymeric substances (EPS) in activated sludge: Separation and characterization of exopolymers between floc level and microcolony level. Water Res. 64, 53–60. https://doi.org/10.1016/j.watres.2014.07.003

Wang, H., Deng, H., Ma, L., Ge, L., 2014. The effect of carbon source on extracellular polymeric substances production and its influence on sludge floc properties. J. Chem. Technol. Biotechnol. 89, 516–521. https://doi.org/10.1002/jctb.4147

Wang, H., Deng, H., Ma, L., Ge, L., 2013. Influence of operating conditions on extracellular polymeric substances and surface properties of sludge flocs. Carbohydr. Polym. 92, 510–515. https://doi.org/10.1016/j.carbpol.2012.09.055

Wang, L., Li, Y., Wang, Li, Zhu, M., Zhu, X., Qian, C., Li, W., 2018. Responses of biofilm microorganisms from moving bed biofilm reactor to antibiotics exposure: Protective role of extracellular polymeric substances. Bioresour. Technol. 254, 268–277. https://doi.org/10.1016/j.biortech.2018.01.063

Wang, X., Xing, H., Jiang, Y., Wu, H., Sun, G., Xu, Q., Xu, S., 2013. Accumulation, histopathological effects and response of biochemical markers in the spleens and head kidneys of common carp exposed to atrazine and chlorpyrifos. Food Chem. Toxicol. 62, 148–158. https://doi.org/10.1016/j.fct.2013.08.044

Wang, Y., Qin, J., Zhou, S., Lin, X., Ye, L., Song, C., Yan, Y., 2015. Identification of the function of extracellular polymeric substances (EPS) in denitrifying phosphorus removal sludge in the presence of copper ion. Water Res. 73, 252–264. https://doi.org/10.1016/j.watres.2015.01.034

Wang, Y., Wang, J., Liu, Z., Huang, X., Fang, F., Guo, J., Yan, P., 2021. Effect of EPS and its forms of aerobic granular sludge on sludge aggregation performance during granulation process based on XDLVO theory. Sci. Total Environ. 795, 148682. https://doi.org/10.1016/j.scitotenv.2021.148682

Wang, Z.W., Liu, Y., Tay, J.H., 2005. Distribution of EPS and cell surface hydrophobicity in aerobic granules. Appl. Microbiol. Biotechnol. 69, 469–473. https://doi.org/10.1007/s00253-005-1991-5

Wang, Z., Gao, M., Wang, S., Xin, Y., Ma, D., She, Z., Wang, Zhe, Chang, Q., Ren, Y., 2014. Effect of hexavalent chromium on extracellular polymeric substances of granular sludge from an aerobic granular sequencing batch reactor. Chem. Eng. J. 251, 165–174. https://doi.org/10.1016/j.cej.2014.04.078

Wang, Z., Gao, M., Wang, Zhe, She, Z., Chang, Q., Sun, C., Zhang, J., Ren, Y., Yang, N., 2013. Effect of salinity on extracellular polymeric substances of activated sludge from an anoxic-aerobic sequencing batch reactor. Chemosphere 93, 2789–2795. https://doi.org/10.1016/j.chemosphere.2013.09.038

Weber, T.J., 2002. Wastewater treatment. Met. Finish. 100, 781–797. https://doi.org/10.1016/S0026-0576(02)82077-3

Wei, D., Wang, B., Ngo, H.H., Guo, W., Han, F., Wang, X., Du, B., Wei, Q., 2015. Role of extracellular polymeric substances in biosorption of dye wastewater using aerobic granular sludge. Bioresour. Technol. 185, 14–20. https://doi.org/10.1016/j.biortech.2015.02.084

Wilén, B.-M., Jin, B., Lant, P., 2003. The influence of key chemical constituents in activated sludge on surface and flocculating properties. Water Res. 37, 2127–2139. https://doi.org/10.1016/S0043-1354(02)00629-2

Wilén, B.-M., Lumley, D., Mattsson, A., Mino, T., 2008. Relationship between floc composition and flocculation and settling properties studied at a full scale activated sludge plant. Water Res. 42, 4404–4418. https://doi.org/10.1016/j.watres.2008.07.033

Wingender, Jost, Neu, T.R., Flemming, H.-C., 1999. What are Bacterial Extracellular Polymeric Substances?, in: Microbial Extracellular Polymeric Substances. Springer Berlin Heidelberg, Berlin, Heidelberg, pp. 1–19. https://doi.org/10.1007/978-3-642-60147-7_1

Wingender, J, Neu, T.R., Flemming, H.C., 1999. Microbial Extracellular Polymeric Substances, Springer. Springer Berlin Heidelberg, Berlin, Heidelberg. https://doi.org/10.1007/978-3-642-

60147-7

Xu, C., Zhang, S., Chuang, C. ying, Miller, E.J., Schwehr, K.A., Santschi, P.H., 2011. Chemical composition and relative hydrophobicity of microbial exopolymeric substances (EPS) isolated by anion exchange chromatography and their actinide-binding affinities. Mar. Chem. 126, 27–36. https://doi.org/10.1016/j.marchem.2011.03.004

Xu, D., Liu, J., Ma, T., Gao, Y., Zhang, S., Li, J., 2021. Rapid granulation of aerobic sludge in a continuous-flow reactor with a two-zone sedimentation tank by the addition of dewatered sludge. J. Water Process Eng. 41, 101941. https://doi.org/10.1016/j.jwpe.2021.101941

Xu, J., Sheng, G.P., Ma, Y., Wang, L.F., Yu, H.Q., 2013. Roles of extracellular polymeric substances (EPS) in the migration and removal of sulfamethazine in activated sludge system. Water Res. 47, 5298–5306. https://doi.org/10.1016/j.watres.2013.06.009

Yang, C., Li, Y., Zhang, K., Wang, X., Ma, C., Tang, H., Xu, P., 2010. Atrazine degradation by a simple consortium of Klebsiella sp. A1 and Comamonas sp. A2 in nitrogen enriched medium. Biodegradation 21, 97–105. https://doi.org/10.1007/s10532-009-9284-9

Yang, J., Liu, X., Wang, D., Xu, Q., Yang, Q., Zeng, G., Li, X., Liu, Y., Gong, J., Ye, J., Li, H., 2019. Mechanisms of peroxymonosulfate pretreatment enhancing production of short-chain fatty acids from waste activated sludge. Water Res. 148, 239–249. https://doi.org/10.1016/j.watres.2018.10.060

Yang, S., Li, X., 2009. Influences of extracellular polymeric substances (EPS) on the characteristics of activated sludge under non-steady-state conditions. Process Biochem. 44, 91–96. https://doi.org/10.1016/j.procbio.2008.09.010

Yang, S.F., Lin, C.F., Wu, C.J., Ng, K.K., Yu-Chen Lin, A., Andy Hong, P.K., 2012. Fate of sulfonamide antibiotics in contact with activated sludge - Sorption and biodegradation. Water Res. 46, 1301–1308. https://doi.org/10.1016/j.watres.2011.12.035

Yanze-Kontchou, C., Gschwind, N., 1994. Mineralization of the herbicide atrazine as a carbon source by a Pseudomonas strain. Appl. Environ. Microbiol. 60, 4297–4302. https://doi.org/10.1128/aem.60.12.4297-4302.1994

Yao, J., Liu, J., Zhang, Y., Xu, S., Hong, Y., Chen, Y., 2019. Adding an anaerobic step can rapidly inhibit sludge bulking in SBR reactor. Sci. Rep. 9, 1–10. https://doi.org/10.1038/s41598-019-47304-3

Ye, F., Peng, G., Li, Y., 2011a. Influences of influent carbon source on extracellular polymeric substances (EPS) and physicochemical properties of activated sludge. Chemosphere 84, 1250–1255. https://doi.org/10.1016/j.chemosphere.2011.05.004

Ye, F., Ye, Y., Li, Y., 2011b. Effect of C/N ratio on extracellular polymeric substances (EPS) and physicochemical properties of activated sludge flocs. J. Hazard. Mater. 188, 37–43. https://doi.org/10.1016/j.jhazmat.2011.01.043

Yin, C., Meng, F., Chen, G.-H., 2015. Spectroscopic characterization of extracellular polymeric substances from a mixed culture dominated by ammonia-oxidizing bacteria. Water Res. 68, 740–749. https://doi.org/10.1016/j.watres.2014.10.046

Yin, C., Meng, F., Meng, Y., Chen, G.H., 2016. Differential ultraviolet-visible absorbance spectra for characterizing metal ions binding onto extracellular polymeric substances in different mixed microbial cultures. Chemosphere 159, 267–274. https://doi.org/10.1016/j.chemosphere.2016.05.089

Yoo, C.K., Vanrolleghem, P.A., Lee, I.B., 2003. Nonlinear modeling and adaptive monitoring with fuzzy and multivariate statistical methods in biological wastewater treatment plants. J. Biotechnol. 105, 135–163. https://doi.org/10.1016/S0168-1656(03)00168-8

Yu, G.H., He, P.J., Shao, L.M., 2009. Characteristics of extracellular polymeric substances (EPS) fractions from excess sludges and their effects on bioflocculability. Bioresour. Technol. 100, 3193–3198. https://doi.org/10.1016/j.biortech.2009.02.009

Yu, G.H., He, P.J., Shao, L.M., He, P.P., 2008. Stratification structure of sludge flocs with implications to dewaterability. Environ. Sci. Technol. 42, 7944–7949. https://doi.org/10.1021/es8016717

Yu, H.Q., 2020. Molecular Insights into Extracellular Polymeric Substances in Activated Sludge. Environ. Sci. Technol. 54, 7742–7750. https://doi.org/10.1021/acs.est.0c00850

Yu, N., Zhao, C., Ma, B., Li, S., She, Z., Guo, L., Zhang, Q., Zhao, Y., Jin, C., Gao, M., 2019. Impact of ampicillin on the nitrogen removal, microbial community and enzymatic activity of activated sludge. Bioresour. Technol. 272, 337–345. https://doi.org/10.1016/j.biortech.2018.10.048

Yu, T., Wang, L., Ma, F., Yang, J., Bai, S., You, J., 2019. Self-immobilized biomixture with pellets of Aspergillus niger Y3 and Arthrobacter. sp ZXY-2 to remove atrazine in water: A bio-functions integration system. Sci. Total Environ. 689, 875–882. https://doi.org/10.1016/j.scitotenv.2019.06.313

Zhang, H., Song, S., Jia, Y., Wu, D., Lu, H., 2019. Stress-responses of activated sludge and anaerobic sulfate-reducing bacteria sludge under long-term ciprofloxacin exposure. Water Res. 164. https://doi.org/10.1016/j.watres.2019.114964

Zhang, H., Song, S., Sun, L., Zhao, Q., Lu, H., 2020. Comparative study on ciprofloxacin removal in sulfur-mediated biological systems. Chinese Chem. Lett. 31, 1432–1437. https://doi.org/10.1016/j.cclet.2020.04.048

Zhang, L., Zhao, Q., Zhang, M., Guo, J., Zheng, J., Chen, Z., Jia, Y., Zhang, J., Li, Z., Zhang, H., 2020. Mg2+ distribution in activated sludge and its effects on the nitrifying activity and the characteristics of extracellular polymeric substances and sludge flocs. Process Biochem. 88, 120–128. https://doi.org/10.1016/j.procbio.2019.10.002

Zhang, P., Chen, Y.P., Guo, J.S., Shen, Y., Yang, J.X., Fang, F., Li, C., Gao, X., Wang, G.X., 2014. Adsorption behavior of tightly bound extracellular polymeric substances on model organic surfaces under different pH and cations with surface plasmon resonance. Water Res. 57, 31–39. https://doi.org/10.1016/j.watres.2014.03.018

Zhang, X., Bishop, P.L., 2003. Biodegradability of biofilm extracellular polymeric substances. Chemosphere 50, 63–69. https://doi.org/10.1016/S0045-6535(02)00319-3

Zhang, Y., Zhang, J., Xu, Q., Wang, Y., Wu, W., Wang, W., Li, X., Zhang, T., 2021. Simultaneous

Determination of Loratadine and Its Metabolite Desloratadine in Beagle Plasma by LC-MS/MS and Application for Pharmacokinetics Study of Loratadine Tablets and Omeprazole-Induced Drug–Drug Interaction. Drug Des. Devel. Ther. 15, 5109–5122. https://doi.org/10.2147/DDDT.S328106

Zhou, G., Li, N., Rene, E.R., Liu, Q., Dai, M., Kong, Q., 2019. Chemical composition of extracellular polymeric substances and evolution of microbial community in activated sludge exposed to ibuprofen. J. Environ. Manage. 246, 267–274. https://doi.org/10.1016/j.jenvman.2019.05.044

Zhou, Q., Chen, L., Wang, Z., Wang, J., Ni, S., Qiu, J., Liu, X., Zhang, X., Chen, X., 2017. Fast atrazine degradation by the mixed cultures enriched from activated sludge and analysis of their microbial community succession. Environ. Sci. Pollut. Res. 24, 22152–22157. https://doi.org/10.1007/s11356-017-9052-z

Zhu, L., Qi, H. ying, Lv, M. Le, Kong, Y., Yu, Y.W., Xu, X.Y., 2012. Component analysis of extracellular polymeric substances (EPS) during aerobic sludge granulation using FTIR and 3D-EEM technologies. Bioresour. Technol. 124, 455–459. https://doi.org/10.1016/j.biortech.2012.08.059

Zhu, L., Zhou, J., Lv, M., Yu, H., Zhao, H., Xu, X., 2015. Specific component comparison of extracellular polymeric substances (EPS) in flocs and granular sludge using EEM and SDS-PAGE. Chemosphere 121, 26–32. https://doi.org/10.1016/j.chemosphere.2014.10.053

Zupanc, M., Kosjek, T., Petkovšek, M., Dular, M., Kompare, B., Širok, B., Blažeka, Ž., Heath, E., 2013. Removal of pharmaceuticals from wastewater by biological processes, hydrodynamic cavitation and UV treatment. Ultrason. Sonochem. 20, 1104–1112. https://doi.org/10.1016/j.ultsonch.2012.12.003

APPENDICES

Chapter 4 - Supplementary Information (SI)

Effect of ibuprofen on extracellular polymeric substances (EPS) production and composition and assessment of microbial structure by quantitative image analysis

Table S4.1 — Average COD, IBU, NH_4^+-N, NO_2^--N, and NO_3^--N concentrations (i - influent, e - effluent), and average removal percentages (r) of COD, NH_4^+-N, and IBU along phases I-III.

Parameter	Unit	Phase I			Phase II			Phase III		
		Mean	SD	N	Mean	SD	N	Mean	SD	N
COD_i		570.9	32.3	17	755.8	216.7	17	621.4	140.7	23
COD_e		19.7	7.4	17	221.8	160.5	17	214.2	118.0	23
IBU_i		0.0	0.0	17	10.5	1.3	17	5.1	0.7	23
IBU_e	mg	0.0	0.0	17	4.4	1.7	17	2.5	0.6	23
NH_4^+-N_i	L^{-1}	27.6	3.9	17	42.1	9.8	17	31.6	6.2	23
NH_4^+-N_e		0.3	0.5	17	10.1	11.4	17	9.0	3.1	23
NO_2^--N_e		0.1	0.4	17	0.7	0.9	17	0.7	1.1	23
NO_3^--N_e		4.6	1.7	17	2.4	3.3	17	0.5	0.4	23
COD_r		97	1.3	17	71	18.8	17	65	15.6	23
NH_4^+-N_r	%	99	2.5	17	77	25.2	17	71	11.7	23
IBU_r		0	0.0	0	58	17.3	17	50	12.0	23

N is the number of samples for the operational period.
SD: standard deviation

Table S4.2 – Statistical analysis of variance (ANOVA) for COD, NH_4^+-N, and IBU removal percentages (r).

		Sum of Squares	df	Mean Square	F test	p-value
ANOVA						
COD_r	Between Groups	10411.40	2	5205.70	25.50	0.000
	Within Groups	11023.28	54	204.13		
	Total	21434.68	56			
NH_4^+-N_r	Between Groups	7950.95	2	3975.47	16.15	0.000
	Within Groups	13291.89	54	246.15		
	Total	21242.84	56			
IBU_r	Between Groups	34374.16	2	17187.08	116.99	0.000
	Within Groups	7932.64	54	146.90		
	Total	42306.79	56			

df: degrees of freedom

Table S4.3 – Tukey's HSD test (difference expressed honestly) to determine if there is a statistically significant difference in the COD and NH_4^+-N removal efficiencies (r) when the IBU was present in the biological systems and whether the assessed concentrations of the IBU had an influence on its removal percentages.

Multiple Comparisons							
Tukey HSD Dependent Variable	(I) Phase	(J) Phase	Mean Difference (I-J)	Std. Error	p-value	95% Confidence Interval	
						Lower Bound	Upper Bound
COD_r	Phase I	Phase II	25.50*	4.90	0.00	13.69	37.31
		Phase III	31.62*	4.57	0.00	20.61	42.63
	Phase II	Phase I	-25.50*	4.90	0.00	-37.31	-13.69
		Phase III	6.12	4.57	0.38	-4.89	17.13
	Phase III	Phase I	-31.62*	4.57	0.00	-42.63	-20.60
		Phase II	-6.12	4.57	0.38	-17.13	4.89
NH_4^+-N_r	Phase I	Phase II	21.47*	5.38	0.00	8.50	34.44
		Phase III	27.88*	5.02	0.00	15.79	39.97
	Phase II	Phase I	-21.47*	5.38	0.00	-34.44	-8.50
		Phase III	6.41	5.02	0.41	-5.68	18.50
	Phase III	Phase I	-27.88*	5.02	0.00	-39.97	-15.79
		Phase II	-6.41	5.02	0.41	-18.50	5.68
IBU_r	Phase I	Phase II	-57.72*	4.16	0.00	-67.74	-47.70
		Phase III	-49.86*	3.88	0.00	-59.21	-40.52
	Phase II	Phase I	57.72*	4.16	0.00	47.70	67.74
		Phase III	7.86	3.88	0.11	-1.48	17.20
	Phase III	Phase I	49.86*	3.88	0.00	40.52	59.21
		Phase II	-7.86	3.88	0.11	-17.20	1.48

*. The mean difference is significant at the 0.05 level.

Std. Error: standard error

Table S4.4 – Average values (mg EPS g_{MLVSS}^{-1}) followed by standard deviation (SD) of EPS and components during phases I-III.

Parameter	Phase I			Phase II			Phase III		
	Mean	SD	N	Mean	SD	N	Mean	SD	N
PS LB-EPS	8.03	1.47	17	1.49	0.16	17	2.45	0.47	23
PN LB-EPS	56.54	17.06	17	9.99	0.84	17	13.95	2.65	23
HAS LB-EPS	73.74	16.24	17	8.54	0.60	17	22.52	2.80	23
PS TB-EPS	8.40	0.58	17	7.79	1.17	17	4.83	2.17	23
PN TB-EPS	38.24	1.66	17	49.67	6.23	17	15.88	1.35	23
HAS TB-EPS	41.86	1.55	17	34.91	3.73	17	18.45	1.80	23
LB-EPS	138.30	23.60	17	20.02	1.04	17	38.92	3.89	23
TB-EPS	88.49	2.35	17	92.37	7.36	17	39.16	3.13	23
Total EPS	226.79	23.72	17	112.38	7.43	17	78.08	4.99	23

Table S4.5 – Statistical analysis of variance (ANOVA) for EPS and its components during phases I-III.

		Sum of Squares	df	Mean Square	F test	p-value
ANOVA						
PS LB-EPS	Between Groups	435.96	2	217.98	36.87	0.000
	Within Groups	319.28	54	5.91		
	Total	755.24	56			
PN LB-EPS	Between Groups	23532.87	2	11766.44	18.16	0.000
	Within Groups	34990.37	54	647.97		
	Total	58523.24	56			
HAS LB-EPS	Between Groups	40878.12	2	20439.06	17.41	0.000
	Within Groups	63402.31	54	1174.12		
	Total	104280.43	56			
PS TB-EPS	Between Groups	149.14	2	74.57	2.20	0.121
	Within Groups	1832.23	54	33.93		
	Total	1981.37	56			
PN TB-EPS	Between Groups	11925.20	2	5962.60	10.11	0.000
	Within Groups	31859.17	54	589.98		
	Total	43784.37	56			
HAS TB-EPS	Between Groups	5860.03	2	2930.01	4.98	0.010
	Within Groups	31789.20	54	588.69		
	Total	37649.23	56			
LB-EPS	Between Groups	141132.29	2	70566.15	20.75	0.000
	Within Groups	183610.99	54	3400.20		
	Total	324743.28	56			
TB-EPS	Between Groups	36192.80	2	18096.40	6.47	0.003
	Within Groups	151075.70	54	2797.70		
	Total	187268.51	56			
Total EPS	Between Groups	226136.01	2	113068.00	13.08	0.000
	Within Groups	466946.25	54	8647.15		
	Total	693082.25	56			

df: degrees of freedom

Table S4.6 – Tukey's HSD test to verify if IBU presence promoted a statistically significant difference in terms of EPS production between phases I, II, and III.

Tukey HSD Dependent Variable	(I) Phase	(J) Phase	Mean Difference (I-J)	Std. Error	Sig.	95% Confidence Interval	
Multiple Comparisons							
						Lower Bound	Upper Bound
PS LB-EPS	Phase I	Phase II	6.53*	0.83	0.00	4.52	8.54
		Phase III	5.57*	0.78	0.00	3.70	7.45
	Phase II	Phase I	-6.53*	0.83	0.00	-8.54	-4.52
		Phase III	-0.95	0.78	0.44	-2.83	0.92
	Phase III	Phase I	-5.57*	0.78	0.00	-7.45	-3.70
		Phase II	0.95	0.78	0.44	-0.92	2.83
PN LB-EPS	Phase I	Phase II	46.54*	8.73	0.00	25.50	67.59
		Phase III	42.59*	8.14	0.00	22.96	62.21
	Phase II	Phase I	-46.54*	8.73	0.00	-67.59	-25.50
		Phase III	-3.96	8.14	0.88	-23.60	15.66
	Phase III	Phase I	-42.59*	8.14	0.00	-62.21	-22.96
		Phase II	3.96	8.14	0.88	-15.66	23.58
HAS LB-EPS	Phase I	Phase II	65.19*	11.75	0.00	36.86	93.51
		Phase III	51.21*	10.96	0.00	24.80	77.63
	Phase II	Phase I	-65.19*	11.75	0.00	-93.51	-36.86
		Phase III	-13.96	10.96	0.41	-40.39	12.44
	Phase III	Phase I	-51.21*	10.96	0.00	-77.63	-24.80
		Phase II	13.96	10.96	0.41	-12.44	40.39
PS TB-EPS	Phase I	Phase II	0.61	2.00	0.95	-4.21	5.42
		Phase III	3.57	1.86	0.14	-0.92	8.06
	Phase II	Phase I	-0.61	2.00	0.95	-5.42	4.21
		Phase III	2.96	1.86	0.26	-1.53	7.45
	Phase III	Phase I	-3.57	1.86	0.14	-8.06	0.92
		Phase II	-2.96	1.86	0.26	-7.45	1.53
PN TB-EPS	Phase I	Phase II	-11.43	8.33	0.36	-31.51	8.65
		Phase III	22.36*	7.77	0.02	3.64	41.08
	Phase II	Phase I	11.43	8.33	0.36	-8.65	31.51
		Phase III	33.79*	7.77	0.00	15.07	52.51
	Phase III	Phase I	-22.36*	7.77	0.02	-41.08	-3.64
		Phase II	-33.79*	7.77	0.00	-52.51	-15.09
HAS TB-EPS	Phase I	Phase II	6.95	8.32	0.68	-13.11	27.00
		Phase III	23.40*	7.76	0.01	4.70	42.11
	Phase II	Phase I	-6.95	8.32	0.68	-27.00	13.11
		Phase III	16.46	7.76	0.09	-2.24	35.16
	Phase III	Phase I	-23.40*	7.76	0.01	-42.11	-4.70
		Phase II	-16.46	7.76	0.09	-35.16	2.24
LB-EPS	Phase I	Phase II	118.28*	20.00	0.00	70.08	166.48
		Phase III	99.38*	18.65	0.00	54.43	144.33
	Phase II	Phase I	-118.28*	20.00	0.00	-166.48	-70.08

				Std. Error			
		Phase III	-18.90	18.65	0.57	-63.85	26.05
	Phase III	Phase I	-99.38*	18.65	0.00	-144.33	-54.43
		Phase II	18.90	18.65	0.57	-26.05	63.85
TB-EPS	Phase I	Phase II	-3.87	18.14	0.97	-47.60	39.85
		Phase III	49.33*	16.92	0.01	8.5629	90.11
	Phase II	Phase I	3.87	18.14	0.97	-39.85	47.60
		Phase III	53.21*	16.92	0.01	12.44	93.98
	Phase III	Phase I	-49.33*	16.92	0.01	-90.11	-8.56
		Phase II	-53.21*	16.92	0.01	-93.98	-12.44
Total EPS	Phase I	Phase II	114.41*	31.89	0.00	37.54	191.27
		Phase III	148.71*	29.74	0.00	77.03	220.39
	Phase II	Phase I	-114.41*	31.89	0.00	-191.27	-37.54
		Phase III	34.30	29.74	0.49	-37.37	105.98
	Phase III	Phase I	-148.71*	29.74	0.00	-220.39	-77.03
		Phase II	-34.30	29.74	0.49	-105.98	37.37

*. The mean difference is significant at the 0.05 level.

Std. Error: standard error

Table S4.7 – Spearman correlation coefficients computed between SVI, ESS, EPS composition, and morphological parameters during phase II (n = 17). Significance of p-values are as followed: $p < 0.01$ represented as **, and $p < 0.05$ represented as *.

Spearman's rho		SVI	ESS	PS LB-EPS	PN LB-EPS	HAS LB-EPS	PS TB-EPS	PN TB-EPS	HAS TB-EPS	TOTAL LB-EPS	TOTAL TB-EPS	TOTAL EPS	TL/Vol	TL/MLSS	TA/Vol	Deq (sml)	Deq (int)	Deq (larg)	%Area$_{sml}$	%Area$_{int}$	%Area$_{larg}$
SVI	r	1.00	-0.20	**0.77**	**0.69**	**0.65**	**0.54***	**0.66**	**0.64**	**0.70**	**0.64**	**0.65**	**-0.65**	**-0.57***	**-0.68**	-0.36	**0.58***	0.22	**-0.50***	0.24	0.19
	p		0.439	0.000	0.002	0.005	0.026	0.004	0.006	0.002	0.006	0.005	0.005	0.016	0.003	0.158	0.014	0.395	0.041	0.353	0.468
ESS	r	-0.20	1.00	-0.14	-0.33	-0.19	-0.05	-0.22	-0.16	-0.25	-0.23	-0.15	-0.05	-0.09	0.22	-0.09	0.14	0.17	-0.04	0.12	-0.01
	p	0.439		0.606	0.194	0.450	0.841	0.400	0.547	0.335	0.368	0.563	0.837	0.733	0.403	0.729	0.606	0.525	0.881	0.639	0.978
PS LB-EPS	r	**0.77**	-0.14	1.00	**0.84**	**0.63**	**0.53***	**0.73**	**0.68**	**0.76**	**0.71**	**0.72**	-0.35	-0.31	**-0.49***	-0.27	0.31	0.34	-0.28	-0.01	0.42
	p	0.000	0.606		0.000	0.007	0.029	0.001	0.003	0.000	0.001	0.001	0.174	0.228	0.048	0.300	0.220	0.181	0.282	0.970	0.094
PN LB-EPS	r	**0.69**	-0.33	**0.84**	1.00	**0.90**	**0.68**	**0.78**	**0.81**	**0.95**	**0.78**	**0.83**	**-0.48***	-0.46	**-0.58***	-0.19	0.36	0.14	-0.41	0.10	0.18
	p	0.002	0.194	0.000		0.000	0.003	0.000	0.000	0.000	0.000	0.000	0.050	0.063	0.016	0.462	0.158	0.586	0.101	0.701	0.492
HAS LB-EPS	r	**0.65**	-0.19	**0.63**	**0.90**	1.00	**0.75**	**0.71**	**0.79**	**0.95**	**0.72**	**0.81**	**-0.75**	**-0.74**	**-0.61**	-0.13	**0.59***	0.02	**-0.67**	0.39	-0.07
	p	0.005	0.450	0.007	0.000		0.001	0.001	0.000	0.000	0.001	0.000	0.001	0.001	0.009	0.633	0.012	0.955	0.003	0.125	0.779
PS TB-EPS	r	**0.54***	-0.05	**0.53***	**0.68**	**0.75**	1.00	**0.86**	**0.90**	**0.74**	**0.87**	**0.90**	**-0.52***	**-0.54***	-0.26	-0.25	0.45	0.41	**-0.61**	0.13	0.29
	p	0.026	0.841	0.029	0.003	0.001		0.000	0.000	0.001	0.000	0.000	0.035	0.024	0.309	0.328	0.069	0.105	0.009	0.633	0.260
PN TB-EPS	r	**0.66**	-0.22	**0.73**	**0.78**	**0.71**	**0.86**	1.00	**0.97**	**0.74**	**0.99**	**0.98**	-0.37	-0.33	-0.26	-0.32	0.34	**0.56***	-0.42	-0.13	**0.55***
	p	0.004	0.400	0.001	0.000	0.001	0.000		0.000	0.001	0.000	0.000	0.147	0.191	0.323	0.205	0.178	0.018	0.096	0.626	0.023
HAS TB-EPS	r	**0.64**	-0.16	**0.68**	**0.81**	**0.79**	**0.90**	**0.97**	1.000	**0.79**	**0.98**	**0.99**	-0.44	-0.42	-0.28	-0.28	0.40	**0.49***	**-0.48***	-0.02	0.43
	p	0.006	0.547	0.003	0.000	0.000	0.000	0.000		0.000	0.000	0.000	0.076	0.094	0.282	0.282	0.112	0.047	0.050	0.940	0.086
TOTAL LB-EPS	r	**0.70**	-0.25	**0.76**	**0.95**	**0.95**	**0.74**	**0.74**	**0.79**	1.00	**0.74**	**0.81**	**-0.64**	**-0.63**	**-0.65**	-0.19	**0.50***	0.09	**-0.56***	0.29	0.06
	p	0.002	0.335	0.000	0.000	0.000	0.001	0.001	0.000		0.001	0.000	0.006	0.007	0.005	0.474	0.041	0.743	0.019	0.264	0.815
TOTAL TB-EPS	r	**0.64**	-0.23	**0.71**	**0.78**	**0.72**	**0.87**	**0.99**	**0.98**	**0.74**	1.00	**0.98**	-0.38	-0.35	-0.23	-0.26	0.34	**0.55***	-0.43	-0.11	**0.53***
	p	0.006	0.368	0.001	0.000	0.001	0.000	0.000	0.000	0.001		0.000	0.135	0.174	0.384	0.314	0.181	0.021	0.086	0.680	0.028
TOTAL EPS	r	**0.65**	-0.15	**0.72**	**0.83**	**0.81**	**0.90**	**0.98**	**0.99**	**0.81**	**0.98**	1.00	-0.46	-0.44	-0.31	-0.29	0.40	**0.49***	**-0.49***	-0.03	0.45
	p	0.005	0.563	0.001	0.000	0.000	0.000	0.000	0.000	0.000	0.000		0.066	0.080	0.220	0.260	0.112	0.046	0.048	0.911	0.071
TL/Vol	r	**-0.65**	-0.05	-0.35	**-0.48***	**-0.75**	**-0.52***	-0.37	-0.44	**-0.64**	-0.38	-0.46	1.00	**0.98**	**0.55***	-0.01	**-0.89**	0.16	**0.89**	**-0.77**	0.38

	p	0.005	0.837	0.174	0.050	0.001	0.035	0.147	0.076	0.006	0.135	0.066		0.000	0.021	0.978	0.000	0.529	0.000	0.000	0.138
TL/MLSS	r	**-0.57***	-0.09	-0.31	-0.46	**-0.74****	**-0.54***	-0.33	-0.42	**-0.63****	-0.35	-0.44	**0.98****	1.00	**0.55***	-0.03	**-0.89****	0.18	**0.93****	**-0.80****	0.41
	p	0.016	0.733	0.228	0.063	0.001	0.024	0.191	0.094	0.007	0.174	0.080	0.000		0.022	0.911	0.000	0.498	0.000	0.000	0.101
TA/Vol	r	**-0.68****	0.22	**-0.49***	**-0.58***	**-0.61****	-0.26	-0.26	-0.28	**-0.65****	-0.23	-0.31	**0.55***	**0.55***	1.00	0.12	-0.42	0.25	0.39	-0.40	0.26
	p	0.003	0.403	0.048	0.016	0.009	0.309	0.323	0.282	0.005	0.384	0.220	0.021	0.022		0.646	0.096	0.343	0.122	0.107	0.323
Deq (sml)	r	-0.36	-0.09	-0.27	-0.19	-0.13	-0.25	-0.32	-0.28	-0.19	-0.26	-0.29	-0.01	-0.03	0.12	1.00	-0.10	**-0.55***	0.04	0.37	-0.47
	p	0.158	0.729	0.300	0.462	0.633	0.328	0.205	0.282	0.474	0.314	0.260	0.978	0.911	0.646		0.701	0.022	0.874	0.149	0.060
Deq (int)	r	**0.58***	0.14	0.31	0.36	**0.59***	0.45	0.34	0.40	**0.50***	0.34	0.40	**-0.89****	**-0.89****	-0.42	-0.10	1.00	-0.14	**-0.92****	**0.79****	-0.35
	p	0.014	0.606	0.220	0.158	0.012	0.069	0.178	0.112	0.041	0.181	0.112	0.000	0.000	0.096	0.701		0.606	0.000	0.000	0.168
Deq (larg)	r	0.22	0.17	0.34	0.14	0.02	0.41	**0.56***	**0.49***	0.09	**0.55***	**0.49***	0.16	0.18	0.25	**-0.55***	-0.14	1.00	0.04	**-0.59***	**0.88****
	p	0.395	0.525	0.181	0.586	0.955	0.105	0.018	0.047	0.743	0.021	0.046	0.529	0.498	0.343	0.022	0.606		0.874	0.011	0.000
%Area (sml)	r	**-0.50***	-0.04	-0.28	-0.41	**-0.67****	**-0.61****	-0.42	**-0.48***	**-0.56***	-0.43	**-0.49***	**0.89****	**0.93****	0.39	0.04	**-0.92****	0.04	1.00	**-0.75****	0.33
	p	0.041	0.881	0.282	0.101	0.003	0.009	0.096	0.050	0.019	0.086	0.048	0.000	0.000	0.122	0.874	0.000	0.874		0.001	0.195
%Area (int)	r	0.24	0.12	-0.01	0.10	0.39	0.13	-0.13	-0.02	0.29	-0.11	-0.03	**-0.77****	**-0.80****	-0.40	0.37	**0.79****	**-0.59***	**-0.75****	1.00	**-0.78****
	p	0.353	0.639	0.970	0.701	0.125	0.633	0.626	0.940	0.264	0.680	0.911	0.000	0.000	0.107	0.149	0.000	0.011	0.001		0.000
%Area (larg)	r	0.19	-0.01	0.42	0.18	-0.07	0.29	**0.55***	0.43	0.06	**0.53***	0.45	0.38	0.41	0.26	-0.47	-0.35	**0.88****	0.33	**-0.78****	1.00
	p	0.468	0.978	0.094	0.492	0.779	0.260	0.023	0.086	0.815	0.028	0.071	0.138	0.101	0.323	0.060	0.168	0.000	0.195	0.000	

r: Spearman correlation coefficient values

p: p-value

Table S4.8 – Spearman correlation coefficients computed between SVI, ESS, EPS composition, and morphological parameters during phase III (n = 23). Significance of p-values are as followed: p < 0.01 represented as **, and p < 0.05 represented as *.

Spearman's rho		SVI	ESS	PS LB-EPS	PN LB-EPS	HAS LB-EPS	PS TB-EPS	PN TB-EPS	HAS TB-EPS	TOTAL LB-EPS	TOTAL TB-EPS	TOTAL EPS	TL/Vol	TL/MLSS	TA/Vol	Deq (sml)	Deq (int)	Deq (larg)	%Area (sml)	%Area (int)	%Area (larg)
SVI	r	1.00	0.29	0.22	0.27	0.35	0.64**	-0.01	0.14	0.42*	0.13	0.22	0.15	0.28	0.03	0.06	-0.38	0.17	0.40	-0.27	0.25
	p		0.183	0.313	0.215	0.102	0.001	0.970	0.539	0.044	0.554	0.322	0.491	0.200	0.881	0.771	0.077	0.441	0.056	0.216	0.243
ESS	r	0.29	1.00	0.35	-0.08	0.11	0.04	-0.45*	-0.18	0.09	-0.33	-0.14	0.61**	0.58**	0.37	0.22	-0.81**	0.35	0.74**	-0.55**	0.46*
	p	0.183		0.100	0.733	0.610	0.870	0.031	0.404	0.677	0.129	0.514	0.002	0.004	0.080	0.317	0.000	0.106	0.000	0.007	0.029
PS LB-EPS	r	0.22	0.35	1.00	0.43*	0.28	-0.08	0.12	0.29	0.37	0.13	0.37	0.53**	0.54**	0.01	-0.19	-0.34	0.39	0.62**	-0.42*	0.28
	p	0.313	0.100		0.040	0.191	0.723	0.593	0.187	0.081	0.570	0.084	0.010	0.008	0.968	0.368	0.114	0.069	0.001	0.046	0.191
PN LB-EPS	r	0.27	-0.08	0.43*	1.00	0.71**	-0.07	0.21	-0.01	0.84**	0.17	0.46*	-0.18	-0.15	-0.36	-0.32	0.15	-0.18	0.07	0.09	-0.11
	p	0.215	0.733	0.040		0.000	0.737	0.340	0.979	0.000	0.446	0.027	0.404	0.508	0.093	0.142	0.483	0.401	0.737	0.673	0.634
HAS LB-EPS	r	0.35	0.11	0.28	0.71**	1.00	0.01	-0.04	-0.04	0.97**	-0.01	0.44*	-0.16	-0.13	-0.29	-0.38	0.08	-0.19	0.14	0.17	-0.15
	p	0.102	0.610	0.191	0.000		0.968	0.868	0.844	0.000	0.970	0.034	0.471	0.541	0.188	0.076	0.720	0.381	0.538	0.446	0.508
PS TB-EPS	r	0.64**	0.04	-0.08	-0.07	0.01	1.00	0.24	0.41	0.05	0.47*	0.26	0.05	0.12	0.17	0.16	-0.03	0.32	-0.06	-0.29	0.36
	p	0.001	0.870	0.723	0.737	0.968		0.264	0.051	0.837	0.022	0.235	0.837	0.587	0.452	0.457	0.907	0.131	0.788	0.188	0.093
PN TB-EPS	r	-0.01	-0.45*	0.12	0.21	-0.04	0.24	1.00	0.66**	0.06	0.94**	0.78**	-0.21	-0.17	-0.13	0.08	0.39	0.05	-0.39	-0.06	0.13
	p	0.970	0.031	0.593	0.340	0.868	0.264		0.001	0.774	0.000	0.000	0.326	0.449	0.553	0.723	0.064	0.826	0.063	0.781	0.544
HAS TB-EPS	r	0.14	-0.18	0.29	-0.01	-0.04	0.41	0.66**	1.00	0.01	0.76**	0.60**	-0.01	0.04	0.05	-0.01	0.18	0.15	-0.05	-0.09	0.12
	p	0.539	0.404	0.187	0.979	0.844	0.051	0.001		0.971	0.000	0.002	0.971	0.854	0.833	0.961	0.401	0.491	0.830	0.690	0.590
TOTAL LB-EPS	r	0.42*	0.09	0.37	0.84**	0.97**	0.05	0.06	0.01	1.00	0.08	0.51*	-0.15	-0.10	-0.29	-0.33	0.08	-0.19	0.16	0.12	-0.11
	p	0.044	0.677	0.081	0.000	0.000	0.837	0.774	0.971		0.723	0.013	0.508	0.660	0.173	0.125	0.733	0.378	0.463	0.593	0.631
TOTAL TB-EPS	r	0.13	-0.33	0.13	0.17	-0.01	0.47*	0.94**	0.76**	0.08	1.00	0.82**	-0.12	-0.08	0.03	0.08	0.29	0.16	-0.33	-0.15	0.23
	p	0.554	0.129	0.570	0.446	0.970	0.022	0.000	0.000	0.723		0.000	0.585	0.732	0.909	0.725	0.178	0.454	0.125	0.490	0.298
TOTAL EPS	r	0.22	-0.14	0.37	0.46*	0.44*	0.26	0.78**	0.60**	0.51*	0.82**	1.00	-0.06	-0.01	-0.07	-0.11	0.14	0.11	-0.08	-0.18	0.22

	p	0.322	0.514	0.084	0.027	0.034	0.235	0.000	0.002	0.013	0.000		0.785	0.950	0.754	0.606	0.511	0.634	0.710	0.419	0.321
TL/Vol	r	0.15	**0.61****	**0.53****	-0.18	-0.16	0.05	-0.21	-0.01	-0.15	-0.12	-0.06	1.00	**0.98****	**0.59****	0.19	**-0.67****	**0.62****	**0.74****	**-0.76****	**0.63****
	p	0.491	0.002	0.010	0.404	0.471	0.837	0.326	0.971	0.508	0.585	0.785		0.000	0.003	0.386	0.000	0.002	0.000	0.000	0.001
TL/MLSS	r	0.28	**0.58****	**0.54****	-0.15	-0.13	0.12	-0.17	0.04	-0.10	-0.08	-0.01	**0.98****	1.00	**0.60****	0.25	**-0.67****	**0.55****	**0.75****	**-0.74****	**0.61****
	p	0.200	0.004	0.008	0.508	0.541	0.587	0.449	0.854	0.660	0.732	0.950	0.000		0.002	0.260	0.000	0.007	0.000	0.000	0.002
TA/Vol	r	0.03	0.37	0.01	-0.36	-0.29	0.17	-0.13	0.05	-0.29	0.03	-0.07	**0.59****	**0.60****	1.00	**0.54****	**-0.49***	0.20	0.26	-0.29	0.23
	p	0.881	0.080	0.968	0.093	0.188	0.452	0.553	0.833	0.173	0.909	0.754	0.003	0.002		0.008	0.017	0.361	0.231	0.171	0.301
Deq (sml)	r	0.06	0.22	-0.19	-0.32	-0.38	0.16	0.08	-0.01	-0.33	0.08	-0.11	0.19	0.25	**0.54****	1.00	-0.35	-0.05	-0.04	-0.08	0.14
	p	0.771	0.317	0.368	0.142	0.076	0.457	0.723	0.961	0.125	0.725	0.606	0.386	0.260	0.008		0.106	0.826	0.840	0.707	0.529
Deq (int)	r	-0.38	**-0.81****	-0.34	0.15	0.08	-0.03	0.39	0.18	0.08	0.29	0.14	**-0.67****	**-0.67****	**-0.49***	-0.35	1.00	-0.36	**-0.81****	**0.58****	**-0.42***
	p	0.077	0.000	0.114	0.483	0.720	0.907	0.064	0.401	0.733	0.178	0.511	0.000	0.000	0.017	0.106		0.091	0.000	0.004	0.045
Deq (larg)	r	0.17	0.35	0.39	-0.18	-0.19	0.32	0.05	0.15	-0.19	0.16	0.11	**0.62****	**0.55****	0.20	-0.05	-0.36	1.00	0.34	**-0.83****	**0.86****
	p	0.441	0.106	0.069	0.401	0.381	0.131	0.826	0.491	0.378	0.454	0.634	0.002	0.007	0.361	0.826	0.091		0.111	0.000	0.000
%Area (sml)	r	0.40	**0.74****	**0.62****	0.07	0.14	-0.06	-0.39	-0.05	0.16	-0.33	-0.08	**0.74****	**0.75****	0.26	-0.04	**-0.81****	0.34	1.00	**-0.59****	0.38
	p	0.056	0.000	0.001	0.737	0.538	0.788	0.063	0.830	0.463	0.125	0.710	0.000	0.000	0.231	0.840	0.000	0.111		0.003	0.073
%Area (int)	r	-0.27	**-0.55****	**-0.42***	0.09	0.17	-0.29	-0.06	-0.09	0.12	-0.15	-0.18	**-0.76****	**-0.74****	-0.29	-0.08	**0.58****	**-0.83****	**-0.59****	1.00	**-0.95****
	p	0.216	0.007	0.046	0.673	0.446	0.188	0.781	0.690	0.593	0.490	0.419	0.000	0.000	0.171	0.707	0.004	0.000	0.003		0.000
%Area (larg)	r	0.25	**0.46***	0.28	-0.11	-0.15	0.36	0.13	0.12	-0.11	0.23	0.22	**0.63****	**0.61****	0.23	0.14	**-0.42***	**0.86****	0.38	**-0.95****	1.00
	p	0.243	0.029	0.191	0.634	0.508	0.093	0.544	0.590	0.631	0.298	0.321	0.001	0.002	0.301	0.529	0.045	0.000	0.073	0.000	

r: Spearman correlation coefficient values

p: p-value

CHAPTER 5 - Supplementary Information (SI)

Effects of desloratadine in activated sludge: behavior of EPS and sludge properties

Table S5.1 – Average COD, DESL, NH_4^+-N, NO_2^--N, and NO_3^--N concentrations in mg L^{-1} followed by standard deviation (i - influent, e - effluent), and average removal percentages (r) of COD, NH_4^+-N and DESL along phases I-IV.

	COD_i	COD_e	NH_4^+-N_i	NH_4^+-N_e	NO_2^--N_e	NO_3^--N_e
Phase I	557.4 ± 22.49	22.20 ± 5.25	45.65 ± 2.22	0.17 ± 0.50	0.00 ± 0.00	10.28 ± 3.61
Phase II	528.87 ± 16.24	65.27 ± 10.53	48.47 ± 4.94	2.92 ± 2.29	0.43 ± 0.64	18.73 ± 1.92
Phase III	525.53 ± 32.61	66.48 ± 44.41	46.55 ± 2.99	1.39 ± 1.19	1.46 ± 1.28	16.52 ± 3.89
Phase IV	605.33 ± 57.23	130.41 ± 83.16	49.40 ± 2.31	13.88 ± 10.35	1.74 ± 1.02	7.01 ± 2.38

	$DESL_i$	$DESL_e$	$DESL_r$	COD_r	NH_4^+-N_r
Phase I	0.00 ± 0.00	0.00 ± 0.00	0.00 ± 0.00	95.93 ± 1.03	99.63 ± 0.99
Phase II	0.99 ± 0.10	0.25 ± 0.14	74.60 ± 10.44	87.70 ± 1.96	94.1 ± 4.44
Phase III	4.95 ± 0.21	1.35 ± 0.35	72.60 ± 7.26	87.40 ± 8.31	97.00 ± 2.25
Phase IV	11.57 ± 0.70	4.21 ± 1.01	63.47 ± 9.33	77.73 ± 14.95	71.30 ± 21.89

Table S5.2 – Statistical analysis of variance (ANOVA) for DESL, COD, and NH_4^+-N removal percentages.

ANOVA						
		Sum of Squares	df	Mean Square	F	Sig.
$DESL_r$	Between Groups	56532.40	3	18844.13	302.98	0.000
	Within Groups	3482.93	56	62.20		
	Total	60015.33	59			
COD_r	Between Groups	2489.73	3	829.91	11.15	0.000
	Within Groups	4167.20	56	74.41		
	Total	6656.93	59			
NH_4^+-N_r	Between Groups	5522.40	3	1840.80	13.97	0.000
	Within Groups	7380.53	56	131.80		
	Total	12902.93	59			

Table S5.3 – Tukey's HSD test (difference expressed honestly) to determine if there is a statistically significant difference in the COD and NH_4^+-N removal when DESL was present in the biological systems and whether the assessed concentrations of the DESL had an influence on its removal percentages.

			Mean Difference (I-J)	Std. Error	Sig.	95% Confidence Interval	
Multiple Comparisons							
Dependent Variable						Lower Bound	Upper Bound
$DESL_r$	Phase I	Phase II	-74.60*	2.88	0.00	-82.23	-66.97
		Phase III	-72.60*	2.88	0.00	-80.23	-64.97
		Phase IV	-63.47*	2.88	0.00	-71.09	-55.84
	Phase II	Phase I	74.60*	2.88	0.00	66.97	82.23
		Phase III	2.00	2.88	0.90	-5.63	9.63
		Phase IV	11.13*	2.88	0.00	3.51	18.76
	Phase III	Phase I	72.60*	2.88	0.00	64.97	80.23
		Phase II	-2.00	2.88	0.90	-9.63	5.63
		Phase IV	9.13*	2.88	0.01	1.51	16.76
	Phase IV	Phase I	63.47*	2.88	0.00	55.84	71.09
		Phase II	-11.13*	2.88	0.00	-18.76	-3.51
		Phase III	-9.13*	2.88	0.01	-16.76	-1.51
COD_r	Phase I	Phase II	8.53*	3.15	0.04	0.19	16.87
		Phase III	8.47*	3.15	0.05	0.13	16.81
		Phase IV	18.20*	3.15	0.00	9.86	26.54
	Phase II	Phase I	-8.53*	3.15	0.04	-16.87	-0.19
		Phase III	-0.067	3.15	1.00	-8.41	8.27
		Phase IV	9.67*	3.15	0.02	1.33	18.01
	Phase III	Phase I	-8.47*	3.15	0.05	-16.81	-0.13
		Phase II	0.07	3.15	1.00	-8.27	8.41
		Phase IV	9.73*	3.15	0.02	1.39	18.07
	Phase IV	Phase I	-18.20*	3.15	0.00	-26.54	-9.86
		Phase II	-9.67*	3.15	0.02	-18.01	-1.33
		Phase III	-9.73*	3.15	0.02	-18.07	-1.39
NH_4^+-N_r	Phase I	Phase II	5.54	4.11	0.54	-5.34	16.42
		Phase III	2.64	4.11	0.92	-8.24	13.52
		Phase IV	28.33*	4.11	0.00	17.45	39.20
	Phase II	Phase I	-5.54	4.11	0.54	-16.42	5.34
		Phase III	-2.90	4.11	0.89	-13.77	7.98
		Phase IV	22.79*	4.11	0.00	11.91	33.67
	Phase III	Phase I	-2.64	4.11	0.92	-13.52	8.24
		Phase II	2.90	4.11	0.89	-7.98	13.77
		Phase IV	25.68*	4.11	0.00	14.81	36.56
	Phase IV	Phase I	-28.33*	4.11	0.00	-39.20	-17.45
		Phase II	-22.79*	4.11	0.00	-33.67	-11.91
		Phase III	-25.68*	4.11	0.00	-36.56	-14.81

*. The mean difference is significant at the 0.05 level.

Table S5.4 – Average values (mg EPS g_{MLVSS}^{-1}) followed by standard deviation (Std. Deviation) of EPS and components during phases I-IV.

	PS LB-EPS		PN LB-EPS		HAS LB-EPS	
	Mean	Std. Deviation	Mean	Std. Deviation	Mean	Std. Deviation
Phase I	7.26	0.21	17.91	2.27	24.27	0.97
Phase II	18.63	0.37	37.89	1.58	43.52	3.10
Phase III	10.84	0.18	40.22	1.47	45.10	0.84
Phase IV	23.96	0.59	23.94	1.30	27.01	1.68

	PS TB-EPS		PN TB-EPS		HAS TB-EPS	
	Mean	Std. Deviation	Mean	Std. Deviation	Mean	Std. Deviation
Phase I	6.97	0.27	24.72	2.04	32.32	1.62
Phase II	16.96	0.30	39.68	1.51	47.66	1.84
Phase III	14.79	0.29	55.92	2.79	54.88	0.98
Phase IV	32.69	0.58	52.45	1.29	64.38	1.35

	LB-EPS		TB-EPS		EPS	
	Mean	Std. Deviation	Mean	Std. Deviation	Mean	Std. Deviation
Phase I	49.45	2.48	64.01	2.62	113.46	3.61
Phase II	100.04	3.50	104.31	2.40	204.35	4.25
Phase III	96.16	1.71	125.59	2.98	221.76	3.43
Phase IV	74.91	2.20	149.53	1.96	224.44	2.95

Table S5.5 – Statistical analysis of variance (ANOVA) for EPS and components during phases I-IV.

ANOVA		Sum of Squares	df	Mean Square	F	Sig.
PS LB-EPS	Between Groups	2557.67	3	852.56	10.29	0.000
	Within Groups	4638.29	56	82.83		
	Total	7195.96	59			
PN LB-EPS	Between Groups	5244.44	3	1748.15	10.73	0.000
	Within Groups	9127.34	56	162.99		
	Total	14371.77	59			
HAS LB-EPS	Between Groups	5301.42	3	1767.14	4.61	0.006
	Within Groups	21478.46	56	383.54		
	Total	26779.88	59			
PS TB-EPS	Between Groups	5233.00	3	1744.33	38.19	0.000
	Within Groups	2557.49	56	45.67		
	Total	7790.49	59			
PN TB-EPS	Between Groups	9018.50	3	3006.17	10.00	0.000
	Within Groups	16831.40	56	300.56		
	Total	25849.90	59			
HAS TB-EPS	Between Groups	8228.03	3	2742.68	3.40	0.024
	Within Groups	45191.67	56	806.99		
	Total	53419.71	59			
LB-EPS	Between Groups	24334.96	3	8111.65	6.00	0.001
	Within Groups	75723.46	56	1352.20		
	Total	100058.43	59			
TB-EPS	Between Groups	59248.64	3	19749.55	8.83	0.000
	Within Groups	125181.97	56	2235.39		
	Total	184430.61	59			
EPS	Between Groups	123829.25	3	41276.42	16.13	0.000
	Within Groups	143333.53	56	2559.53		
	Total	267162.77	59			

Table S5.6 – Tukey's HSD test to verify if DESL presence promoted a statistically significant difference in terms of EPS production along phases I-IV.

Multiple Comparisons							
Tukey HSD							
Dependent Variable			Mean Difference (I-J)	Std. Error	Sig.	95% Confidence Interval	
						Lower Bound	Upper Bound
PS LB-EPS	Phase I	Phase II	-11.37*	3.32	0.01	-20.17	-2.57
		Phase III	-3.59	3.32	0.70	-12.39	5.21
		Phase IV	-16.70*	3.32	0.00	-25.50	-7.90
	Phase II	Phase I	11.37*	3.32	0.01	2.57	20.17
		Phase III	7.78	3.32	0.10	-1.02	16.58
		Phase IV	-5.33	3.32	0.38	-14.13	3.46
	Phase III	Phase I	3.59	3.32	0.70	-5.21	12.39
		Phase II	-7.78	3.32	0.10	-16.58	1.02
		Phase IV	-13.12*	3.32	0.00	-21.91	-4.32
	Phase IV	Phase I	16.70*	3.32	0.00	7.90	25.50
		Phase II	5.33	3.32	0.38	-3.46	14.13
		Phase III	13.12*	3.32	0.00	4.32	21.91
PN LB-EPS	Phase I	Phase II	-19.98*	4.66	0.00	-32.33	-7.64
		Phase III	-22.31*	4.66	0.00	-34.65	-9.97
		Phase IV	-6.03	4.66	0.57	-18.37	6.32
	Phase II	Phase I	19.98*	4.66	0.00	7.64	32.33
		Phase III	-2.33	4.66	0.96	-14.67	10.02
		Phase IV	13.95*	4.66	0.02	1.61	26.30
	Phase III	Phase I	22.31*	4.66	0.00	9.97	34.65
		Phase II	2.33	4.66	0.96	-10.02	14.67
		Phase IV	16.28*	4.66	0.01	3.94	28.63
	Phase IV	Phase I	6.03	4.66	0.57	-6.32	18.37
		Phase II	-13.95*	4.66	0.02	-26.30	-1.61
		Phase III	-16.28*	4.66	0.01	-28.63	-3.94
HAS LB-EPS	Phase I	Phase II	-19.25*	7.15	0.04	-38.18	-0.31
		Phase III	-20.82*	7.15	0.03	-39.76	-1.89
		Phase IV	-2.74	7.15	0.98	-21.67	16.20
	Phase II	Phase I	19.25*	7.15	0.04	0.31	38.18
		Phase III	-1.57	7.15	1.00	-20.51	17.36
		Phase IV	16.51	7.15	0.11	-2.42	35.45
	Phase III	Phase I	20.82*	7.15	0.03	1.89	39.76
		Phase II	1.57	7.15	1.00	-17.36	20.51
		Phase IV	18.09	7.15	0.07	-0.85	37.02
	Phase IV	Phase I	2.74	7.15	0.98	-16.20	21.67
		Phase II	-16.51	7.15	0.11	-35.45	2.42
		Phase III	-18.09	7.15	0.07	-37.02	0.85
PS TB-EPS	Phase I	Phase II	-9.99*	2.47	0.00	-16.53	-3.46
		Phase III	-7.83*	2.47	0.01	-14.36	-1.29

			Mean Diff	Std. Error	Sig.	Lower	Upper
		Phase IV	-25.73*	2.47	0.00	-32.26	-19.19
	Phase II	Phase I	9.99*	2.47	0.00	3.46	16.53
		Phase III	2.17	2.47	0.82	-4.36	8.70
		Phase IV	-15.73*	2.47	0.00	-22.26	-9.20
	Phase III	Phase I	7.83*	2.47	0.01	1.29	14.36
		Phase II	-2.17	2.47	0.82	-8.70	4.36
		Phase IV	-17.90*	2.47	0.00	-24.43	-11.37
	Phase IV	Phase I	25.73*	2.47	0.00	19.19	32.26
		Phase II	15.73*	2.47	0.00	9.20	22.26
		Phase III	17.90*	2.47	0.00	11.37	24.43
PN TB-EPS	Phase I	Phase II	-14.96	6.33	0.10	-31.72	1.80
		Phase III	-31.20*	6.33	0.00	-47.96	-14.44
		Phase IV	-27.73*	6.33	0.00	-44.49	-10.97
	Phase II	Phase I	14.96	6.33	0.10	-1.80	31.72
		Phase III	-16.24	6.33	0.06	-33.00	0.53
		Phase IV	-12.77	6.33	0.19	-29.53	3.99
	Phase III	Phase I	31.20*	6.33	0.00	14.44	47.96
		Phase II	16.24	6.33	0.06	-0.53	33.00
		Phase IV	3.47	6.33	0.95	-13.30	20.23
	Phase IV	Phase I	27.73*	6.33	0.00	10.97	44.49
		Phase II	12.77	6.33	0.19	-3.99	29.53
		Phase III	-3.47	6.33	0.95	-20.23	13.30
HAS TB-EPS	Phase I	Phase II	-15.34	10.37	0.46	-42.81	12.13
		Phase III	-22.56	10.37	0.14	-50.03	4.90
		Phase IV	-32.06*	10.37	0.02	-59.53	-4.59
	Phase II	Phase I	15.34	10.37	0.46	-12.13	42.81
		Phase III	-7.22	10.37	0.90	-34.69	20.24
		Phase IV	-16.72	10.37	0.38	-44.19	10.75
	Phase III	Phase I	22.56	10.37	0.14	-4.90	50.03
		Phase II	7.22	10.37	0.90	-20.24	34.69
		Phase IV	-9.50	10.37	0.80	-36.96	17.97
	Phase IV	Phase I	32.06*	10.37	0.02	4.59	59.53
		Phase II	16.72	10.37	0.38	-10.75	44.19
		Phase III	9.50	10.37	0.80	-17.97	36.96
LB-EPS	Phase I	Phase II	-50.60*	13.43	0.00	-86.15	-15.04
		Phase III	-46.72*	13.43	0.01	-82.27	-11.16
		Phase IV	-25.46	13.43	0.24	-61.02	10.09
	Phase II	Phase I	50.60*	13.43	0.00	15.04	86.15
		Phase III	3.88	13.43	0.99	-31.67	39.43
		Phase IV	25.13	13.43	0.25	-10.42	60.69
	Phase III	Phase I	46.72*	13.43	0.01	11.16	82.27
		Phase II	-3.88	13.43	0.99	-39.43	31.67
		Phase IV	21.25	13.43	0.40	-14.30	56.81
	Phase IV	Phase I	25.46	13.43	0.24	-10.09	61.02
		Phase II	-25.13	13.43	0.25	-60.69	10.42

		Phase III	-21.25	13.43	0.40	-56.81	14.30
TB-EPS	Phase I	Phase II	-40.29	17.26	0.10	-86.01	5.42
		Phase III	-61.58*	17.26	0.00	-107.30	-15.87
		Phase IV	-85.51*	17.26	0.00	-131.23	-39.80
	Phase II	Phase I	40.29	17.26	0.10	-5.42	86.01
		Phase III	-21.29	17.26	0.61	-67.00	24.42
		Phase IV	-45.22	17.26	0.05	-90.94	0.49
	Phase III	Phase I	61.58*	17.26	0.00	15.87	107.30
		Phase II	21.29	17.26	0.61	-24.42	67.00
		Phase IV	-23.93	17.26	0.51	-69.65	21.78
	Phase IV	Phase I	85.51*	17.26	0.00	39.80	131.23
		Phase II	45.22	17.26	0.05	-0.49	90.94
		Phase III	23.93	17.26	0.51	-21.78	69.65
Total EPS	Phase I	Phase II	-90.89*	18.47	0.00	-139.81	-41.98
		Phase III	-108.30*	18.47	0.00	-157.22	-59.39
		Phase IV	-110.98*	18.47	0.00	-159.90	-62.06
	Phase II	Phase I	90.89*	18.47	0.00	41.98	139.81
		Phase III	-17.41	18.47	0.78	-66.32	31.51
		Phase IV	-20.09	18.47	0.70	-69.00	28.83
	Phase III	Phase I	108.30*	18.47	0.00	59.39	157.22
		Phase II	17.41	18.47	0.78	-31.51	66.32
		Phase IV	-2.68	18.47	1.00	-51.60	46.24
	Phase IV	Phase I	110.98*	18.47	0.00	62.06	159.90
		Phase II	20.09	18.47	0.70	-28.83	69.00
		Phase III	2.68	18.47	1.00	-46.24	51.60

*. The mean difference is significant at the 0.05 level.

Table S5.7 – Spearman correlation coefficients between SVI and EPS composition, from start to day 49 of phase II (n = 7). Significance (Sig.) of p-values are as followed: $p < 0.01$ represented as **, and $p < 0.05$ represented as *.

		PS LB-EPS	PN LB-EPS	HAS LB-EPS	PS TB-EPS	PN TB-EPS	HAS TB-EPS	LB-EPS	TB-EPS	EPS	SVI
PS LB-EPS	Correlation Coefficient	1.00	0.64	0.64	-0.04	-0.43	-0.43	0.86*	-0.43	0.07	-0.04
	Sig. (2-tailed)		0.12	0.12	0.94	0.34	0.34	0.01	0.34	0.88	0.94
PN LB-EPS	Correlation Coefficient	0.64	1.00	1.00**	0.32	-0.07	-0.07	0.93**	-0.07	0.71	0.39
	Sig. (2-tailed)	0.12			0.48	0.88	0.88	0.00	0.88	0.07	0.38
HAS LB-EPS	Correlation Coefficient	0.64	1.00**	1.00	0.32	-0.07	-0.07	0.93**	-0.07	0.71	0.39
	Sig. (2-tailed)	0.12			0.48	0.88	0.88	0.00	0.88	0.07	0.38
PS TB-EPS	Correlation Coefficient	-0.04	0.32	0.32	1.00	0.71	0.71	0.21	0.71	0.68	0.04
	Sig. (2-tailed)	0.94	0.48	0.48		0.07	0.07	0.64	0.07	0.09	0.94
PN TB-EPS	Correlation Coefficient	-0.43	-0.07	-0.07	0.71	1.00	1.00**	-0.14	1.00**	0.54	-0.32
	Sig. (2-tailed)	0.34	0.88	0.88	0.07			0.76		0.22	0.48
HAS TB-EPS	Correlation Coefficient	-0.43	-0.07	-0.07	0.71	1.00**	1.00	-0.14	1.00**	0.54	-0.32
	Sig. (2-tailed)	0.34	0.88	0.88	0.07			0.76		0.22	0.48
LB-EPS	Correlation Coefficient	0.86*	0.93**	0.93**	0.21	-0.14	-0.14	1.00	-0.14	0.54	0.18
	Sig. (2-tailed)	0.01	0.00	0.00	0.64	0.76	0.76		0.76	0.22	0.70
TB-EPS	Correlation Coefficient	-0.43	-0.07	-0.07	0.71	1.00**	1.00**	-0.14	1.00	0.54	-0.32
	Sig. (2-tailed)	0.34	0.88	0.88	0.07			0.76		0.22	0.48
EPS	Correlation Coefficient	0.07	0.71	0.71	0.68	0.54	0.54	0.54	0.54	1.00	0.21
	Sig. (2-tailed)	0.88	0.07	0.07	0.09	0.22	0.22	0.22	0.22		0.64
SVI	Correlation Coefficient	-0.04	0.45	0.45	0.04	-0.32	-0.32	0.30	-0.32	0.21	1.00
	Sig. (2-tailed)	0.94	0.35	0.35	0.94	0.48	0.48	0.70	0.48	0.64	

*. Correlation is significant at the 0.05 level (2-tailed).

**. Correlation is significant at the 0.01 level (2-tailed).

CHAPTER 6 – Supplementary Information (SI)

Assessing extracellular polymeric substances in activated sludge under atrazine exposure

Table S6.1 – Average of performance parameters (ATZ, COD, NH_4^+-N, NO_2^--N, and NO_3^--N) concentrations in mg L^{-1} followed by standard deviation (i - influent, e - effluent), and average removal percentages (r) of ATZ, COD and NH_4^+-N along phases I-IV.

					Descriptives			
		Mean	Std. Deviation	Std. Error	95% Confidence Interval for Mean Lower Bound	Upper Bound	Minimum	Maximum
ATZ_i	Phase I	0.00	0.00	0.00	0.00	0.00	0.00	0.00
(mg L^{-1})	Phase II	2.05	0.06	0.02	2.01	2.08	2.00	2.20
	Phase III	5.87	1.56	0.40	5.01	6.74	2.20	8.40
	Phase IV	12.53	2.73	0.70	11.02	14.04	8.50	16.50
ATZ_e	Phase I	0.00	0.00	0.00	0.00	0.00	0.00	0.00
(mg L^{-1})	Phase II	1.22	0.21	0.05	1.10	1.34	1.00	1.90
	Phase III	3.06	0.77	0.20	2.63	3.49	1.60	4.20
	Phase IV	6.26	1.80	0.47	5.26	7.26	3.40	9.60
COD_i	Phase I	547.80	39.28	10.14	526.05	569.55	445.00	585.00
(mg L^{-1})	Phase II	531.67	9.78	2.53	526.25	537.08	510.00	545.00
	Phase III	566.47	26.65	6.88	551.71	581.22	501.00	595.00
	Phase IV	664.93	50.44	13.02	637.00	692.87	549.00	762.00
COD_e	Phase I	27.67	10.77	2.78	21.71	33.64	15.50	55.20
(mg L^{-1})	Phase II	59.81	13.21	3.41	52.49	67.12	31.10	85.00
	Phase III	116.01	69.06	17.83	77.77	154.26	30.50	232.00
	Phase IV	155.13	81.81	21.12	109.83	200.44	45.00	290.50
NH_4^+-N_i	Phase I	45.45	2.76	0.71	43.92	46.97	38.30	50.40
(mg L^{-1})	Phase II	48.37	2.03	0.53	47.24	49.49	45.00	51.10
	Phase III	46.73	2.83	0.73	45.16	48.30	41.70	50.23
	Phase IV	49.78	1.60	0.41	48.90	50.67	46.60	52.20
NH_4^+-N_e	Phase I	0.04	0.03	0.01	0.02	0.06	0.00	0.10
(mg L^{-1})	Phase II	2.71	2.23	0.57	1.47	3.94	0.15	6.15
	Phase III	17.95	5.16	1.33	15.09	20.80	10.60	27.40
	Phase IV	18.10	7.57	1.96	13.90	22.29	6.96	32.50
NO_2^--N_e	Phase I	0.00	0.00	0.00	0.00	0.00	0.00	0.00
(mg L^{-1})	Phase II	0.21	0.18	0.05	0.11	0.31	0.00	0.71
	Phase III	0.36	0.24	0.06	0.23	0.50	0.20	1.16
	Phase IV	2.07	1.38	0.36	1.30	2.83	0.08	4.27
NO_3^--N_e	Phase I	10.65	1.06	0.27	10.07	11.24	8.04	12.30
(mg L^{-1})	Phase II	20.41	2.39	0.62	19.08	21.73	14.50	23.70

	Phase III	13.13	3.67	0.95	11.10	15.17	7.82	22.20
	Phase IV	4.82	1.80	0.46	3.83	5.82	2.12	8.81
ATZ_r	Phase I	0.00	0.00	0.00	0.00	0.00	0.00	0.00
	Phase II	40.60	10.93	2.82	34.55	46.65	3.00	49.00
	Phase III	49.21	6.50	1.74	45.46	52.97	33.00	58.00
	Phase IV	50.53	6.16	1.59	47.12	53.95	39.00	68.00
COD_r	Phase I	94.80	2.48	0.64	93.42	96.18	88.00	97.00
	Phase II	88.53	2.50	0.65	87.15	89.92	84.00	94.00
	Phase III	79.53	11.87	3.06	72.96	86.11	60.00	94.00
	Phase IV	76.53	12.76	3.29	69.47	83.60	55.00	92.00
$NH_4^+\text{-}N_r$	Phase I	100.00	0.00	0.00	100.00	100.00	100.00	100.00
	Phase II	94.67	4.56	1.18	92.14	97.19	88.00	100.00
	Phase III	61.53	11.29	2.92	55.28	67.79	41.00	78.00
	Phase IV	63.27	16.21	4.19	54.29	72.25	31.00	86.00

Table S6.2 – Statistical analysis of variance (ANOVA) for NO_2^--N and NO_3^--N concentration, and ATZ, COD, and NH_4^+-N removal percentages (r).

		Sum of Squares	df	Mean Square	F	Sig.
ANOVA						
NO_2^--N_e	Between Groups	40.54	3	13.51	27.21	0.000
	Within Groups	27.80	56	0.50		
	Total	68.34	59			
NO_3^--N_e	Between Groups	1875.24	3	625.08	106.25	0.000
	Within Groups	329.47	56	5.88		
	Total	2204.71	59			
ATZ_r	Between Groups	25291.94	3	8430.65	168.39	0.000
	Within Groups	2753.69	55	50.08		
	Total	28045.627	58			
COD_r	Between Groups	3150.05	3	1050.02	13.29	0.000
	Within Groups	4423.60	56	78.99		
	Total	7573.65	59			
NH_4^+-N_r	Between Groups	18540.93	3	6180.31	60.11	0.000
	Within Groups	5758.00	56	102.82		
	Total	24298.93	59			

df: degrees of freedom

178

Table S6.3 – Tukey's HSD test (difference expressed honestly) to determine if there is a statistically significant difference in the NO_2^--N and NO_3^--N concentration and COD and NH_4^+-N removal efficiencies (r) when the ATZ was present in the biological systems and whether the assessed concentrations of the ATZ had an influence on its removal percentages.

Multiple Comparisons							
Tukey HSD							
Dependent Variable			Mean Difference (I-J)	Std. Error	Sig.	95% Confidence Interval Lower Bound	Upper Bound
NO_2^--N$_e$	Phase I	Phase II	-0.21	0.26	0.845	-0.89	0.47
		Phase III	-0.36	0.26	0.497	-1.04	0.32
		Phase IV	-2.07*	0.26	0.000	-2.75	-1.38
	Phase II	Phase I	0.21	0.26	0.845	-0.47	0.89
		Phase III	-0.15	0.26	0.934	-0.83	0.53
		Phase IV	-1.85*	0.26	0.000	-2.54	-1.17
	Phase III	Phase I	0.36	0.26	0.497	-0.32	1.04
		Phase II	0.15	0.26	0.934	-0.53	0.83
		Phase IV	-1.70*	0.26	0.000	-2.38	-1.02
	Phase IV	Phase I	2.07*	0.26	0.000	1.38	2.75
		Phase II	1.86*	0.26	0.000	1.17	2.54
		Phase III	1.70*	0.26	0.000	1.02	2.38
NO_3^--N$_e$	Phase I	Phase II	-9.75*	0.89	0.000	-12.10	-7.41
		Phase III	-2.48*	0.89	0.034	-4.82	-0.13
		Phase IV	5.83*	0.89	0.000	3.48	8.17
	Phase II	Phase I	9.75*	0.89	0.000	7.41	12.10
		Phase III	7.27*	0.89	0.000	4.93	9.62
		Phase IV	15.58*	0.89	0.000	13.24	17.93
	Phase III	Phase I	2.48*	0.89	0.034	0.13	4.82
		Phase II	-7.27*	0.89	0.000	-9.62	-4.93
		Phase IV	8.31*	0.89	0.000	5.96	10.65
	Phase IV	Phase I	-5.83*	0.89	0.000	-8.17	-3.48
		Phase II	-15.58*	0.89	0.000	-17.93	-13.24
		Phase III	-8.31*	0.89	0.000	-10.65	-5.96
ATZ_r	Phase I	Phase II	-40.60*	2.58	0.001	-47.44	-33.75
		Phase III	-49.21*	2.63	0.001	-56.18	-42.25
		Phase IV	-50.53*	2.58	0.001	-57.37	-43.69
	Phase II	Phase I	40.60*	2.58	0.001	33.75	47.44

		Phase III	-8.61	2.63	0.01	-15.58	-1.65
		Phase IV	-9.93*	2.58	0.002	-16.78	-3.09
	Phase III	Phase I	49.21*	2.63	0.001	42.25	56.18
		Phase II	8.61	2.63	0.010	1.65	15.58
		Phase IV	-1.32	2.63	0.958	-8.28	5.65
	Phase IV	Phase I	50.53*	2.58	0.001	43.69	57.38
		Phase II	9.93*	2.58	0.002	3.09	16.78
		Phase III	1.32	2.63	0.958	-5.65	8.29
COD_r	Phase I	Phase II	6.27	3.25	0.227	-2.33	14.86
		Phase III	15.27*	3.25	0.000	6.67	23.86
		Phase IV	18.27*	3.25	0.000	9.67	26.86
	Phase II	Phase I	-6.27	3.25	0.227	-14.86	2.33
		Phase III	9.00*	3.25	0.037	0.41	17.59
		Phase IV	12.00*	3.25	0.003	3.41	20.59
	Phase III	Phase I	-15.27*	3.25	0.000	-23.86	-6.67
		Phase II	-9.00*	3.25	0.037	-17.59	-0.41
		Phase IV	3.00	3.25	0.792	-5.59	11.59
	Phase IV	Phase I	-18.27*	3.25	0.000	-26.86	-9.67
		Phase II	-12.00*	3.25	0.003	-20.59	-3.41
		Phase III	-3.00	3.25	0.792	-11.59	5.59
$NH_4^+-N_r$	Phase I	Phase II	5.33	3.70	0.480	-4.47	15.14
		Phase III	38.46*	3.70	0.000	28.66	48.27
		Phase IV	36.73*	3.70	0.000	26.93	46.54
	Phase II	Phase I	-5.33	3.70	0.480	-15.14	4.47
		Phase III	33.13*	3.70	0.000	23.33	42.94
		Phase IV	31.40*	3.70	0.000	21.60	41.20
	Phase III	Phase I	-38.47*	3.70	0.000	-48.27	-28.66
		Phase II	-33.13*	3.70	0.000	-42.94	-23.33
		Phase IV	-1.73	3.70	0.966	-11.54	8.07
	Phase IV	Phase I	-36.73*	3.70	0.000	-46.54	-26.93
		Phase II	-31.40*	3.70	0.000	-41.20	-21.60
		Phase III	1.73	3.70	0.966	-8.07	11.54

*. The mean difference is significant at the 0.05 level.
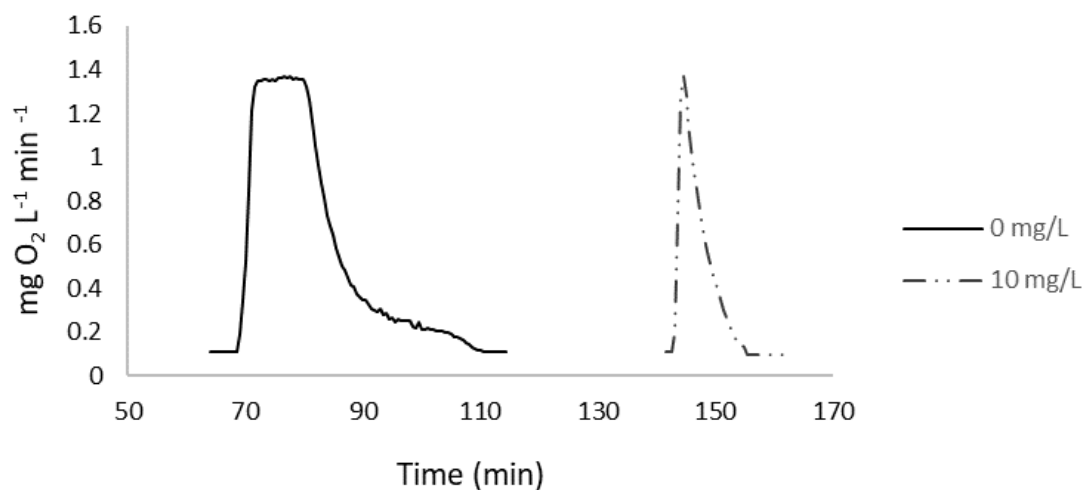
Figure S6.1 – OUR profile illustration for measure of the total oxygen consumed during the peak with carbon source and the peak with canbon source and ATZ at 10 mg L^{-1}.
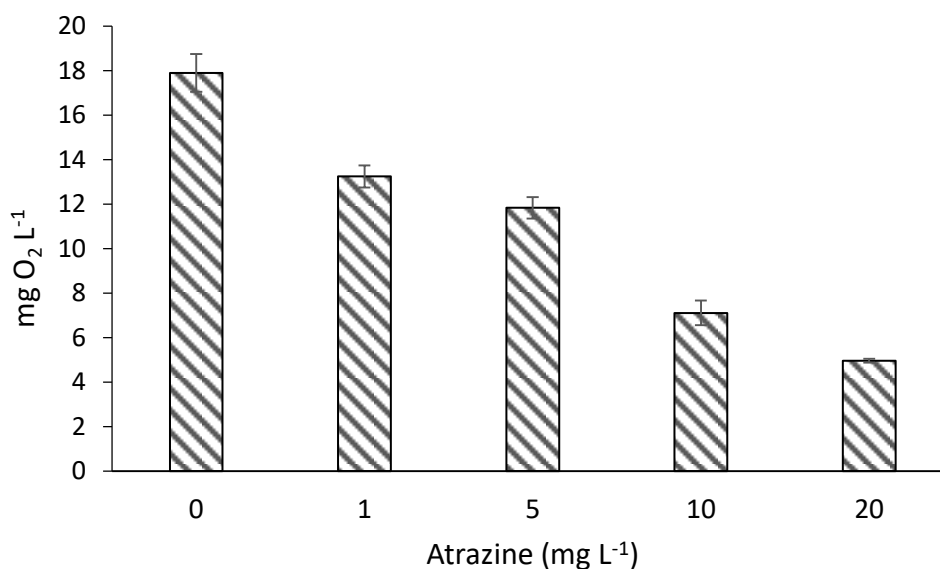
Figure S6.2 – Oxygen consumed for concentrations ranging from 0 to 20 mg L^{-1} of ATZ during OUR assays.

Table S6.4 – Parameters values on average from respirometric assays.

ATZ (mg L^{-1})	K_{La} (1 min^{-1})	Oxygen consumed (mg O_2 L^{-1})	OUR_{Max} (mg O_2 g^{-1} MLVSS min^{-1})
0	0.210	17.7	0.83
1	0.217	13.3	0.69
5	0.217	11.8	0.58
10	0.155	7.1	0.78
20	0.210	5.0	0.75

Table S6.5 – Average values (mg EPS g_{MLVSS}^{-1}) followed by standard deviation (Std. Deviation) of EPS and components during phases I-IV.

Descriptives		Mean	Std. Deviation	95% Confidence Interval for Mean		Minimum	Maximum
				Lower Bound	Upper Bound		
PS LB-EPS	Phase I	5.74	0.37	3.59	7.89	1.10	14.73
	Phase II	10.27	0.26	8.42	12.11	2.85	15.00
	Phase III	4.97	0.19	3.59	6.34	1.18	10.39
	Phase IV	10.80	0.26	7.67	13.93	2.98	20.32
PN LB-EPS	Phase I	11.97	0.90	6.94	16.99	0.69	31.41
	Phase II	39.00	1.07	32.91	45.09	18.20	54.94
	Phase III	32.16	1.18	22.66	41.65	9.11	58.36
	Phase IV	33.94	1.20	25.54	42.33	14.55	56.04
PS TB-EPS	Phase I	9.96	0.86	6.54	13.39	2.17	22.01
	Phase II	10.41	0.37	7.62	13.20	5.25	22.60
	Phase III	17.42	0.56	12.45	22.39	9.93	38.12
	Phase IV	13.79	0.24	9.91	17.67	5.66	27.04
PN TB-EPS	Phase I	24.16	1.48	14.64	33.67	3.47	50.60
	Phase II	36.10	1.06	29.48	42.72	16.99	52.64
	Phase III	39.85	1.63	29.41	50.29	14.70	71.85
	Phase IV	52.61	1.12	41.73	63.50	25.25	83.49
LB-EPS	Phase I	17.71	0.98	11.02	24.40	1.79	46.14
	Phase II	49.26	1.10	41.44	57.09	21.05	69.94
	Phase III	37.12	1.20	26.55	47.69	10.48	66.28
	Phase IV	44.74	1.23	33.52	55.95	18.92	73.83
TB-EPS	Phase I	34.12	1.71	21.95	46.29	5.78	72.61
	Phase II	46.51	1.13	37.41	55.60	22.24	71.63
	Phase III	57.27	1.73	42.25	72.29	26.41	109.97
	Phase IV	66.40	1.14	52.03	80.78	32.20	109.69
EPS	Phase I	51.82	1.97	39.67	63.98	23.36	95.60
	Phase II	95.77	1.57	84.21	107.33	55.10	141.57
	Phase III	94.39	2.10	77.93	110.86	48.73	141.68
	Phase IV	111.14	1.68	93.08	129.20	60.34	154.78

Table S6.6 – Statistical analysis of variance (ANOVA) for EPS and its components during phases I-IV.

		Sum of Squares	df	Mean Square	F	Sig.
ANOVA						
PS LB-EPS	Between Groups	409.07	3.00	136.36	8.48	0.000
	Within Groups	900.02	56.00	16.07		
	Total	1309.09	59.00			
PN LB-EPS	Between Groups	6361.70	3.00	2120.57	11.67	0.000
	Within Groups	10176.31	56.00	181.72		
	Total	16538.01	59.00			
PS TB-EPS	Between Groups	540.96	3.00	180.32	3.73	0.016
	Within Groups	2704.45	56.00	48.29		
	Total	3245.40	59.00			
PN TB-EPS	Between Groups	6181.59	3.00	2060.53	6.99	0.000
	Within Groups	16511.38	56.00	294.85		
	Total	22692.96	59.00			
LB-EPS	Between Groups	8732.87	3.00	2910.96	10.39	0.000
	Within Groups	15686.46	56.00	280.12		
	Total	24419.33	59.00			
TB-EPS	Between Groups	8727.17	3.00	2909.06	5.38	0.003
	Within Groups	30263.74	56.00	540.42		
	Total	38990.90	59.00			
EPS	Between Groups	29177.15	3.00	9725.72	13.58	0.000
	Within Groups	40118.19	56.00	716.40		
	Total	69295.34	59.00			

df: degrees of freedom

Table S6.7 – Tukey's HSD test to verify if ATZ presence promoted a statistically significant difference in terms of EPS production along phases I to IV.

			Mean Difference (I-J)	Std. Error	Sig.	95% Confidence Interval	
Multiple Comparisons							
Tukey HSD							
Dependent Variable						Lower Bound	Upper Bound
PS LB-EPS	Phase I	Phase II	-4.53*	1.46	0.016	-8.40	-0.65
		Phase III	0.78	1.46	0.952	-3.10	4.65
		Phase IV	-5.06*	1.46	0.006	-8.93	-1.18
	Phase II	Phase I	4.53*	1.46	0.016	0.65	8.40
		Phase III	5.30*	1.46	0.003	1.43	9.18
		Phase IV	-0.53	1.46	0.983	-4.41	3.34
	Phase III	Phase I	-0.78	1.46	0.952	-4.65	3.10
		Phase II	-5.30*	1.46	0.003	-9.18	-1.43
		Phase IV	-5.83*	1.46	0.001	-9.71	-1.96
	Phase IV	Phase I	5.06*	1.46	0.006	1.18	8.93
		Phase II	0.53	1.46	0.983	-3.34	4.41
		Phase III	5.83*	1.46	0.001	1.96	9.71
PN LB-EPS	Phase I	Phase II	-27.03*	4.92	0.000	-40.06	-14.00
		Phase III	-20.19*	4.92	0.001	-33.22	-7.16
		Phase IV	-21.97*	4.92	0.000	-35.00	-8.94
	Phase II	Phase I	27.03*	4.92	0.000	14.00	40.06
		Phase III	6.84	4.92	0.511	-6.19	19.87
		Phase IV	5.06	4.92	0.734	-7.98	18.09
	Phase III	Phase I	20.19*	4.92	0.001	7.16	33.22
		Phase II	-6.84	4.92	0.511	-19.87	6.19
		Phase IV	-1.78	4.92	0.984	-14.82	11.25
	Phase IV	Phase I	21.97*	4.92	0.000	8.94	35.00
		Phase II	-5.06	4.92	0.734	-18.09	7.98
		Phase III	1.78	4.92	0.984	-11.25	14.82
PS TB-EPS	Phase I	Phase II	-0.45	2.54	0.998	-7.17	6.27
		Phase III	-7.46*	2.54	0.024	-14.18	-0.74
		Phase IV	-3.83	2.54	0.439	-10.55	2.89
	Phase II	Phase I	0.45	2.54	0.998	-6.27	7.17
		Phase III	-7.01*	2.54	0.038	-13.73	-0.29
		Phase IV	-3.38	2.54	0.547	-10.10	3.34
	Phase III	Phase I	7.46*	2.54	0.024	0.74	14.18
		Phase II	7.01*	2.54	0.038	0.29	13.73
		Phase IV	3.63	2.54	0.486	-3.09	10.35
	Phase IV	Phase I	3.83	2.54	0.439	-2.89	10.55
		Phase II	3.38	2.54	0.547	-3.34	10.10

		Phase III	-3.63	2.54	0.486	-10.35	3.09
PN TB-EPS	Phase I	Phase II	-11.94	6.27	0.238	-28.54	4.66
		Phase III	-15.69	6.27	0.070	-32.30	0.91
		Phase IV	-28.46*	6.27	0.000	-45.06	-11.85
	Phase II	Phase I	11.94	6.27	0.238	-4.66	28.54
		Phase III	-3.75	6.27	0.932	-20.36	12.85
		Phase IV	-16.52	6.27	0.052	-33.12	0.09
	Phase III	Phase I	15.69	6.27	0.070	-0.91	32.30
		Phase II	3.75	6.27	0.932	-12.85	20.36
		Phase IV	-12.76	6.27	0.187	-29.36	3.84
	Phase IV	Phase I	28.46*	6.27	0.000	11.85	45.06
		Phase II	16.52	6.27	0.052	-0.09	33.12
		Phase III	12.76	6.27	0.187	-3.84	29.36
LB-EPS	Phase I	Phase II	-31.55*	6.11	0.000	-47.74	-15.37
		Phase III	-19.41*	6.11	0.013	-35.59	-3.23
		Phase IV	-27.03*	6.11	0.000	-43.21	-10.84
	Phase II	Phase I	31.55*	6.11	0.000	15.37	47.74
		Phase III	12.14	6.11	0.205	-4.04	28.32
		Phase IV	4.53	6.11	0.880	-11.66	20.71
	Phase III	Phase I	19.41*	6.11	0.013	3.23	35.59
		Phase II	-12.14	6.11	0.205	-28.32	4.04
		Phase IV	-7.61	6.11	0.601	-23.80	8.57
	Phase IV	Phase I	27.03*	6.11	0.000	10.84	43.21
		Phase II	-4.53	6.11	0.880	-20.71	11.66
		Phase III	7.61	6.11	0.601	-8.57	23.80
TB-EPS	Phase I	Phase II	-12.39	8.49	0.468	-34.87	10.09
		Phase III	-23.15*	8.49	0.041	-45.63	-0.68
		Phase IV	-32.29*	8.49	0.002	-54.76	-9.81
	Phase II	Phase I	12.39	8.49	0.468	-10.09	34.87
		Phase III	-10.76	8.49	0.587	-33.24	11.71
		Phase IV	-19.90	8.49	0.100	-42.37	2.58
	Phase III	Phase I	23.15*	8.49	0.041	0.68	45.63
		Phase II	10.76	8.49	0.587	-11.71	33.24
		Phase IV	-9.13	8.49	0.705	-31.61	13.34
	Phase IV	Phase I	32.29*	8.49	0.002	9.81	54.76
		Phase II	19.90	8.49	0.100	-2.58	42.37
		Phase III	9.13	8.49	0.705	-13.34	31.61
EPS	Phase I	Phase II	-43.95*	9.77	0.000	-69.82	-18.07
		Phase III	-42.57*	9.77	0.000	-68.45	-16.69
		Phase IV	-59.32*	9.77	0.000	-85.20	-33.44
	Phase II	Phase I	43.95*	9.77	0.000	18.07	69.82
		Phase III	1.38	9.77	0.999	-24.50	27.25
		Phase IV	-15.37	9.77	0.402	-41.25	10.51
	Phase III	Phase I	42.57*	9.77	0.000	16.69	68.45
		Phase II	-1.38	9.77	0.999	-27.25	24.50

	Phase IV	-16.75	9.77	0.326	-42.63	9.13
Phase IV	Phase I	59.32*	9.77	0.000	33.44	85.20
	Phase II	15.37	9.77	0.402	-10.51	41.25
	Phase III	16.75	9.77	0.326	-9.13	42.63

*. The mean difference is significant at the 0.05 level.